UNIVERSITÀ
DEGLI STUDI
DI PADOVA

Università degli Studi di Padova

Dipartimento di Biologia

SCUOLA DI DOTTORATO DI RICERCA
IN BIOSCIENZE E BIOTECNOLOGIE

INDIRIZZO IN BIOTECNOLOGIE
CICLO XXIV°

Nanovehicles for medical use: an *in vitro* evaluation of cytotoxicity and drug delivery efficiency

Direttore della scuola: Ch.mo Prof. Giuseppe Zanotti

Coordinatore d'indirizzo: Ch.mo Prof.ssa Lo Schiavo Fiorella

Supervisore: Ch.mo Prof.ssa Lucia Celotti

Co-supervisore: Ch.mo Dott.ssa Elena Reddi

Dottorando: Francesca Moret

Contents

List and summary of papers

The thesis is based on the following papers, which are referred to by roman numerals in the text:

I Chiara Compagnin[†], Francesca Moret[†], Lucia Celotti, Giovanni Miotto, Josephine H. Woodhams, Alexander J. MacRobert, Dietrich Scheglmann, Selma Iratni and Elena Reddi.

"*Meta*-tetra(hydroxyphenyl)chlorin-loaded liposomes sterically stabilised with poly(ethylene glycol) of different length and density: characterisation, *in vitro* cellular uptake and phototoxicity."

II Francesca Moret, Dietrich Scheglmann and Elena Reddi.

"Folate-targeted PEGylated liposomes improve the selectivity of PDT with *meta*-tetra(hydroxyphenyl)chlorin (*m*-THPC)."

III Matija Rojnik, Petra Kocbek, Francesca Moret, Chiara Compagnin, Lucia Celotti, Melissa J. Bovis, Josephine H Woodhams, Alexander J MacRobert, Dietrich Scheglmann, Wijnand Helfrich, Marco J Verkaik, Emanuele Papini, Elena Reddi and Janko Kos.

"*In vitro* and *in vivo* characterization of temoporfin-loaded PEGylated PLGA nanoparticles for use in photodynamic therapy."

IV Francesco Selvestrel[†], Francesca Moret[†], Daniela Segat[†], Josephine H. Woodhams[†], Giulio Fracasso[†], Iria M. Rio Echevarria, Luca Baù, Federico Rastrelli, Chiara Compagnin, Elena Reddi, Chiara Fedeli, Emanuele Papini, Regina Tavano, Alexandra Mackenzie, Melissa Bovis, Elnaz Yaghini, Alexander MacRobert, Silvia Zanini, Anita Boscaini, Marco Colombatti and Fabrizio Mancin.

***"*Targeted delivery of photosensitizers: efficacy and selectivity issues revelead by multifunctional ORMOSIL nanovectors in cellular systems."**

V Francesca Moret, Francesco Selvestrel, Elisa Lubian, Chiara Compagnin, Maddalena Mognato, Lucia Celotti, Fabrizio Mancin and Elena Reddi.

"PEGylation of ORMOSIL nanoparticles abolishes the toxicity toward some lung cells but not alveolar type II epithelial cells *in vitro.*"

† The authors contributed equally to the study.

The papers were written in co-authorship, reflecting the collaboration among authors. Papers I, II and III are already published and collected data obtained during the European project NANOPHOTO, in which 4 academic groups (Padova University, Ljubljana University, University College London, Groningen University) and the industry Biolitec Research GmbH collaborated at the development of a nanovehicle for the delivery of the photosensitizer m*eta*-tetra(hydroxyphenyl)chlorin (*m*-THPC) for photodynamic therapy (PDT) of cancer. In particular, I am the first author of both papers I and II since the majority of the data were produced in my research group and during my PhD experience. My contribution to paper III is related to the studies on *m*-THPC-loaded PLGA nanoparticles uptake, dark and photo-toxicity *in vitro*. Paper IV that has been accepted by Nanoscale for publication but not already published, collected results related to different aspects of using functionalized ORMOSIL nanoparticles as drug delivery systems. My contribution is referred to the *in vitro* studies of intracellular uptake of nanoparticles functionalized with folate or RGD peptide. For paper V, that is being submitted, I had the main responsibility for the experiments as well as for writing the paper.

Summary of Paper I

The study reports the *in vitro* characterization of PEGylated liposomes (namely Fospeg®) developed for the delivery of the photosensitizer *m*-THPC to cancer cells. In particular, the effects of liposome PEG density and thickness on *m*-THPC cellular uptake as well as on dark and phototoxicity were evaluated in normal (CCD-34Lu) and in cancer (A549) lung cells. The photodynamic efficiency of the different Fospeg® formulations was compared to those of the photosensitizer delivered to cells by the standard solvent (Foscan®). The study highlighted how the delivery of *m*-THPC by PEGylated liposomes drastically reduced the dark side effects of the drug, and how the reduction of cytotoxicity correlated with the increase of the percentage of PEGylation. In addition, even if the encapsulation of the photosensitizer in PEGylated liposomes reduced by 30-40% his intracellular uptake with respect to the free drug, phototoxicity was only slightly affected. Intracellular localization studies revealed that both Foscan® and Fospeg® localized in endoplasmic reticulum and Golgi apparatus, suggesting that part of the drug effectively entered the cells with the delivery systems but also that part of the drug is release before internalization and entered cells as complexes with serum proteins.

Summary of Paper II

In this paper the design, the synthesis and the *in vitro* specific uptake and phototoxicity of a novel folate-targeted liposomal formulation (FA-Fospeg) for the delivery of *m*-THPC to cells over-expressing folate receptors (FR) are reported. Thus, *m*-THPC PEGylated liposomes (PEG750) bearing folate at the distal end of a PEG spacer (PEG5000) were synthesized and their specific internalization were compared to those of un-targeted liposomes in KB (FR-positive) and A549 (FR-negative) cells. Since, as demonstrated in Paper I, *m*-THPC release from Fospeg®

occurs and very likely affects the measure of the specific internalization of the drug via the targeted nanovehicles, preliminary experiments were carried out using liposomes covalently labelled with carboxyfluorescein (CF-liposomes). Competition experiments using free FA revealed that only a modest fraction (~15%) of FA-targeted CF-liposomes entered KB cells via FR-mediated endocytosis while non-specific uptake of liposomes prevailed in both cell lines regardless the presence of the targeting agent. Instead, when FA-Fospeg was used, the selective uptake in KB cells was measured only at short incubation time (3h) while no difference in the photosensitizer uptake was measure after 24 h in both cell lines and for both liposome formulations due to the release of a large fraction of the drug at long incubation time. Nevertheless, despite the low contribution of FR-mediated uptake of FA-Fospeg, in KB cells the *m*-THPC uptake was doubled and translated into a 1.5-foldenhanced photo-killing efficiency.

Summary of Paper III

The paper reports on an *in vitro* and *in vivo* evaluation of PEGylated poly-($_{D,L}$-lactide-co-glycolide) nanoparticles (PEG PLGA NPs) as *m*-THPC drug delivery system for use in PDT and in fluorescence-based imaging of tumours. In the study bare and PEGylated PLGA NPs were synthesized using nanoprecipitation method, were photo-physically characterized and their ability to deliver *m*-THPC was evaluated *in vitro* in 3 different cell lines (A549, MCF10A neo T, U937) while their biodistribution was evaluated *in vivo* in mice. The results showed that within NPs *m*-THPC was aggregated with consequent self-quenching and that it was promptly released in the presence of serum proteins with a kinetics faster for PEG with respect non PEG PLGA NPs. Nevertheless, by using both bare and PEGylated NPs, *m*-THPC was efficiently delivered to the cells and localized in perinuclear region and/or acidic compartments. The reduced drug uptake measured for PEGylated NPs with respect to bare NPs confirmed the sheathing features of the delivery system. Interestingly, the dark cytotoxicity of *m*-THPC was highly reduced with the encapsulation in PEG PLGA NPs while photo-toxicity resulted comparable to that of mTHPC delivered by standard solvent (Foscan®), notwithstanding the double uptake measured for Foscan®. Reduced uptake of NPs with respect to Foscan® was confirmed *in vivo* measuring the total body fluorescence of mice 24 h post-injection while biodistribution experiments revealed higher tumour-to-skin ratio for PLGA NPs with respect to Foscan® and reduced accumulation in lungs and colon of PEG PLGA NPs with respect to bare NPs.

Summary of Paper IV

The study highlighted potentialities and limitations of ORganically MOdified SILica nanoparticles (ORMOSIL NPs) as targeted drug delivery system. For the first time the synthesis of highly PEGylated VTES-ORMOSIL NPs in which *m*-THPC was covalently entrapped after mono- or tetra-functionalisation with alkoxysilane was reported together with a detailed photophysical characterisation of the entrapped drug. It was found that the singlet oxygen

quantum yield was comparable to that of the free drug for the mono-silane derivative of *m*-THPC in NPs while was strongly reduced in the case of the tetra-silane in NPs. *In vitro* experiments revealed that the embedding of the photosensitizer in PEG NPs highly reduced his uptake in normal as well in cancer cells with respect to Foscan®, indicating that targeting of NPs could be a useful strategy in order to improve the selective uptake of *m*-THPC in cancer cells. Thus, NPs were functionalized with folate, RGD peptide or Cetuximab antibody and their ability was measured to target selectively cells over-expressing folate receptor (FR), integrin $\alpha_5\beta_3$ receptor and epidermal growth factor receptor (EGFR), respectively,. Folate-targeted NPs displayed no selective uptake very likely because of scarce exposure of the hydrophobic targeting agents that hides itself in the PEG layer. On the contrary, RGD-targeted and Cetuximab-targeted NPs were selectively taken up with respect to their control NPs RAD-NPs and BSA-NPs, respectively. However, selective targeting did not correlate with enhanced PDT efficiency since a modest increase of phototoxicity was measured for Cetuximab NPs but not for RGD NPs. The results obtained arise the paradox that at least *in vitro* selectivity of uptake by the targeted NPs is achievable only in conditions of low NP cell-loading with consequent delivery of an amount of *m*-THPC that is insufficient for inducing satisfactory cell photo-killing.

Summary of Paper V

The paper reports an *in vitro* characterization of the cytotoxic profiles of bare and PEGylated ORMOSIL NPs in different normal (CCD-34Lu) and cancer (A549, NCI-H2347) lung cells. Cell viability measurements revealed that un-PEGylated NPs were highly cytotoxic toward all cell lines while PEGylation abolished cytotoxicity in CCD-34Lu and NCI-H2347 but not in A549 cells. PEG NP exposure determined A549 cell death via necrosis since membrane permeabilization and LDH release were measured. In addition, gene expression profile studies using Agilent microarray revealed that the expression of hundred of genes involved in inflammation, receptor-mediated cell signalling and cell death were altered after A549 NP exposure. Furthermore, a significant increase in reactive oxygen species (ROS) production was measured but oxidative stress cannot be considered the determinant of A549 cell mortality since incubation of cells with ROS inhibitors reduced ROS level while did not protect cells from NP-induced death. The uptake of PEG NPs in CCD-34Lu fibroblasts was comparable to that of A549 cells, ROS were produced following the 24 h incubation with NPs but cytotoxic effects could not be detected in these cells. Analysing the intracellular fate of NPs by transmission electron microscopy, we found that in A549 cells NPs were internalized in pulmonary surfactant-containing lamellar bodies, peculiar of alveolar type II cells of which A549 represents a model. Immunofluorescence studies showed that PEG NPs caused a decrease of expression of specific pulmonary surfactant proteins (SP-A, SP-C). Overall the results suggest that the sensitivity of A549 to PEG ORMOSIL NPs was triggered by the interference of the nanostructures with the lung surfactant production and recycling.

Abstract

The recent progresses offered by nanotechnology in the manipulation of matter lead to the development of several nanoparticles (NPs) and nanodevices for medical applications. In oncology, nanosized objects are particularly attractive as drug delivery systems since it is expected that engineered nanovehicles of appropriate size and functionalised with specific ligands/antibodies will improve the efficacy and selectivity of cancer therapies by exploiting both the passive and active mechanism of tumour targeting. The use of delivery systems is particularly appealing in those therapies in which the administration of the drug in aqueous formulations leads to drug aggregation with decreased activity or scarce bioavailability and tumour selectivity. This is the case of most of the photosensitizers used in photodynamic therapy (PDT), which display hydrophobicity and poor selective accumulation in malignant tissues. In the last decades, PDT is emerging as a promising cancer treatment modality in alternative to conventional therapies, which often demonstrate systemic drug toxicity and multidrug-resistance phenomena. PDT is based on the administration of a photosensitizer (PS) that accumulates in the tumour and after activation with light of appropriate wavelengths, reacts with surrounding molecular oxygen leading to the formation of cytotoxic reactive oxygen species (ROS) with consequent cellular and vasculature damages.

In this PhD thesis, three different nanosystems, namely, liposomes, poly-($_{D,L}$-lactide-co-glycolide) nanoparticles (PLGA NPs) and ORganically Modified SILica nanoparticles (ORMOSIL NPs) were considered for the delivery of the second generation PS *meta*-tetra(hydroxyphenyl)chlorin (*m*-THPC, Temoporfin) to cancer cells *in vitro*. In particular, drug delivery efficiency, dark and phototoxicity of the *m*-THPC nanoparticle-based formulations were evaluated. To improve *m*-THPC bioavailability and tumour selectivity, in the design of the nanovehicles PEGylation and targeting of NPs were considered as essential strategies in order to prolong NP circulation in the bloodstream and exploit active mechanisms of tumour targeting.

For the delivery of *m*-THPC using unilamellar liposomes, four different PEGylated liposomal formulations (trade name Fospeg®, provided by Biolitec Research) in which the length (PEG750, PEG2000, PEG5000) and the density (2%, 8%) of PEG were varied, were tested *in vitro* in normal lung fibroblasts CCD-34Lu and in cancer A549 lung epithelial cells. Compared to drug delivered in the standard solvent (Foscan®, ethanol/PEG 400/water (20:30:50, by vol.)), liposomal *m*-THPC showed a decreased intracellular uptake in both cell lines, but the presence of the delivery system highly reduced the dark cytotoxicity of the drug. The reduction of the PS dark toxicity increased with the increasing of PEG density on liposome surface, while the length of PEG chains did not affect significantly the toxic effect of *m*-THPC in the dark. However, photo-toxicity measured in A549 cells was only slightly affected by the reduced uptake of *m*-THPC delivered by Fospeg®, and the efficiency of PDT-induced cell killing was comparable among the different liposomal formulations. Interestingly, the intracellular localization of *m*-THPC delivered as Fospeg® or Foscan® was the same (Golgi apparatus and endoplasmic reticulum) suggesting drug release from liposomes, especially in the presence of the serum

proteins, being *m*-THPC only physically entrapped within liposomes. *m*-THPC release was confirmed by the fact that liposomes covalently labelled with rhodamine were effectively were taken up by cells but, differently from *m*-THPC, localized in the acidic compartments of the cells. In spite of *m*-THPC release from liposomes, the Fospeg® formulation was exploited to target actively cancer cells by liposome conjugation with folic acid (FA), being FA-receptors (FRs) over-expressed in several human tumours. Thus, specific uptake and photo-toxicity of FA-targeted liposomes (FA-Fospeg) with respect to liposomes of the same composition but lacking FA (un-targeted Fospeg) was evaluated in KB (FR-positive) and in A549 (FR-negative) cells. The uptake of *m*-THPC delivered as FA-Fospeg was twice that of un-targeted Fospeg in KB cells; however only a modest fraction (~ 15%) of the targeted vehicle was effectively internalized by FR-mediated endocytosis while nonspecific internalization remained the prevailing mechanism of liposomes uptake in both cell lines. The improved *m*-THPC uptake obtained with FA-Fospeg in FR over-expressing cells translated into a 1.5 higher photo-induced toxicity.

A novel formulation of bare and PEGylated PLGA NPs in which *m*-THPC was physically entrapped were synthesized (Prof J. Kos, University of Ljubljana) and evaluated *in vitro* and *in vivo* for phototherapy and fluorescence-based tumour imaging applications. *In vitro* studies carried out on A549, MCF10A neo T (breast cancer cells) and U937 (lymphoma derived pro-monocytic cells) cell lines, showed reduced uptake of PEGylated NPs with respect to non PEGylated NPs. As for Fospeg®, the use of the delivery system led to a significant reduction of *m*-THPC dark toxicity.. As expected for PEGylated NPs, the efficiency of cell internalization of *m*-THPC entrapped in PEG PLGA was reduced by 50% with respect to that in the standard solvent, but surprisingly cytotoxicity induced in irradiated A549 cells was quite comparable. At 24 h post-injection *in vivo* biodistribution of bare and PEGylated PLGA NPs compared to Foscan® was assessed in mice, showing very similar drug accumulation in the major organs but reduced skin uptake for both NP formulations. Thus, even if *m*-THPC release in the presence of serum proteins was measured *in vitro*, PEGylated PLGA NPs appeared potentially useful as stealth and biodegradable PS delivery systems.

The premature release of the PS from the delivery system was completely avoided with the covalent link of *m*-THPC to the silane matrix of highly PEGylated ORMOSIL NPs (Prof. F. Mancin, University of Padova). This type of NPs exhibited a very low extent of cell internalization *in vitro* due to their high degree of PEGylation, making NP targeting an essential prerequisite to enhance intracellular drug delivery. In addition to FA, the RGD peptide and the antibody Cetuximab, which bind respectively the integrin $\alpha_5ß_3$ receptor and epidermal growth factor receptor (EGFR), were exploited as targeting agents for ORMOSIL NPs and the specific uptake and photo-toxicity of *m*-THPC delivered by conjugated NPs were evaluated *in vitro*. The study revealed how the characteristics of the targeting agents are of crucial importance in determining the performances of targeted PEGylated nanosystems. In fact, the hydrophobic FA was very likely buried in the PEG layer and was unable to drive the selective uptake of

ORMOSIL NPs while RGD peptide and Cetuximab antibody displayed some selectivity toward cells over-expressing their receptors (HUVEC cells over-expressing integrin $\alpha_5\beta_3$ receptors and A431 cells over-expressing EGFR). Unfortunately, the enhanced and selective uptake of *m*-THPC obtained by the two latter targeted ORMOSIL NPs was not accompanied by efficient and selective photo-induced cytotoxicity; it appeared that the selectivity of NP uptake was achieved in scarce drug cell loading conditions, determining only low PDT efficacy.

The assessment of the biocompatibility of NPs is of fundamental importance for their safe use in nanomedicine. Since ORMOSIL NPs are not well characterised from this point of view, a toxicological characterization of empty ORMOSIL NPs were carried out *in vitro* in normal (CCD-34Lu) and cancer (A549, NCIH-2347) lung cells. The study included traditional cell viability and cytotoxicity tests (MTS test, LDH release assay, ROS production, cell membrane permeabilization measurements and electron microscopy analyses) in combination with a genome-wide analysis of gene expression profiles of cells exposed to NPs. The results pointed out that different types of cells respond quite differently to NPs and PEGylation of NPs highly affected the cytotoxicity profiles. PEGylation of ORMOSIL NPs completely abolished the toxicity of the nanosystem in CCD-34Lu and NCIH-2347 cells. On the contrary PEG ORMOSIL NPs induced necrotic cell death of A549 by increasing the permeability of the plasma membrane. At sub-lethal concentrations alteration of gene expression and inflammation were measured in A549 cells exposed to. The different response to PEG NPs is very likely explained considering the peculiarity of the cell type and the particular interaction of NPs with cell and internalization mechanisms. In fact, it was shown clearly that NPs internalized in A549 cells localized in and affected the morphology and the functioning of pulmonary surfactant containing lamellar bodies, peculiar of alveolar type II cells of which A459 cells represents an *in vitro* models.

Riassunto

Il recente progresso apportato dalla nanotecnologia nella manipolazione della materia ha portato al conseguente sviluppo di diversi tipi di nanoparticelle e *nanodevices* per applicazioni biomediche. In campo oncologico, oggetti dalle dimensioni nanometriche si sono dimostrati particolarmente interessanti in qualità di sistemi per la veicolazione di farmaci, poiché si presume che l'ingegnerizzazione dei nanoveicoli e la loro funzionalizzazione con specifici ligandi/anticorpi possa portare ad un miglioramento dell'efficacia e della selettività delle terapie antitumorali sfruttando meccanismi di *targeting* del tumore sia passivi che attivi. L'utilizzo di sistemi di veicolazione è particolarmente importante nel caso di terapie nelle quali la somministrazione dei farmaci in formulazioni acquose conduce a fenomeni di aggregazione con conseguente diminuzione di attività e di disponibilità nel circolo sanguineo, o nel caso di farmaci con scarsa selettività per il tumore. Appartengono a queste categorie la maggior parte dei fotosensibilizzanti utilizzati in terapia fotodinamica (PDT), poiché farmaci di natura idrofobica e con scarsa selettività di accumulo nei tessuti maligni. Negli ultimi decenni, la PDT si è dimostrata una promettente tecnica di trattamento del cancro in alternativa alle terapie convenzionali che invece generalmente dimostrano alta tossicità sistemica e fenomeni di farmaco-resistenza. La PDT si basa sulla somministrazione di un fotosensibilizzante (PS) che accumulatosi nel tumore, e dopo essere stato attivato con opportune lunghezze d'onda di luce, è in grado di reagire con l'ossigeno molecolare che lo circonda generando specie reattive dell'ossigeno (ROS) altamente citotossiche con conseguente danno cellulare e vascolare. In questa tesi di dottorato, tre diversi nanosistemi quali liposomi, nanoparticelle PLGA (poly-($_{D,L}$-lactide-co-glycolide)) e nanoparticelle di silice organicamente modificata (ORMOSIL), sono stati presi in considerazione per la veicolazione del fotosensibilizzante di seconda generazione *meta*-tetra(hydroxyphenyl)chlorin (*m*-THPC, Temoporfin) in cellule tumorali *in vitro*. In particolare, sono state valutate l'efficienza di veicolazione del farmaco, la tossicità buia e fotoindotta delle diverse formulazioni di *m*-THPC. Per migliorare la biodisponibilità e la selettività per il tumore della *m*-THPC, nella progettazione dei nanoveicoli sono state considerate quali strategie essenziali la pegilazione e il *targeting* delle particelle, in modo da prolungare la circolazione dei nanosistemi nel flusso sanguineo e in modo da sfruttare meccanismi attivi di *targeting* del tumore.

Per la veicolazione della *m*-THPC utilizzando liposomi unilamellari sono state saggiate *in vitro* quattro diverse formulazioni liposomiali pegilate (Fospeg®, fornito dalla ditta Biolitec Research) con lunghezza (PEG750, PEG2000, PEG5000) e densità del PEG (2%, 8%) variabili, utilizzando come linee cellulari fibroblasti di polmone normali (CCD-34Lu) e cellule tumorali di epitelio polmonare (A549). Se paragonate al farmaco somministrato in forma libera in soluzione (Foscan®, etanolo/PEG 400/acqua (20:30:50, vol/vol)), le formulazioni liposomiali di *m*-THPC hanno mostrato una ridotta internalizzazione in entrambe le linee cellulari, ma nello stesso tempo la presenza del sistema di veicolazione ha portato alla significativa riduzione della tossicità buia del farmaco. La riduzione della tossicità buia del farmaco è risultata proporzionale all'aumento

della densità di PEG sulla superficie del liposoma mentre la lunghezza delle catene di PEG sembra essere ininfluente nel limitare l'effetto tossico della *m*-THPC al buio. Comunque, la ridotta internalizzazione della *m*-THPC veicolata tramite Fospeg® influenza in modo solo parziale la fototossicità misurata in cellule A549, mentre l'efficienza d'induzione di mortalità in seguito a trattamento fotodinamico è risultata paragonabile tra le diverse formulazioni saggiate. Indipendentemente dalla veicolazione tramite Fospeg® o Foscan®, è stata riscontrata la medesima localizzazione intracellulare della *m*-THPC (apparato del Golgi e reticolo endoplasmatico) suggerendo il possibile rilascio del farmaco dalla formulazione liposomiale in presenza di proteine del siero, essendo la *m*-THPC solamente fisicamente intrappolata all'interno dei liposomi. Il rilascio della *m*-THPC è stato confermato dal fatto che liposomi nei quali viene legata covalentemente rodamina vengono effettivamente internalizzati dalle cellule e, differentemente dalla *m*-THPC, si accumulano nei compartimenti acidi intracellulari.
Nonostante il rilascio del fotosensibilizzante dai liposomi, la formulazione Fospeg® è comunque stata utilizzata per veicolare selettivamente la *m*-THPC in cellule cancerose tramite la coniugazione dei liposomi con acido folico, essendo i recettori del folato sovraespressi in diversi tumori umani. Quindi sono state valutate l'internalizzazione specifica e la fototossicità di liposomi coniugati con folato (liposomi folato) rispetto a liposomi della stessa composizione ma privi di acido folico (liposomi non coniugati) in cellule KB e A549, rispettivamente positive e negative per l'espressione di recettori del folato. In cellule KB, l'internalizzazione della *m*-THPC si è rivelata doppia in caso di veicolazione con liposomi folato, malgrado solo una modesta parte (~15%) dei nanosistemi coniugati con folato siano effettivamente internalizzati tramite meccanismi di endocitosi mediata da recettore, essendo invece un'internalizzazione di tipo aspecifico il meccanismo prevalente per l'internalizzazione dei liposomi in entrambe le linee cellulari saggiate. In ogni caso, all'aumentato accumulo di *m*-THPC ottenuto tramite la veicolazione con Fospeg coniugato con folato in cellule che sovra esprimono il recettore, ne è conseguita una tossicità dopo irradiamento aumentata di circa 1.5 volte.
Riguardo invece la veicolazione di *m*-THPC tramite particelle PLGA, formulazioni nude o pegilate sono state sintetizzate (Prof. J. Kos, Università di Lubiana) e saggiate sia *in vitro* che *in vivo* per la loro potenziale applicazione in fototerapia o in diagnosi dei tumori, sfruttando la fluorescenza del fotosensibilizzante fisicamente intrappolato all'interno delle particelle. Studi *in vitro* condotti su cellule A549, MCF10A neo T (derivate da tumore del seno) e U937 (cellule pro-monocitiche derivate da linfoma), hanno mostrato una ridotta internalizzazione della formulazione di *m*-THPC pegilata rispetto a quella nuda. Anche con particelle PLGA e come già visto per il Fospeg®, l'utilizzo di un sistema di veicolazione porta alla significativa riduzione della citotossicità buia della *m*-THPC. L'efficienza d'internalizzazione del fotosensibilizzante veicolato tramite particelle PLGA pegilate viene ridotta circa del 50% rispetto alla sua veicolazione nella formulazione standard ma sorprendentemente l'effetto citotossico indotto in cellule A549 irradiate è quasi paragonabile. La biodistribuzione della *m*-THPC (veicolata tramite nanoparticelle PLGA nude o pegilate o nella formulazione standard) è stata valutata 24 ore dopo

la sua iniezione in topi, mostrando una simile distribuzione nei vari organi ma una significativa riduzione dell'accumulo a livello epidermico per entrambe le formulazioni nanoparticellari. Quindi, nonostante anche per le particelle PLGA pegilate sia stato misurato il rilascio di *m*-THPC in presenza di proteine sieriche, esse appaiono un buon sistema di veicolazione di fotosensibilizzanti soprattutto per le loro caratteristiche *'stealth'* e per la loro biodegradabilità.
Il rilascio prematuro del fotosensibilizzante è stato invece completamente limitato con il legame covalente della *m*-THPC alla matrice silanica di particelle ORMOSIL altamente pegilate (Prof. F. Mancin, Università di Padova). Tuttavia questo tipo di particelle ha mostrato un'internalizzazione intracellulare estremamente bassa derivata dall'elevato grado di pegilazione, ponendo come requisito essenziale il *targeting* delle particelle. In qualità di agenti di *targeting* per le particelle ORMOSIL pegilate sono stati valutati, oltre al folato, anche il peptide ciclico RGD e l'anticorpo Cetuximab, essendo questi ultimi in grado di legarsi rispettivamente ad integrine $\alpha_5ß_3$ e al recettore del fattore di crescite dell'epidermide (EGFR). L'internalizzazione selettiva e la fototossicità della *m*-THPC veicolata tramite le tre diverse nanoparticelle funzionalizzate sono state valutate *in vitro* in opportuni sistemi cellulari. Tale studio ha mostrato come le caratteristiche dell'agente di *targeting* influenzino in modo sostanziale la selettività di tali nanosistemi pegilati. Infatti, mentre il folato altamente idrofobico si ripiega verosimilmente verso la corona di PEG rendendosi inefficace nel guidare selettivamente le particelle ORMOSIL, il peptide RGD e l'anticorpo Cetuximab hanno mostrato una certa selettività nei confronti di cellule sovraesprimenti i rispettivi recettori (cellule HUVEC sovraesprimenti recettori per le integrine $\alpha_5ß_3$ e cellule A431 sovraesperimenti EGFR). Tuttavia, l'aumentato accumulo selettivo della *m*-THPC ottenuto tramite la coniugazione delle nanoparticelle con RGD e Cetuximab non ha portato ad una conseguente aumentata efficienza e selettività nell'induzione di citotossicità in seguito ad irradiamento. Tale risultato è verosimilmente imputabile al fatto che la selettività di accumulo delle nanoparticelle viene raggiunta in condizioni nelle quali la disponibilità del farmaco nelle cellule è troppo bassa, con conseguente scarsa efficacia dopo trattamento fotodinamico.
La valutazione della biocompatibilità delle nanoparticelle risulta di fondamentale importanza per un'applicazione sicura della nanotecnologia in campo medico. Quindi, poiché le nanoparticelle ORMOSIL non sono ancora state ben caratterizzate da tale punto di vista, un loro profilo tossicologico è stato tracciato *in vitro* in cellule polmonari normali (CCD-34Lu) e tumorali (A549, NCIH-2347). Nello studio sono stati combinati esperimenti tradizionali di valutazione della vitalità cellulare e della citotossicità (test MTS, saggio del rilascio di LDH, valutazione della produzione di ROS, misure di permeabilizzazione di membrana, analisi di microscopia elettronica) con un'analisi dei profili di espressione genica estesa all'intero genoma di cellule esposte alle nanoparticelle. I risultati hanno mostrato come diversi tipi di cellule rispondono in modo abbastanza differente all'esposizione alle nanoparticelle e come la pegilazione influisce fortemente sui profili di citotossicità. Infatti, la pegilazione delle particelle ORMOSIL è in grado di abolire completamente la tossicità dei nanosistemi in cellule CCD-34Lu e NCIH-2347 mentre

le stesse particelle pegilate inducono morte per necrosi in cellule A549, aumentandone la permeabilità di membrana. Inoltre nelle medesime cellule, concentrazioni sub-letali di nanoparticelle inducono infiammazione e alterazione dell'espressione genica. La differente risposta all'esposizione alle nanoparticelle pegilate delle cellule A549 è spiegabile considerando la peculiarità di questo tipo cellulare, e in particolare l'interazione delle particelle stesse con le cellule e il loro meccanismo d'internalizzazione. Infatti, è stato mostrato in modo chiaro che le nanoparticelle vengono internalizzate in corpi lamellari contenenti il surfattante polmonare, peculiari di cellule alveolari di tipo II, delle quali le cellule A549 rappresentano un modello *in vitro*. Tale accumulo delle nanoparticelle nei corpi lamellari porta alla modifica della morfologia degli stessi e una pesante alterazione della loro funzionalità.

Abbreviations

5-ALA: 5-aminolevulinic acid

EGFR epidermal growth factor receptor

EMA: european medicines agency

EPR: enhanced permeability and retention effect

FDA: food and drug administration

HPD: hematoporphyrin derivative

HPPH: 2-devinyl-2-(1-hexyloxyethyl)pyropheophorbide

ICS: inter crossing system

InTPP: In(III)-*meso*-tetraphenylporphyrin

i.v.: intravenous injection

LDL: low density lipoproteins

MB: methylene blue

m-THPC: *meta*-tetra(hydroxyphenyl)chlorin

m-THPP: 5,10,15,20-tetra(*m*-hydroxyphenyl)porphyrin

MPS: mononuclear phagocytic system

NPs: nanoparticles

ORMOSIL NPs: ORganically MOdified SILica nanoparticles

PDT: photodynamic therapy

PEG: poly (ethylene glycol)

PpIX: protoporphyrin IX

PPT: photothermal therapy

PS: photosensitizer

PLGA NPs: p*oly-($_{D,L}$-lactide-co-glycolide)* nanoparticles

RES: reticulo-endothelial system

ROS: reactive oxygen species

TPDT: targeted photodynamic therapy

ZnPc: zinc phthalocyanine

Introduction

In the last decades, the scientific knowledge in cancer biology has come on in leaps and bounds but has not translated into comparable advances in clinic practice. Thus, one of the major challenges still remains the improvement of cancer therapy, especially as regards an increase of the efficiency of therapeutics delivery and the concomitant obtainment of tumour selectivity. In fact, most of the conventional chemotherapeutics, after systemic administration, distribute in cancerous as well in healthy tissues with consequent side-effects and sub-optimal accumulation in the tumour (Wang *et al.* 2009). It appears that extraordinary opportunities to improve cancer therapy are offered by the emerging science of nanotechnology, which offers new starting point to be integrated with the established cancer research (Ferrari 2005, Ahmed *et al.* 2012). However, even if many products developed with nanotechnological approaches have entered the market and clinical practice, most of the concepts that grounded under the term 'nanomedicine', are for the most under continuous investigation by university and industry researchers. To date, many nanomaterials are at their infancy in the knowledge of their properties and require to be well characterized *in vitro* as well *in vivo* in animal models before their full potentials for application in medicine are completely understood. In fact, even if part of the research community is very confident in exploiting the potential of nanomedicine in the very near future (5-10 years), others are more cautious and feel that more time is needed before obtaining nanomaterials produced by large scale processes that can be safely used for disease treatments (Aguilar 2012).

In the following paragraphs the concepts of nanotechnology and nanomedicine are expanded, with particular attention dedicated to the development of nanomaterials for drug delivery applications in photodynamic therapy of cancer that is the main topic of this thesis.

Nanotechnology and Nanomedicine

The science of *nanotechnology* manipulates matter properties at the nanoscale level in order to develop new capabilities of materials for potential applications in engineering, technology and medicine. Nanotechnology products, which have at least one dimension in the range of 1 to 100 nm, possess unique chemical, electronic, optical, magnetic and catalytic properties, with respect to the bulk materials, that make them very attractive. Two different strategies of matter control and manipulation have been developed, the "bottom-up" and the "top-down" approaches. In the first, smaller molecules and atoms are assembled to form the nanoscale materials, while in the second micron-sized components are used to manipulate submicron materials. However, a convergence of the two approaches is needed for a practical use of the new developed nanomaterials in order to engineer nanoscale devices and to interface them with the outside world (Mazzola 2003). In the last 10 years, nanostructured material advantages have been

exploited in many different commercial fields with the development of several products for application in electronic industry, computer technology, pharmaceutical and medical research, food industry and agriculture. Thus, nanotechnology market is growing exponentially with an increasing number of commercial products which are introduced every week, with a tremendous worldwide socio-economic impact (Roco 2003). Nanomaterials are currently introduced in sunscreen, cosmetics, food products, food packaging, paints, varnishes, clothing, computer hardware, and as catalysts in fuels. In addition, in the 20th century, in the second half, growing synthetic polymer chemistry and pioneering nanotechnologies led to the development of the first nano-drugs which entered routine clinical use two decades later (Duncan and Gaspar 2011). From the 1930s, iron oxide nanoparticles appeared useful as parental iron infusion solution for the treatment of anemia (Marchasin and Wallerstein 1964, Silverstein and Rodgers 2004) while from the 1990s they were used as magnetic resonance imaging (MRI) contrasting agents with the acronym of SPIONs (Ferrucci 1991, Lin *et al.* 2008). Examples of first generation nano-drugs and imaging agents marketed and approved in clinical trials are liposome-based formulation such as the liposomal doxorubicin Myocet for cancer treatment or the liposomal morphine Depodur for pain relief, SPION dextran (Feridex, Endorem) coated nanoparticles for liver imaging, Abraxane albumin-based paclitaxel loaded nanoparticles for breast cancer therapy and polymeric drugs such as Copaxane, Renagel and Genoxol-PM (Duncan and Gaspar 2011, Cattaneo *et al*. 2010). However, the application of nanotechnology in medicine, referred with the term *nanomedicine*, not only provides new pharmaceutical formulations for optimized drug delivery but also exploits fields such as surgery (*nanosurgery*) (Ebbesen 2006), tissue engineering (Weeldon *et al.* 2011), DNA and RNA intracellular delivery for gene therapy (Chen *et al.* 2012, Shen *et al.* 2012) and molecular diagnosis for the early detection of diseases (Namiki *et al.* 2011). The concept that nanometric devices, with dimensions comparable with those of biological molecules such as proteins (5-50 nm), viruses (20-450 nm), genes (2 nm wide, 10-100 nm long), can be used to exploit biological signature of diseases and at the same time to treat them, lay beside the term *theranostic*. Theranostics are ideally integrated nanotherapeutic systems which can diagnose, deliver targeted drugs and finally monitor the response to therapy (Warner 2004, Sumer and Gao 2008). Theranostic research is growing up very fast and has already resulted in the development of products made of different nanomaterials carrying contrasting agents and active drugs. Examples are represented by gold nanoparticles loaded with doxorubicin for diagnosis, tumour targeting and photothermal therapy (PPT) (Prabaharan *et al.* 2009), carbon nanotubes loaded with doxorubicin, paclitaxel or plasmid DNA for diagnosis, drug and gene delivery (Pantarotto *et al.* 2004, Liu *et al.* 2008), luminescent quantum dots containing methotrexate or doxorubicin for imaging, therapy and sensing (Savla *et al.* 2008, Yuan *et al.* 2009).

The use of nanoparticles (NPs) as drug delivery systems in cancer makes them attractive for improving traditional chemotherapies since the pharmacokinetic profile of the drugs can be favourably modulated and therefore the therapeutic index can be improved and the systemic

toxicity reduced. To obtain these results, the so called "multifunctional nanoparticles" have been properly engineered, possessing 'stealthlike feature' to evade the immune system and prevent opsonization but also carrying targeting molecules to improve the selectivity of tumour uptake (Torchilin 2006, Cheng *et al*. 2012).

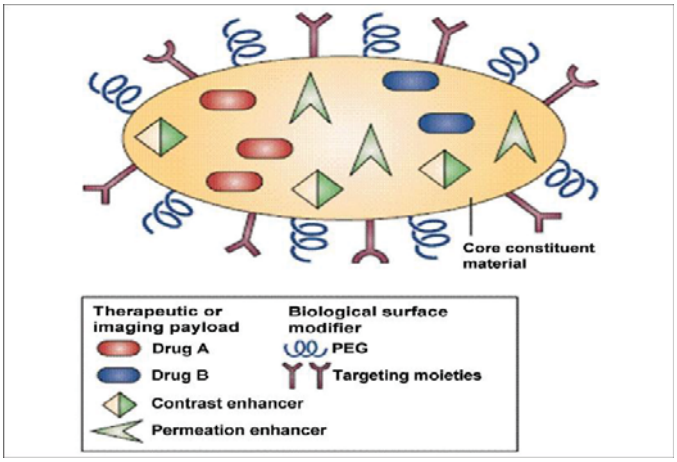

Figure 1: Example of a multifunctional nanocarrier (figure from Ferrari 2005, with license from Nature Publishing Group).

At the moment, several thousands of different types of nanovehicles are under investigations, and the flexibility offered by nanotechnological approaches to modulate NP characteristics, to select therapeutics and biological targets, represents the ideal starting point for the future of a personalized medicine.

Passive and active targeting of drug delivery systems to tumours

All nano-formulations already approved by the Food and Drug Administration (FDA) are examples of non-targeted NPs based on polymers or liposomes, which accumulates within malignant lesions due to *passive targeting*. With the term passive targeting we refer to the ability of NPs to accumulate in the tumour matrix as the result of their nanometric size and the particular architecture of the tumour vasculature. In fact, the rapid angiogenesis in solid tumours produce blood vessels with large gaps (600-800 nm) between adjacent endothelial cells which, together with the poor lymphatic drainage of cancer tissues, creates the enhanced permeability and retention (EPR) effect (Maeda *et al.* 2000, Hirsjärvi *et al.* 2011). Thus, the leaky vasculature allows nanovehicles to accumulate and reside in tumour cell interstitial space. EPR-based drug delivery strategies have been exploited in clinical practice especially using liposomes and experiments in animal models showed that the EPR effect can increase by more than 50-folds NP accumulation within tumour with respect to healthy tissues (Peer *et al*. 2007).

Several factors such as NP dimension, surface properties and circulation half-life but also the degree of tumour angiogenesis, may affect the selectivity of drug delivery (Allen and Cullis

2004). Regarding size, NPs with diameter between 10 and 100 nm exhibited the most efficient tumour accumulation escaping renal filtering, but also particles of > 400 nm in size were shown to extravasate in animal tumour models (Torchilin 2000). However, it must be taken in account that the EPR effect is very heterogeneous and can vary substantially from one tumour model to another and there is no doubt that it is more evident in tumour models in animals than in patients. In addition, the EPR can vary even within the same tumour, with areas in which particles up to 200 nm can easily extravasate and areas in which the endothelial lining is intact and constituted of pericytes, smooth muscle cells or fibroblasts, which compromise vascular permeability (Lammers *et al.* 2012). Thus, to evaluate the usefulness of EPR-based therapy considering EPR heterogeneity, theranostics to pre-screen patients and to monitor efficiency of tumour accumulation have been developed (Sun 2010). Nevertheless, upon reaching tumour extracellular matrix, for an effective delivery of the drug, NPs have to penetrate into tumour cells. Penetration is strongly affected and hampered by the high tumour cell density and high interstitial density of the extracellular matrix, which prevent NPs from crossing more than one or two cell layers. The NP size also plays a pivotal role in determining efficiency of penetration. It has been reported that upon intravenous injection (i.v.) of quantum dots of different diameters (12, 60, 125 nm) in mouse bearing Mu89 melanoma, only the smallest one penetrated into tumour cells efficiently, while larger NPs remained confined in the peri-vascular regions (Popovic *et al.* 2010). Strategies to overcome penetration barrier have been developed, including stimuli sensitive delivery systems for drug release in peri-vascular regions or pharmacological treatments (inflammatory mediators, inhibitors of fibrosis, matrix-degrading enzymes) (Kano *et al.* 2007) or radiotherapy (Davies *et al.* 2004) and are proposed in association to NP delivery.

However, before extravasate and reaching tumour, the drug delivery system has to circulate in the bloodstream for long period, without being captured and cleared by monocytes and macrophages of the mononuclear phagocytic system (MPS), which identify NPs as foreign materials. In fact, once in the bloodstream, unprotected NPs interact and associate with plasma components such as serum proteins that favour the recognition by elements of the reticulo-endothelial system (RES), especially hepatic Kupffer cells (Moghimi *et al.* 2001). This phenomenon has been extensively investigated using liposomes, studying the association of opsonins such as immunoglobulins, complement components and lipoproteins with the phospholipid outer monolayer, promoting clearance of opsonised liposomes by receptor-mediated phagocytosis in liver and spleen (Moghimi 1998, Moghimi and Patel 1998, Yan *et al.* 2005). The degree of opsonization of particles depends on different factors such as NP size and shape (Canelas *et al.* 2009, Longmire *et al.* 2011, Albanese *et al.* 2012), but the surface properties of the delivery system are the major determinants of opsonisation. It has been shown that neutral NPs exhibit lower opsonin association than charged NPs (Roser *et al.* 1998) and hydrophobic surfaces enhance adsorption of blood proteins compared to hydrophilic ones (Carstensen *et al.* 1992, Norman *et al.* 1992). Therefore, it is expected that the modification of NP surface by the addition of groups that minimize those electrostatic and hydrophobic

interactions leading to opsonin absorption, creates the so called "stealth NP" with prolonged circulation in the bloodstream (Moghimi and Szebeni 2003, Owens III and Peppas, 2006). Non-ionic surfactants incorporated during NP synthesis as well as hydrophilic polymers (polysaccharides, polyacrylamide, poly(vinyl alcohol)) have been exploited as coating elements and among the different molecules used polyethylene glycol (PEG) and PEG-containing copolymers were found to be the most effective. The conjugation of PEG molecules on NP surface (PEGylation) forms a flexible layer and creates a sort of steric hindrance not only preventing opsonin adsorption but also increasing biocompatibility (Romberg et al. 2008). PEG is poorly toxic, immunogenic and antigenic, is not biodegradable and consequently does not form toxic metabolites and is not accumulated by RES cells (Zalipsky 1995, Yamaoka *et al.* 1994). Prolonged circulation time and reduced toxicity have been reported for different types of PEGylated drug delivery systems such as liposomes, polymeric NPs and micelles (Amoozgar and Yeo 2012), dendrimers (Svenson 2009) and quantum dots (Clift and Stone 2012). As an example, the PEGylated liposomal formulation of doxorubicin Doxil/Caelix, clinically approved for the treatments of ovarian cancer and Kaposi's sarcoma, exhibits a 100 time longer circulation half life compared to the free drug and a sevenfold reduced cardio-toxicity (O'Brien *et al.* 2004).
However, despite the presence of the PEG coating which ensure prolonged circulation, to some extent also stealth particles are captured in the MPS organs and cleared (Moghimi and Szebeni 2003). Beyond size, it seems that the PEG layer characteristics are of crucial importance in determining the final distribution and the clearance rate of the drug delivery system since PEG thickness, charge, surface density and conformation affected opsonin interaction. Even if literature data on the most suitable PEG layer conformation are still conflicting across the various animal model tested, it appears that high molecular weight PEG polymers favoured longer blood circulation half-lives *in vitro* and *in vivo* (Gref *et al.* 1995, Gref *et al.* 2000, Dos *et al.* 2007).
Recent studies reported on the so called "PEG dilemma", since while PEGylation is fundamental for imparting favourable properties to NPs until their extravasation into tumour extracellular matrix, it interferes in the interaction between NPs and tumour cells, compromising the intracellular delivering of the payloads. Interferences of PEGylation have been reported especially in gene delivery therapy using liposomes, since DNA or siRNA must be internalized in the cytosol or in the nucleus to be efficacious and the surface aqueous phase formed by PEG corona limited the interactions of the gene delivery system with cell surface, resulting in very poor uptake (Hatakeyama *et al.* 2011). Furthermore, stabilization of NPs with the PEG layer resulted in increased stability of the nanocarriers, favouring poor endosomal escape and consequent degradation of cargos in the digestive compartments of the cells (Remaut *et al.* 2007). Thus, the ideal strategy to overcome the dilemma is represented by nanocarriers which during circulation carry the PEG corona while, after NP extravasation in the target site, lose PEG molecules by external stimuli (Kuai *et al.* 2010).

Alternatively, increased intracellular accumulation of nanovehicles in tissues and cells can be achieved exploiting targeted NPs, carrying on surface, specific ligands in addition to PEG. Thus, *active targeting* strategies (targeted drug delivery), complementing with EPR effect, propose to enhance drug accumulation and selectivity taking advantage of specific recognition and binding of the targeting moieties by tumour-associated antigens or receptors, leading to the internalization of the drug delivery system via receptor-mediated endocytosis. The targeting agent has to be specific for receptors that are over-expressed by cancer cells but minimally expressed in normal cells, in order to minimize drug accumulation in healthy tissues and reduce toxicity (Wang and Thanou 2010). The selection of targeted receptors/antigens and NP ligands are of crucial importance in the design of the targeted nanosystem, since the firsts should be highly and uniquely expressed on cancer cells, while the second has to trigger the internalization process for the optimization of drug therapeutic responses. In addition, it is expected that targeted delivery, which promotes drug internalization by endocytic processes, and therefore by-passing glycoprotein efflux pumps, lead to reduced multidrug resistance (Yu *et al.* 2011). Numbers of ligands such as transferrin (Ishida *et al.* 2001), urokinase plasminogen activator (uPA) (Yang *et al.* 2009), RGD peptide (Schiffelers *et al.* 2003), folate (Pan and Lee 2004, Gabizon *et al.* 2003), anti human epidermal growth factor HER-2 antibodies (Park *et al.* 2002, Sheeda *et al.* 2009), prostate cancer-specific antigen (PSMA) antibodies (Gu *et al.* 2008) have been successfully conjugated with different types of nanovehicles, showing NP-targeting in cancer cells. In particular, folate, RGD peptide and Cetuximab antibody (monoclonal antibody against epidermal growth factor receptor (EGFR)) has been selected as targeting agents for the drug delivery systems objective of this PhD thesis and their advantages/disadvantages will be discussed in paper II and IV as ligands for liposomes and silica NPs, respectively.

Nevertheless, even if the idea of targeted nanomedicine has been developed more than 30 years ago, only few targeted drug formulations have been proposed for clinical trials and none have been approved. Limits are represented especially by the targeting agent conjugation techniques which in some cases affects the affinity of binding of the ligands as a consequence of conformational changes, steric hindrance or inadequate orientation (Cheng *et al.* 2012). Finding the optimal density of targeting ligands on NP surface is of crucial importance in the design of targeted nanovehicles, since ligands concentration has to exceed a minimum threshold for binding. Nevertheless, it has been reported that an excess of targeting agent diminishes binding affinity, promotes non-specific interactions with endothelial and other non-cancerous cells, and increases immunogenicity, thereby causing the clearance of the NPs (Yu *et al.* 2012). Thus, the targeting ligands and the stealth layers on NP surfaces have to cooperate in the global process of intracellular internalization. In the case of PEGylated drug delivery systems, the use of PEG spacers carrying the targeting moieties at the extremity represented one of the most exploited strategies in order to avoid the shielding of the ligands into the polymer chains (Gabizon 1999, Gref *et al.* 2003, Shenoy *et al.* 2006, Kawano and Maitani 2011). However, optimized targeted drug delivery systems which have demonstrate successful targeting in cancer cells *in vitro,*

demonstrated completely different behaviours in experimental models consequent to accelerated plasma clearance of targeted NPs (Gu *et al.* 2008, Sheeda *et al.* 2009). These observations stress the fact that *in vivo* experiments are absolutely required to follow targeted NP distribution throughout the body after i.v. administration, in normal and neoplastic tissues as well as to asses RES interference with targeting. Thus, multifunctional nanocarrier optimization cannot abstract from a complete understanding of the tumour biology and physiology as a basis for truly targeted drug delivery.

Nanotechnologies in Photodynamic therapy

Photodynamic therapy: an overview

In cancer treatment, photodynamic therapy (PDT) has emerged as a compelling alternative or adjuvant to traditional chemotherapy, radiotherapy or surgery. PDT is a minimally invasive technique which exerts selective cytotoxic effects in target tissues (Agostinis *et al.* 2011). Currently, PDT is used in clinical for the treatments of several types of malignancies as well as for non-oncological diseases such as endometriosis, arteriosclerosis and age-related macular degeneration (Levy and Obochi 1996) but also for antimicrobial purposes (Hamblin and Hasan 2004).

PDT is based on the administration of three components which are individually non toxic: the photosensitizer (PS), light and molecular oxygen. Nevertheless the PSs, upon activation with appropriate wavelengths of light, exert cytotoxicity in the site of accumulation via production of highly reactive oxygen species (ROS), mainly singlet oxygen ($^1O_2$), which lead rapidly to cell death (Dougherty *et al.* 1998).

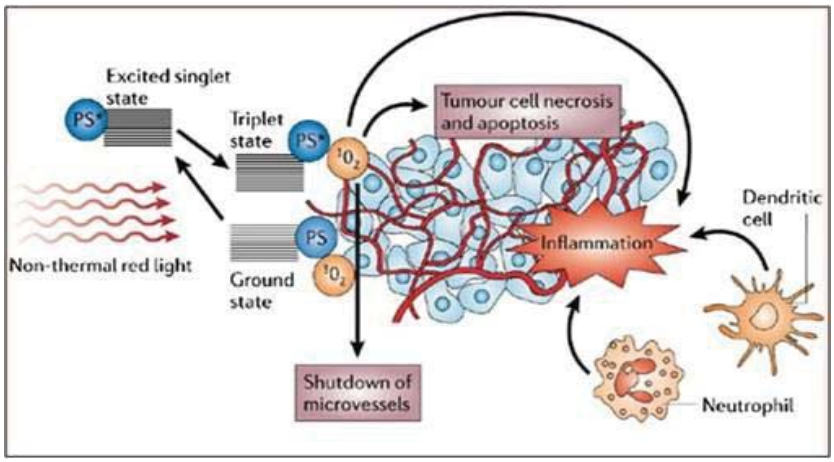

Figure 1: PDT mechanisms of action (figure from Castano *et al.* 2005, with license from Nature Publishing Group).

PDT selectivity is due not only to the possibility to deliver the light from lasers to desired areas of the body using optical fibres but also to the tendency of PSs to localize in neoplastic lesions with some degree of selectivity (Konan *et al.* 2002). In fact, tumour peculiar characteristics such high proliferation rate and vascularisation, low extracellular pH values compared to surrounding healthy tissues, high expression of lipoprotein receptors (LDLs) together with the high hydrophobic nature of the PSs, lead to increased accumulation of PS drugs in malignancies with respect to healthy tissues offering a great opportunity for a targeted therapy based on EPR effect (Oenbrink *et al.* 1988, Friberg *et al.* 2003). It has been reported that hydrophobic PSs bind with high affinity to LDL and then are endocytosed by LDL receptor in cancer cells (Allison 1994, Polo *et al.* 2002) while more hydrophilic PSs tend to localize in the interstitial space and in the vascular stroma of tumours. Thus, the antitumor effects of PDT derive from the cytotoxicity exerted directly in tumour cells, but also to the tumour vasculature, accompanied by a significant inflammatory response, consequent of PDT-induced oxidative stress (Bhuvaneswari *et al.* 2009, Korbelik 2006).

Most of the PSs used in PDT of cancer are chlorins, porphyrins and phthalocyanins which, with their tetrapyrrolic structures, efficiently absorb light in the red and far red regions of the visible spectrum, the so called 'PDT therapeutic window' (600-800 nm). Local irradiation with red light wavelengths, allows deep penetration (> 1 cm) in the tissues as well as limited absorption of light by endogenous chromophores, limiting undesired cytotoxicity (Allison *et al.* 2006). In addition, the confined damages elicited by PDT are determined also by the very short lifetime of $^1O_2$ in biological systems (~10-320 ns), which is able to diffuse from the site of production for at least 10-55 nm (Dysart and Patterson 2005).

Photochemical reactions which lead to the production of the highly reactive radicals and $^1O_2$ upon irradiation of the PS proceed across the following steps (see Jablonski diagram, figure 3):

i) Absorption of photon by PS leads to the promotion of one PS's electron from a low energy level in the singlet ground state (S_0) (electrons with opposite spins) to an exited singlet level (S_2) characterized by higher energy level ii) Excited PS instability leads to emission of excess of energy by non-radiative processes to return to a lower energy level (S_1) iii) The short-lived S_1 (in the order of nanoseconds) can undergo inter system crossing (ICS) to form a long lived triplet state (T_1) with inverted spin of one electron iii) From T_1 the PS can either decay to S_0 via radiative decay (phosphorescence) or can transfer its energy to molecular oxygen (O_2), which is unique in being a triplet in its ground state, leading to the direct formation of $^1O_2$ (Type II process). Instead, if a Type I processes occurs, the T_1 state of PS reacts directly with neighbouring organic molecules, acquiring a hydrogen atom or electron to form a radical. In turn, radical intermediates may react with molecular oxygen to form several radical oxygen species (ROS) such as superoxides ($\bullet O_2^-$), peroxidises (H_2O_2), and hydroxyl radicals ($\bullet$OH).

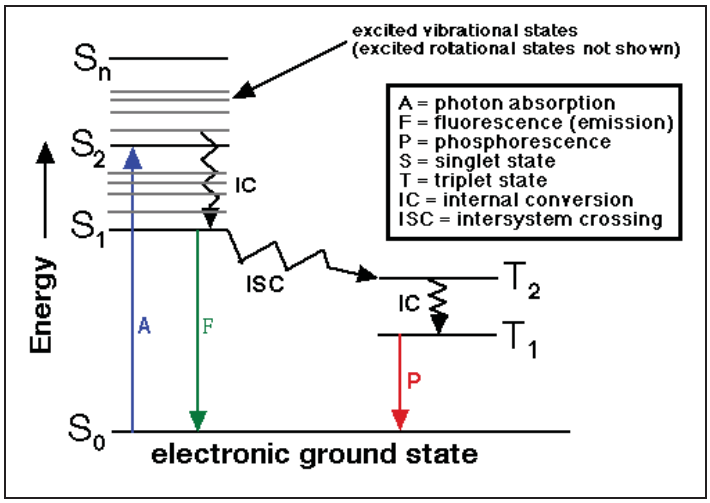

Figure 3: Simplified Jablonski diagram showing electronic transitions of a PS after photon absorption.

At cellular level, produced ROS can trigger the activation of several biochemical, immunological and physiological responses consequent to the destruction of the cells of the irradiated tissues via apoptosis or necrosis; the mechanism of death mainly depends on the type of PS used and its intracellular localization (Castano *et al.* 2005, Oleinick *et al.* 2002). PSs can accumulated in plasma membrane, Golgi apparatus, endoplasmic reticulum, mitochondria, lysosomes while nuclear accumulation is not observed with the currently used PSs; this excludes DNA damages, mutation and carcinogenesis as a consequence of PDT. PS accumulation in plasma membranes leads to cell death mainly via necrosis while PS accumulation in mitochondria induces apoptosis (Calzavara-Pinton *et al.* 2006).

To obtain efficient PDT damages, the PS has to posses several ideal characteristics such as a high quantum yield of generation of long-lived triplet state and ROS to assure damage to targeted molecules, efficient absorption in the therapeutic window, high chemical purity, solubility and low tendency to aggregation in formulations suitable for i.v. administration. In addition, for a safe medical use, PS has to be not toxic in the absence of light (negligible dark cytotoxicity), exhibit high selectivity for tumour tissues and be rapidly cleared from healthy tissues in order to avoid systemic toxicity and generalized skin photosensitization (Allison *et al.* 2004).

Many different PS molecules have been approved for clinics and they are usually classified as first, second and third generation photosensitizers. Among the first generation PSs, Photofrin®, a purified form of an hematoporphyrin derivative (HPD), was the first approved in 1995 by the FDA. Although Photofrin® remains one of the most used PSs for treating cancer in patients, it is not very selective for tumours leading to long-lasting skin photosensitivity, it absorbs light in the red region very inefficiently and its chemical formulation and biological activity are difficult to be reproduced (Lam *et al.* 1987). Thus, second generation PSs such as porphyrins, chlorins, texaphyrins, purpurins and phthalocyanines have been developed with improved chemical properties (high purity, stability, solubility, optimal photo-physical properties) and improved

selectivity of tumour accumulation (Nyman and Hynninen 2004). Their improved PDT efficacy is related to a high singlet oxygen quantum yield and by the presence of chemical groups at the periphery of the tetrapyrrolic structure that positively affect photophysical and pharmacological properties. In the recent years, different strategies, such as peptides or antibodies conjugation, have been proposed in order to further increased tumour selectivity of these second generation PSs, leading to the development of the 'third generation PSs'. In addition, the so called 'pro-drugs' has been exploited in PDT, being molecules that are not PSs but that are converted in active PSs once inside the cells by metabolic processes. The most widely studied pro-drug in PDT is 5-aminolevulinic acid (5-ALA), a precursor in the biosynthetic of heme, that can induce the formation of the potent PS protoporphyrin IX (PpIX) and to his accumulation especially in cancer cells (Uehlinger *et al.* 2000, Collaud *et al.* 2004). PpIX natural fluorescence is exploited also for fluorescence diagnosis (ALA-FD) and fluorescence-guided resection of malignant tissues together with ALA-PDT are successfully applied since more than 25 years in dermatology, urology, neurosurgery, otorhinolaryngology, gynecology and gastroenterology (Krammer and Plaetzer 2008).

Among the second generation PSs, *meta*-tetra(hydroxyphenyl)chlorin (*m*-THPC) also known as Temoporfin, is one of the most potent PSs used in clinics. It has been approved by the European Medicines Agency (EMA) for the palliative PDT treatment of advanced head and neck carcinoma and for oral squamous carcinoma (Senge and Brandt 2011). *m*THPC is a chlorin derived from the parent porphyrin 5,10,15,20-tetra(*m*-hydroxyphenyl)porphyrin) (*m*-THPP) and is formed by four pyrrolic sub-units linked by four carbon atoms which are *meso*-substituted with four hydroxylated phenyl groups. *m*-THPC absorption spectra is characterized by a high absorption peak (Soret band) set at 420 nm and by four absorption peaks of lower intensities (Q bands) in the region 500-700 nm (50, 540, 600, 650 nm). In addition *m*-THPC exhibits a red fluorescence with a maximum settled around 652 nm that makes it potentially useful for imaging and monitoring of drug accumulation, but it not yet approved for photodiagnosis.

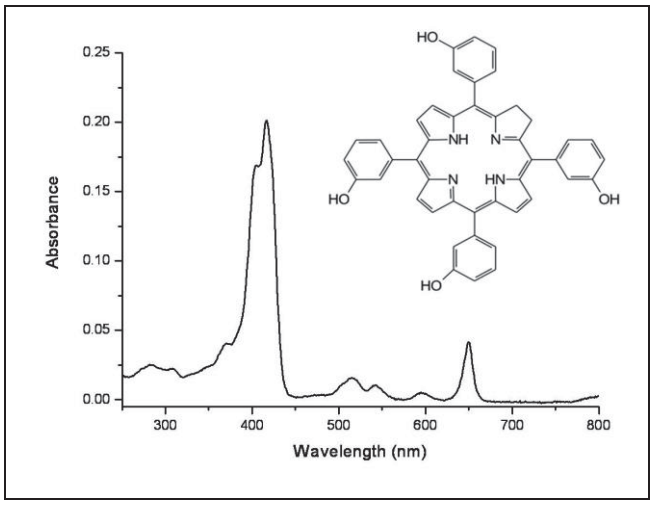

Figure 4: chemical structure and absorption spectra of *m*-THPC.

For clinical application, because of his high hydrophobic degree, *m*-THPC is administered intravenously in a formulation containing ethanol and propylene glycol as co-solvent (Foscan® formulation). To avoid unwanted phototoxic effects, in Foscan® PDT light treatment is performed 24 - 96 h after injection of the drug to guarantee sufficient clearance from healthy tissues Several studies reported a 100-200 fold increased PDT efficacy of Foscan® with respect to Photofrin®. Foscan® doses low as 0.1-0.15 mg kg^{-1} combined with low light fluences (10-20 J cm^{-2}) gave tumour responses comparable to those elicited with 2 mg kg^{-1} Photofrin® and 100 J cm^{-2} of light (van Geel *et al.* 1995, Mlkvy *et al.* 1998, Ball *et al.* 1999, Mitra and Foster 2005). However, in spite of the improvement obtained with Foscan®-PDT, the drawbacks of the therapy remain considerable. Foscan® is only partially selective for malignant tissues and distribution and retention throughout the body determine prolonged skin and eye photosensivity (up to 6 weeks) as well as hemorrage, constipation, vomiting, mouth necrosis and face edema (D'Cruz *et al.* 2004, Hopper *et al.* 2004). The high hydrophobic nature of the PS induces drug precipitation inside blood vessels, especially at the injection site with consequent local pains and decreased drug concentration in the bloodstream. In addition, the low water-solubility of *m*-THPC favour aggregation in aqueous media that compromise photodynamic efficiency, being aggregated PSs much less efficient than monomeric PSs in the $^1O_2$ production (Bonnet *et al.* 2001). Thus, new formulations for *m*-THPC and other potentially useful hydrophobic PSs are needed in order to improve bio-distribution, pharmacokinetics and PDT efficacy. In the development of these new PS formulations, it appears that nanotechnology offers unique opportunities for the engineering of nanovehicles that overcome problems related to drug hydrophobicity from one hand and takes the drug specifically into target tissue and cells on the other.

Drug delivery systems in PDT

Different types of delivery systems for PSs have been developed. These include liposomes, micelles, bio-degradable and non-biodegradable polymeric NPs, metallic NPs and ceramic NPs, often functionalised to impart stealthy properties or carrying targeting agent for the so called targeted PDT (TPDT) (Zeisser-Labouèbe *et al.* 2006, Bugaj 2011). However, the majority of the results so far published are limited to *in vitro* investigations probably because many of the *in vivo* challenges have not been adequately addressed and inconsistent levels of drug accumulated in tissues.have been reported (Master *et al.* 2013).

In addition to modulation of size, shapes and superficial characteristics of nanocarriers to fully exploit passive and active targeting, PS loading efficiency is a crucial parameter in the design of the delivery system. In fact, differently from conventional chemotherapeutics, where the higher drug loading produces the higher cytotoxic effects, for PS, high loading can lead to drug aggregation and self-quenching of ROS during irradiation, with consequent reduced photo-efficiency. Therefore, nanoparticles based formulations of PS have to ensure the delivery of optimal doses of photodinamically active drug and ideally, PS molecules within the nanocarrier should be monomers or become monomers soon after delivery at the target site. Loss of the drug cargo has been reported for different types of NPs and payloads, especially after incubation in

the presence of serum proteins. It is well known that most the PSs possess high affinity for serum proteins that easily adsorb on NP surface forming a corona. As a consequence PSs are transferred from the inside of the NPs to serum proteins and PS-protein complexes are formed (Konan *et al.* 2003, Sasnouski *et al.* 2005, Cedervall *et al.* 2007, Compagnin *et al.* 2009). Thus, to avoid PS release and partitioning to plasma proteins before reaching target sites, strategies has been developed to chemically conjugate the PS to the vehicles, without interfering with the PS photo-physical properties. In fact, once in targeted cells, the release of PSs from the carrier is not required, since the nanometric dimensions of NPs allows the diffusion of oxygen and ROS out of the vehicle to cause cellular damages. In addition, it is expected that the dark cytotoxicity of the PS can be significantly reduced embedding the drug within the NPs and preventing his escape and accumulation in healthy tissues.

Theranostic approaches have been exploited also in PDT with the developing of multifunctional delivery systems carrying PSs, fluorescent probes (or the PS itself if fluorescent) or magnetic resonance agents for the *in situ* evaluation of PDT-induced effects (Kopelman *et al.* 2005, van Vlerken *et al.* 2006). As an example, Reddy *et al.* designed a multifunctional nanoplatform for TPDT based on polyacrylamide NPs loaded with Photofrin® and with iron oxide as imaging agent and bearing F3 peptide linked by PEG spacer on NP surface for the selective targeting of brain tumour cells and vasculature. Multifunctionality of NPs leads also to the combination of different therapies, as PDT and chemotherapy, using as an example the same delivery system for the PS methylene blue (MB) and doxorubicin (Khdair *et al*. 2009). Moreover, the introduction of magnetic components offers the possibilities of combining PDT with radiotherapy or hyperthermia (Chen and Zhang 2006, Zhang *et al.* 2008). Zhang *et al.* demonstrated the efficacy *in vitro* and *in vivo* of a novel nanosystem for combined PDT and photohyperthermia, using zinc phthalocyanine (ZnPc) as PDT agent loaded in single-wall carbon nanohorns with holes opened (SWNHox) conjugates with bovine serum albumin (BSA) to enhance NP biocompatibility. Recently, the development of the so called ‘upconversion nanoparticles’ seem to offers the opportunity to enhance the activation of PSs using deep penetrating light making PDT useful for the treatment of deep-seated tumours. PDT upconversion-based NPs, exploited the capability of upconversion elements to absorb light in the near infrared region (NIR, 700-1110 nm) having great penetration in tissue, and to re-emitted light at shorter wavelength in order to activated PSs loaded in the same nanovehicles (Chatterjee and Yong 2008, Cui *et al.* 2012). However, even if the efficacy of upconversion NPs have been demonstrated *in vitro* and *in vivo* (Idris *et al.* 2012), the safe biomedical use of upconverting elements need to be further assessed before starting clinical trials (Chen and Zhao 2012).

Nanoparticles as drug delivery system for *m*-THPC

Several studies reported the successful loading of *m*-THPC in different type of NPs including liposomes (Buchholz *et al.* 2005, Pegaz *et al.* 2006, Lasalle *et al.* 2009, Kiesslich *et al.* 2007),

micelles (Hofman *et al.* 2008, Shieh *et al.* 2010, Syu *et al*. 2012), nanocapsules (Bourdon *et al.* 2002), silica-based NPs (Yan and Kopelman 2003), human serum bovine based polymers (HSA) NPs (Wacker *et al.* 2010), pH-sensitive methacrylate-based NPs (Peng *et al.* 2010), calcium phosphate NPs (Klesing *et al.* 2010), and their ability to deliver the PS to cancer cells both *in vitro* and *in vivo.*

In the European project called "Nanophoto", of which the work of this thesis is part, the main purpose was the design of one or more nanosystems for the improvement of efficiency and selectivity of *m*-THPC-based PDT and *m*-THPC fluorescence-based diagnosis of cancer. For this purpose, three different types of nanovehicles were selected, namely, liposomes, poly-($_{D,L}$-lactide-co-glycolide) (PLGA) NPs, and silica NPs, that for their different chemical characteristics could differently affect biodistribution and biocompatibility of the drug. The prolonged circulation in the blood and improved biodistribution of NPs, biocompatibility and selective accumulation in tumours, are ideally guaranteed by the stealth-like features of these PEGylated nanocarriers and by their specific targeting to cancer cells. In the following paragraphs each type of drug delivery system is described with some hints on the state of the art, general chemical features and synthesis processes, potential advantages/disadvantages in *m*-THPC delivery.

Liposomes

Liposomes are extensively investigated as drug carriers since 50 years, due to their high biocompatibility and versatility of drug entrapment, being artificial spherical vesicles composed of phospholipid bilayers surrounding an internal aqueous space. Therefore, they can carry both hydrophilic and hydrophobic drugs entrapped in the aqueous space or within the phospholipid bilayer, respectively. Thus, liposomes are suitable nanocarriers also for the hydrophobic *m*-THPC and may offer the opportunity of creating a *m*-THPC formulation guaranteeing improved drug bioavailability and less side effects when compared to the currently used formulation Foscan®.

Biolitec, the producer/distributor of Foscan®, developed two *m*-THPC liposomal formulations, Foslip® and Fospeg® made respectively of non PEGylated and PEGylated liposomes.

Both formulations are dipalmitoylphosphatydilcholine/dipalmitoylphosphatydilglycerol (DPPC/DPPG) based unilamellar liposomes in which *m*-THPC is only physically entrapped in the bilayers during synthesis using the conventional film method followed by extrusion (Bangham and Lea 1978).

Several studies reported the improvement of *m*-THPC PDT using liposomal formulations with respect to Foscan®. The comparative pharmacokinetics in mice with an HT29 tumour model, showed more rapid accumulation and slightly higher selectivity for tumour and muscle for Foslip® compared to Foscan® but also lower blood concentration indicating faster biodistribution and clearance of liposomal *m*-THPC. D'Hallewin and colleagues studied Foslip®-PDT in a mouse mammary carcinoma and found low and inhomogeneous tumour accumulation of drug at short times with a maximun 24 h post-injection as a consequence of *m*-THPC release from

liposomes. Drug release from liposomes and redistribution of *m*-THPC to serum components was studied *in vitro* by Reshetov *et al.* who reported faster drug release from Fospeg® than from Foslip®, as confirmed in Paper I and Paper II of this thesis. Despite faster *m*-THPC release, improved PDT efficiency using Fospeg® was reported by Pegaz *et al.* in an *in vivo* preclinical study with a chicken chorioallontoic membrane (CAM) model. They measured significantly higher photothrombic activities on CAM model using Fospeg® with respect to Foslip®. Accordingly, Buchholz *et al*. treated with PDT spontaneous feline squamous cell carcinoma *in vivo* and reported higher drug bioavailability, shorter biodistribution half-life and improved selectivity for Fospeg® compared to Foscan®. In addition, it has been reported that the delivery of *m*-THPC using liposome formulations limited the dark cytotoxicity of the drug at least *in vitro* (Berlanda *et al.* 2010, Kiesslich *et al.* 2007). Hence in this compelling context, the advantages of using three different formulations of Fospeg® with different density and thickness of the PEG layer has been evaluated in comparison to Foscan® *in vitro* (see Paper I). Further, attempts were made to improve the selectivity of Fospeg®-PDT by conjugating liposomes with folic acid to target ovarian cancer cells *in vitro* (see Paper II).

Poly-($_{D,L}$-lactide-co-glycolide) (PLGA) NPs

The use of biodegradable polymeric NPs as carriers for PSs has been widely investigated, with several polymers and methods of synthesis that can be selected based on the physicochemical characteristics of the incorporated drug. A definition of polymeric NPs classified them as submicron (<1000 nm) colloidal systems made of solid polymers. These NPs are generally classified in nanocapsules and nanospheres, with the drug entrapped in a liquid core or entrapped/adsorbed on the surface of the polymeric matrix, respectively. For drug delivery applications, polyesters as poly(lactic acid) (PLA) and copolymers as poly(lactic-co-glycolic acid) (PLGA) are the mostly used since they have been approved for use in humans by FDA and by EMA. It is expected that PLGA hydrolysis proceeds within the body, and that the metabolites lactic acid and glycolic acid enter Krebs cycle, minimizing systemic toxicity (Kumari *et al.* 2010). PLA is used less than PLGA for the synthesis of NPs for medical applications because its degradation rate is lower (Danhier *et al.* 2012). The degradation rate can vary from several months to years and can be easily modulated during the design of NPs because it strictly depends on the molecular weight and ratio of the copolymers (Vert *et al.* 1994). Despite the high versatility of composition and surface modification (e.g. addition of PEG, poloxamer, poloxamine, chitosan to impart stealthy properties and/or addition of targeting moieties for selective drug delivery), two main pitfalls limited the efficacy of PLGA NPs as delivery systems: the poor drug loading (usually around 1%) and the release of the drug. The latter was largely documented by Kumari *et al.* that identified five mechanisms of drug release from polymeric NPs that are determined by the polymers used and the drug loading. Thus, if the drug is adsorbed on NP surface can desorb, while if the drug is entrapped in the NP core can diffuse through the

polymer matrix and escape from NPs. In addition to diffusion, drug release can be triggered by the erosion of the NP matrix due to degradation.
Different methods of PLGA NPs preparation have been reported; the drug can be incorporated in the NPs during synthesis or can be adsorbed on NPs after the synthesis. For the preparation of NPs containing hydrophobic drugs two methods are generally considered: the emulsification-solvent evaporation technique and nanoprecipitation method. Using the first technique, which is based on the formation of an emulsion in which polymers and drugs are solubilised in an organic solvent, several PS-loaded NPs have been prepared, as for example PLGA NPs containing ZnPc (Ricci-Júnior and Marchetti 2006, Fadel *et al.* 2010), *meso*-tetra(p-hydroxyphenyl)porphyrin (mTHPP) (Vargas *et al.* 2009), In(III)-*meso*-tetraphenylporphyrin (InTPP) (Da Silva *et al.* 2009) and have been tested for PDT-efficacy *in vitro* and *in vivo*. Regarding the nanoprecipitation method, Paper III is the first published report on PS-loaded PLGA NPs synthesized using this method. The synthesis of bare or PEGylated *m*-THPC-loaded PLGA NPs, has been successfully accomplished (Kocbek *et al.* 2010), by dissolving PLGA or/and PEG-PLGA copolymers and *m*-THPC in acetone and slowly injecting the resulting solution into a Poloxamer 188 water solution to form NPs. Non incorporated drug and excess of stabilizer were removed by NP dispersion, and centrifugation followed by resuspension in trehalose and freeze drying.
The loading of *m*-THPC in bare PLGA NPs was reported also by Löw group, which compared accumulation and PDT-induced toxicity of such NPs to Foscan® in human colon carcinoma cells. In Paper III, the photo-physical characterization, PDT efficiency *in vitro* and fluorescence-based imaging *in vivo* of bare and, for the first time PEGylated *m*-THPC PLGA NPs, are reported.

ORganically MOdified SILica (ORMOSIL) NPs
Among ceramic nanomaterials, silica NPs and ORMOSIL NPs have been exploited as useful PS delivery systems because they are chemically inert, not susceptible to swelling or changes with varying pH, or vulnerable to microbial attack (Weetall 1970). Particle dimension, shape, mono-dispersibility and porosity can be controlled during the simple process of synthesis that requires ambient temperature conditions (Couleaud *et al.* 2010). The porosity of silica matrix allows the molecular oxygen diffusion through the pores and interaction with the irradiated PS while the produced $^1O_2$ can diffuse out to exert cytotoxicity and this does not require the release of PS once the NPs are inside the cells. Therefore, the PS can be either physically entrapped within the silica matrix or covalently linked to the matrix to avoid the release of the PS before internalisation into the target cell.
Silica NPs are synthesized by the base-catalyzed polymerization of silicon alkoxides (pure silica) or of organosilane precursors (ORMOSIL NPs) in an ethanol-water solution (Stöber protocol) (Stöber *et al.* 1968), or in reverse microemulsions (Osseo-Asare and Arriagada 1999), or in aqueous micellar solutions (Prasad method) (Roy *et al.* 2003, Roy *et al.* 2005).
In 2003 the group of Prasad reported a new method for the entrapment of the PS 2-devinyl-2-(1-hexyloxyethyl)pyropheophorbide (HPPH) in ORMOSIL NPs, synthesized in the non polar core

of micelles by hydrolysis of triethoxyvinylsilane (Roy *et al.* 2003). They demonstrated that the encapsulated PS maintained the ability to produces $^1O_2$ upon irradiation and that PS loaded NPs taken up by UCI-107 and Hela cells, were able to induce cytotoxicity after PDT. In 2007, the same group reported the covalent incorporation of HPPP in ORMOSIL NPs, without alteration of PS spectroscopic and photophysical properties (Ohulchanskyy *et al.* 2007).

Regarding *m*-THPC, the first example of loading this PS in Stöber-like silica NPs was reported in 2003 by Yan and Kopelman that also reported higher production of $^1O_2$ for NP-embedded PS than for PS in solution. More recently, our group (Compagnin *et al.* 2009) reported on the physical entrapment of *m*-THPC in ORMOSIL NPs synthesized with the Prasad's method. Interestingly, we reported that the monomeric NP-entrapped *m*-THPC was able to produce $^1O_2$ with high efficiency but, when NPs were incubated in the presence of serum, the PS was rapidly transferred to serum proteins. PS delivery and PDT efficiency of *m*-THPC NPs compared to Foscan® were studied *in vitro* in KYSE-510 cells, showing comparable cytotoxic effects upon irradiation notwithstanding the 50% reduced uptake of NPs. In the same work we reported that PEGylation of NPs is a strategy to limit *m*-THPC escape from NPs by decreasing protein absorption. In any case, the release can be completely prevented only with the covalent linking of the PS to the silane matrix. Thus, since PEGylation revealed itself an efficient strategy to limited NP-proteins interactions, within Nanophoto project the group of Prof. Mancin (Chemical Science Department, Padova University) developed a one-pot procedure to synthesize highly PEGylated ORMOSIL NPs (Rio-Echevarria IM *et al.* 2010). *In vitro* studies confirmed the stealthy features of these NPs compared to non-PEGylated NPs, as documented by reduced macrophage capture.

NP preparation procedure consists in the ammonia-catalyzed co-polymerization of vinyltriethoxy silane (VTES) and PEG-silane derivatives in an aqueous solution of a non-ionic surfactant (Brij35) and *n*-butanol. The easy and controlled synthesis, as well as fast purification procedure using surfactant-removing resin, offers potential large scale preparation. In addition, the use of VTES offers a low polarity NP interior that favours the inclusion of hydrophobic drugs while PEG-silane derivatives can be easily functionalized for the bioconjugation of NPs. Thus, the potentialities offer by PEG ORMOSIL NPs has been explored in Paper IV, with the synthesis of covalently linked *m*-THPC NPs carrying different targeting agents (folic acid, RGD peptide, Cetuximab antibody) for targeted PDT. In additional, a toxicological profile of empty PEGylated ORMOSIL NPs against cancer and normal cells *in vitro* is reported for the first time in Paper V.

Safe use of NPs as drug delivery systems

In addition to nanomedicine, nanotoxicology is growing up in order to address the potential adverse health effects caused by nanomaterials (Donaldson *et al.* 2004). To this purpose nanotoxicology analyzes NP physicochemical determinants, routes of exposure, nanoparticulate biodistribution, interactions with/and effects on cellular components, and dictates the use of

robust test protocols for nanomaterial risk assessment for human and environment (Lewinski *et al.* 2008). The knowledge of the toxicological profiles of nanosized materials is of fundamental importance especially in the case of medical applications in which NPs are directly ingested or injected but also unintentional exposure (e.g. occupational, environmental) to NPs may represent a serious danger. Health risks are very likely related to the unusual physicochemical properties of engineered nanomaterials determined by small size (surface area and size distribution), chemical composition (purity, cristallinity, electronic properties), surface structure (surface reactivity, surface groups, inorganic/organic coatings), solubility, shape and aggregation. Thus, this combination of effects may generate adverse biological responses in living cells otherwise not seen with the bulk materials (Nel *et al.* 2006). Especially the extremely small size of NPs, which determines the high surface area to volume ratio with an increased numbers of potential reactive groups, renders them highly harmful toward biological systems (Arora *et al.* 2012). In addition, the effects of particle size can be further modified by surface coating and treatments, and by particle aggregation. Therefore, it is possible that contrary to monodisperse NPs, aggregates exert toxicity, even if for general assumption smaller particles easily enter and pass through tissues, cells and organelles (Fadeel and Garcia-Bennet 2010).

Nanomaterials can enter the body by intentional or non intentional routes. Intravenous administration, inhalation, oral, intraperitoneal, dermal, and subcutaneous exposure represent the main route of entrance of NPs into the organism. Intravenously, administered NPs have been found to be distributed in various organs such as colon, lungs, bone marrow, liver, spleen and lymphatic system, even if their distribution is followed by their clearance from systemic circulation by macrophages of liver and spleen (Hagens *et al.* 2007). Even in the case of inhalation, NP distribution in lungs, hearth, liver, spleen and brain occurs, while clearance is promoted especially in the alveolar region via phagocytosis by macrophages facilitated by chemotactic attraction of alveolar macrophages in the site of NP deposition (Garnett and Kallinteri 2006). Interestingly, Oberdörster *et al.* calculated that the average half-life of NPs in the human respiratory tract is about 700 days. NPs administered orally distribute mainly in the kidneys, liver, spleen, lungs, brain and gastrointestinal tract, where NPs pass through and are absorbed in the systemic circulation and eliminated with feces and urines. Regarding NPs administered via intraperitoneal injection, they can cross transplacental membrane or peritoneal cavity into uterus, affecting embryo development and even causing embryo death (Vega-Villa *et al.* 2008). Dermal exposure to nanomaterials, which occurs in the occupational environment as well as during the intentional application of topical creams and drug treatments, can lead to NP penetration in the dermis and translocation to the systemic circulation via lymphatic system and regional lymph (Oberdörster *et al.* 2005).

It is well accepted that the interaction of nanomaterials with biological tissue culminates in free radicals generation and oxidative stress is the best-developed paradigm to explain cytotoxic effects (Shvedova *et al.* 2005, Nel *et al.* 2006). The extent of ROS generation depends on size, shape and aggregation state of NPs but also surface coating, metal impurities or experimental

conditions (e.g. UV light exposure) can contribute to trigger oxidative stress. One of the direct consequences of oxidative stress is the activation of an inflammatory response through the activation of pro-inflammatory signalling cascades (e.g. mitogen-activated protein kinase (MAPK) and nuclear factor κB (NF- κB) cascades) (Curtis *et al.* 2006). NP-promoted ROS can react with DNA, proteins, carbohydrates and lipids leading to genotoxicity, protein denaturation, lipid peroxidation and finally to cell death via apoptosis or necrosis. In addition, nanomaterials can display antigenicity, evoking immunogenic response due to their intrinsic characteristics or/and to the complexes that they form with cellular biomolecules. Thus, the cytotoxic profile of nanomaterials is highly dependent on the microenvironment conditions and is determined by NP opsonization by serum components, NP surface modification by absorbed proteins or lipids such as albumin and surfactants (Unfried *et al.* 2007). The NP-corona, which can be constituted by the adsorption of over 3700 plasma proteins, is continuously modified in the biological fluids and is highly dependent on protein concentrations and protein affinity for NPs (Lynch and Dawson 2008). Beyond affecting NP internalization, proteins interacting with the large surface area of NPs can be modified or denatured, with consequent mal-functioning which in turn may lead to pathogenesis (Borm and Kreyling 2004). Thus, since the numbers of new nanosized materials is increasing exponentially while toxicological aspects are not adequately addressed, there is the urgent need of standard protocols for *in vitro* and *in vivo* evaluation of cytotoxicity in order to guarantee a safe use of nanotechnology products. *In vitro* studies using different cell lines present several advantages such as i) the assessment of primary effects on target cells without secondary effects caused by inflammation or physiological and compensatory factors, ii) efficiency, iii) rapidity, iv) cost-effectiveness, v) reduction of variability between experiments vi) reduced requirement of test materials vii) models for the design of subsequent whole animal studies (Huang *et al.* 2010, Takhar and Mahant 2011, Arora *et al.* 2012). However, the experimental condition used for the *in vitro* assays (i.e. cell type, differentiation status, incubation carried out in the presence/absence of serum, time of NP exposure, etc) may influence the toxicological profile of a nanomaterial. Hence, *in vitro* studies represent the starting point for the knowledge of nanomaterial interaction with biological systems, knowledge that require further evaluation *in vivo* in animal models and possibly in whole ecosystems.

Aim of the thesis

The overall aim of this thesis is the *in vitro* characterization of the cytotoxicity and the delivery efficiency of 3 different nanosystems loaded with the second generation photosensitizer *meta*-tetra(hydroxyphenyl)chlorin (*m*-THPC), used for photodynamic therapy (PDT) of cancer. Thus, in 4 of the 5 papers collecting the work of this thesis the potentialities and limits of using liposomes (**Paper I, II**), poly-($_{D,L}$-lactide-co-glycolide) nanoparticles (PLGA NPs) (**Paper III**) and ORganically Modified SILica nanoparticles (ORMOSIL NPs) (**Paper IV**) as *m*-THPC nanocarriers are critically discussed. In addition, in **Paper V** the potential adverse health effects of using ORMOSIL NPs for medical applications were investigated *in vitro* in different lung cell models.

Firstly, un-targeted PEGylated nanovehicles were synthesized and characterized for their PDT efficiency *in vitro* and secondly the potentialities of targeted PDT were evaluated by the functionalisation of PEGylated liposomes (**Paper II**) and ORMOSIL NPs (**Paper IV**) with selected targeting agents (folic acid, RGD peptide, Cetuximab antibody).

The suitability of the three delivery systems as nanocarriers of *m*-THPC and associated PDT efficiency was evaluated with:

-measurements of photochemical and photophysical properties of *m*-THPC in nanovehicles with respect to *m*-THPC in the standard solvent (**Paper I, III, IV**).
-investigations of nanovehicles PEGylation influences on *m*-THPC intracellular delivery and cytotoxicity (**Paper I, III**).
-measurements of intracellular uptake and localization of *m*-THPC delivered by nanoparticles with respect to *m*-THPC delivered in the standard solvent (**Paper I, III, IV**)
-investigations of targeted nanosystem selective uptake in cells over-expressing receptors able to be recognized by the targeting agents (**Paper II, Paper IV**).
-evaluation of phototoxic effects (PDT *in vitro*) of *m*-THPC delivered by un-targeted NPs (**Paper I, III**) and targeted NPs (**Paper II, IV**).

The toxicological profile of ORMOSIL NPs was evaluated in normal and cancer lung cells by performing:

- i*n vitro* tests for the measurement of cell viability and cytotoxicity.
-genome-wide studies of gene expression alteration using Agilent microarray.
-investigations of NP intracellular uptake using fluorescence-based imaging techniques or electron microscopy techniques (scanning electron microscopy and transmission electron microscopy.

Papers

I

Photochemical & Photobiological Sciences

Cite this: *Photochem. Photobiol. Sci.*, 2011, **10**, 1751

www.rsc.org/pps

PAPER

Meta-tetra(hydroxyphenyl)chlorin-loaded liposomes sterically stabilised with poly(ethylene glycol) of different length and density: characterisation, *in vitro* cellular uptake and phototoxicity

Chiara Compagnin,†[a] Francesca Moret,†[a] Lucia Celotti,[a] Giovanni Miotto,[b] Josephine H. Woodhams,[c] Alexander J. MacRobert,[c] Dietrich Scheglmann,[d] Selma Iratni[d] and Elena Reddi*[a]

Received 27th May 2011, Accepted 21st July 2011
DOI: 10.1039/c1pp05163f

We studied the effects of density and thickness of PEG coating on *in vitro* cellular uptake, and dark- and photo-toxicity of liposomal formulations (Fospeg) of the photodynamic agent *meta*-tetrahydroxyphenyl chlorin (*m*-THPC). The cellular uptake of various Fospeg formulations was determined by flow cytometry in CCD-34Lu human normal fibroblasts and A549 lung cancer cells. Dark and light-induced cytotoxicity was measured by MTS assay after exposure to increasing concentrations of Fospeg only and followed by irradiation with red light. Intracellular localization of *m*-THPC delivered by Fospeg was determined by fluorescence microscopy. The studies were carried out in comparison with *m*-THPC delivered by the standard solvent. In the dark all Fospeg formulations were less cytotoxic than *m*-THPC in standard solvent (ethanol/poly(ethylene glycol 400/water; 20 : 30 : 50 by vol.) and cytotoxicity decreased by increasing PEGylation. *m*-THPC delivered as Fospeg was internalised by endocytosis and localised mainly in the Golgi apparatus and endoplasmic reticulum. The efficiency of cellular uptake of Fospeg was reduced by 30–40% with respect to *m*-THPC in standard solution causing a slight reduction of the phototoxicity but without serious impairment of the efficacy of the treatment. Our study suggests that PEGylated liposomes are promising nanocarriers for the delivery of photosensitisers for photodynamic therapy because they reduce dark cytotoxicity while preserving therapeutic efficacy.

Introduction

It is well established that photodynamic therapy (PDT) is a valuable method for treatment of a number of oncological, dermatological and ophthalmological diseases.[1,2] PDT is based on the light-activation of a photosensitising molecule that localises in the diseased tissue and produces reactive oxygen species (ROS), mainly singlet oxygen, to induce cell death.[3] These cytotoxic species are short lived and cannot diffuse far from the site of production, therefore the tissue damage is limited to the proximity of their site of production. PDT is becoming widely accepted and has been approved for the treatment of several types of solid tumours. *Meta*-tetra(hydroxyphenyl)chlorin (*m*-THPC, temoporfin) is one of the most potent second generation photosensitisers and is approved in Europe for the palliative treatment of patients with advanced head and neck cancers.[4,5] Clinical trials have shown that basal cell carcinomas,[6] pancreatic[7] and prostate cancers[8] can also be treated successfully with PDT. While the clinical benefit of PDT has been demonstrated, various strategies are being considered to optimise its efficacy and selectivity. In the past, various delivery systems have been proposed to overcome the problems related to the administration of the hydrophobic photosensitisers[9] and in this context liposomes were particularly useful for their capacity to solubilise such molecules in their phospholipid bilayer. The major draw-back of these conventional liposomes is the rapid clearance from plasma caused by the recognition and uptake in the phagocytic cells of the reticulo-endothelial system (RES) following systemic administration.[10] Stealth or long-circulating liposomes, having the surface coated with a hydrophilic polymer, which prevents the adsorption of blood plasma opsonins and recognition by macrophages, appear to be promising delivery systems for targeting the tumour, passively taking advantage of the enhanced permeability and retention (EPR) effect.[11,12] It is expected that hydrophobic photosensitisers can be administered in the form of highly photoactive monomers by using stealth liposomes as delivery vehicles, which should also lead to more efficient and selective targeting of the tumour. Hopefully, the increased and

[a]*Department of Biology, University of Padova, via U. Bassi 58/B, 35121, Padova, Italy. E-mail: elena.reddi@unipd.it; Fax: +39 049 8276300; Tel: +39 049 8276335*
[b]*Department of Biological Chemistry, University of Padova, via U. Bassi 58/B, 35121, Padova, Italy*
[c]*National Medical Laser Centre, University College London, London, UK*
[d]*Research & Development Biolitec AG, Otto-Schott-Strasse 15, 07745, Jena, Germany*
† These authors contributed equally to the study

selective accumulation of the photosensitiser in the target tissue should allow the administration of lower doses of drug with fewer side effects, in particular less skin photosensitivity.

The method largely used for the production of stealth nanoparticles and liposomes is based on the coating of their surface with poly(ethylene glycol) (PEG), which is inert and biocompatible.[13] Pre-clinical studies using the chick chorioallantoic membrane model showed that *m*-THPC encapsulated in PEGylated liposomes (Fospeg) exhibited a rate of extravasation similar to that of conventional liposomes (Foslip) but the phototrombic activity was much higher, making the Fospeg a suitable formulation for the treatment of choroidal neovascularisation associated with age-related macular degeneration.[14] PEGylated liposomal *m*-THPC was also proven to be suitable for the PDT treatment of rheumatoid arthritis, due to more favourable accumulation in the inflamed arthritic joints in comparison to *m*-THPC in standard solvent or non-PEGylated liposomes.[15] Buchholz *et al.*[16] reported that the plasma concentration and bioavailability were approx. 3 times higher with the PEGylated liposomes compared to the standard formulation of *m*-THPC. The superior pharmacokinetic properties resulted in a more favourable response to PDT of feline squamous carcinomas. Thus, it appears that PEGylated liposomes may be a useful tool to increase the therapeutic response to PDT in various pathological situations. In this context, we felt it was important to establish how the density and thickness of the PEG corona could affect the stability of the *m*-THPC liposomal formulation and its ability to deliver the photosensitizer to cultured cells. In this paper, we report the characterisation of several liposomal formulations of *m*-THPC (Fospeg) in which the PEG length and density was varied. Furthermore the efficiency of uptake of various Fospeg formulations in normal and cancer cells, as well as cytotoxicity in the dark and after irradiation with red light are reported in comparison with *m*-THPC delivered to the cells in the standard solvent.

Experimental

Materials

Rhodamine–DPPE [1,2-dipalmitoyl-*sn*-*glycero*-3-phosphoethanolamine-*N*-(lissamine rhodamine B sulfonyl)] was purchased from Avanti Polar Lipids (Alabaster, USA). DPPC [1,2-Dipalmitoyl-*sn*-*glycero*-3-phosphocholine]; DPPG [1,2-dipalmitoyl-*sn*-*glycero*-3-phosphoglycerol]; mPEG-750-DSPE [*N*-(carbonyl-methoxypolyethyleneglycol 750)-1,2 distearoyl-*sn*-*glycero*-3-phosphoethanolamine]; mPEG-2000-DSPE [*N*-(carbonyl-methoxypolyethyleneglycol 2000)-1,2 distearoyl-*sn*-*glycero*-3-phosphoethanolamine]; and mPEG-5000-DSPE [*N*-(carbonyl-methoxypolyethyleneglycol 5000)-1,2 distearoyl-*sn*-*glycero*-3-phosphoethanolamine] were purchased from Genzyme Pharmaceuticals (Liestal, Switzerland). Temoporfin (*m*-THPC) [3,3′,3″,3‴-(2,3-dihydroporphyrin-5,10,15,20-tetrayl)tetraphenol] was provided by Biolitec AG (Jena, Germany). Rhodamine 123 (R123), *N*-(4,4-difluoro-5,7-dimethyl-4-bora-3a,4a-diaza-*s*-indacene-3-pentanoyl)sphingosine (BODIPY® FL C_5-ceramide), LysoTracker Green DND-26 and ER-Tracker™ Green (glibenclamide BODIPY® FL) were purchased from Invitrogen Molecular Probes (Milan, Italy). Bicinchoninic acid (BCA) assay was from Pierce (Rockford, IL). The CellTiter 96® Aqueous One Solution Cell proliferation Assay (MTS) was from Promega Co (Madison, WI, USA). Genistein, filipin III, chlorpromazine hydrochloride, amiloride, 5-(*N*,*N*-dimethyl)-hydrochloride were obtained from Sigma-Aldrich (St. Louis, MO, USA). Solvents and commercially available reagents were used as received.

Preparation and characterization of *m*-THPC liposomal formulations (Fospeg). Liposomes were prepared by the conventional film method. *m*-THPC was dissolved in an organic solution of phospholipids (chloroform/methanol). This mixture was dried to a thin film at 50 °C using the rotary evaporator. The obtained film was kept under vacuum (1 mbar) for 2 h at room temperature and afterwards flushed with nitrogen. The film was then hydrated with 10 mM histidine buffer pH 6.5 with 5% glucose for 30 min. Afterwards the liposome dispersion was extruded through polycarbonate membranes of different pore sizes (400 nm, 200 nm, 100 nm). Liposomal size was measured by Photon Correlation Spectroscopy (PCS) with a Zetasizer Nano S90 from Malvern Instruments GmbH (Herrenberg, Germany). *m*-THPC concentration was determined by UV-Vis spectroscopy. In Table 1, we report the list and composition of the Fospeg preparations considered in this study.

For the photophysical studies, Fospeg 2%-2000 and Fospeg 8%-2000 stock solutions were diluted in 10 mM histidine buffer, containing 5% glucose at pH 6.5, to give a 0.5 μM *m*-THPC concentration. The *m*-THPC loading was the same for both formulations with a dye : lipid ratio of 13.3. Comparative studies were carried out in dimethyl sulfoxide (DMSO, Sigma–Aldrich, UK) at the same *m*-THPC concentration.

Cell cultures. The cell line A549, derived from human lung carcinoma, and the human normal lung fibroblasts CCD-34Lu were obtained from American Type Culture Collection (ATCC, Rockville, USA). The cells were maintained at 37 °C in a humidified atmosphere containing 5% CO_2. A549 cells were cultured in F-12 K medium supplemented with 10% heat-inactivated foetal bovine serum (FBS) (Gibco, Invitrogen, Milan, Italy),

Table 1 Composition of the Fospeg liposomal formulations

Formulation	DPPC	DPPG	mPEG-750-DSPE	mPEG-2000-DSPE	mPEG-5000-DSPE	*m*-THPC
Fospeg 2%-2000	18.0	2.0	—	2.0	—	1.5
Fospeg 8%-750	18.0	2.0	3.7	—	—	1.5
Fospeg 8%-2000	18.0	2.0	—	6.8	—	1.5
Fospeg 8%-5000	18.0	2.0	—	—	14.1	1.5

Values are in mg ml^{-1} of the preparation after extrusion. Watery phase in all formulations: 10 mM histidine buffer with 5% glucose. The concentrations of mPEG-DSPE correspond to 2 or 8 mol% of total phospholipids.

2 mM L-glutamine, 2.5 g l^{-1} sodium bicarbonate, 38 units ml^{-1} streptomycin and 100 units ml^{-1} penicillin G (Sigma-Aldrich). CCD-34Lu cells were grown in Dulbecco's Modified Eagle's Medium (DMEM) with 3.7 g l^{-1} sodium bicarbonate, 4.5 g l^{-1} glucose, and supplemented with 38 units ml^{-1} streptomycin and 100 units ml^{-1} penicillin G, 0.1 mM MEM non essential amino acids, 0.02 M HEPES and 10% FBS. A549 and CCD-34Lu cells have a doubling time of 22 and 24 h, respectively.

Photophysical characterisation

Absorption spectra were measured using a Perkin–Elmer Lambda 25 UV/Vis spectrometer (Perkin–Elmer, Beaconsfield, UK) with quartz cuvettes. Fluorescence emission spectra were measured using a LS50B Perkin–Elmer spectrofluorimeter (Perkin–Elmer, Beaconsfield, UK). Spectra were acquired using a multimode bifurcated fibre-optic probe to provide front surface excitation/detection geometry, which is unaffected by polarization effects, unlike the conventional orthogonal excitation/detection configuration. Fluorescence lifetimes were measured using the time-correlated single photon counting method (TCSPC). For the fluorescence studies, dilute solutions were employed with an *m*-THPC concentration of 0.5 μM. The light source for TCSPC was a 405 nm picosecond laser diode (EPL-405, Edinburgh Instruments Ltd., Livingston, UK) with a pulse duration of 90 picoseconds, and a 5 MHz repetition rate. Fluorescence was detected using a fast multialkali photomultiplier module (model H5773-04, Hamamatsu Photonics UK Ltd, Hertfordshire, UK) *via* a longpass filter (OG510, Schott, Stafford, UK) and a monochromator (model M300, Bentham Instrument Ltd, Berkshire, UK). A Lyot depolarizer (Thorlabs Ltd, Ely, UK) was used to minimise any fluorescence polarization effects. TCSPC was carried out using a PC-mounted board (TimeHarp100, PicoQuant GmbH, Berlin, Germany) and lifetimes were derived using FluoFit software (PicoQuant GmbH, Berlin, Germany). The Instrument Response Function (IRF) was obtained from a non-fluorescent scattering Ludox® solution (Sigmal–Aldrich, Gillingham, UK). Optimum fitting with minimisation of the residuals was confirmed using a chi-squared value $\chi^2 < 1.4$.

Dark and photo toxicity of *m*-THPC delivered by standard solvent or by Fospeg

For the dark cytotoxicity experiments A549 and CCD-34Lu cells were seeded in 96-well plates (3000 cells $well^{-1}$) in 200 μl of culture medium (F-12 K and DMEM, respectively) supplemented with 10% FBS. After 24 h the medium was removed and replaced with 150 μl of fresh medium containing 3% FBS and increasing concentrations of *m*-THPC delivered in free form by standard solvent (ethanol/poly(ethylene glycol) 400/water; 20:30 : 50, by vol.) or by liposomal formulations (Fospeg). Before the addition to the cells, Fospeg was diluted 1 : 10 in sterile water and then 1 : 2 in culture medium added with 3% FBS. The cells were incubated in the dark and cell viability was measured with MTS test after 24 h of treatment (24 h) as well as after 24 h of treatment followed by additional 24 h in which the cells were kept in *m*-THPC-free medium containing 10% FBS (24 + 24 h). For MTS assay the cell medium was replaced with 100 μl of serum-free medium and 20 μl of CellTiter 96® Reagent and the wells were incubated for 1.5 h at 37 °C. The absorbance at 492 nm was measured with Biotrak II (Amersham, GE Healthcare, NJ, USA) plate reader and the viability of treated cells was expressed as percentage of the absorbance of control cells that was taken as 100% viability.

The *in vitro* phototoxic effect of *m*-THPC delivered by standard solvent or Fospeg was evaluated in A549 cells. The cells were seeded in 96-well plates and incubated for 24 h at 37 °C in the dark with increasing and non toxic concentrations of *m*-THPC (0.25–1.5 μM) as determined with the experiments of dark toxicity. At the end of the incubation time, cells were washed twice with 150 μl of PBS with Ca^{2+} and Mg^{2+}, and irradiated in PBS with 0.24 J cm^{-2} of red light (600–700 nm) emitted from a Waldmann PDT 1200 lamp (Waldmann Medizintechnik, Germany). The fluence rate at level of the cell monolayer was 12 mW cm^{-2}, as measured with the radiometer IL 1700 (International Light, Newburyport, MA). Immediately after irradiation the cells were brought back to the incubator after replacement of PBS with fresh medium containing 10% FBS. Cell viability was measured with the MTS test after additional 24 h.

Cellular uptake of *m*-THPC delivered by standard solvent or Fospeg

A549 or CCD-34Lu cells (10^5) were seeded in 2 ml of complete medium in 35 mm diameter tissue culture dishes. After 24 h, the cells were incubated with increasing concentrations of *m*-THPC (0.25–1.75 μM), delivered by standard solvent or Fospeg, in culture medium supplemented with 3% FBS. After 24 h of incubation with *m*-THPC the cells were washed twice with 2 ml of versene, detached with 500 μl of trypsin (Gibco) that was neutralized with the addition of 200 μl of FBS. Cells were centrifuged and resuspended in 700 μl of versene before measuring *m*-THPC fluorescence by flow cytometry with a BD FACSCanto™ II (Becton Dickinson, San Jose, California, USA) instrument. The blue laser at 488 nm was used as the excitation source and wavelengths longer than 670 nm (PerCP channel) were used for the detection of the *m*-THPC fluorescence. 10^5 events $sample^{-1}$ were acquired and analyzed with the FACSDiva Software. The uptake of *m*-THPC in A549 cells was also determined as a function of the incubation time, up to 24 h, with 1 μM *m*-THPC in standard solvent or Fospeg 8%-2000. The uptake of Fospeg 8%-2000 (1.5 μM *m*-THPC) was also measured after 2 h of incubation in the presence of 3 and 10% FBS or without FBS.

To study the effect of the incubation temperature on the uptake of 1 μM *m*-THPC in standard solvent and Fospeg 8%-2000, A549 cells were incubated at 4 °C and 37 °C and then analyzed by flow cytometry. Furthermore, cell samples were preincubated (30 min) with selected inhibitors of endocytosis before the addition of *m*-THPC to the culture medium. The inhibitors tested were: chlorpromazine hydrochloride (10 μg ml^{-1}), filipin III (5 μg ml^{-1}), amiloride, 5-(*N*,*N*-dimethyl)-hydrochloride (34 μg ml^{-1}) and genistein (54 μg ml^{-1}). For these experiments the cells were incubated with *m*-THPC for 2 h.

Quantification of cellular uptake of *m*-THPC

For selected concentrations of *m*-THPC in standard solvent and Fospeg 8%-2000, the data of cellular uptake measured by flow cytometry were validated with the traditional chemical extraction

method. After 24 h incubation with 0.5 or 1 μM *m*-THPC, A549 cells were washed twice with 2 ml of PBS with Ca^{2+} and Mg^{2+} and lysed with 800 μl of 2% sodium-dodecyl sulfate (SDS). Cell lysates were kept under magnetic stirring for 1 h before measuring the *m*-THPC fluorescence with a fluorescence spectrophotometer (Cary Eclipse). The intensity of the fluorescence emission spectrum of *m*-THPC in the 600–800 nm range ($\lambda_{max\ em} = 652$ nm) was registered after excitation with 420 nm light. The *m*-THPC concentrations in the cell lysates was calculated from calibration plots built up with known *m*-THPC concentrations. The solutions for the calibration plot were prepared by adding known amounts of *m*-THPC from stocks in standard solution or in Fospeg to aliquots of lysate obtained from cells not incubated with the photosensitizer and containing the same amounts of cellular protein as the samples. The protein content of the cell lysates was measured by the bicinchoninic acid (BCA) assay and was used to express the *m*-THPC uptake in cells as nmoles of *m*-THPC mg^{-1} of proteins.

Fluorescence microscopy

The intracellular localization of *m*-THPC in A549 cells was determined by fluorescence microscopy taking advantage of its red fluorescence. 10^5 cells were seeded in complete medium in 35 mm diameter tissue culture dishes containing a glass coverslip. After 24 h, the cells were incubated at 37 °C for 5 h with fresh F-12 K medium supplemented with 3% FBS and 1.5 μM *m*-THPC delivered by standard solvent or Fospeg 8%-2000. The intracellular localization of the PEGylated liposomes was determined in cells incubated with liposomes with the same composition as Fospeg 8%-2000 and labeled with the fluorescent phospholipid rhodamine–DPPE. At the end of the incubation time, the cells were washed twice with 2 ml of PBS and observed with the Olympus IMT-2 microscope equipped with a refrigerated CCD camera (Micromax, Princeton Instruments) and a 75 W xenon lamp. Fluorescence images obtained with 60× 1.4 NA oil immersion objective (Olympus) were acquired and analyzed with the imaging software Metamorph (Universal Imaging). The cellular distribution of the fluorescence of *m*-THPC or rhodamine-DPPE was compared with that of R123, LysoTracker Green DND-26, BODIPY® FL C_5-ceramide and ER-Tracker™ Green, used as markers for mitochondria, lysosomes, Golgi apparatus and endoplasmic reticulum, respectively. R123 (0.2 μM), Lysotracker Green (75 nM), BODIPY® FL C_5-ceramide (5 μM) and ER-Tracker™ Green (1 μM) were added to the cell monolayers 15 min before completing the incubation with *m*-THPC or fluorescent liposomes. For the *m*-THPC fluorescence detection a set of filters with 400 nm excitation and 620 nm emission were used, whereas 475 nm excitation and 520 nm emission were used for the other probes.

Results

Characterisation of Fospeg formulations

Each liposomal formulation used during this study was prepared with the same method and identical devices. The composition of each formulation as determined after extrusion is reported in Table 1.

To evaluate particle size and storage stability, size measurements were carried out after extrusion and after storage at 25 °C for 6 months. Directly after extrusion, the mean particle size (PCS *z*-average) of the liposomes was between 105 and 125 nm. Polydispersity indices (PDI) were between 0.04 and 0.15 in all cases, indicating narrow size distributions.

The liposomes have been found to be stable with respect to size and optical appearance over the storage time of 6 months. A small decrease in size (about 5%) was only detected in liposomes containing PEG 2000 or 5000, whereas the PEG 750 preparations have been found to be completely stable in size. Further, no drug precipitates or aggregates were observed in light microscopy.

Fluorescence spectroscopic studies

The fluorescence emission spectra and lifetimes were recorded for the liposomes at 2 and 8% PEGylation and identical *m*-THPC loading diluted in buffer. Peak emission using 423 nm excitation was recorded at 652 nm in each case but a higher peak intensity was noted for the 8% PEGylation: the ratio of fluorescence intensities for the solutions containing 8 *vs.* 2% PEGylated liposomes was 1.25. Peak absorption in the Soret band was at 423 nm for both liposomes.

In DMSO, a mono-exponential decay was observed with a lifetime of 9.6 ns. In liposomes, multi-exponential decays with significantly shorter lifetimes were observed for the PEGylated liposomes. Using tri-exponential fitting, both 2% and 8% PEGylated liposomes exhibited long lived lifetime components of 7.3 and 9.8 ns, respectively but the pre-exponential factor (normalized to unity) was significantly larger at 0.22 for 8% compared with 0.02 for 2% PEGylation. For a mono-exponential decay, the pre-exponential factor or effectively the 'weighting' is unity, whereas for multi-exponential decays the sum of various pre-exponential factors is unity. Therefore pre-exponential factors of 0.22 and 0.02 for these longer lifetimes show that they are minor components in the decay profile. Both liposomes exhibited two similar short-lived lifetime components with comparable pre-exponential factors: for 2% PEGylation, 2.5 and 0.9 ns with corresponding pre-exponential factors of 0.53 and 0.45, and for 8% PEGylation, 3.0 and 1.1 ns with pre-exponential factors of 0.35 and 0.43.

Dark cytotoxicity of Fospeg *vs.* *m*-THPC in standard solvent

The Fospeg formulations listed in Table 1 were used to evaluate the cytotoxicity of liposomal *m*-THPC in the dark toward the A549 tumour cells and the CCD-34Lu normal fibroblasts in comparison to *m*-THPC in standard solvent. The cells were incubated with concentrations of *m*-THPC up to 5 μM for 24 h. The MTS test showed that all formulations were non-toxic to the cells with *m*-THPC concentrations lower than 1 μM. However, higher concentrations of *m*-THPC caused a reduction of the cell viability that was dependent on the concentration and the formulation. Five micromolar *m*-THPC in standard solvent reduced the viability of both cell lines to about 20% (Fig. 1, A and C) at 24 h and close to zero, especially in CCD-34Lu, at 24 + 24 h (Fig. 1, B and D). All liposomal formulations were less toxic than the *m*-THPC standard and the decreased toxicity was dependent on the degree of PEGylation. Fospeg 2%-2000 reduced the viability of A549 cells to about 70% at 24 and 24 + 24 h and to about 30% in

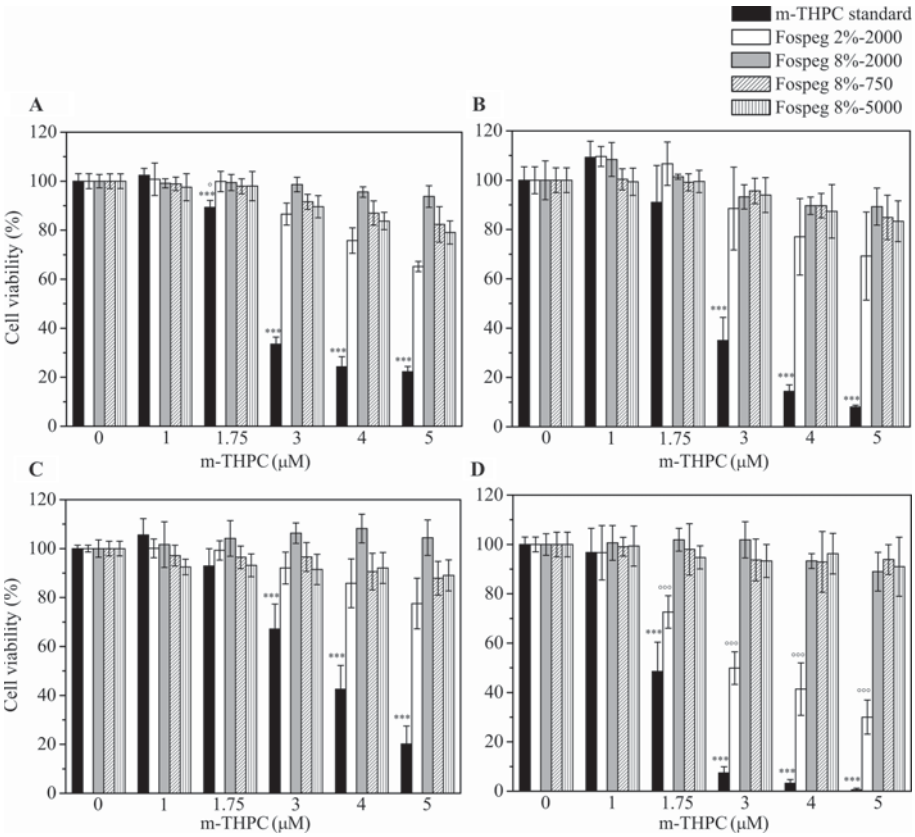

Fig. 1 Viability of A549 (A, B) and CCD-34Lu (C, D) cells after exposure to *m*-THPC standard formulation and different Fospeg formulations. Cell viability was measured by MTS assay at the end of 24 h of incubation in the dark (24 h) with increasing concentrations of *m*-THPC, delivered by standard formulation or Fospeg (A, C), and 24 h after the release in *m*-THPC-free complete medium (24 + 24 h) (B, D). Data are presented as means ± S.D. (n = 9) from three independent triplicate experiments. A and B: °, $p < 0.01$ *vs.* Fospeg 8%-5000; ***, $p < 0.001$ *vs.* Fospeg 2%-2000, 8%-2000, -750, -5000. C and D: °°°, $p < 0.001$ *vs.* Fospeg 8%-2000, -750, -5000; ***, $p < 0.001$ Fospeg 2%-2000, 8%-2000, -750, -5000 (Student t test).

CCD-34Lu fibroblasts. Cell toxicity was abolished when PEGylation was increased to 8% with PEG ranging from 750 to 5000.

Cellular uptake of Fospeg *vs. m*-THPC in standard solvent

The uptake of *m*-THPC delivered as Fospeg in comparison to standard formulation was determined in A549 cells and CCD-34Lu fibroblasts after 24 h of incubation in medium with 3% FCS. The uptake studies were performed with *m*-THPC concentrations up to 1.75 μM because below this concentration none of the formulations showed dark toxicity at 24 h (Fig. 2). The relative amount of *m*-THPC taken up by the cells was determined by flow cytometry. The data showed less uptake (about 30%) of *m*-THPC in the CCD-34Lu in comparison to A549 cells with all formulations. In both cell lines the uptake of *m*-THPC delivered with the Fospeg formulations reached or approached a plateau as with Fospeg 2% 2000, at concentrations above 1.5 μM while the uptake steadily increased with the standard formulation. This difference could suggest a different modality of *m*-THPC uptake with the standard formulation in comparison to Fospeg or the presence of scarcely fluorescent aggregates of *m*-THPC in the Fospeg formulations with the consequent underestimate of its intracellular concentration when measured by flow cytometry. To rule out the latter possibility, in selected samples of cells incubated with Foscan or Fospeg, cell lysates were analysed by spectrofluorimetry to determine the intracellular concentration of *m*-THPC. The results (Table 2) confirmed that, especially at the high concentrations, *m*-THPC standard formulation is taken up more efficiently than Fospeg.

In A549 cells, we measured the time-dependent uptake of *m*-THPC standard formulation and Fospeg 8%-2000 and found that uptake of *m*-THPC in standard solvent steadily increased with time while with Fospeg was biphasic. At short times the rate of uptake of Fospeg was lower than that of free *m*-THPC standard

Table 2 Uptake in A549 cells of 0.5 and 1 μM *m*-THPC delivered with standard formulation, Fospeg 2%-2000 and Fospeg 8%-2000 quantified by the chemical extraction method

	nmol *m*-THPC/mg cell proteins	
Formulation	*m*-THPC 0.5 μM	*m*-THPC 1 μM
Standard	0.62 ± 0.02	1.52 ± 0.27
Fospeg 2%-2000	0.46 ± 0.01	0.90 ± 0.02
Fospeg 8%-2000	0.52 ± 0.09	0.94 ± 0.18

The cellular uptake was determined after 24 h of incubation at 37 °C in culture medium containing 3% FBS and expressed as nmoles of *m*-THPC mg^{-1} of cell proteins. The data represent means ±S.D. from three independent experiments.

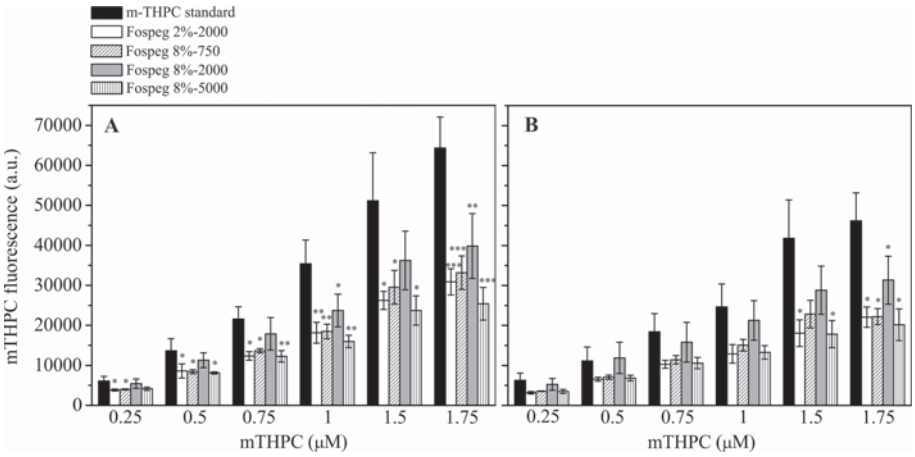

Fig. 2 Cellular uptake of increasing concentrations of *m*-THPC delivered by standard formulation or Fospeg in A549 (A) and CCD-34Lu (B) cells. Flow cytometry was used for measuring *m*-THPC fluorescence signals after 24 h of incubation. Data are presented as means ± S.D. ($n = 3$) from three independent experiments. *, $p < 0.05$; **, $p < 0.005$; ***, $p < 0.001$ compared to *m*-THPC in standard solvent (Student t test).

formulation and a plateau could be detected around 7 h, but later the uptake raised again with no sign of plateau up to 24 h (Fig. 3).

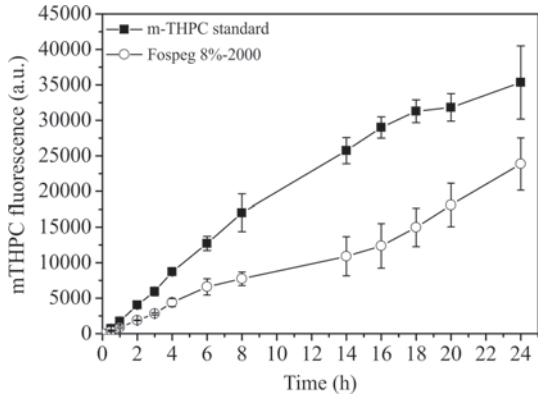

Fig. 3 Time-dependent uptake in A549 cells of 1 μM *m*-THPC in standard solvent or Fospeg 8%-2000. The uptake was measured by flow cytometry at various times up to 24 h of incubation. Data are presented as means ± S.D. from three independent experiments.

In the absence of FBS in the incubation medium the uptake of Fospeg 8%-2000 was about twice that in the presence of 3% FBS and about three times higher than with 10% FBS (Table 3).

The uptake of Fospeg 8%-2000 and free *m*-THPC was inhibited by about 95% by lowering the temperature from 37 °C to 4 °C during the incubation, suggesting that the internalisation of both formulations occurred *via* endocytosis. The addition of 10 μg ml^{-1} of chlorpromazine, an inhibitor of the clathrin-mediated endocytosis, to the cell medium 30 min before starting the incubation, reduced the uptake of free *m*-THPC and Fospeg 8%-2000 by about 30 and 20%, respectively. On the contrary, the addition of filipin III or genistein, used as inhibitors of the caveolae-mediated endocytosis, and amiloride, an inhibitor of macropinocytosis, did not reduce the uptake of free *m*-THPC or Fospeg 8%-2000 in A549 carcinoma cells (data not shown).

Table 3 Uptake in A549 cells of *m*-THPC (1.5 μM) delivered as Fospeg 8%-20000 in absence and presence of 3 and 10% FBS

FBS (%)	*m*-THPC fluorescence (a.u.)
0	3299 ± 116
3	1776 ± 532
10	1130 ± 71

The intracellular uptake was determined by flow cytometry after 2 h of incubation at 37 °C. The data represent means ± S.D. from three independent experiments.

Fluorescence microscopy studies

Fluorescence microscopy analyses of A549 cells incubated for 5 h with 1.5 μM *m*-THPC standard formulation or Fospeg 8%-2000 showed an intracellular distribution of *m*-THPC fluorescence, which co-localised with that of BODIPY® FL C5-ceramide and ER-Tracker™ Green (Fig. 4), indicating that the Golgi apparatus and endoplasmic reticulum were the major sites of localisation of *m*-THPC. In the cells incubated with Fospeg 8%-2000 in absence of FBS, the intracellular localisation of *m*-THPC was the same as in cells incubated in presence of 3 or 10% FBS (not shown). PEGylated liposomes with the same composition as in Fospeg 8%-2000 and containing rhodamine–DPPE were used to assess the intracellular localisation of the liposomes in comparison to *m*-THPC. After 5 h of incubation at 37 °C the liposome fluorescence appeared punctuated throughout the cytoplasm and colocalised with Lysotracker Green suggesting an endosome/lysosome localisation (Fig. 5).

Phototoxicity of Fospeg formulations *vs.* *m*-THPC in standard solvent

The phototoxicity of the Fospeg formulations was determined in A549 carcinoma cells in comparison with free *m*-THPC in standard solvent. The cells incubated with 0.25–1.5 μM *m*-THPC for 24 h were irradiated with 0.24 J cm^{-2} of red light. The dose-response curves (Fig. 6) showed that the tested Fospeg formulations had very similar phototoxic effects on A549 cells and were slightly less phototoxic than free *m*-THPC. The lower

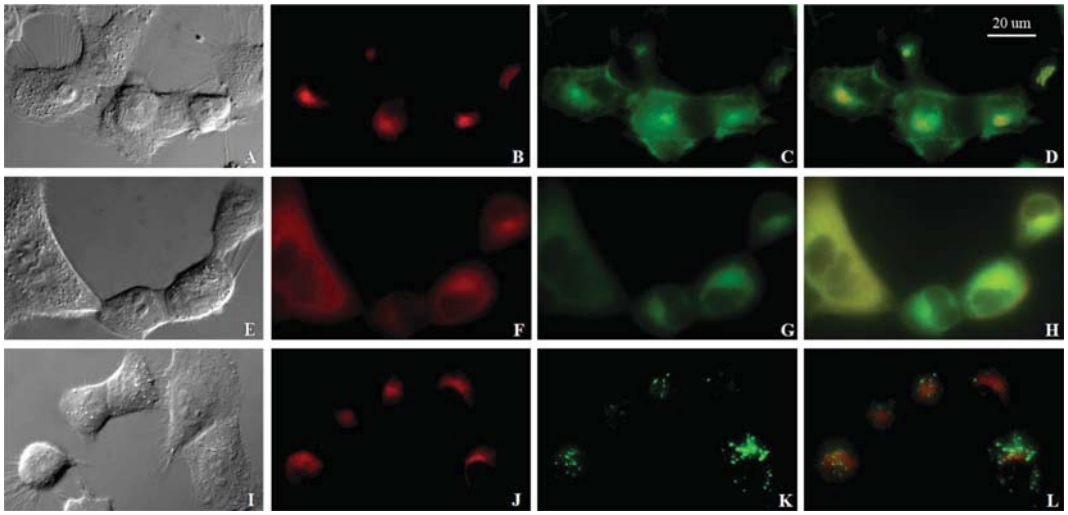

Fig. 4 Subcellular distribution of the red fluorescence of *m*-THPC (1.5 μM) delivered as Fospeg 8%-2000 (B, F and J) in A549 cells after 5 h of incubation at 37 °C. The *m*-THPC fluorescence co-localised with the green fluorescence of BODIPY® FL C_5-ceramide(C) and ER-Tracker™ Green (G), but not with LysoTracker Green DND-26 (K), used respectively as markers for the Golgi apparatus, endoplasmic reticulum and lysosomes. The Differential Interference Contrast images of cells are shown in A, E and I; the merge images for each probe are shown in D, H, and L.

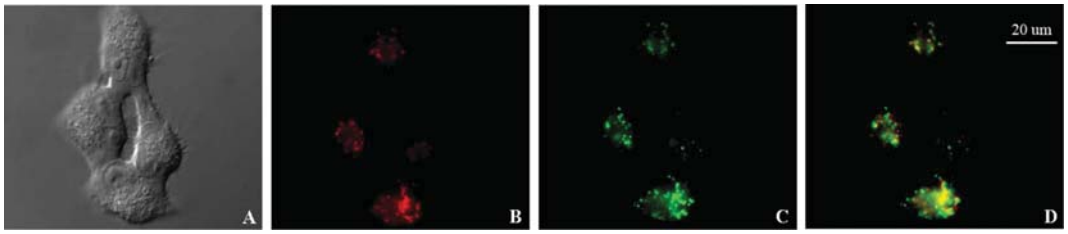

Fig. 5 Localisation in A549 cells of PEGylated liposomes with the same phospholipid composition as Fospeg 8%-2000 and labeled with rhodamine-DPPE. The punctuated red fluorescence of the rhodamine–DPPE (B) co-localised (merge image D) with that of LysoTracker Green DND-26 (C), used as marker for lysosomes. The differential interference contrast image of cells is shown in A.

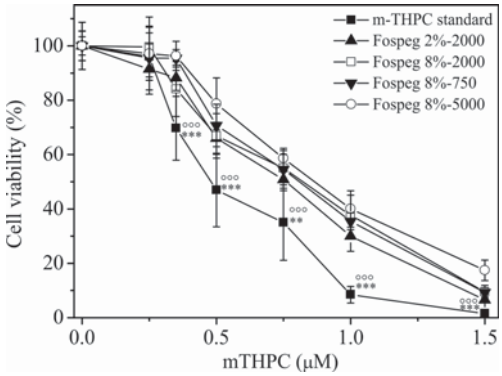

Fig. 6 Light-induced toxicity in A549 cells. Cells were irradiated with 0.24 J cm^{-2} of red light (600–700 nm) after 24 h incubation with increasing doses of *m*-THPC in standard solvent or Fospeg. Cell viability was measured 24 h post-irradiation by MTS assay and expressed as mean percentage ± S.D. (n = 12) with respect to untreated and unirradiated control cells. °°°, $p < 0.001$ *vs.* Fospeg 8%-2000 and -5000; **, $p < 0.005$; ***, $p < 0.001$ Fospeg 2%-2000 and 8%-750 (Student t test).

phototoxicity correlated with the lower uptake of the liposomal *m*-THPC in comparison to the free form.

Discussion

One of the ideal properties of a photosensitising agent for the PDT of tumours is low toxicity in the absence of light. For this reason, we have tested the dark toxicity of the Fospeg formulations towards A549 carcinoma cells and CCD-34Lu normal fibroblasts *in vitro*. We had already reported that free *m*-THPC in the standard formulation is toxic to oesophageal carcinoma cells in the dark at concentrations above 1.75 μM.[17] Here, we found a similar threshold of dark toxicity in two other cell lines and confirmed that *m*-THPC can cause cell death without irradiation at rather low concentrations. In this context, the findings reported here on the dark toxicity of Fospeg appear particularly interesting. We have found that all Fospeg formulations with 8% PEGylation did not cause any toxicity to the cells up to the *m*-THPC concentration of 5 μM (Fig. 1). On the contrary, Fospeg with a lower degree of PEGylation (2%) exhibited some dark toxicity especially to CDD-34Lu fibroblasts. In any case, the cytotoxicity of Fospeg 2%-2000 was much reduced in comparison to free *m*-THPC. Lower dark cytotoxicity of *m*-THPC liposomal formulation in comparison to Foscan was reported also by Kiesslich *et al.*, who tested Foslip, the non PEGylated liposomal formulation of *m*-THPC, on biliary tract cancer cells.[18] Similarly, Berlanda *et al.* found that a Fospeg formulation was less toxic than Foscan to epidermoid carcinoma

cells, but the characteristics of the PEG layer coating the liposome surface were not reported.[19] Our data suggest that the length of PEG chains had no influence on dark toxicity of Fospeg while the increasing density of PEG layer coating the liposomes decreased the cytotoxicity. Because of the loss of stability of the liposomal vesicles in Fospeg formulations with a degree of PEGylation higher than 8%, we could not test the effects of higher levels of PEGylation. The much lower toxicity of Fospeg in comparison to *m*-THPC in standard solvent may be attributed to multiple factors. The lower uptake of *m*-THPC in Fospeg formulation in comparison to standard solvent certainly accounts for the lower toxicity. In fact a significantly lower uptake of *m*-THPC was found in A549 and CCD-34Lu cells after 24 h of incubation with Fospeg in comparison to the standard formulation. Both flow cytometry (Fig. 2) and chemical extraction (Table 2) showed reduced uptake of Fospeg. The reduction was concentration dependent and increased by increasing concentrations of *m*-THPC. In A549 cells the uptake of Fospeg was reduced by 25–30% and about 40% at, respectively, 0.5 and 1 μM *m*-THPC. However, the lower uptake of *m*-THPC does not fully explain our dark toxicity data because the uptake of Fospeg 2%-2000 was not significantly different from that of Fospeg 8% PEG but its toxicity was higher. Thus, it appears that the increasing level of PEGylation of liposomes diminishes the dark toxicity of *m*-THPC. The different kinetics of cellular uptake of Fospeg *vs.* *m*-THPC standard formulation may also have an effect on dark toxicity of *m*-THPC. Our studies showed that the uptake of Fospeg was biphasic and slower than that of free *m*-THPC (Fig. 3), suggesting some differences in their modality of cell internalisation. Kiesslich *et al.*[18] reported that the kinetics of Foslip and extent of cellular uptake in the presence of FBS were very similar to Foscan and concluded that, in both cases *m*-THPC attached to the serum components that mediated its cellular uptake. The coating of the liposomes with a layer of PEG should limit the interaction with serum proteins and increase the probability that the photosensitiser can enter the cells while still encapsulated in the liposomes.

The fluorescence lifetime data indicate that the *m*-THPC fluorescence is strongly quenched in the liposomes, in comparison to monomeric *m*-THPC, which exhibits a longer mono-exponential lifetime of 9.6 ns in DMSO. The results are consistent with the occurrence of fluorescence self-quenching due to dimerisation in combination with energy-transfer between adjacent *m*-THPC monomers and weakly fluorescent aggregates within the liposomes. These time-resolved data are in accordance with the steady-state studies reported by Reshetov *et al.*,[20] who observed lower fluorescence yields when *m*-THPC was incorporated in both PEGylated (Fospeg 2%-2000, as used here) and unPEGylated liposomes (Foslip). We also studied *m*-THPC in Fospeg 8% and observed higher fluorescence emission by a factor of 1.25 over that from the same concentration of *m*-THPC in the Fospeg 2% solution. Although the fluorescence lifetimes are multi-exponential, the higher fluorescence efficiency of *m*-THPC in Fospeg 8% appears to correlate with the higher pre-exponential factor observed for the long-lived lifetime component with Fospeg 8%.

Since *m*-THPC is water-insoluble it should reside within the liposomal membrane but it has recently been suggested that some partitioning of *m*-THPC may also occur in the PEGylated coating of the liposomes.[20] The higher degree of PEGylation for Fospeg 8% may favour more partioning of *m*-THPC to this layer. Multi-exponential fluorescence decays usually arise from the presence of aggregates as well as monomers and/or the presence of different microenvironments. In the latter case, the measured pre-exponential factors would then correlate with the relative concentrations or populations of the fluorophore in the different microenvironments. From the fluorescence lifetime analysis, the significantly higher pre-exponential factor (0.22) observed for the long-lived lifetime component (9.8 ns) for Fospeg 8% could be explained by the presence of a higher relative population of *m*-THPC dispersed within the PEGylated layer either as aggregates or more likely in monomeric form. Our studies were carried out at 25 °C, which, as noted by Reshetov *et al.*,[20] should promote more partitioning into the PEGylated layer compared to 37 °C. However, further studies using much lower *m*-THPC loading would be required before drawing any firm conclusion.

We have previously reported that PEGylation of ORMOSIL nanoparticles limits the release of the physically entrapped *m*-THPC[17] and a similar effect could be expected also for liposomes. Contrary to this hypothesis, it was found that about 40% of *m*-THPC was released more rapidly from Fospeg 2% than from Foslip and only the remaining fraction redistributed much slower.[20] We found that the time-dependent cellular uptake of Fospeg 8% is biphasic and this might be explained by the initial slow uptake of *m*-THPC still entrapped in the liposomes while the second fast wave of uptake could depend on *m*-THPC that with time escaped from liposomes and associated to serum proteins. The fluorescence microscopy studies performed with the fluorescent labelled liposomes (rhodamine–DPPE) suggest that at least some liposomes enter the cells and localise in the endosomal/lysosomal compartments, as shown by their colocalisation with LysoTracker Green (Fig. 5). Fospeg is a DPPC-based liposomal formulation with a phase transition temperature of 41 °C and liposomes are stable also in the presence of serum proteins. In this connection, Pegaz *et al.*, in their studies on the chick chorioallantoic membrane model, found that the extravasation of *m*-THPC delivered with Fospeg was strongly reduced when compared to Visudyne®, which is based on more fluid lipids, namely dimyristoylphosphatidylcholine and egg yolk phosphatidylglycerol.[14] The authors concluded that the leakage of *m*-THPC from Fospeg was slow and its transfer to serum proteins delayed. Our studies also suggest that, following liposome internalisation, *m*-THPC was promptly released and localised mainly in the Golgi apparatus and endoplasmic reticulum (Fig. 4) as reported for other types of cells.[18,21] In fact, the red fluorescence of *m*-THPC co-localized with the green fluorescence of BODIPY® FL C5-ceramide and ER-Tracker™ but not LysoTracker Green as did the fluorescence of the labelled phospholipid (Fig. 4 and 5). The images of Fig. 4 and 5 were acquired after 5 h of incubation but a very similar *m*-THPC localisation was found at shorter and longer (up to 24 h) incubation times. Some uptake experiments with Fospeg 8%-2000 were carried out in the absence of FBS and showed a very efficient uptake of *m*-THPC (Table 3). It is reasonable to assume that, because of its lipophilicity, in the absence of FBS, *m*-THPC was internalised only entrapped in the PEGylated liposomes, but, also in this case, was localised (not shown) in the Golgi apparatus and endoplasmic reticulum, confirming its release from liposomes after internalisation. The presence of FBS clearly inhibited the uptake of *m*-THPC delivered as Fospeg (Table 3),

suggesting some competition for *m*-THPC binding, interactions between liposomes and serum components, possible release of *m*-THPC to serum components and consequent cellular internalisation as serum protein complexes. With increasing incubation time, the *m*-THPC uptake mediated by serum proteins prevails over the uptake mediated by liposomes that takes place at the beginning of the incubation. In all cases the internalisation of *m*-THPC occurred *via* endocytosis because at 4 °C the process was inhibited by 95%. The reduced *m*-THPC uptake in the presence of chlorpromazine, an inhibitor of clathrin-mediated endocytosis, suggested that some *m*-THPC enters the cells with this type of endocytosis.

The A549 carcinoma cells were irradiated with red light (0.24 J cm^{-2}) following incubation with increasing concentrations of *m*-THPC in the various formulations. As expected based on the uptake of *m*-THPC delivered by the different formulations (Fig. 2), a slightly lower phototoxic effect was found with Fospeg in comparison to standard formulation (Fig. 6). The LD_{50} for free *m*-THPC was approx 0.5 μM while it was in the range of 0.75–0.85 μM for the Fospeg formulations with no significant differences among the various types of Fospeg.

Conclusions

We have shown that Fospeg formulations with a degree of PEGylation up to 8% are stable over time with respect to the size of the liposomes and the content of *m*-THPC. The *in vitro* cellular studies demonstrated that the uptake of Fospeg was lower than that of *m*-THPC in standard solvent but the photo-toxicity was only slightly reduced. On the contrary, the dark toxicity of Fospeg was strongly reduced especially with the formulations containing 8% PEG. These findings suggest that PEGylated liposome-based formulations are promising for the delivery of photosensitising drugs, such as *m*-THPC, to cancer cells. Future investigations with tumor-bearing animals will define pharmacokinetic properties, *in vivo* PDT efficacy and side effects of Fospeg with respect to *m*-THPC in standard formulation and further assess their potential benefit for clinical PDT.

Acknowledgements

The research leading to these results has received funding from the European Community's Seventh Framework Programme (FP7/2007-2013) under Grant Agreement No. 201031 (NANOPHOTO).

References

1 R. E. Dolmans, D. Fukumura and R. K. Jain, Photodynamic therapy for cancer, *Nat. Rev. Cancer*, 2003, **3**, 380–387.
2 J. N. Silva, P. Filipe, P. Morlière, J. C. Mazière, J. P. Freitas, M. M. Gomes and R. Santus, Photodynamic therapy: dermatology and ophthalmology as main fields of current applications in clinic, *Biomed. Mater. Eng.*, 2008, **18**, 319–327.
3 N. L. Oleinick and H. H. Evans, The photobiology of photodynamic therapy: cellular targets and mechanisms, *Radiat. Res.*, 1998, **150**, S146–S156.
4 K. J. Lorenz and H. Maier, Photodynamic therapy with meta-tetrahydroxyphenyl chlorine (Foscan) in the management of squamous cell carcinoma of the head and neck: experience with 35 patients, *Eur. Arch. Oto-Rhino-Laryngol.*, 2009, **266**, 1937–1944.
5 C. S. Betz, W. Rauschning, E. P. Stranadko, M. V. Riavow, V. Albrecht, N. E. Nifantiev and C. Hopper, Optimization of treatment parameters for Foscan-PDT of basal cell carcinomas, *Lasers Surg. Med.*, 2008, **40**, 300–311.
6 P. Baas, A. E. Saarnak, H. Oppelaar, H. Neering and F. A. Stewart, Photodynamic therapy with meta-tetrahydroxyphenylchlorin for basal cell carcinoma: a phase I/II study, *Br. J. Dermatol.*, 2001, **145**, 75–78.
7 S. G. Bown, A. Z. Rogowska, D. E. Whitelaw, W. R. Lees, L. B. Lovat, P. Ripley, L. Jones, P. Wyld, A. Gillams and A. W. R. Hatfield, Photodynamic therapy for cancer of the pancreas, *Gut*, 2002, **50**, 549–557.
8 C. M. Moore, T. R. Nathan, W. R. Lees, C. A. Mosse, A. Freeman, M. Emberton and S. G. Bown, Photodynamic therapy using meso tetra hydroxyl phenyl chlorine (m-THPC) in early prostate cancer, *Lasers Surg. Med.*, 2006, **38**, 356–363.
9 E. Reddi, Role of delivery vehicles for photosensitizers in the photodynamic therapy of tumours, *J. Photochem. Photobiol., B*, 1997, **37**, 189–195.
10 G. L. Scherphof, Uptake and intracellular processing of targeted and non targeted liposomes by rat Kupffer cells in vivo and in vitro, *Ann. N. Y. Acad. Sci.*, 1985, **446**, 368–384.
11 D. C. Drummond, O. Meyer, K. Hong, D. B. Kirpotin and D. Papahadjopoulos, Optimizing liposomes for delivery of chemotherapeutic agents to solid tumours, *Pharmacol. Rev*, .1999, **51**, 691–743.
12 H. Maeda, J. Wu, T. Sawa, Y. Matsumura and K. Hori, Tumour vascular permeability and the EPR effect in macromolecular therapeutics: a review, *J. Controlled Release*, 2000, **65**, 271–284.
13 B. Romberg, W. E. Hennink and G. Storm, Sheddable coating for long-circulating nanoparticles, *Pharm. Res.*, 2008, **25**, 55–71.
14 B. Pegaz, E. Debefve, J. P. Ballini, G. Wagnieres, S. Spaniol, V. Albrecht, D. V. Scheglmann, N. E. Nifantiev, H. van den Bergh and Y. N. Konan-Kouakou, Photothrombic activity of m-THPC-loaded liposomal formulations: pre-clinical assessment on chick chorioallantoic membrane model, *Eur. J. Pharm. Sci.*, 2006, **28**, 134–140.
15 A. Hansch, O. Frey, M. Gajda, S. Graefe, J. Boettcher, R. Bräuer and W. A. Kaiser, Photodynamic treatment as a novel approach in the therapy of arthritic joints, *Lasers Surg. Med.*, 2008, **40**, 265–272.
16 J. Buchholz, B. Kaser-Hotz, T. Khan, B. C. Rohrer, K. Melzer, R. A. Schwendener, M. Roos and H. Walt, Optimizing photodynamic therapy: in vivo pharmacokinetics of liposomal meta-(tetrahydroxyphenyl)chlorin in feline squamous cell carcinoma, *Clin. Cancer Res.*, 2005, **11**, 7538–7544.
17 C. Compagnin, L. Baù, M. Mognato, L. Celotti, G. Miotto, M. Arduini, F. Moret, C. Fede, F. Selvestrel, I. M. Rio Echevarria, F. Mancin and E. Reddi, The cellular uptake of meta-tetra(hydroxyphenyl)chlorin entrapped in organically modified silica nanoparticles is mediated by serum proteins, *Nanotechnology*, 2009, **20**, 345101.
18 T. Kiesslich, J. Berlanda, K. Plaetzer, B. Krammer and F. Berr, Comparative characterisation of the efficiency and cellular pharmacokinetics of Foscan®- and Foslip®-based photodynamic treatment in human biliary tract cancer cell lines, *Photochem. Photobiol. Sci.*, 2007, **6**, 619–627.
19 J. Berlanda, T. Kiesslich, V. Engelhardt, B. Krammer and K. Plaetzer, Comparative in vitro study on the characteristics of different photosensitizers employed in PDT, *J. Photochem. Photobiol., B*, 2010, **100**, 173–180.
20 V. Reshetov, D. Kachatkou, T. Shmigol, V. Zorin, M. A. D'Hallewin, F. Guillemin and L. Bezdetnaya, Redistribution of meta-tetra(hydroxyphenyl)chlorin (m-THPC) from conventional and PEGylated liposomes to biological substrates, *Photochem. Photobiol. Sci.*, 2011, **10**, 911–919.
21 M. H. Teiten, L. Bezdetnaya, P. Morlière, R. Santus and F. Guillemin, Endoplasmic reticulum and Golgi apparatus are the preferential sites of Foscan® localisation in cultured tumour cells, *Br. J. Cancer*, 2003, **88**, 146–152.

II

Photochemical & Photobiological Sciences

RSC Publishing

PAPER

Folate-targeted PEGylated liposomes improve the selectivity of PDT with *meta*-tetra(hydroxyphenyl)-chlorin (*m*-THPC)†

Francesca Moret,[a] Dietrich Scheglmann[b] and Elena Reddi*[a]

Cite this: *Photochem. Photobiol. Sci.*, 2013, **12**, 823

Received 12th November 2012,
Accepted 16th January 2013

DOI: 10.1039/c3pp25384h

www.rsc.org/pps

The folate receptor (FR) is over-expressed in many human tumours and is being intensively studied also in the field of nanomedicine as a target to enhance the selectivity of drug delivery to cancer cells by using nanocarriers bearing folic acid (FA) on their surface. In this study we report the encapsulation of the photosensitizer (PS) *meta*-tetra(hydroxyphenyl)chlorin (*m*-THPC) in FA-targeted PEGylated liposomes used as a novel drug delivery system for photodynamic therapy (PDT) of cancer. Our *in vitro* investigations revealed that only a modest fraction of targeted liposomes were internalized by specific endocytosis in FR-positive KB cells. However, FA-liposomes doubled the uptake of the entrapped *m*-THPC with respect to un-targeted liposomes and enhanced the photo-induced cytotoxicity in KB cells. In contrast, in FR-negative A549 cells FA-targeted or un-targeted liposomes exhibited a very similar extent of internalization and as a consequence the same photo-killing efficiency.

Introduction

Photodynamic therapy (PDT) is a clinically approved, minimally invasive therapeutic procedure that can induce cytotoxic effects in tumour tissues with some selectivity.[1] PDT is based on the administration of a photosensitizer (PS) which displays no detectable toxicity in the absence of light but, after activation with light of suitable wavelengths, generates highly reactive oxygen species, inducing oxidative damage mainly in the cellular compartments of PS accumulation.[2] Currently, PDT is applied for the treatment of different types of solid tumours as well as some non-cancerous diseases, such as age-related macular degeneration, endometriosis,[3] and microbial infections.[4] Unlike conventional cancer treatments, PDT does not cause major systemic toxicity; however, it has some important limitations that prevent PDT from becoming a more widely established method for treating cancer. Following systemic administration, PSs accumulate in the tumour as well as in the normal tissues and cause prolonged skin photosensitivity.[5] In addition, most of the PSs for PDT exhibit low water solubility that makes drug delivery difficult and impairs efficacy because of the formation of aggregates with poor photoactivity.[6] In recent years, it appears that the development of various types of nanocarriers as delivery systems for photosensitizing agents can bring substantial improvement of PDT outcome.[7–11] Following intravenous administration, properly engineered nanocarriers can accumulate selectively in tumours, which have relatively "leaky" vasculature, and deliver high concentrations of PS photoactive monomers.[12] Based on this a number of PSs encapsulated in a variety of biodegradable or non-biodegradable nanocarriers were investigated. Hydrophobic PSs such as 5,10,15,20-tetrakis(*meso*-hydroxyphenyl) porphyrin (*m*-THPP) and silicon phthalocyanine (Pc4) loaded in the internal core of biodegradable synthetic polymeric micelles were highly phototoxic to cancer cells while micelles without PS did not show cytotoxicity.[13,14] Protoporphyrin IX (PpIX) encapsulated into chitosan nanoparticles or PEG–polypropylene imine dendrimers was more phototoxic both *in vitro* and *in vivo* than free PpIX.[15,16] Non-biodegradable, silica-based or gold nanoparticles were also investigated and are considered promising nanocarriers of hydrophobic PSs.[17,18]

meta-Tetra(hydroxyphenyl)chlorin (*m*-THPC, temoporfin, trade name Foscan®) is a highly potent second generation PS approved, in Europe and in Japan, for the palliative treatment of patients with advanced head and neck cancers. *m*-THPC was efficiently loaded in micelles,[19,20] organically modified silica nanoparticles,[21] poly-(D,L-lactide-*co*-glycolide) (PLGA) nanoparticles[22] and liposomes and all these nanosystems could deliver the drug to cancer cells.[23–25] However, liposomes were shown to be particularly suitable for the encapsulation of large amounts of the hydrophobic *m*-THPC within their lipid

[a]*Department of Biology, University of Padova, via Ugo Bassi 58/B, 35121 Padova, Italy. E-mail: elena.reddi@unipd.it; Fax: +39 049 8276300; Tel: +39 049 8276335*
[b]*Biolitec Research GmbH, Otto-Schott-Strasse 15, 07745 Jena, Germany*
†Electronic supplementary information (ESI) available. See DOI: 10.1039/c3pp25384h

bilayer without altering its photo-physical properties. Liposomes also showed long-term stability and suitability for the addition of a poly(ethylene glycol) (PEG) corona.[26] The PEG coating sterically stabilises the liposomes, minimises the adhesion of opsonins and the recognition and clearance by the macrophages of the reticuloendothelial system (RES).[27,28] Recently, decreased pro-coagulant activity of PEGylated *vs.* non-PEGylated liposomes has been also reported,[29] indicating that PEGylation is a successful strategy to increase the liposome biocompatibility in addition to circulation lifetimes in the blood stream.

Previously, we have reported on the characterization, *in vitro* uptake and phototoxicity of *m*-THPC loaded in liposomes sterically stabilised with PEG (Fospeg®).[30] Compared to Foscan®, Fospeg® decreased significantly the dark cytotoxicity of *m*-THPC and decreased to a minor extent the cell photokilling efficiency. *In vivo*, Fospeg® showed improved biodistribution and tumour uptake leading to higher tumour necrosis after PDT, in comparison to Foscan®.[31] The increased selectivity was explained with the passive targeting of the tumour by the PEGylated liposomes exploiting the enhanced permeability and retention (EPR) effect.[32] Despite the substantial improvement of PDT with *m*-THPC using Fospeg® formulation, we attempted to further optimise the delivery of *m*-THPC to cancer cells by adding a targeting agent on the liposome surface. This strategy allows the exploitation of active mechanisms of targeting with delivery of the drugs carried by the nanocarriers specifically inside cancer cells or cells of the tumour vasculature over-expressing receptors for the targeting agents on their surface. To enable selective drug delivery to cancer tissue, the ideal targeting ligand needs to bind receptors that are homogeneously over-expressed by tumour cells or tumour vasculature, but are poorly expressed in normal cells and vasculature. The drug-loaded nanocarrier is then internalized *via* receptor-mediated endocytosis.[33] The most studied and promising targets are transferrin receptors, folate receptors (FR) and epidermal growth factor receptors (EGFR) for targeting cancer cells and vascular endothelial growth factor receptors (VEGFR), $\alpha_v\beta_3$ integrins, vascular cell adhesion molecule-1 (VCAM-1) and matrix metalloproteinases (MMPs) for targeting tumour vasculature.

The vitamin folic acid (FA) is very attractive as a targeting molecule because it binds a high affinity receptor over-expressed in about 40% of human tumours and absent in most normal tissues.[33] Furthermore, when compared to other targeting agents, FA presents several advantages: (i) it is inexpensive; (ii) it is not toxic or immunogenic; (iii) it is stable, and (iv) it can be easily coupled to the surface of nanocarriers properly functionalised or can be conjugated to PS with the aid of suitable spacers. Schneider *et al.* conjugated FA to 4-carboxyphenylporphyrin *via* a short PEG spacer and showed that the conjugate accumulated 7-fold more efficiently than the free porphyrin in FR-overexpressing KB cells and induced more efficient cell photo-killing.[34] The *in vivo* studies carried out by Gravier *et al.* demonstrated that a *m*-THPC-like PS conjugated to FA with the same PEG spacer accumulated more efficiently (~2-fold) than the unconjugated PS in KB tumours with a tumour to normal tissue ratio of 5 : 1 at 4 h post-injection.[35] Similarly, pyropheophorbide a conjugated to FA *via* a short peptide showed enhanced accumulation and PDT efficacy in FR-positive KB cells with respect to FR-negative HT 1080 cells. *In vivo*, the selective accumulation in KB tumours of the construct carrying FA was confirmed by detection of the PS fluorescence 24 h after injection; at this post-injection time no fluorescence could be detected in normal tissues and HT 1080 tumours. Interestingly, the peptide inserted as a spacer favourably modulated the PS biodistribution and this observation makes this construct very promising for diagnosis and PDT.[36] As the use of nanocarriers has emerged as a strategy to achieve efficient and selective delivery of PSs in tumours, FA has been exploited also as a homing molecule for carrying PS-loaded nanocarriers into FR-overexpressing cancer cells. The FR-mediated pathway allowed the cell internalisation of FA-conjugated liposomes loaded with a sulphonated phthalocyanine unable to efficiently cross the plasma membrane of target cells without a nanocarrier.[37] FA-conjugated chitosan nanoparticles were developed for enhancing the selective delivery of 5-aminolaevulinic acid and the synthesis of PpIX in colorectal cancers to facilitate their detection by an endoscopic fluorescence-based technique. Only *in vitro* data are reported showing that the intracellular accumulation of PpIX correlated with the expression of FR in the cell models used.[38] Recently, Syu *et al.* developed FA-conjugated polymeric micelles loaded with *m*-THPC and showed accumulation in FR-overexpressing KB cells *in vitro* and *in vivo*. The FA-conjugated delivery system reduced skin photosensitivity and one third the usual dose of *m*-THPC required to achieve *in vivo* the same PDT effect as with free PS.[20] NIR absorbing quantum dots have emerged as an alternative to the existing organic PSs and it has been reported that their conjugation to FA, using the short PEG 2,2′-(ethylenedioxy)-bis-ethylamine as a spacer, significantly improved photodynamic efficiency in FR-positive KB cells but not in FR-negative HT 29 cells.[39]

In the present work, FA was used as a targeting ligand for PEGylated liposomes with the aim to obtain selective delivery of *m*-THPC to FR-overexpressing cells. The *in vitro* intracellular uptake of FA-targeted PEGylated liposomes mediated by FR was first assessed with liposomes labelled with carboxyfluorescein (CF) covalently linked to the lipid bilayer. Subsequently, the uptake and photoactivity of *m*-THPC were defined by delivering the drug *via* FA-targeted or un-targeted liposomes to FR-positive KB cells and FR-negative A549 cells.

Experimental

Materials

DPPC [1,2-dipalmitoyl-*sn-glycero*-3-phosphocholine], DPPG [1,2-dipalmitoyl-*sn-glycero*-3-phosphoglycerol], DOPE [1,2-dioleoyl-*sn-glycero*-3-phosphoethanolamine], mPEG-750-DSPE [*N*-(carbonyl-methoxypolyethyleneglycol 750)-1,2 distearoyl-*sn-glycero*-3-phosphoethanolamine], and mPEG-5000-DSPE

[*N*-(carbonyl-methoxypolyethyleneglycol 5000)-1,2 distearoyl-*sn-glycero*-3-phosphoethanolamine] were purchased from Genzyme Pharmaceuticals (Liestal, Switzerland) while FA-5000-PEG-DSPE (1,2-distearoyl-*sn-glycero*-3-phosphoethanolamine-*N*-FA(polyethylene glycol)-5000) and DOPE-CF [1,2-dioleoyl-*sn-glycero*-3-phosphoethanolamine-*N*-(carboxyfluorescein)] were purchased from Avanti Polar (Alabaster, AL, USA). Temoporfin (*m*-THPC) [3,3′,3″,3‴-(2,3-dihydroporphyrin-5,10,15,20-tetrayl)-tetraphenol] and liposomal formulations of *m*-THPC were provided by Biolitec Research GmbH (Jena, Germany). The CellTiter 96® Aqueous One Solution Cell Proliferation Assay (MTS) was from Promega Co. (Madison, WI, USA). Solvents and commercially available reagents were used as received.

Preparation and characterization of liposomal formulations

All liposomal formulations were prepared by the conventional film method followed by extrusion. In Table 1, we report the list and the composition of the different preparations considered in this study. For liposomes containing *m*-THPC (Fospeg), a chloroform solution of *m*-THPC and phospholipids (DPPC, DPPG, DOPE, mPEG-750-DSPE, mPEG-5000-DSPE and FA-5000-PEG-DSPE when required) was evaporated and the lipid film was hydrated by adding 10 mM histidine buffer, pH 6.5, with 5% (w/w) glucose for 30 min. Afterwards the liposome dispersion was extruded through polycarbonate membranes with pore sizes between 100 and 400 nm using an EmulsiFlex-C5® or LiposoFast-extruder®. Carboxyfluorescein doped liposomes (CF-liposomes), with phospholipid compositions as Fospeg, were prepared by adding DOPE-CF to the mixture of phospholipids. Liposomal suspensions were characterised by photon correlation spectroscopy (PCS) with a Zetasizer Nano S90 from Malvern Instruments GmbH (Herrenberg, Germany), by differential scanning calorimetry with a Pyris 1 instrument (Perkin Elmer, MA, USA) and by cryo-transmission electron microscopy with a Philips CM 120 instrument (Eindhoven, The Netherlands). *m*-THPC and CF concentrations were determined by UV-Vis absorption spectroscopy.

Cell cultures

A549 cells derived from a human lung carcinoma do not express FR, while KB cells, derived *via* HeLa contamination, express high levels of FR. Both cell lines were obtained from American Type Culture Collection (ATCC, Rockville, MD, USA). These cell lines were maintained at 37 °C in a humidified atmosphere containing 5% CO_2. A549 cells were cultured in F-12K medium supplemented with 10% heat-inactivated foetal bovine serum (FBS, Life Technologies, Milan, Italy), 38 units ml^{-1} streptomycin and 100 units ml^{-1} penicillin G (Sigma-Aldrich, St. Louis, MO, USA). KB cells were grown in modified Eagle's medium (MEM, Life Technologies, Milan, Italy) and supplemented with 38 units ml^{-1} streptomycin and 100 units ml^{-1} penicillin G and 10% FBS.

Cellular uptake of FA-targeted and un-targeted CF-liposomes

Preliminary uptake experiments were carried out with FA-targeted and un-targeted CF-doped liposomes to assess the involvement of FR in the uptake of the targeted liposomes. In these liposomes the release of the fluorescent probe is avoided by its covalent binding to phospholipids and therefore they can be safely used for monitoring cellular entry and localisation of liposomes. KB and A549 cells (10^5) were seeded in 35 mm diameter tissue culture dishes containing 2 ml of FA-deficient RPMI medium (Life Technologies, Milan, Italy). After 24 h at 37 °C, the cells had reached the exponential phase of growth and were incubated for 5 h with increasing concentrations of liposomes in a culture medium supplemented with 3% FBS or for different time periods (from 1 to 24 h) with a liposome concentration equivalent to 11 μg ml^{-1} of phospholipids. At the end of the incubation time the cell monolayers were washed and detached from the plates with trypsin (Life Technologies, Milan, Italy). Cells were centrifuged and re-suspended in versene before measuring CF fluorescence by flow cytometry using a BD FACSCanto™ II instrument (Becton Dickinson, San Jose, CA, USA). The blue laser at 488 nm was used as an excitation source and FITC channel was selected for the detection of the CF fluorescence. Ten thousand events/samples were acquired and analyzed with the FACSDiva software. Competition experiments with 1 mM free folic acid (Sigma-Aldrich, St. Louis, MO, USA) were carried out incubating the cells for 1 h prior to the addition of liposomes in order to saturate FRs present on the cell surface.

Cellular uptake of FA-targeted and un-targeted Fospeg formulations was determined by using incubation protocols as described for CF-liposomes and measuring *m*-THPC fluorescence (PerCP channel of the flow cytometry) after 3 or 24 h of incubation. The influence of serum proteins on the uptake of targeted Fospeg was evaluated after 1 h of cell incubation in a medium supplemented with 0, 3 or 10% FBS.

Table 1 Composition of the Fospeg liposomal formulations

Formulation	DPPC	DPPG	mPEG-750-DSPE	mPEG-5000-DSPE	Folate-PEG5000-DSPE	DOPE	DOPE-CF	*m*-THPC
FA-targeted CF-liposomes	18	2	4	—	1	—	1	—
Un-targeted CF-liposomes	18	2	4	1	—	—	1	—
FA-Fospeg	18	2	4	—	1	1	—	1.5
Un-targeted Fospeg	18	2	4	1	—	1	—	1.5

Values are expressed in mg ml^{-1} of the preparation. The watery phase in all formulations is 10 mM histidine buffer with 5% of glucose. The concentrations of mPEG-750-DSPE correspond to 8 mol% while mPEG-5000-DSPE or folate-PEG5000-DSPE (if present) corresponds to 0.5 mol% of the total phospholipids.

Confocal microscopy

KB cells incubated with FA-targeted or un-targeted CF-labelled liposomes were visualized with a Leica SP5 confocal laser scanning microscope (Leica Microsystems Srl, Milan, Italy) and the images were analyzed with the ImageJ software. Twenty-four hours before the experiments, 2×10^5 cells per sample were seeded in 35 mm diameter tissue culture dishes containing a glass cover slip. Cells were incubated for 5 h with CF-labelled liposomes (11 μg ml^{-1} phospholipids) diluted in a medium supplemented with 3% FBS. At the end of the incubation time, cells were washed twice with PBS and fixed with 4% paraformaldehyde in PBS at 37 °C for 15 min. The fixed cells were washed again three times with PBS in order to remove excess formaldehyde. Cells were counterstained with 2 μg ml^{-1} DAPI (4,6-diamidino-2-fenilindole) in antifade solution (Vectashield, Vector Laboratories, Burlingame, CA, USA) and glass cover slips were mounted.

Phototoxicity of *m*-THPC delivered by FA-targeted or un-targeted liposomes (Fospeg)

The *in vitro* photodynamic efficiency of FA-targeted and un-targeted Fospeg was evaluated in cells incubated with liposomes for 3 h. KB and A549 cells were seeded in 96-well plates (3000 cells per well) 24 h before starting the incubation. Cells were incubated in the dark with increasing and not toxic concentrations of *m*-THPC (0.1 to 2 μM), delivered as Fospeg in a culture medium supplemented with 3% FBS. At the end of the incubation time, cells were washed twice with PBS with Ca^{2+} and Mg^{2+}, and irradiated in PBS with 0.8 J cm^{-2} of red light (600–700 nm) emitted from a Waldmann PDT 1200 lamp (Waldmann Medizintechnik, Villingen-Schwenningen, Germany). The fluence rate at the level of the cell monolayer was 12 mW cm^{-2} as measured with a radiometer IL 1700 (International Light, Newburyport, MA, USA). Immediately after irradiation the cells were brought back to the incubator after replacement of PBS with fresh medium containing 10% FBS and cell viability was measured with the MTS test after an additional 24 h. For the MTS test the cell medium was replaced with 100 μl of a serum-free medium and 20 μl of CellTiter 96® Reagent and the wells were incubated for 1.5 h at 37 °C. The absorbance at 492 nm was measured with a Biotrak II (GE Healthcare, Piscataway, NJ, USA) plate reader and the viability of the treated cells was expressed as the percentage of the absorbance of the control cells that was taken as 100% viability.

Dose–response curves were determined as a function of the light dose (from 0 to 2.4 J cm^{-2}) for KB cells incubated for 3 h with 3 selected doses of FA-targeted and un-targeted Fospeg corresponding to *m*-THPC concentrations of 0.5, 0.75, 1 μM.

Statistical analysis

The Primer software for biostatistics (McGraw-Hill, Columbus, OH, USA) was used for statistical analysis of the data. The data are expressed as means ± standard deviations (SD) of at least 3 experiments. The differences between groups were evaluated with the Student's *t*-test and considered significant for $p < 0.05$.

Results

Characterization of liposomal formulations

The composition of the formulations used in the present work is reported in Table 1. The mean particle size (PCS *z*-average) and the polydispersity indices (PDI) were measured directly after liposome extrusion. CF-doped liposomes had a PCS *z*-average between 97 and 117 nm whereas the PDI was between 0.077 and 0.160. Fospeg formulations had a PCS *z*-average between 105 and 122 nm whereas the PDI was lower, between 0.061 and 0.056, indicating a very narrow size distribution. Cryo-transmission electron microscopy images of a FA-targeted Fospeg formulation confirmed the monodispersity of liposome suspensions and indicated that no micellar structures were detectable (Fig. 1A). Each preparation of FA-targeted liposomes was analysed by column chromatography to test if free FA was present in the suspension. The analysis showed that free FA was not detectable and confirmed the validity of the used production procedure (Fig. 1B). CF-labelled liposomes as well as liposomes in Fospeg were PEGylated on the surface because they contained 8 mol% of PEG750 and 0.5 mol% of PEG5000 or FA-PEG5000, respectively, in the un-targeted and targeted versions. The liposomes were found to be stable with respect to size and optical appearance over the storage time of 6 months.

Uptake of FA-targeted and un-targeted CF-liposomes

It was already reported that in the presence of serum proteins an important fraction of *m*-THPC is released from non-PEGylated (Foslip®) and PEGylated (Fospeg®) liposomes.[30,41,42] Therefore to study the receptor-mediated uptake and to follow the cell internalization of the FA-targeted liposomes, we prepared CF-doped liposomes in which the fluorescent tracer was covalently linked to one phospholipid of the bilayer (DOPE-CF). The time-dependent and concentration-dependent uptake of FA-targeted and un-targeted CF-liposomes was measured by flow cytometry in KB and A549 cells. The time-dependent uptake was measured with a CIF-liposome

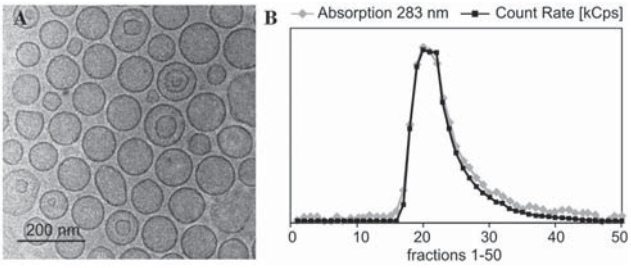

Fig. 1 (A) Cryotransmission electron microscopy image of a representative FA-targeted Fospeg formulation. (B) Column chromatography analysis of free folic acid in a folate-decorated liposome sample, indicating the absence of released targeting molecules.

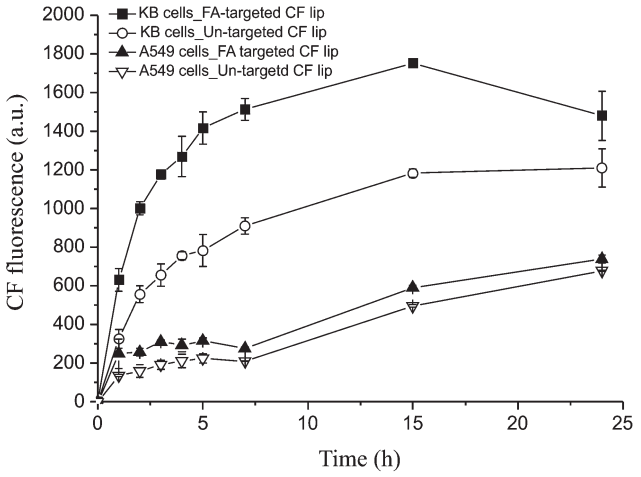

Fig. 2 Time-dependent uptake of FA-targeted or un-targeted CF-labelled liposomes in KB and A549 cells. Liposome concentration was equivalent to 11 μg ml^{-1} of phospholipid and uptake was measured by flow cytometry at different times up to 24 h of cell incubation. Data are means ± SD (n = 3).

concentration of 11 μg ml^{-1} of phospholipid; that with Fospeg corresponds to a *m*-THPC concentration of 1 μM, frequently used in *in vitro* uptake and phototoxicity studies. The time-dependent studies showed that in KB cells liposome internalization was very fast, especially for FA-targeted liposomes, during the first 5 h and then tended to a plateau (Fig. 2). The highest ratio (1.94) for FA-targeted *vs.* un-targeted liposomes was measured after 1 h, it remained around 1.8 until 5 h and decreased to 1.2 at 24 h very likely because of a higher contribution of non-specific uptake. In A549 cells, the uptake was slower and was still slightly increasing at 24 h.

The concentration-dependent uptake was measured at 5 h, the incubation time approaching maximum uptake and ratio of targeted *vs.* un-targeted (Fig. 2). As reported in Fig. 3A, in KB cells the uptake of FA-targeted liposomes was about twice that of the un-targeted counterpart (average ratio of FA-targeted *vs.* un-targeted is 1.8). In A549 cells, the uptake of both targeted and un-targeted liposomes was lower than in KB cells but also in these FR negative cells the uptake of targeted liposomes was slightly higher than that of the un-targeted ones. However, the higher ratio of uptake between targeted and un-targeted liposomes in KB with respect to A549 cells suggested some involvement of FR and therefore competition experiments were carried out to confirm this hypothesis. In cells pre-incubated for 1 h with 1 mM free FA before liposome addition, we actually measured a significant reduction of uptake of the FA-targeted liposomes in KB cells (Fig. 3B) while the uptake of un-targeted liposomes was almost unaffected. The inhibitory effect of 1 mM FA was very similar for the two tested liposome concentrations of 11 and 16.5 μg ml^{-1} phospholipids, suggesting no dependency on liposome concentration at least in this range. In A549 cells the preincubation with 1 mM FA decreased to a lesser extent the uptake of targeted and un-targeted liposomes. Nevertheless, in KB cells 1 mM FA did not inhibit the uptake of the FA-targeted liposomes to the level of the un-targeted ones, while 1 mM FA almost totally inhibited the uptake of a simple FA-FITC conjugate (Fig. S1†). The latter observation suggested that 1 mM FA was sufficient to saturate all FRs on the surface of KB cells.

Confocal microscopy studies

In order to confirm the cellular uptake of CF-liposomes measured with flow cytometry, KB cells were incubated with 11 μg ml^{-1} of CF-liposomes for 5 h and analysed by confocal microscopy. Both targeted and un-targeted liposomes were internalized as shown by the CF green fluorescence localised in the cytoplasm of the cells. As expected, the fluorescence signal in cells incubated with FA-targeted liposomes (Fig. 4A)

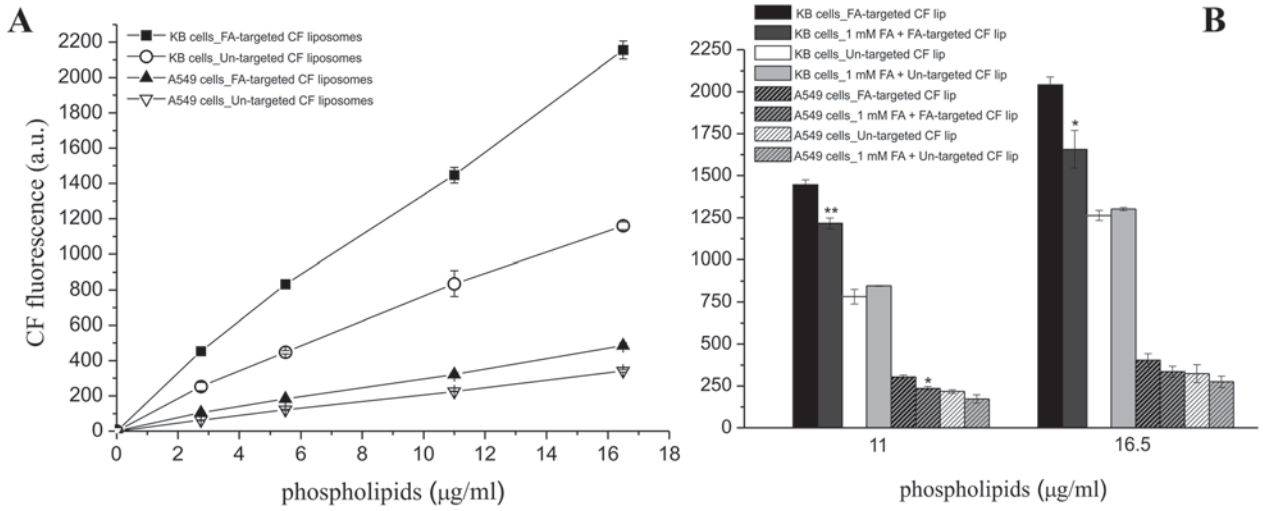

Fig. 3 Flow cytometry measurements of CF-labelled liposome uptake in KB (FR-positive) and A549 (FR-negative) cells. (A) Cells were incubated for 5 h with increasing concentrations of FA-targeted or un-targeted liposomes. (B) Competition experiment: cells were pre-treated (1 h) with 1 mM free folic acid and then incubated for 5 h with CF-labelled liposomes. Data are means ± SD (n = 3). *p < 0.005; **p < 0.001 with respect to the corresponding sample not pre-incubated with 1 mM FA (Student's t-test).

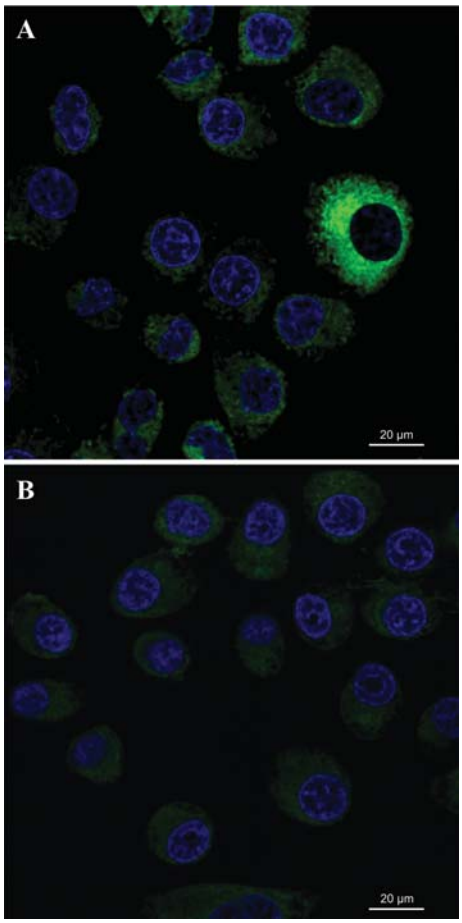

Fig. 4 Confocal microscopy images of KB cells incubated for 5 h with FA-targeted (A) or un-targeted (B) carboxyfluorescein doped liposomes at a concentration of 11 μg ml^{-1} of phospholipids.

was higher with respect to that of cells incubated with the un-targeted liposomes (Fig. 4B). Moreover, it appeared that the fluorescence intensity of targeted liposomes was very high only in some cells of the sample whereas in the case of the un-targeted ones the distribution appeared more homogeneous. This may be related to different levels of expression of FR on KB cells. The fluorescence signals in A549 cells were very low and the differential uptake between targeted and un-targeted liposomes was not appreciable (images not shown).

Uptake of FA-targeted and un-targeted Fospeg

Based on the results of the CF-liposomes, we evaluated the uptake of increasing concentrations of *m*-THPC loaded in liposomes (Fospeg) of the same phospholipid composition, after 3 and 24 h of incubation. The long incubation of 24 h was selected because it was frequently used by us[21,30] and other authors[34] for similar studies, while the incubation of 3 h approached the time of maximum liposome uptake (Fig. 2) and was sufficiently short to ensure that a large fraction of *m*-THPC had not escaped the liposomes before being internalised by the cells. As reported in Fig. 5A, after 3 h of incubation, the mean fluorescence intensity of cells incubated with FA-Fospeg was higher than that of the cells incubated with un-targeted Fospeg. In KB cells the ratio of FA-targeted *vs.* un-targeted Fospeg was significantly higher than in A549 cells (*e.g.* 1.94 *vs.* 1.34 for 0.5 μM *m*-THPC). In A549 cells the uptake of FA-targeted Fospeg was not significantly ($p > 0.05$) higher than that of the un-targeted Fospeg. When the incubation time was prolonged to 24 h, the mean fluorescence intensity of the cells was very similar for both the targeted and un-targeted Fospeg and the cell lines (Fig. 5B).

It is well known that serum proteins compete with the cells for the binding of *m*-THPC[42] and decrease the cell photosensitizer uptake. We checked whether serum proteins could affect differently the internalisation of targeted and un-targeted Fospeg and their FR-mediated or non-specific mechanism of entry. Thus, the uptake of the Fospeg formulations was evaluated after 1 h of cell incubation in a medium supplemented with 0, 3 or 10% FBS (Table 2). As expected, in both types of

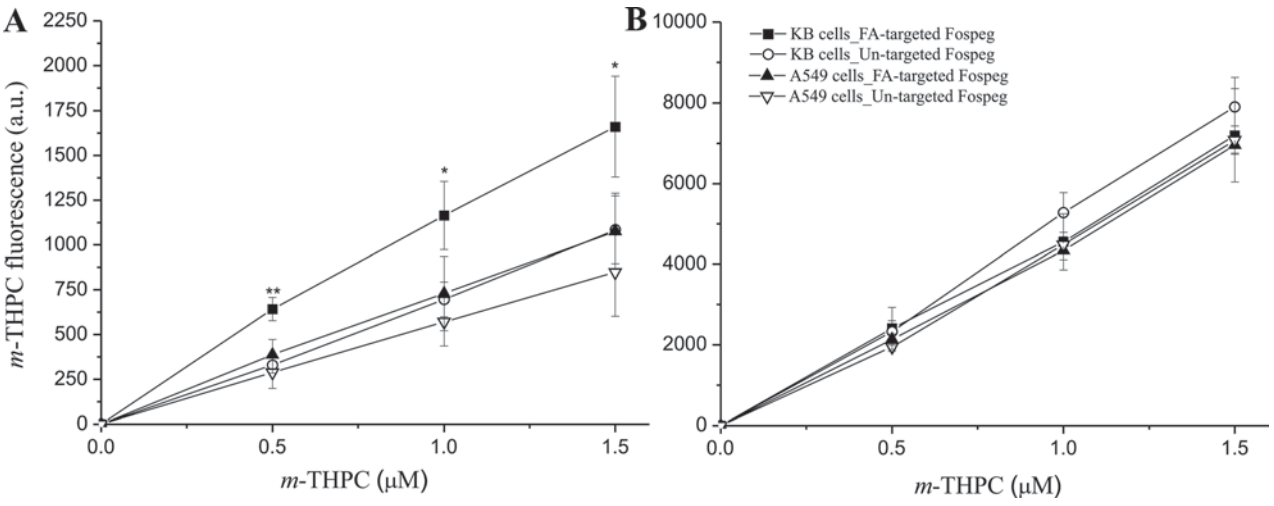

Fig. 5 Cellular uptake of FA-targeted and un-targeted *m*-THPC loaded liposomes (Fospeg). KB and A549 cells were incubated for (A) 3 h or (B) 24 h with increasing doses of Fospeg. Data are means ± SD ($n = 3$). *$p < 0.05$; **$p < 0.005$ with respect to un-targeted Fospeg (Student's *t*-test).

Table 2 Uptake of 1 μM *m*-THPC delivered to KB and A549 cells with FA-targeted or un-targeted liposomes diluted in a culture medium supplement with different percentage of serum. The values represent the mean fluorescence intensity (a.u.) of *m*-THPC internalized by the cells as measured by flow cytometry after 1 h of incubation. Values ± SD from three independent experiments

	KB cells			A549 cells		
Serum concentration (%)	FA-Fospeg	Un-targeted Fospeg	Ratio	FA-Fospeg	Un-targeted Fospeg	Ratio
0	1005.00 ± 127.05	771.00 ± 12.77	1.3	754 ± 14.47	719.33 ± 95.13	1.04
3	707.33 ± 77.47	390.67 ± 39.51	1.81	382 ± 72.81	406.33 ± 30.35	0.94
10	515.00 ± 24.27	249.00 ± 17.35	2.09	281.33 ± 28.04	266 ± 19.70	1.05

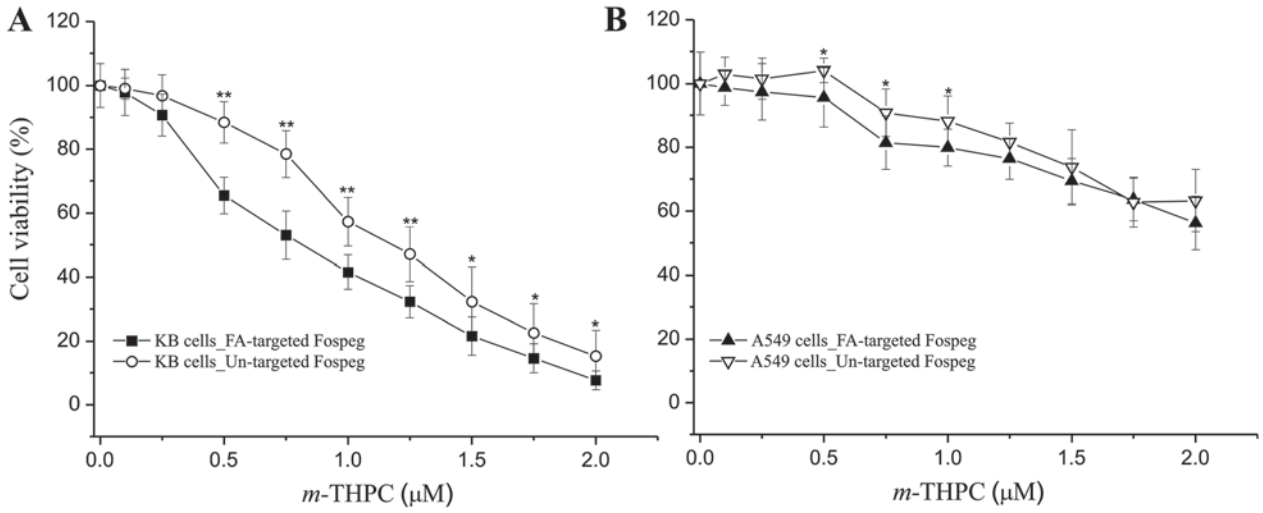

Fig. 6 *In vitro* phototoxicity of KB (A) and A549 (B) cells incubated for 3 h with increasing doses of FA-targeted or un-targeted Fospeg and irradiated with 0.8 J cm^{-2} of red light (600–700 nm). Cell viability was measured with the MTS test 24 h after irradiation and expressed as mean percentage ± SD (n = 9) with respect to untreated and un-irradiated control cells. *p < 0.05 and **p < 0.001 significantly different from FA-targeted Fospeg values (Student's t-test).

cells and for both targeted and un-targeted Fospeg formulations, the increasing percentage of FBS decreased the uptake of *m*-THPC. However, it is worth noting that in KB cells the uptake of *m*-THPC was inhibited less when delivered by targeted instead of un-targeted Fospeg and when compared to A549 cells. As a consequence in A549 cells the ratio of FA-targeted *vs.* un-targeted Fospeg remained around 1 in all tested serum conditions while in KB cells the ratio increased with the increasing percentage of FBS.

Phototoxicity of FA-targeted and un-targeted Fospeg

The *in vitro* phototoxicity of *m*-THPC delivered with the Fospeg formulations was evaluated in cells incubated for 3 h with increasing concentrations of the photosensitizer and irradiated with 0.8 J cm^{-2} of red light. Photosensitisation studies were carried out only with the 3 h incubation because at this time enhanced uptake of *m*-THPC delivered with targeted Fospeg was measured. In line with this, in KB cells, the photo-killing efficiency of FA-targeted Fospeg was approximately 1.5-fold higher with respect to un-targeted Fospeg (Fig. 6A) as deduced also from the IC_{50} values of 0.81 and 1.17 μM, respectively, of FA-targeted and un-targeted Fospeg. Indeed, in A549 cells the cytotoxicity was lower and similar for both Fospeg formulations and the *m*-THPC concentration decreasing the cell viability by 50% was higher than 2 μM (Fig. 6B).

From the dose–response curves of Fig. 6 it appears that the best selectivity in killing KB cells was achieved with *m*-THPC concentrations in the range 0.5–1 μM. For such a reason, KB cells were incubated with 0.5, 0.75, and 1 μM *m*-THPC Fospeg formulations and then irradiated with increasing doses of light (0–2.4 J cm^{-2}) (Fig. 7). For each *m*-THPC concentration, targeted and un-targeted Fospeg induced a light-dose-dependent decrease of cell viability that was, however, more severe with FA-Fospeg especially at low light doses (0.4–1.2 J cm^{-2}). In all cases, dark incubation alone (0 J cm^{-2}) induced no detectable decrease of cell viability, indicating that both Fospeg formulations were not cytotoxic in the absence of light.

Discussion

Specific delivery of photosensitizers to tumour cells is one of the most important challenges of PDT and nanotechnologies appear to offer great opportunities for reaching this goal. Thus we explored the possibility of obtaining selective delivery of

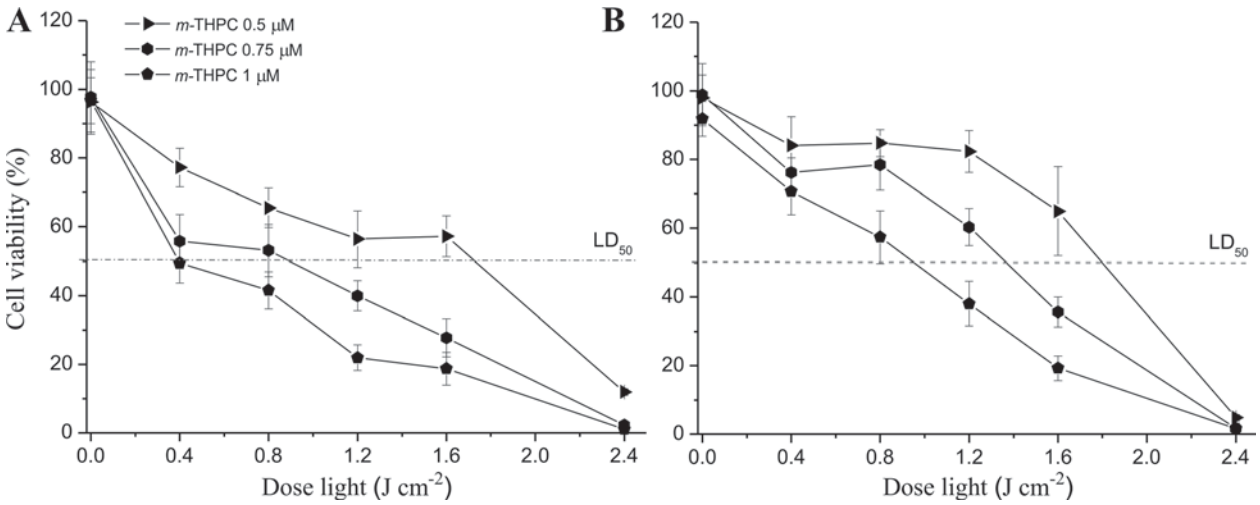

Fig. 7 Light-dose-dependent photo-killing of KB cells incubated for 3 h with selected doses of FA-targeted (A) or un-targeted (B) Fospeg and then irradiated with increasing doses of red light. Cell viability was measured with the MTS test 24 h after irradiation and expressed as mean percentage ± SD (n = 9) with respect to untreated control cells.

m-THPC to cancer cells by using PEGylated liposomes targeted with folic acid, since FR is overexpressed in many types of human tumours.[43]

Our *in vitro* work included two steps: in the first one, FA-targeted and un-targeted CF-labelled liposomes were used to assess FR involvement in the nanocarrier uptake; in the second step, we studied delivery and phototoxicity of *m*-THPC entrapped in FA-liposomes.

The liposomes used in the formulations are "stealth" since they contain 8 mol% of phospholipid PEGylated with PEG750 while the FA molecule is coupled to a PEG5000 chain. It was already shown that in the construction of targeted nanovehicles the length of the PEG chain used for the coupling of the targeting agent (PEG spacer) is crucial and a compromise must be found with the lengths of the PEG chains forming the coating. Lee and Low[44] studied the influence of the PEG spacer in calcein loaded liposomes and found that if FA was directly linked to the amino group of phospholipids (no spacer), liposomes were not taken up by KB cells while the addition of a PEG spacer permitted efficient uptake of the liposomes. The nature and the length of the spacer were shown to play a role also in the FR-mediated uptake of FA-conjugated PSs and quantum dots.[34,39]

Based on this, we synthesized two formulations of FA-targeted CF-liposomes coated with PEG750 in which PEG2000 or PEG5000 was used as a spacer to expose the FA molecules on the surface of liposomes. Intracellular uptake studies demonstrated the uselessness of PEG2000 as a spacer for FA since no increased uptake was measured for this type of liposomes in KB cells incubated for 5 h (data not shown). In contrast, the coupling of FA to PEG5000 produced a 2-fold increase of the uptake of the targeted with respect to the un-targeted liposomes in KB cells (Fig. 3A). The higher uptake of FA-liposomes in FR-positive cells was also appreciated by the confocal microscopy analysis carried out after 5 h of incubation (Fig. 4). Our findings are in agreement with those of Yamada *et al.*[45] who studied the *in vitro* and *in vivo* cellular uptake of doxorubicin delivered by FA-liposomal formulation and found the highest uptake for FA-PEG5000 liposomes with respect to FA-PEG3400 or FA-PEG2000 liposomes. Thus, it appears that the longer PEG chains favour FR-mediated liposome internalization.

We found that the uptake of FA-targeted was higher with respect to the un-targeted liposomes also in A549 cells which are negative for the expression of FR (Fig. 3A). This result may indicate that the coupling of FA molecules induces changes of the liposome surface favouring un-specific internalization. This effect is very likely mediated by the association of extracellular and serum components on the surface of FA-targeted liposomes.[46] Thus, when the incubation is carried out in the presence of serum, as in our experiments, the association of proteins favoured by the FA molecules might lead to the formation of complexes that are easily internalized by the cells. Nevertheless, the involvement of FR-mediated endocytosis in the uptake of FA-liposomes in KB cells was confirmed with competition experiments (Fig. 3B). In these cells, the pre-incubation with 1 mM free FA determined a significant decrease of the internalization of FA-liposomes and did not affect the internalization of un-targeted nanocarriers. However, 1 mM FA did not reduce the uptake of FA-liposomes to the level of the un-targeted liposomes as found by Kawano and Maitani[47] who studied the specific internalization of FA-targeted liposomes loaded with doxorubicin in the same cellular system. Therefore, based on the competition experiment we deduced that only a small fraction (about 15%) of FA-targeted liposomes entered the cells *via* FR-mediated endocytosis while nonspecific endocytosis seems to be the predominant mechanism of uptake. Some improvements with regard to the specific uptake are very likely obtained by reducing the numbers of FA molecules conjugated to the liposomes.[47,48]

The experiments on the time-dependent internalization of liposomes, up to 24 h, in KB cells showed that the differential uptake of FA-targeted *vs.* un-targeted liposomes reached the maximum (1.94) after 1 h and decreased (1.2) after 24 h (Fig. 2). Notwithstanding the mild gain of intracellular uptake of CF-liposomes targeted with FA, we evaluated the uptake of *m*-THPC delivered with liposomes of the same composition. A significantly higher uptake of *m*-THPC delivered with FA-Fospeg with respect to un-targeted Fospeg was observed only in KB cells after a short incubation time (3 h) (Fig. 5A). In the Fospeg formulations *m*-THPC is not covalently linked to phospholipids but only physically entrapped into the bilayer; therefore, drug release can occur in the presence of serum proteins. The kinetics of redistribution of *m*-THPC from Foslip® (non-PEGylated *m*-THPC liposomes) or Fospeg® to biological substrates were well characterised by Reshetov and co-workers.[40,41] In particular, they found that in the presence of 5% serum, *m*-THPC release from Fospeg® showed two phase kinetics: a fast one with more than 20% released in the first minutes of incubation and a slow one (from 30 minutes onward) in which the release is less consistent with a maximum of about 70%. In the Fospeg® formulations used by Reshetov PEG2000 was used for the coating while in our case PEG750 was used. Nevertheless, the photosensitizer release from our targeted liposomes must be considered already after few minutes of incubation in a medium added with the serum. The cell fluorescence signals measured by flow cytometry derive from *m*-THPC molecules entering the cells still entrapped in liposomes as well as those associated with serum proteins as a consequence of premature release from liposomes. In all cases, higher (~2-fold) *m*-THPC fluorescence signals were measured after 3 h of incubation of KB cells with FA-Fospeg with respect to un-targeted Fospeg, showing some contribution of FR-mediated endocytosis. A similar increase of *m*-THPC fluorescence was found in KB cells incubated, under conditions comparable to ours, with FA-conjugated polymeric micelles as PS nanocarriers.[20] The enhancement of PS uptake mediated by the FR receptor was higher when using simple FA–PS conjugates[34,36] and this is very likely explained with a different ability of FA to bind its receptor as can be expected by changing the nature of its cargo (a simple PS molecule or a nanoparticle). In all cases, it is worth noting that in A549 cells *m*-THPC uptake for FA-Fospeg and un-targeted Fospeg was very similar to that of un-targeted Fospeg in KB cells. This is different from the results obtained with the CF-labelled liposomes (Fig. 3A) and confirmed the hypothesis that an important fraction of *m*-THPC molecules enter the cells with a mechanism not involving liposomes. After 24 h of incubation, no significantly different uptake of *m*-THPC was measured between the two cell lines and the two formulations (Fig. 5B), in agreement with the release of most of the drug molecules from liposomes and the decreased contribution of FR-mediated endocytosis already highlighted for FA-targeted CF-liposomes (Fig. 2).

The influence of serum protein concentration on the specific uptake of *m*-THPC was evaluated by increasing the percentage of FBS during liposome incubation (Table 2). In a serum-free medium *m*-THPC delivered with FA-Fospeg entered the cells only by a specific and non-specific endocytosis of liposomes. Therefore, in this condition the fraction of liposomal *m*-THPC taken up by FR-mediated endocytosis can be better appreciated. From the data of Table 2, it appears that serum proteins inhibited more the non-specific with respect to the FR-mediated uptake of *m*-THPC because only in KB cells and using FA-Fospeg, 3% and 10% FBS inhibited *m*-THPC uptake by about 30% and 50%, respectively, with respect to the uptake in the absence of serum. In all other conditions, inhibition of *m*-THPC uptake accounted for about 50% and 65% respectively for 3% and 10% FBS. As a consequence, the ratio of *m*-THPC uptake in FR-positive cells increased with the increasing serum percentage while it remained constant in FR-negative cells.

The more selective *m*-THPC uptake obtained with FA-liposomes translated to higher photo-induced toxicity in cells incubated with Fospeg formulations for 3 h and then irradiated with 0.8 J cm^{-2} of light (Fig. 6). The decrease of viability of KB cells was approx. 1.5 times more if *m*-THPC was delivered with FA-targeted with respect to un-targeted liposomes, while in A549 cells the mortality was not appreciably influenced by the Fospeg formulations. Hence, the contribution of FR-mediated endocytosis of FA-targeted liposomes yielded enhanced phototoxicity (~30%) with equal concentrations of *m*-THPC administered to FR-expressing cells. The enhancement of phototoxicity afforded by the conjugation of Fospeg to FA is lower than expected but not very different from that observed in KB cells with FA-conjugated liposomes loaded with a tetrasulphonated phthalocyanine[37] and with FA-conjugated quantum dots[39] in comparison with their un-targeted counterparts. Our results are also in line with those of García-Diaz[49] *et al.*, reporting modest enhancement of internalization of the PS ZnTPP and phototoxicity in FR-positive HeLa cells with FA-targeted liposomes. Similarly to us they concluded that FA-liposomes are mainly internalized by non-specific endocytosis.

While the biodistribution, selectivity of uptake and PDT efficiency of FA-Fospeg *in vivo* need to be defined, we can speculate that, in spite of limited selectivity emerging from our *in vitro* data, FA-Fospeg would favourably affect the outcome of PDT in FR-overexpressing tumours. Bovis *et al.*[31] have clearly shown that un-targeted Fospeg® accumulates rapidly and efficiently in the MC28 fibrosarcoma. Fospeg® uptake in tumour increased about 3-fold compared to Foscan® with a maximal tumour to skin ratio of 6 (*vs.* 1.4 of Foscan®) at 6 h after injection. Overall, the data indicated that for clinical PDT a shorter drug light interval and a lower dose of *m*-THPC in Fospeg® can be adopted over those currently used for Foscan®. The tumour to skin ratio of un-targeted Fospeg® is comparable to that reported for a *m*-THPC-like PS conjugated to folate and tested in KB tumour[25] and is higher than that of *m*-THPC delivered with FA-conjugated polymeric micelles.[20] Conjugation with FA should not affect negatively the pharmacokinetic properties and bioavailability of Fospeg;

instead, a further improvement is expected since the targeted formulation slightly favours cellular internalisation of *m*-THPC. Because of the prolonged circulation of Fospeg in the bloodstream, the damage to the vasculature largely contribute to the PDT-induced tumour damage.[31] The FA-Fospeg favouring the cellular internalisation of the PS might increase the contribution of the direct tumour cell damage and therefore the tumour response to PDT.

Conclusions

We have reported that the selectivity of *m*-THPC uptake and phototoxicity in FR-expressing cells can be improved by delivering the photosensitising drug *via* FA-targeted Fospeg. However, our results show modest selectivity of uptake of FA-liposomes and suggest that non-specific endocytosis remains the prevailing mechanism of cell internalisation also for the targeted nanocarriers. In spite of the modest contribution of the specific uptake on the total of *m*-THPC uptake, in FR-positive KB cells, the photo-killing effect produced with FA-Fospeg was 1.5 times stronger when compared to un-targeted Fospeg. The limited selectivity of the uptake of *m*-THPC delivered by FA-liposomes is explained with the modest contribution of FR-mediated endocytosis to the overall liposome internalisation and premature escape of the drug from liposomes in the presence of serum proteins. It appears that the attachment of FA to PEG diminishes by 5–10-fold the extent of binding of FA to its receptor.[46] In addition the presence of the PEG corona on the liposome surface, while conferring stealth properties to the particles and prolonging their systemic circulation *in vivo*, interferes with the targeting effect of FA.[46,50] Recently, it has been suggested that a FA-poly(L-lysine) conjugate might be more promising than FA–PEG–lipid as a coating and coupling element in the development of liposomal formulations for targeting FR.[51] Therefore, additional investigations can further optimise the targeting of liposomal nanocarriers and fully exploit the potential of FA as a targeting agent for cancer cells.

Acknowledgements

The research leading to these results has received funding from European Community's Seventh Framework Programme (FP7/2007–2013) under Grant Agreement No. 201031 (NANOPHOTO).

References

1 P. Agostinis, K. Berg, K. A. Cengel, T. H. Foster, A. W. Girotti, S. O. Gollnick, S. M. Hahn, M. R. Hamblin, A. Juzeniene, D. Kessel, M. Korbelik, J. Moan, P. Mroz, D. Nowis, J. Piette, B. C. Wilson and J. Golab, Photodynamic therapy of cancer: an update, *CA Cancer J. Clin.*, 2011, **61**, 250–281.

2 T. J. Dougherty, C. J. Gomer, B. W. Henderson, G. Jori, D. Kessel, M. Korbelik, J. Moan and Q. Peng, Photodynamic therapy, *J. Natl. Cancer Inst.*, 1998, **90**, 889–905.

3 S. B. Brown, E. A. Brown and I. Walker, The present and future role of photodynamic therapy in cancer treatment, *Lancet Oncol.*, 2004, **5**, 497–508.

4 M. R. Hamblin and T. Hasan, Photodynamic therapy: a new antimicrobial approach to infectious disease?, *Photochem. Photobiol. Sci*, 2004, **3**, 436–450.

5 C. Hopper, Photodynamic therapy: a clinical reality in the treatment of cancer, *Lancet Oncol.*, 2000, **1**, 212–219.

6 C. Hadjur, N. Lange, J. Rebstein, P. Monnier, H. Van der Bergh and G. Wagnières, Spectroscopic studies of photobleaching and photoproduct formation of *meta*(tetrahydroxyphenyl)chlorin (*m*THPC) used in photodynamic therapy. The production of singlet oxygen by *m*THPC, *J. Photochem. Photobiol., B*, 1998, **45**, 170–178.

7 D. Bechet, P. Couleaud, C. Frochot, M. L. Viriot, F. Guillemin and M. Barbery-Heyob, Nanoparticles as vehicles for delivery of photodynamic therapy agents, *Trends Biotechnol.*, 2008, **26**, 612–621.

8 A. Gupta, S. Wang, P. Pera, K. V. Rao, N. Patel, T. Y. Ohulchanskyy, J. Missert, J. Morgan, Y. E. Koo-Lee, R. Kopelman and R. K. Pandey, Multifunctional nanoplatforms for fluorescence imaging and photodynamic therapy developed by post-loading photosensitizer and fluorophore to polyacrylamide nanoparticles, *Nanomedicine*, 2012, **8**, 941–950.

9 P. Couleaud, V. Morosini, C. Frochot, S. Richeter, L. Raehmaand and J. O. Durand, Silica-based nanoparticles for photodynamic therapy applications, *Nanoscale*, 2010, **2**, 1083–1095.

10 B. Klajnert, M. Rozanek and M. Bryszewska, Dendrimers in photodynamic therapy, *Curr. Med. Chem.*, 2012, **19**, 4903–412.

11 A. M. Bugaj, Targeted photodynamic therapy – a promising strategy of tumour treatment, *Photochem. Photobiol. Sci.*, 2011, **10**, 1097–1109.

12 D. S. Kohane, Microparticles and nanoparticles for drug delivery, *Biotechnol. Bioeng.*, 2007, **96**, 203–209.

13 E. M. Cohen, H. Ding, C. W. Kessinger, C. Khemtong, J. Gao and B. D. Sumer, Polymeric micelle nanoparticles for photodynamic treatment of head and neck cancer cells, *Otolaryngol Head Neck Surg.*, 2010, **143**, 109–115.

14 A. M. Master, M. E. Rodriguez, M. E. Kenney, N. L. Oleinick and A. S. Gupta, Delivery of the photosensitizer Pc4 in PEG-PCL micelles for *in vitro* PDT studies, *J. Pharm. Sci.*, 2010, **99**, 2386–2398.

15 S. J. Lee, K. Park, Y.-K. Oh, S.-H. Kwon, S. Her, I.-S. Kim, K. Choi, S. J. Lee, H. Kim, S. G. Lee, K. Kim and I. C. Kwon, Tumour specificity and therapeutic efficacy of photosensitizer-encapsulated glycol chitosan-based nanoparticles in tumour-bearing mice, *Biomaterials*, 2009, **30**, 2929–2939.

16 C. Kojima, Y. Toi, A. Harada and K. Kono, Preparation of poly(ethylene glycol)-attached dendrimers encapsulating

photosensitizers for application to photodynamic therapy, *Bioconjugate Chem.*, 2007, **18**, 663–670.
17 I. Roy, T. Y. Ohulchanskyy, H. E. Pudavar, E. J. Bergey, A. R. Oseroff, J. Morgan, T. J. Dougherty and P. N. Prasad, Ceramic-based nanoparticles entrapping water-insoluble photosensitizing anticancer drugs: a novel drug-carrier system for photodynamic therapy, *J. Am. Chem. Soc.*, 2003, **125**, 7860–7865.
18 Y. Cheng, A. C. Samia, J. D. Meyers, J. Panagopoulos, B. Frei and C. Burda, Highly efficient drug delivery with gold nanoparticles vectors for *in vivo* photodynamic therapy of cancer, *J. Am. Chem. Soc.*, 2008, **130**, 10634–10647.
19 M. J. Shieh, C. L. Peng, W. L. Chiang, C. H. Wang, C. Y. Hsu, S. J. Wang and P. S. Lai, Reduced skin photosensitivity with *meta*-tetra(hydroxyphenyl)chlorin-loaded micelles based on a poly(2-ethyl-2-oxazoline)-*b*-poly(D,L-lactide) diblock copolymer *in vivo*, *Mol. Pharm.*, 2010, **7**, 1244–1253.
20 W. J. Syu, H. P. Yu, C. Y. Hsu, Y. C. Rajan, Y. H. Hsu, Y. C. Chang, W. Y. Hsieh, C. H. Wang and P. S. Lai, Improved photodynamic cancer treatment by folate-conjugated polymeric micelles in a KB xenografted animal model, *Small*, 2012, **13**, 2060–2069.
21 C. Compagnin, L. Baù, M. Mognato, L. Celotti, G. Miotto, M. Arduini, F. Moret, C. Fede, F. Selvestrel, I. M. Rio Echevarria, F. Mancin and E. Reddi, The cellular uptake of *meta*-tetra(hydroxyphenyl)chlorin entrapped in organically modified silica nanoparticles is mediated by serum proteins, *Nanotechnology*, 2009, **20**, 345101.
22 M. Rojnik, P. Kocbek, F. Moret, C. Compagnin, L. Celotti, M. J. Bovis, J. H. Woodhams, A. J. MacRobert, D. Scheglmann, W. Helfrich, M. J. Verkaik, E. Papini, E. Reddi and J. Kos, *In vitro* and *in vivo* characterization of temoporfin-loaded PEGylated PLGA nanoparticles for use in photodynamic therapy, *Nanomedicine*, 2012, **7**, 663–667.
23 B. Pegaz, E. Debefve, J. P. Ballini, G. Wagnieres, S. Spaniol, V. Albrecht, D. V. Scheglmann, N. E. Nifantiev, H. Van der Bergh and Y. N. Konan-Kouakou, Photothrombic activity of *m*-THPC-loaded liposomal formulations: pre-clinical assessment on chick chorioallantonic membrane model, *Eur. J. Pharm. Sci.*, 2006, **28**, 134–140.
24 J. Buchholz, B. Kaser-Hotz, T. Khan, B. C. Rohrer, K. Melzer, R. A. Schwendener, M. Roos and H. Walt, Optimizing photodynamic therapy: *in vivo* pharmacokinetics of liposomal *meta*-(tetra-hydroxyphenyl)chlorin in feline squamous cell carcinoma, *Clin. Cancer Res.*, 2005, **11**, 7538–7544.
25 H. P. Lasalle, D. Dumas, S. Gräfe, M. A. D'Hallewin, F. Guillemin and L. Bezdetnaya, Correlation between *in vivo* pharmakinetics, intratumoral distribution and photodynamic efficiency of liposomal *m*THPC, *J. Controlled Release*, 2009, **134**, 118–124.
26 J. Kuntsche, I. Freislebena, F. Steinigerb and A. Fahra, Temoporfin-loaded liposomes: physicochemical characterization, *Eur. J. Pharm. Sci.*, 2010, **40**, 305–315.
27 A. L. Klibanov, K. Maruyama, V. P. Torchilin and L. Huang, Amphipathic polyethyleneglycols effectively prolong the circulation time of liposomes, *FEBS Lett.*, 1990, **268**, 235–237.
28 S. N. Dos, C. Allen, A. M. Doppen, M. Anantha, K. A. Cox, R. C. Gallagher, G. Karlsson, K. Edwards, G. Kenner, L. Samuels, M. S. Webb and M. B. Bally, Influence of poly-(ethyleneglycol) grafting density and polymer length on liposomes: relating plasma circulation lifetimes to protein binding, *Biochim. Biophys. Acta*, 2007, **1768**, 1367–1377.
29 R. Tavano, D. Segat, E. Reddi, J. Kos, M. Rojnik, P. Kocbek, S. Iratni, D. Scheglmann, M. Colucci, I. M. Rio Echevarria, F. Selvestrel, F. Mancin and E. Papini, Procoagulant properties of bare and highly PEGylated vinyl-modified silica nanoparticles, *Nanomedicine*, 2010, **5**, 881–896.
30 C. Compagnin, F. Moret, L. Celotti, G. Miotto, J. H. Woodhams, A. J. MacRobert, D. Scheglmann, S. Iratni and E. Reddi, *Meta*-tetra(hydroxyphenyl)chlorin-loaded liposomes sterically stabilised with poly(ethylene glycol) of different length and density: characterisation, *in vitro* cellular uptake and phototoxicity, *Photochem. Photobiol. Sci.*, 2011, **10**, 1751–1759.
31 M. J. Bovis, J. H. Woodhams, M. Loizidou, D. Scheglmann, S. G. Bown and A. J. MacRobert, Improved *in vivo* delivery of *m*-THPC *via* pegylated liposomes for use in photodynamic therapy, *J. Controlled Release*, 2012, **30**, 196–205.
32 N. Solban, I. Rizvi and T. Hasan, Targeted photodynamic therapy, *Lasers Surg. Med.*, 2006, **38**, 522–531.
33 F. Danhier, O. Feron and V. Préat, To exploit the tumor microenvironment: passive and active tumor targeting of nanocarriers for anti-cancer drug delivery, *J. Controlled Release*, 2010, **148**, 135–146.
34 R. Schneider, F. Schmitt, C. Frochot, Y. Fort, N. Lourette, F. Guillemin, J.-F. Müller and M. Barberi-Heyob, Design, synthesis, and biological evaluation of folic acid targeted tetraphenylporphyrin as novel photosensitizers for selective photodynamic therapy, *Bioorg. Med. Chem.*, 2005, **13**, 2799–2808.
35 J. Gravier, R. Schneider, C. Frochot, T. Bastogne, F. Schmitt, J. Didelon, F. Guillemin and M. Barberi-Heyob, Improvement of *meta*-tetra(hydroxyphenyl)chlorin-like photosensitizer selectivity with folate-based targeted delivery. Synthesis and *in vivo* delivery studies, *J. Med. Chem.*, 2008, **51**, 3867–3877.
36 C. Stefflova, H. Li, J. Chen and G. Zheng, Peptide-based pharmacomodulation of a cancer-targeted optical imaging and photodynamic therapy agent, *Bioconjugate Chem.*, 2007, **18**, 379–388.
37 M. M. Qualls and D. H. Thompson, Chloroaluminum phthalocyanine tetrasulfonate delivered *via* acid-labile diplasmenylcholine-folate liposome: intracellular localisation and synergistic phototoxicity, *Int. J. Cancer*, 2001, **93**, 384–392.
38 S.-J. Yang, F.-H. Lin, K.-C. Tsai, M.-F. Wei, H.-M. Tsai, J.-M. Wong and M.-J. Shieh, Folic acid-conjugated chitosan nanoparticles enhanced protoporphyrin IX accumulation

in colorectal cancer cells, *Bioconjugate Chem.*, 2010, **21**, 679–689.

39 V. Morosini, T. Bastogne, C. Frochot, R. Schneider, A. François, F. Guillemin and M. Barberi-Heyob, Quantum dot-folic acid conjugates as potential photosensitizers in photodynamic therapy of cancer, *Photochem. Photobiol. Sci.*, 2011, **10**, 842–851.

40 V. Reshetov, D. Kachatkou, T. Shmigol, V. Zorin, M. D'Hallewin, F. Guillemin and L. Bezdetnaya, Redistribution of *meta*-tetra(hydroxyphenyl)chlorin (*m*-THPC) from conventional and PEGylated liposomes to biological substrates, *Photochem. Photobiol. Sci.*, 2011, **10**, 911–919.

41 V. Reshetov, V. Zorin, A. Siupa, M. D'Hallewin, F. Giullemin and L. Bezdetnaya, Interaction of liposomal formulations of *meta*-tetra(hydroxyphenyl)chlorin (temoporfin) with serum proteins: protein binding andliposome destruction, *Photochem. Photobiol.*, 2012, **88**, 1256–1264.

42 S. Sasnouski, V. Zorin, I. Khludeyev, M. A. D'Hallewin, F. Guillemin and L. Bezdetnaya, Investigation of Foscan® interactions with plasma proteins, *Biochim. Biophys. Acta*, 2005, **1725**, 394–402.

43 N. Parker, M. J. Turk, E. Westrick, J. D. Lewis, P. S. Low and C. P. Leamon, Folate receptor expression in carcinomas and normal tissues determined by a quantitative radioligand binding assay, *Anal. Biochem.*, 2005, **338**, 284–293.

44 R. J. Lee and P. S. Low, Delivery of liposomes into cultured KB cells via folate receptor-mediated endocytosis, *J. Biol. Chem.*, 1994, **269**, 3198–3204.

45 A. Yamada, Y. Taniguchi, T. Honda, Y. Hattori and Y. Maitani, Design of folate-linked liposomal doxorubicin to its antitumor effect in mice, *Clin. Cancer Res.*, 2008, **14**, 8161–8168.

46 A. Gabizon, A. T. Horowitz, D. Goren, D. Tzemach, F. Mandelbaum-Shavit, M. M. Qazen and S. Zalipsky, Targeting folate receptor with folate linked to extremities of poly(ethylene glycol)-grafted liposomes: *in vitro* studies, *Bioconjugate Chem.*, 1999, **10**, 289–298.

47 K. Kawano and Y. Maitani, Effects of polyethylene glycol spacer length and ligand density on folate receptor targeting of liposomal doxorubicin *in vitro*, *J. Drug Deliv.*, 2011, 160967.

48 A. R. Hilgenbrink and P. S. Low, Folate receptor-mediated drug targeting: from therapeutics to diagnostics, *J. Pharm. Sci.*, 2005, **94**, 2135–2146.

49 M. García-Díaz, S. Nonell, A. Villanueva, J. C. Stockert, M. Cañete, A. Casadò, M. Mora and M. L. Sagristá, Do folate-receptor targeted liposomal photosensitizers enhance photodynamic therapy selectivity?, *Biochim. Biophys. Acta*, 2011, **1808**, 1063–1071.

50 H. Shmeeda, Y. Amitay, J. Gorin, D. Tzemach, L. Mak, J. Ogorka, S. Kumar, J. A. Zhang and A. Gabizon, Delivery of zoledronic acid encapsulated in folate-targeted liposome results in potent *in vitro* cytotoxic activity on tumor cells, *J. Controlled Release*, 2010, **146**, 76–83.

51 K. Watanabe, M. Kaneko and Y. Maitani, Functional coating of liposomes using a folate-polymer conjugate to target folate receptors, *Int. J. Nanomed.*, 2012, **7**, 3679–3688.

Electronic Supplementary Material (ESI) for Photochemical & Photobiological Science

Supplementary Information

Folate-targeted PEGylated liposomes improve the selectivity of PDT with *meta*-tetra(hydroxyphenyl)chlorin (*m*-THPC)

Francesca Moret,[a] Dietrich Scheglmann,[b] and Elena Reddi*[a]

[a] *Department of Biology , University of Padova, via Ugo Bassi 58/B, 35121, Padova, Italy. Fax: +39 049 8276300; Tel: +39 049 8276335; E-mail: elena.reddi@unipd.it*
[b] *Biolitec Research GmbH, Otto-Schott-Strasse 15, 07745, Jena, Germany.*

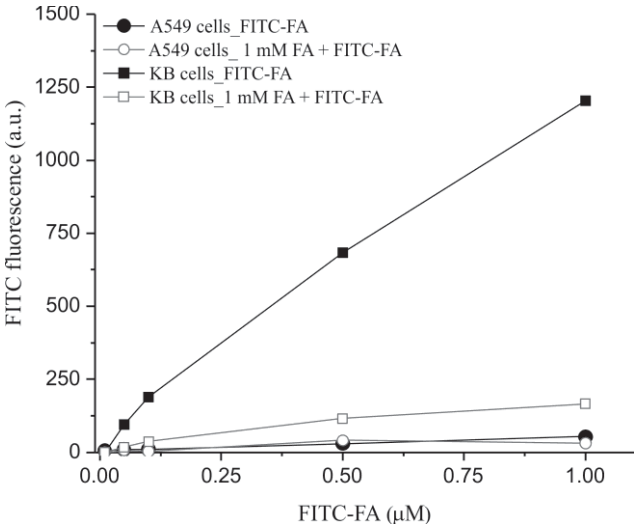

Fig. S1. Flow cytometry measurements of FITC-folate (FITC-FA) conjugate uptake in KB and A549 cells. The uptake in cells incubated 5 h with increasing concentration of FITC-FA was compared with the uptake in cells pre-treated for 1 h with 1 mM free folic acid and then incubated with the FITC-FA conjugate.

III

In vitro and *in vivo* characterization of temoporfin-loaded PEGylated PLGA nanoparticles for use in photodynamic therapy

Aims: In this study we evaluated temoporfin-loaded polyethylene glycol (PEG) poly-(D,L-lactide-co-glycolide) (PLGA) nanoparticles (NPs) as a new formulation for potential use in cancer treatment. **Materials & methods:** NPs were characterized for their photophysical properties, temoporfin release, cellular uptake and intracellular localization, and dark and photocytotoxicities of temoporfin by using A549, MCF10A neoT and U937 cell lines. *In vivo* imaging was performed on athymic nude-Foxn1 mice. **Results:** Temoporfin was highly aggregated within the NPs and the release of temoporfin monomers was faster from PEGylated PLGA NPs than from non-PEGylated ones. PEGylation significantly reduced the cellular uptake of NPs by the differentiated promonocytic U937 cells, revealing the stealth properties of the delivery system. Dark cytotoxicity of temoporfin delivered by NPs was less than that of free temoporfin in standard solution (Foscan®, Biolitec AG [Jena, Germany]), whereas phototoxicity was not reduced. Temoporfin delivered to mice by PEGylated PLGA NPs exhibits therapeutically favorable tissue distribution. **Conclusion:** These encouraging results show promise in using PEGylated PLGA NPs for improving the delivery of photosensitizers for photodynamic therapy.

Original submitted 30 March 2011; Revised submitted 9 July 2011

KEYWORDS: cytotoxicity ■ meta-tetra(hydroxyphenyl)chlorin ■ nanoparticles ■ PEGylation ■ photodynamic therapy ■ poly-(D,L-lactide-co-glycolide)

Matija Rojnik[1], Petra Kocbek[1], Francesca Moret[2], Chiara Compagnin[2], Lucia Celotti[2], Melissa J Bovis[3], Josephine H Woodhams[3], Alexander J MacRobert[3], Dietrich Scheglmann[4], Wijnand Helfrich[5], Marco J Verkaik[5], Emanuele Papini[2], Elena Reddi[2] & Janko Kos*[1]

[1]Faculty of Pharmacy, University of Ljubljana, Askerceva 7, 1000, Ljubljana, Slovenia
[2]Department of Biology, Interdepartmental Research Center for Innovative Biotechnology, University of Padova, via U.Bassi 58/B, 35131 Padova, Italy
[3]National Medical Laser Centre, University College London, Charles Bell House, 677–3 Riding House St, London W1W 7EJ, UK
[4]Research & Development Biolitec AG, Winzerlaer Strasse 2, 07745 Jena, Germany
[5]Department of Surgery, Surgical Research Laboratory, University Medical Center Groningen, University of Groningen, Hanzeplein 1, 9713 GZ Groningen, The Netherlands
**Author for correspondence:*
Tel.: +386 1 4769 604
Fax: +386 1 4258 031
janko.kos@ffa.uni-lj.si

Photodynamic therapy (PDT) is a promising treatment for cancer, its aim being to specifically destroy the malignant tissue [1,2]. To be effective, PDT requires a photosensitizer (PS) that accumulates preferentially in malignant tissue, nonthermal visible light and molecular oxygen. Upon absorption of photons, the PS is activated and can undergo two different types of reactions, one producing oxygen radicals and the other, singlet oxygen. These reactive oxygen species can induce damage in malignant and nonmalignant cells alike, depending on the PS distribution [3,4].

Meta-tetra(hydroxyphenyl)chlorin (mTHPC, temoporfin) is a highly potent second generation PS [5]. After systemic administration, the distribution of temoporfin between the tumor and the skin, the tumor to skin ratio, is significantly better than that obtained with previous PSs (e.g., hematoporphyrin derivates and photofrin), resulting in reduced side effects [6]. Temoporfin-mediated PDT has been shown to be an effective treatment for head and neck cancer [7], early stage oral squamous cell carcinoma [8] and prostate cancer [9]. A solution of temoporfin in ethanol and propylene glycol (Foscan®, Biolitec AG [Jena, Germany]) has been approved in the EU, Norway and Iceland as a local therapy for the palliative treatment of patients with advanced head and neck cancer who have failed prior therapies and are unsuitable for radiotherapy, surgery or systemic chemotherapy.

Bioavailability and biodistribution of PSs can be improved by nanoparticulate delivery systems such as liposomes and polymer particulate carriers [10]. These nanoscale delivery systems are capable of accumulating in tumor tissues due to the phenomenon known as the enhanced permeability and retention effect, or by targeting ligands designed to selectively bind over-expressed tumor-associated antigens [11]. Biodegradable poly-(D,L-lactide-co-glycolide) (PLGA) nanoparticles (NPs) constitute a delivery system that can be loaded with a variety of therapeutic agents, including low-molecular-weight drugs, as well as macromolecules such as proteins and plasmid DNA [12]. They are degraded to biocompatible, nontoxic products that are removed from the body by physiological pathways and clearance mechanisms. By changing the composition of the copolymeric system, it is possible to regulate the rate of degradation and the pore size, consequently releasing incorporated therapeutic molecules. Owing to excellent biocompatibility and biodegradability, the PLGA co-polymer has been approved by the US FDA [13] and has received wide attention as a promising biomaterial for the formulation of NPs for delivery of anti-tumor agents including PSs [14–17].

However, systemic use of NPs, including PLGA NPs, is limited due to their rapid opsonization and removal from the body by the

Future Medicine part of fsg

mononuclear phagocytic system. Several methods for modifying or masking the NP surface have been developed that allow NPs to temporarily evade recognition by the mononuclear phagocytic system and reach the target site. The most commonly used method for development of what are known as stealth NPs is to bind polyethylene glycol (PEG) chains to the NP surface [18]. PEGylated PLGA NPs have been shown to be retained in the blood significantly longer than the bare PLGA NPs [19,20].

The aim of this study was to prepare a PLGA NP delivery system loaded with the PS temoporfin to be used in PDT. PLGA NPs were optimized with respect to their average particle size, surface charge, drug loading and degradation rate. Furthermore, the effect of PEGylation on cell internalization, intracellular distribution and cell viability was evaluated *in vitro* in different cell lines. Dark cytotoxicity and photocytotoxicity of temoporfin-loaded PEGylated PLGA NPs were determined and compared with those of free temoporfin in a standard solution (Foscan). Finally, the performance of all three formulations (Foscan, PEGylated and non-PEGylated PLGA NPs) has been characterized *in vivo* using fluorescence-based imaging.

Materials & methods

Materials

Temoporfin (3,3′,3′′,3′′′-(2,3-dihydroporphyrin-5,10,15,20-tetrayl)tetraphenol) was provided by Biolitec AG (Jena, Germany) and dissolved in ethanol and propylene glycol – standard solution (Foscan). Resomers RG 503H and RGP d 50155 were obtained from Boehringer (Ingelheim, Germany), poloxamer 188 (Lutrol F68) and dimethyl sulfoxide (DMSO) were supplied by Sigma-Aldrich (MO, USA).

Cell lines

The human-transformed breast MCF10A neoT cell line was provided by Bonnie F Sloane (Wayne State University, MI, USA). The cells were cultured in DMEM/F12 (1:1) medium (Gibco, Invitrogen, CA, USA) supplemented with 5% fetal bovine serum (FBS), 1 µg/ml insulin (σ), 0.5 µg/ml hydrocortisone (σ), 50 ng/ml EGF (σ), 2 mM L-glutamine and antibiotics (38 units/ml streptomycin and 100 units/ml penicillin G). Human promonocytic cell line U937 (CRL-1593.2; ATCC, VA, USA) was grown in Advanced RPMI 1640 (Gibco, Invitrogen) supplemented with 2 mM L-glutamine, antibiotics (38 units/ml streptomycin and 100 units/ml penicillin G) and 10% FBS. Human lung carcinoma A549 cells (CCL-185, ATCC, MA, USA) were cultured in F-12K medium supplemented with 10% FBS (Gibco, Invitrogen), 2 mM L-glutamine, 2.5 g/l sodium bicarbonate, 38 units/ml streptomycin and 100 units/ml penicillin G (σ). HCT116-luc is a human colorectal adenocarcinoma cell line stably transfected with firefly luciferase gene (Caliper, MA, USA). HCT116-luc cells were cultured in Advanced RPMI 1640 (Gibco, Invitrogen) supplemented with 2 mM L-glutamine, antibiotics (38 units/ml streptomycin and 100 units/ml penicillin G) and 10% FBS.

Preparation of temoporfin-loaded PLGA & PEGylated PLGA NPs

PLGA and PEGylated PLGA NPs were prepared by a modified nanoprecipitation method [21]. In short, 45 mg of PLGA (Resomer RG 503H) and 5 mg of temoporfin were dissolved in 1 ml acetone and the solution was slowly injected into 50 ml of 0.25% (weight/volume) poloxamer 188 water solution with moderate magnetic stirring. The resulting NP dispersion was stirred for 15 min at room temperature and then centrifuged at 15,000 rpm for 15 min to separate NPs from nonincorporated temoporfin and excess stabilizer. Subsequently, the NPs were washed with 20 ml of distilled water, centrifuged at 15,000 rpm for 15 min, and then dispersed in 10 ml of 5% (weight/volume) aqueous trehalose solution. The NPs were freeze-dried at room temperature and 0.090 mbar for 24 h (Christ Beta 18–K, Germany). PEGylated NPs were prepared by the same procedure, the only difference being the polymer composition. The weight ratio of PLGA (Resomer RG 503H) and PEG PLGA (Resomer RGP d 50155) used for preparation of PEGylated NPs was 1:1.

Characterization of NPs

The mean particle diameter and width of the particle distribution (polydispersity index) were determined by photon correlation spectroscopy using a Zetasizer Nano ZS (Malvern Instruments, Worcestershire, UK). Particle charge was quantified as ζ-potential by laser Doppler anemometry using a Zetasizer Nano ZS (Malvern). Freeze-dried NPs were dispersed in 10% FBS solution in phosphate buffered saline (PBS) prior to measurement. All measurements were made in triplicate.

The total amount of temoporfin entrapped in NPs was measured by fluorescence spectroscopy after complete dissolution of the NPs in DMSO. The temoporfin fluorescence (λ

excitation 423 nm, λ emission 652 nm) was recorded on a Tecan Safire[2] and compared with the corresponding standard curve.

Photophysical characterization

The measurements of absorption spectra, fluorescence emission spectra and fluorescence lifetimes are shown in SUPPLEMENTARY MATERIAL, see online: www.futuremedicine.com/doi/suppl/10.2217/NNM.11.130.

Release of temoporfin from NPs

PEGylated and bare freeze-dried PLGA NPs loaded with temoporfin were dispersed in PBS containing 10% FBS. The samples were incubated at 37°C (to mimic cell culture conditions) for 1–24 h then centrifuged for 20 min at 50,000 × g using a Thermo Scientific Sorvall® WX100 ultracentrifuge with rotor F50L-24 × 1.5 ml. After ultracentrifugation, the supernatants were removed and DMSO was added to dissolve the temoporfin-loaded NPs. Temoporfin fluorescence (λ excitation 423 nm, λ emission 652 nm) was recorded on Tecan Safire® and compared with the corresponding standard curve.

Cellular uptake of temoporfin

A549 and MCF10A neoT cells (1×10^5) were seeded in 24-well culture plates with appropriate medium and grown to confluence. U937 (4×10^5 cells/ml of medium) were differentiated with 50 nM phorbol 12-myristate 13-acetate (Sigma, MO, USA) for 24 h to induce macrophage-like properties and attached on a polystyrene plate [22]. Cells were washed with PBS and incubated for 4 h and 24 h with 0.5 or 1 µM temoporfin, respectively, delivered by NPs in culture medium supplemented with 10% FBS. Cells were then washed twice with PBS to remove NPs not internalized by the cells, detached from plates and immediately analyzed by flow cytometry (4-h and 24-h time points). Additional samples were washed and incubated in NP-free medium for an additional 20 h or 24 h (4 + 20 h and 24 + 24 h time points). The mean fluorescence intensity (MFI) of a population of 1×10^4 cells was determined using a FACSCalibur (Becton Dickinson, CA, USA). An argon ion laser at 488 nm was used for excitation, and fluorescence emission was measured at 670 nm (FL-3 detector).

Intracellular localization of temoporfin

The intracellular localization of temoporfin delivered by PEGylated PLGA NPs was assessed by fluorescence microscopy, taking advantage of temoporfin's red fluorescence. For these experiments 3×10^4 MCF10A neoT cells were seeded in a 24-well cell culture plate containing glass coverslides. After 1, 3, 6 and 10 h incubation, cells were washed using PBS and then fixed with 4% paraformaldehyde in PBS (pH 7.4) for 30 min. After washing with PBS, ProLong Antifade kit (Gibco, Invitrogen) was mounted on dried coverslides and allowed to dry overnight at 4°C. Labeling of cells with markers of subcellular structures was performed separately. For labeling of the Golgi apparatus, cells were fixed with 4% paraformaldehyde in PBS (pH 7.4) for 30 min and permeabilized with 0.1% Triton X-100 in PBS (pH 7.4) for 10 min. Nonspecific staining was blocked with 3% BSA in PBS (pH 7.4). The Golgi was labeled with primary rabbit polyclonal anti-GM130 antibody (Sigma) with a working concentration of 0.4 µg/ml in 3% BSA in PBS. After 2 h of incubation, cells were washed three-times with PBS and incubated with Alexa 488-labeled donkey anti-rabbit (2:1000, Molecular Probes®, Invitrogen) antibodies for 2 h. After washing with PBS, ProLong Antifade kit was mounted on dried coverslides and allow to dry overnight at 4°C. Endosomal and lysosomal labeling were performed using Organelle Lights™ Endosomes and Lysosomes (Gibco, Invitrogen), following the manufacturer's protocol. Fluorescence microscopy was performed at room temperature using an Olympus IX/81 inverted fluorescence microscope equipped with a Dapi/FITC/TxRed filter set (E0435016) and immersion oil was used as imaging medium. Images were analyzed using CellR Imaging software.

Dark cytotoxicity studies

The dark cytotoxicity of temoporfin-loaded PEG-PLGA NPs was evaluated in A549 cells using the MTS test (Promega Co., WI, USA) and compared with that of temoporfin in standard solution (Foscan). Cytotoxicity of empty PEGylated NPs was evaluated with both the MTS test and lactate dehydrogenase (LDH) assays. For both tests, A549 cells were seeded in 96-well plates (3×10^3 cells/well) in culture medium supplemented with 10% FBS. After 24 h, cells were incubated with fresh medium containing 3% FBS and increasing concentrations of empty or temoporfin-loaded PEG-PLGA NPs or Foscan. The cells were incubated in the dark for 24 h and cell viability was then measured with the MTS test, as well as after an additional 24 h during which the cells were kept in

Table 1. Particle size, polydispersity index and ζ-potential of temoporfin-loaded poly-(D,L-lactide-co-glycolide) and polyethylene glycol–poly-(D,L-lactide-co-glycolide) nanoparticles.

Formulation	Particle size (nm)	PI	ζ-potential (mV)	Temoporfin loading (%, weight/weight)
PLGA NPs	179.0 ± 0.3	0.27 ± 0.01	-5.5 ± 0.4	6.90
PEG-PLGA NPs	144.7 ± 2.0	0.13 ± 0.01	-2.5 ± 1.1	6.70

NP: Nanoparticle; PEG: Polyethylene glycol; PI: Polydispersity index; PLGA: Poly-(D,L-lactide-co-glycolide).

temoporfin-free medium containing 10% FBS in the dark (24 + 24 h). For the MTS assay, the cell medium was replaced with 100 µl of serum-free medium and 20 µl of CellTiter 96® Reagent (Promega Co.) and the wells were incubated for 1.5 h at 37°C. The absorbance at 492 nm was measured with a Biotrack II (GE Healthcare, Little Chalfont, UK) visible plate reader, and the survival of the treated cells expressed as a percentage of the absorbance of the untreated control, which was set to 100%. The activity of the LDH released in the culture medium during incubation of the cells with empty PEG-PLGA NPs for 24 h was measured according to the manufacturer's instructions (Promega Co.). This, and the activity of the total cellular LDH content, were measured in order to calculate the percentage of enzyme released during the treatment.

Photocytotoxicity studies (PDT) *in vitro*

The phototoxic effects of temoporfin loaded in PEG-PLGA NPs or dissolved in the standard solution (Foscan) were evaluated using carcinoma A549 cells. Cells were seeded in 96-well plates and incubated for 24 h at 37°C in the dark with temoporfin concentrations from 0.25–1.5 µM, which were not toxic without light activation. After incubation, the cells were washed twice with PBS containing Ca^{2+} and Mg^{2+}, and irradiated in PBS with 0.24 J/cm^2 of red light (600–700 nm) emitted from a Waldmann PDT 1200 lamp (Waldmann Medizintechnik, Schwenningen, Germany). The fluence rate at the level of the cell monolayer was 12 mW/cm^2 as measured with a radiometer IL 1700 (International Light, MA, USA). Immediately after irradiation, PBS was replaced with fresh medium containing 10% FBS and the cells were incubated in the dark at 37°C. Cell viability was determined with the MTS test after an additional 24 h. Using the same protocols, irradiation experiments were also performed with cells incubated with empty PEG-PLGA NPs at doses equivalent to those loaded with temoporfin, to exclude any light-induced toxic effect in the presence of the nanovehicle alone.

HCT116-luc xenograft mouse model

Animal experiments were approved by the local Committee for Research and Animal Ethics in compliance with the law on experimental animals. Ten-week-old male Hsd:Athymic nude-Foxn1 mice were purchased from Harlan (Horst, The Netherlands). Mice were housed in individually ventilated cages and fed *ad libitum* with an alfalfa-free diet and sterilized water. Twelve mice were subcutaneously inoculated with 5 × 10^6 HCT-116-luc cells in 100 µl PBS supplemented with matrigel (1:1). Tumor growth was monitored by bioluminescence imaging.

Bioluminescence & fluorescence imaging

Bioluminescence imaging was performed using the IVIS® Spectrum Imaging System (Xenogen,

Table 2. Fluorescence lifetimes of PEGylated and non-PEGylated poly-(D,L-lactide-co-glycolide) nanoparticles in phosphate-buffered saline or dimethyl sulfoxide, together with pre-exponential factors.

Formulation	τ_1 (ns)	A_1 (%)	τ_2 (ns)	A_2 (%)
PLGA in PBS	6.2	67	2.3	32
PEG-PLGA in PBS	3.2	27	1.4	73
Temoporfin in DMSO	9.6	100	–	–
PLGA in DMSO	9.5	100	–	–
PEG–PLGA in DMSO	9.5	100	–	–

τ: Fluorescence lifetime; A: Pre-exponential factor; DMSO: Dimethyl sulfoxide; PBS: Phosphate-buffered saline; PEG: Polyethylene glycol; PLGA: Poly-(D,L-lactide-co-glycolide).

CA, USA) every other day until day 10, after which imaging was performed daily. Ten minutes prior to imaging, animals were injected intraperitoneally with D-luciferin (25 mg/ml; Xenogen). Imaging of animals was performed under general anesthesia (2.5% isoflurane in oxygen). First, a gray-scale reference photo was taken of the animal from the lateral side. Bioluminescence images were acquired using the following settings: integration time 1 s; binning factor 8; field of view 21.2; and f/stop 1 open filter. Living Image 3.1 software (Xenogen) was used for data analysis and to create a pseudo-color image representing light intensity (blue: low intensity; red: high intensity). Bioluminescence images were quantified in radiance (photons/s/cm^2/sr) for reliable comparisons between the various images.

After reaching a tumor size of 0.5 cm^3, corresponding to radiation of 10^9 photons/s/cm^2/sr, mice were assigned randomly into four groups of three animals each. In each group, animals were injected in the penile vein with 100 µl PBS or 100 µl of a specified temoporfin formulation. A total of 0.3 mg of temoporfin/kg bodyweight was used to ensure a detectable fluorescence signal in a new *in vivo* imaging model. Animals were injected with PBS (group 1), Foscan (group 2), PLGA NPs (group 3) and PEGylated PLGA NPs (group 4).

After injection, fluorescence imaging was performed every 24 h for 4 days using the following settings: integration time 1 s; binning factor 8; field of view 21.2; f/stop 2; lamp level high; excitation filter 430 nm; and emission filter 660 nm. After imaging at t = 96 h, the animals were terminated. Subsequently, tumor, liver, spleen, kidney, muscle, lungs, heart, bladder, skin and colon were surgically procured. Fluorescence was quantified in the harvested tumors and the separate organs.

Statistical analysis

The SPSS PC software (Release 13.0) was used for the statistical analysis of all of the data. The differences between the groups were evaluated using Student's t-test. $p < 0.05$ was considered to be statistically significant.

Results

Preparation & characterization of temoporfin-loaded NPs

Polymeric NPs loaded with temoporfin were formed by the nanoprecipitation method and their physicochemical parameters, such as mean diameter, size distribution and ζ-potential, were determined (Table 1). The ζ-potential was significantly more negative for PLGA NPs compared with PEGylated PLGA NPs ($p < 0.05$), indicating the presence of a larger number of free carboxyl groups on the PLGA NP surface than on the PEGylated PLGA NPs, which, in addition, have uncharged PEG chains on their surface. The particle size of PLGA NPs was larger than that of PEGylated PLGA NPs, probably due to the incorporation of more hydrophilic PEG chains in the hydrophobic PLGA polymer. Covalently linked hydrophilic PEG blocks changed physicochemical properties of PLGA polymer enabling formation of smaller particles. Both NP formulations showed low polydispersity index and low negative surface charge. Low surface charge of NPs indicates low stability, resulting in aggregation and sedimentation of NPs from the aqueous dispersion. Therefore, to obtain long-term stable NP samples, the dispersions were freeze-dried and NPs were redispersed in suitable medium prior to the *in vitro* or *in vivo* experiments.

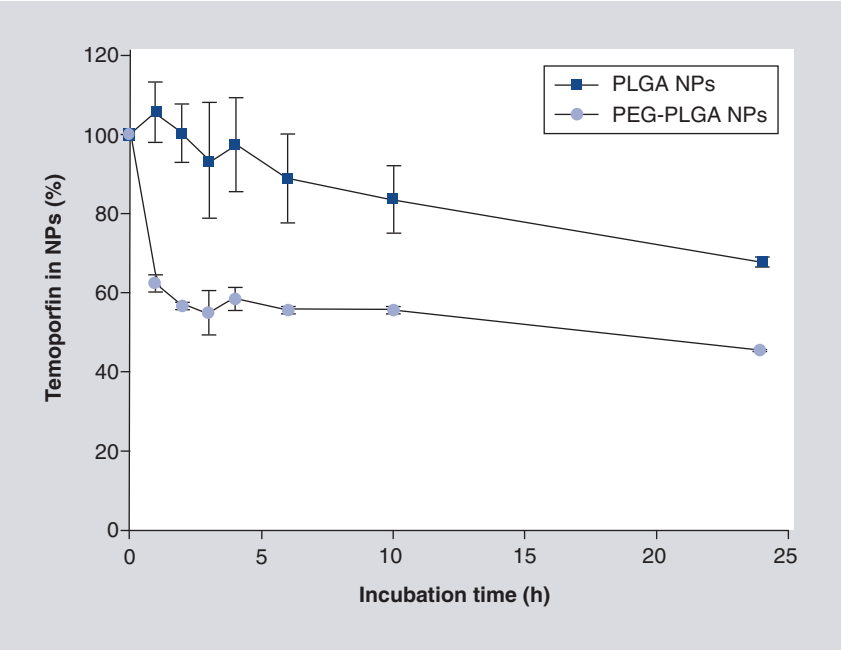

Figure 1. The release of temoporfin from polyethylene glycol-poly-(D,L-lactide-co-glycolide) and poly-(D,L-lactide-co-glycolide) nanoparticles. The percentage of loaded temoporfin left in NPs after 1, 2, 3, 4, 6, 10 and 24 h incubation in phosphate-buffered saline with 10% fetal bovine serum. Temoporfin retained in NPs was measured after ultracentrifugation and dissolution of NPs in dimethyl sulfoxide.
NP: Nanoparticle; PEG: Polyethylene glycol; PLGA: Poly-(D,L-lactide-co-glycolide).

Fluorescence properties of temoporfin-loaded NPs

The fluorescence emission spectra and lifetimes were recorded for NP stock solutions diluted in PBS (pH 7.4), in comparison to the same sample

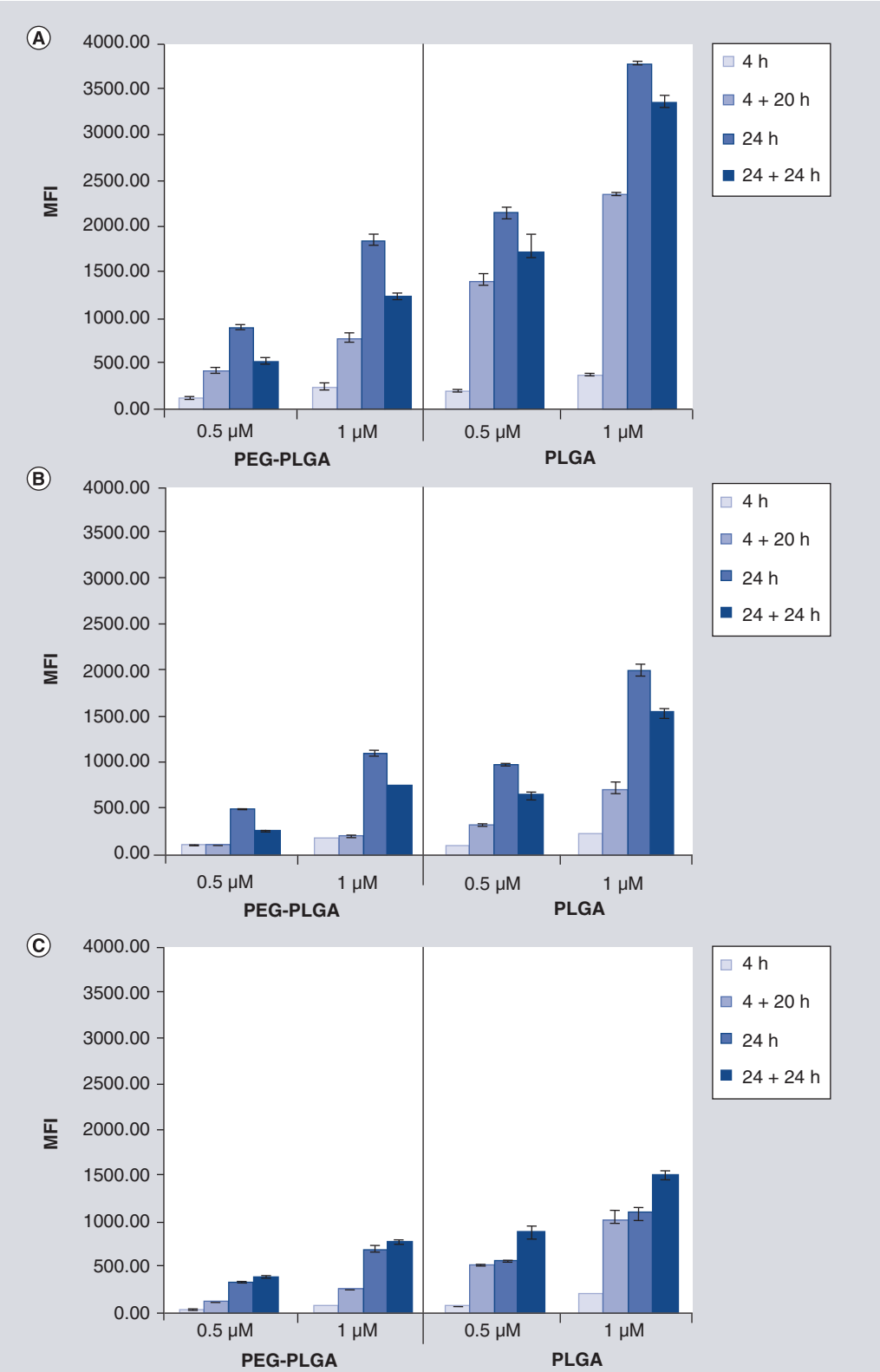

Figure 2. Cellular uptake of temoporfin-loaded nanoparticles. Uptake of temoporfin-loaded PEGylated and non-PEGylated PLGA nanoparticles by **(A)** MCF10A neoT, **(B)** A549 and **(C)** differentiated U937 cells. Cells were treated with 0.5 or 1 µM temoporfin delivered by nanoparticles for 4 and 24 h. After incubation, the cells were washed and fresh nanoparticle-free medium was added for an additional 20 h (4 + 20 h) and 24 h (24 + 24 h).
MFI: Mean fluorescence intensity; PEG: Polyethylene glycol; PLGA: Poly-(D,L-lactide-co-glycolide).

dissolved in DMSO at an equivalent temoporfin concentration. SUPPLEMENTARY FIGURE 1 shows the fluorescence emission spectra recorded for the NP solutions diluted at the same concentrations in PBS versus DMSO. For both the PEGylated and non-PEGylated PLGA NPs, much lower fluorescence intensities were noted for the PBS solutions compared to DMSO solutions, by factors of 21 and 11, respectively. Likewise, a significant change in fluorescence lifetimes was observed between the two solvents, as shown in TABLE 2. In DMSO, mono-exponential decays with identical lifetimes (within experimental error) were observed for all samples. In PBS, multiexponential decays with significantly shorter lifetimes were observed for both the PEGylated and non-PEGylated NPs in comparison to DMSO solutions of the NPs. Using bi-exponential fitting, the lifetimes of the PEGylated NPs in PBS (3.2 and 1.4 ns) were shorter than for the non-PEGylated NPs. Temoporfin itself is insoluble in PBS and so no lifetime data are given.

Release of temoporfin from the NPs

Temoporfin is noncovalently entrapped inside the copolymeric matrix and partially bound to the NP surface, and therefore its binding to serum proteins is possible only after its release from the NPs. Temoporfin still present in NPs was separated from the released temoporfin by ultracentrifugation and quantified. Results showed sustained release of temoporfin from PLGA NPs. After 1 h no significant change was observed, whereas after 24 h 68 ± 1% of temoporfin was still present in NPs ($t = 0$ vs 24 h; $p < 0.001$) (FIGURE 1). PEGylated PLGA NPs showed faster release of the drug immediately after incubation with serum proteins, after 1 h incubation 62 ± 2% of the temoporfin was present in NPs ($t = 0$ vs 1 h; $p < 0.05$). Release then became slower, with 45% of temoporfin still present in NPs after 24 h ($t = 0$ vs 24 h; $p < 0.001$).

Cellular uptake of temoporfin-loaded NPs

Cellular uptake of temoporfin-loaded NPs was evaluated by flow cytometry in A549, MCF10A neoT and differentiated U937 cells at four time points (FIGURE 2). MCF10A neoT cells internalized larger amounts of drug than the other cell lines, especially following delivery with PLGA NPs ($p < 0.05$). Moreover, the uptake of temoporfin was significantly increased ($p < 0.05$) when delivered by PLGA NPs compared with PEGylated PLGA NPs in all cell lines at 4 and 24 h.

Differences between the single time points were the most obvious at 24 and 24 + 24 h. The MFI of temoporfin in U937 cells at 24 + 24 h was greater than at the 24 h time point ($p < 0.01$), except in the case of the epithelial cell lines A549 and MCF10A neoT, most probably because the differentiated U937 cells are not able to proliferate. Another major difference between A549 and MCF10A neoT cells and promonocytic U937 cells concerns the internalization rate of PLGA NPs. The MFI of temoporfin in U937 cells was almost identical at 4 + 20 h and 24 h ($p > 0.05$), while in the epithelial cell lines a significant difference was observed between these two time points ($p < 0.001$).

The data obtained from experiments with U937 cells can be useful in clarifying the fate of PLGA NPs after their cellular uptake. An increase in temoporfin MFI was observed in U937 cells, even after cell washing with PBS and incubation in NP-free medium (4 + 20 h, 24 + 24 h time points), indicating continuous intracellular degradation of the PLGA matrix. Furthermore, the degradation of PEGylated NPs was significantly lower than that of PLGA NPs in all the selected cell lines.

Internalization of temoporfin-loaded NPs depends on the PEGylation of the NPs. The ratio between the MFI for PLGA NPs and PEGylated PLGA NPs (PLGA/PEG-PLGA ratio) [23] clearly shows a lower uptake of PEGylated PLGA NPs than the non-PEGylated version in all the tested cell lines after 4 and 24 h of incubation (FIGURE 3). U937 cells exhibit the highest MFI PLGA/PEG-PLGA ratio

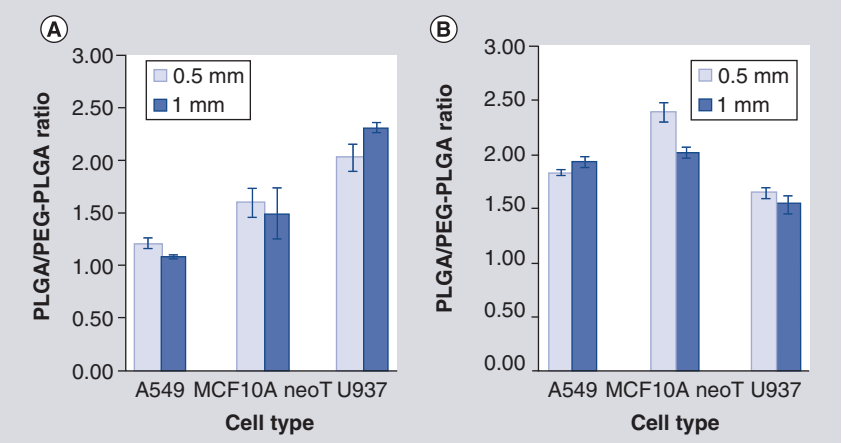

Figure 3. The effect of PEGylation on the cellular uptake of nanoparticles. Ratio of the mean fluorescence intensities of PLGA nanoparticles (NPs) and PEGylated PLGA NPs (PLGA/PEG-PLGA ratio) indicating the stealth properties of PEGylated PLGA NPs. Ratio after 4 h **(A)** and 24 h **(B)** of cell treatment with temoporfin-loaded NPs. The values were calculated from mean fluorescence intensitys presented in FIGURE 2.
PEG: Polyethylene glycol; PLGA: Poly-(D,L-lactide-co-glycolide).

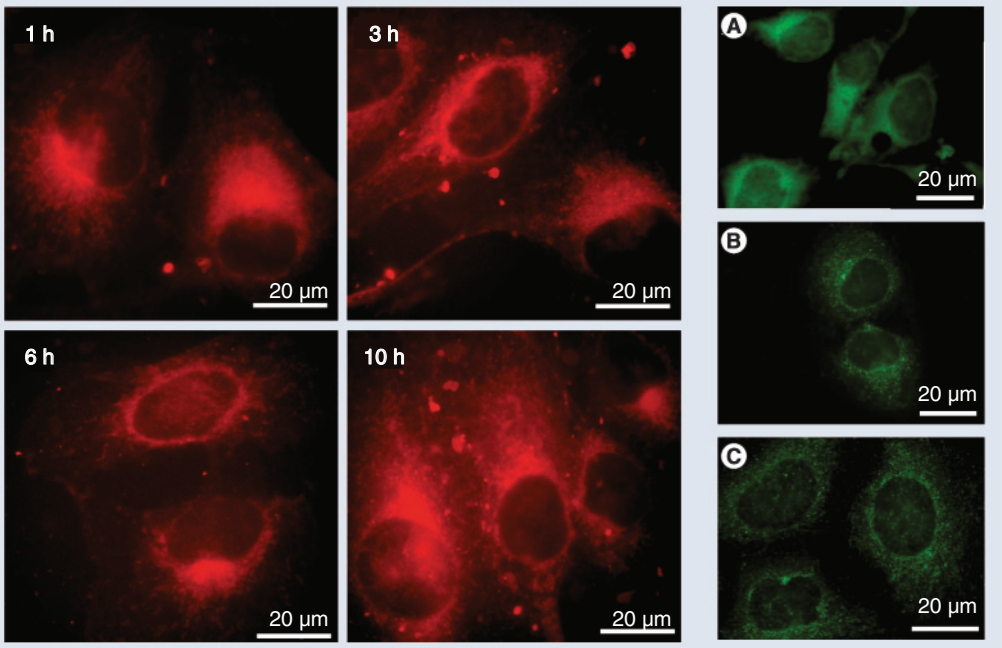

Figure 4. Localization of temoporfin-loaded PEGylated poly-(D,L-lactide-co-glycolide) nanoparticles in MCF10A neoT cells (red fluorescence). Cells were incubated with 50 µg /ml of nanoparticles in cell medium supplemented with 10% fetal bovine serum for 1, 3, 6 and 10 h (left panel). Separately, Golgi **(A)** was labeled with anti-GM130 antibody (Sigma, MO, USA) using Alexa 488-labeled donkey anti-rabbit (Gibco, Invitrogen, CA, USA) IgG as secondary antibody. Endosomes **(B)** and lysosomes **(C)** were labeled with Organelle Lights™ (Molecular Probes, Invitrogen). Scale bars represent 20 µm.

after 4 h of incubation ($p < 0.05$), followed by MCF10A neoT cells, while the ratio is barely above one for A549 cells. After 24 h of incubation, the PLGA/PEG-PLGA ratio decreases in U937 cells ($p < 0.01$), while in A549 ($p < 0.001$) and MCF10A neoT ($p < 0.05$) cells the ratio increases significantly compared with the 4-h time point.

Intracellular localization of temoporfin-loaded PEGylated PLGA NPs

Localization of temoporfin-loaded PEGylated PLGA NPs in MCF10A neoT cells was visualized using fluorescence microscopy after 1, 3, 6 and 10 h incubation. After 1 h of incubation, the red fluorescence corresponding to the internalized temoporfin was distributed throughout the cell cytoplasm (Figure 4). However, it was more intense in regions corresponding to the endoplasmic reticulum and Golgi apparatus, as previously reported [24]. On incubation of cells for 3, 6 and 10 h, increasing numbers of red spots appeared, corresponding to accumulated temoporfin or temoporfin-loaded NPs in lysosomal–endosomal compartments. Similar intracellular localization was reported for PLGA NPs [25].

Dark cytotoxicity of empty & temoporfin-loaded PEGylated PLGA NPs

Empty PEGylated PLGA NPs did not affect the survival of A549 cells exposed to NP concentrations up to 100 µg/ml for 24 h, much higher than those used to deliver the highest temoporfin concentration of 5 µM used in our experiments. The MTS assay showed that the number of metabolically active cells at 24 and 24 + 24 h after exposure to NPs was not reduced relative to controls (Figure 5A). The biocompatibility of the empty nanocarrier was confirmed by the LDH assay, which showed no increase in the cytosolic enzyme in the medium of cells exposed to NPs. Only 6.2 ± 1.1% of LDH was measured in the culture medium of A549 cells exposed to 100 µg/ml of empty PEGylated NPs, which was not different from the 7.8 ± 1% measured in untreated cells.

The dark cytotoxicity of temoporfin in concentrations up to 5 µM loaded in PEGylated PLGA NPs was evaluated and compared with temoporfin delivered as Foscan in the standard solution (Figure 5B). The MTS assay showed no decrease in survival of A549 cells at the end of the 24 h incubation with temoporfin-loaded PEGylated PLGA NPs. However, a decrease in

cell survival was observed with temoporfin at concentrations above 3 µM after 24 h of NP exposure and the additional 24 h of cell incubation in NP-free medium (24 + 24 h). In any case, the dark toxicity of temoporfin delivered as Foscan was much greater than that of temoporfin delivered by PEGylated PLGA NPs at both investigated time points. At concentrations above 2 µM Foscan was highly cytotoxic and the cell survival was reduced to 10–20% at 5 µM. Concentrations of 0.5 and 1 µM temoporfin used in other experiments are therefore below the threshold of dark toxicity of all temoporfin formulations.

Phototoxicity studies of empty & temoporfin-loaded PEGylated PLGA NPs

Phototoxicity studies were carried out with A549 cells preincubated with empty PEGylated PLGA NPs, temoporfin-loaded PEGylated PLGA NPs and with Foscan standard solution. The cells, preincubated for 24 h in the dark, were irradiated with a light dose of 0.24 J/cm^2. As shown in Figure 6, the reduction in cell survival measured 24 h after irradiation was dependent on temoporfin dose, but was similar for both temoporfin formulations. To assess whether the comparable phototoxic effect correlated with a similar intracellular drug concentration at the time of irradiation, the amount of temoporfin internalized by the cells was determined by flow cytometry. Surprisingly, the results showed that the cellular uptake of free temoporfin was significantly higher than when delivered by PEGylated PLGA NPs. In fact, by expressing the uptake as the ratio between the MFI for Foscan standard solution and temoporfin loaded in PEGylated PLGA NPs, we found ratio values of 2.2 and 2.3 for 0.5 and 1 µM temoporfin, respectively.

The empty PEGylated PLGA NPs exhibited no cytotoxic effects on cells after irradiation, confirming that they are photochemically inert and, therefore, any contribution of the drug delivery system to the phototoxic effect of temoporfin-loaded PEGylated PLGA NPs can be ruled out.

In vivo distribution of temoporfin

Total body fluorescence of mice (Figure 7) indicates no significant difference between temoporfin-loaded PLGA and PEGylated PLGA NPs at 24h postinjection. At this time point, the fluorescence was significantly lower ($p < 0.01$) for

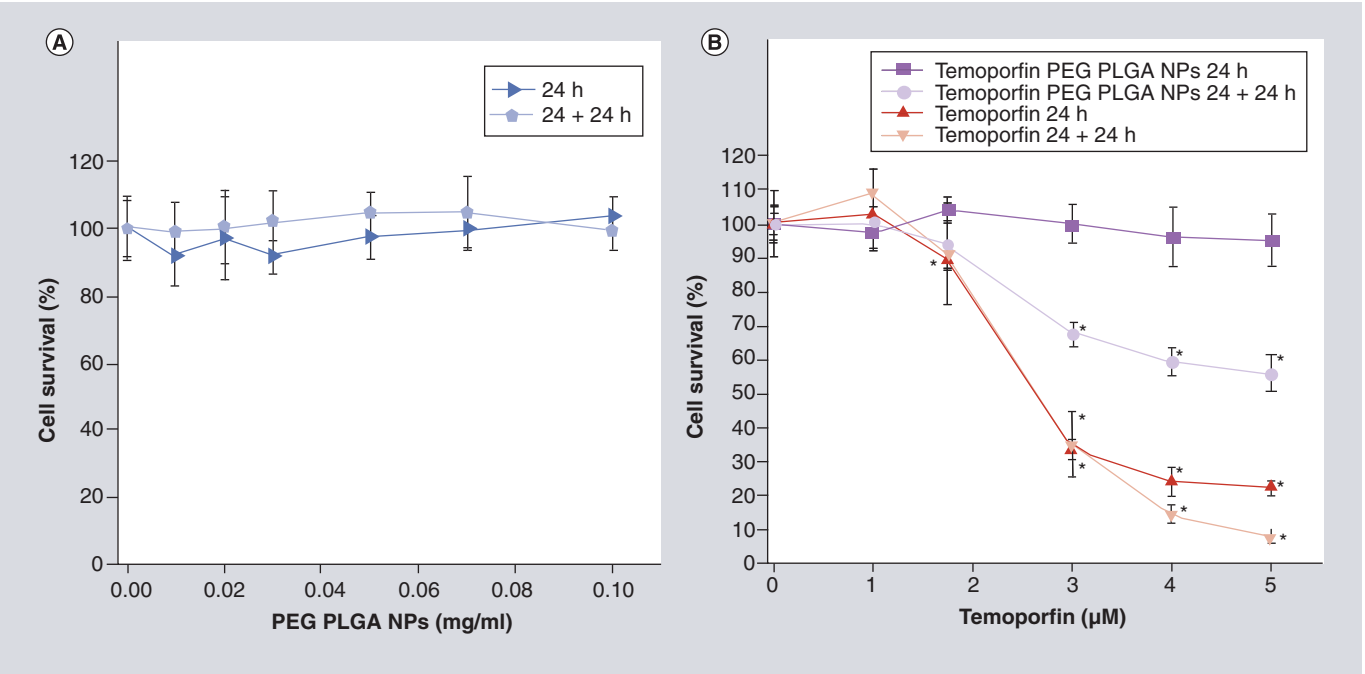

Figure 5. Dark cytotoxicity of empty and temoporfin-loaded PEGylated poly-(D,L-lactide-co-glycolide) nanoparticles in A549 cells. (A) Viability of cells incubated in the dark with increasing doses of empty nanoparticles for 24 h (24 h) and for 24 h and an additional 24 h in NP-free medium (24 + 24 h). **(B)** Dark cytotoxicity of temoporfin-loaded NPs compared with that of temoporfin in the standard solution (Foscan®, Biolitec AG [Jena, Germany]) after 24 h or 24 + 24 h of incubation. Viabilities are expressed as mean percentages ± standard deviation (n = 9) relative to control cells.
*$p < 0.001$ vs controls (t-test).
NP: Nanoparticle; PEG: Polyethylene glycol; PLGA: Poly-(D,L-lactide-co-glycolide).

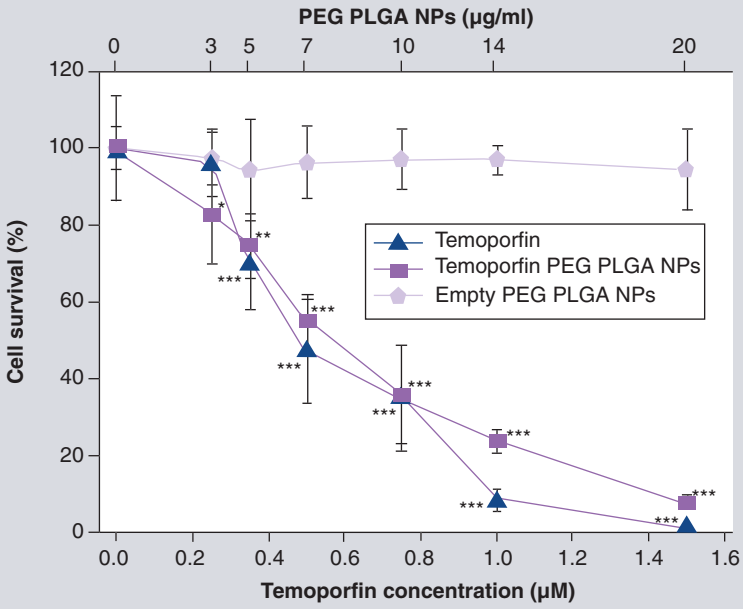

Figure 6. Dose-response curves after photodynamic therapy in A549 cells preincubated for 24 h with temoporfin in PEGylated poly-(D,L-lactide-co-glycolide) nanoparticles or as Foscan® (Biolitec AG [Jena, Germany]) and then irradiated with 0.24 J/cm² of red light. Viability was also evaluated in cells incubated for 24 h with empty PLGA NPs at the same concentrations as used for the delivery of temoporfin and irradiated. Data are expressed as mean percentages ± standard deviation (n = 6) with respect to untreated and nonirradiated control cells.
*p < 0.05; **p < 0.01; ***p < 0.001 vs controls (t-test).
NP: Nanoparticle; PEG: Polyethylene glycol; PLGA: Poly-(D,L-lactide-co-glycolide).

both nanoparticulate systems than for Foscan, and remained so until the end of the experiment at 96 h postinjection. Overall body fluorescence showed time-dependent increases for both PLGA NPs and PEGylated PLGA NPs during a 96 h follow-up (Figure 8). Mouse organs were harvested 96 h postintraperitoneal injection of temoporfin formulations, and scanned for temoporfin fluorescence (Figure 9). The data have been normalized using the IVIS imaging software. Fluorescence of each tissue sample taken is indicated as a percentage of the sum of fluorescence of all organs evaluated, which was set at 100%. The highest levels for all three formulations were observed in the skin, followed by tumor and bladder tissue. However, different levels can partially be due to different optical properties of tissues. In all the tissues, the fluorescence of temoporfin was higher when delivered by PEGylated PLGA NPs than by PLGA NPs, although the difference was not statistically significant. Interestingly, delivery of temoporfin to colon tissue was higher with PEGylated and PLGA NPs than Foscan (Foscan to PLGA NPs; p = 0.007; Foscan to PEGylated PLGA NPs; p = 0.058). In lung tissue, the concentration of temoporfin was higher when delivered by PLGA NPs than Foscan and PEGylated PLGA NPs (Foscan to PLGA NPs; p = 0.006; PLGA NPs to PEGylated PLGA NPs; p = 0.038). The skin uptake of the drug, which results in skin photosensitivity, appeared lower for the NPs; however, this was not significantly different from Foscan, as shown in Figure 9.

Discussion

The use of NPs as drug delivery systems can significantly improve the distribution of the PS for PDT and the efficacy of the treatment in cancer patients. In this study, we formulated PLGA NPs with incorporated PS temoporfin. The average particle size of 150 nm enables NP accumulation at the tumor site by the enhanced permeability and retention effect [26] and their internalization in tumor cells. PEG chains bound to the surface of PLGA NPs did not significantly change the physical properties of the delivery system; however, PEGylation may prolong the retention time in the blood stream. The PEG chains prevent the adhesion of opsonins present in the blood serum to the NPs surface, making the surface of the NP unrecognizable by the mononuclear phagocyte system [18].

In the present study, we showed that PEGylation of PLGA NPs did not significantly affect the loading of temoporfin to the polymeric matrix. The monomeric form of porphyrin-based PSs, including temoporfin, is well known to possess more advantageous fluorescence properties (in terms of longer fluorescence lifetimes) and higher triplet state yields, and thus higher photodynamic efficiency than the aggregates [27]. PSs entrapped inside PLGA NPs were suggested to form aggregates that dissociate to monomeric forms after their release from the NPs and transfer to plasma proteins [16]. Furthermore, the PS release from NPs and its activity were shown to be controlled by the NP size, composition and surface properties [28]. The fluorescence emission and lifetime data shown in Supplementary Figure 1 & Table 2 indicate that temoporfin fluorescence is strongly quenched in NPs, in comparison to monomeric temoporfin. This comparison was achieved by dissolving the NPs in DMSO to induce release of the temoporfin in monomeric form, which resulted in a large increase in fluorescence intensity and lifetime. These results are consistent with the occurrence of fluorescence self-quenching due to aggregation of the temoporfin within the intact NPs. The degree of quenching appeared to be greater for the PEGylated NPs, despite the comparable temoporfin loading, which could be explained by

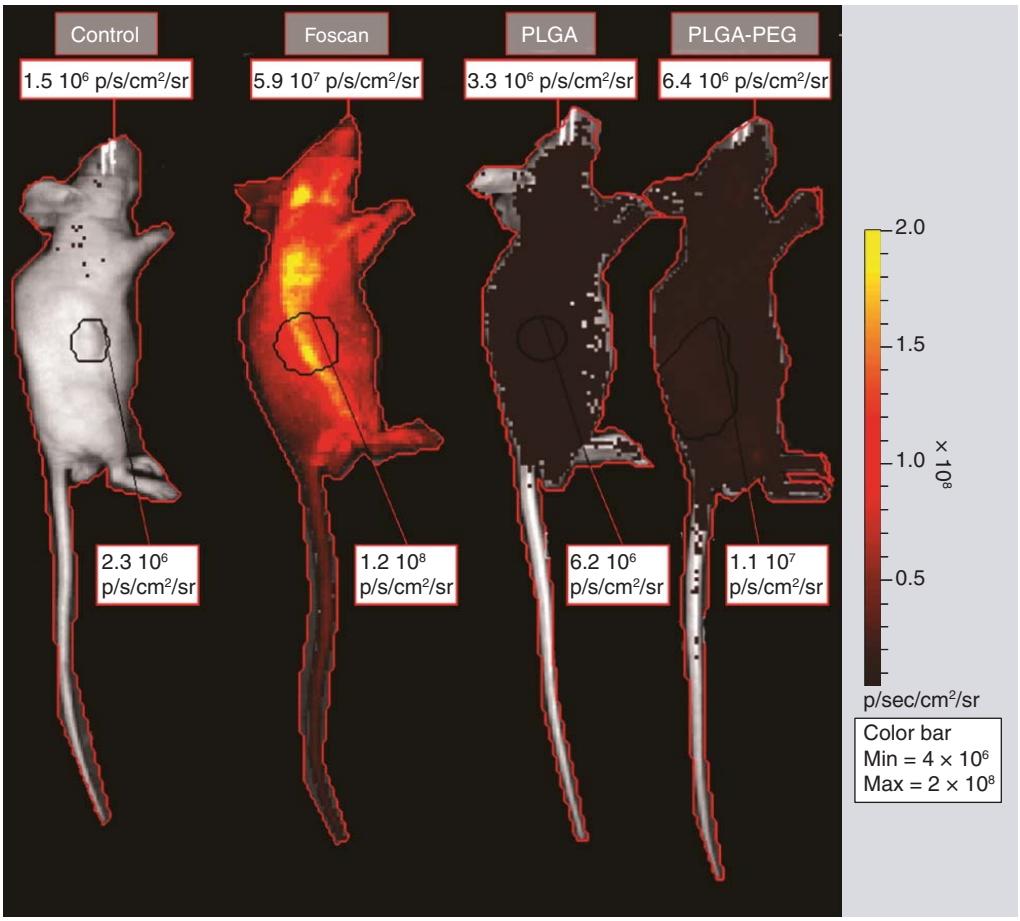

Figure 7. Total body fluorescence of mice 24 h postinjection with phosphate-buffered saline (control), Foscan® (Biolitec AG [Jena, Germany]), poly-(D,L-lactide-co-glycolide) nanoparticles and PEGylated poly-(D,L-lactide-co-glycolide) nanoparticles loaded with temoporfin. The total body fluorescence values are presented in upper inserts and the fluorescence localized to tumors in lower inserts.
PEG: Polyethylene glycol; PLGA: Poly-(D,L-lactide-co-glycolide).

their smaller size resulting in a higher local temoporfin concentration and thus greater propensity for aggregation. Similar fluorescence quenching effects are observed for temoporfin incorporated in liposomal membranes where the fluorescence lifetime was reduced to 1 ns, which was attributed to aggregation [28–30]. The other technique we could use would be absorption spectroscopy, but the spectral differences between the monomeric and dimerized forms are less easy to interpret.

It was shown that temoporfin can readily be released from PLGA NPs when reaching tumors and it was demonstrated that it is able to associate with various serum protein fractions [31,32]. Therefore, we may expect that, when delivered to the site of action, temoporfin is monomerized, a form that is preferable for effective PDT. When PLGA NPs were resuspended in cell culture medium containing serum proteins, most of the temoporfin remained entrapped inside NPs after 1 h of incubation and was released at the rate of degradation of the polymer. On the other hand, more than 30% (weight/weight) of temoporfin was immediately released from PEGylated PLGA NPs after incubation in medium containing serum proteins. This burst release could be a consequence of the temoporfin fraction that was adsorbed on the NP surface and released immediately to the medium due to incompatibility with the hydrophilic PEG chains on the surface of PEGylated PLGA NPs. The difference in release profiles of temoporfin from these two delivery systems could also result in different time courses of temoporfin-dependent total body fluorescence in mice. Again, temoporfin released from PLGA NPs revealed a continuous increase until reaching the 96-h time point, whereas peak temoporfin release from PEGylated PLGA NPs was at 48 h (FIGURE 8).

The availability and photo-activity of the intracellular temoporfin delivered by PEGylated PLGA NPs is dependent on its monomerization, which follows the degradation of the polymer

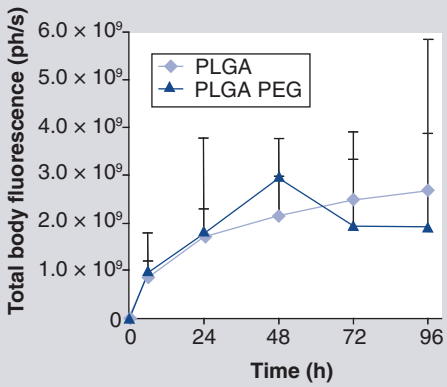

Figure 8. Time-dependent total body fluorescence of temoporfin delivered by poly-(D,L-lactide-co-glycolide) nanoparticles or PEGylated poly-(D,L-lactide-co-glycolide) nanoparticles.
PEG: Polyethylene glycol; PLGA: Poly-(D,L-lactide-co-glycolide).

and the release of the temoporfin from NPs. The dissociation may occur before or after the cellular uptake of NPs, and temoporfin released from NPs prior to internalization may also contribute to intracellular activity, if internalized. On the other hand, cell division continuously decreases the intracellular concentration of temoporfin [24]. We have shown that the intracellular monomerization of temoporfin delivered by PLGA NPs is a preferred process in all cell lines studied. During the first 24 h of incubation, temoporfin fluorescence increased. The effect was lower because of cell division, in particular in MCF10A neoT and A549 cells, whereas in differentiated U937 cells the fluorescence increased, even up to 24 + 24 h (Figure 2). The PEGylation of NPs significantly decreased the rate of temoporfin intracellular monomerization, probably due to its faster release into the cell medium, lower internalization or slower intracellular degradation of PEGylated PLGA NPs. The effect of PEGylation on cellular uptake can be deduced by evaluating the PLGA/PEG-PLGA ratio (Figure 3). In the first 4 h of incubation, the internalization of PEGylated PLGA NPs was significantly slower than that of PLGA NPs. The difference was particularly evident in U937 cells, indicating the ability of PEGylation to confer stealth properties on PLGA NPs, at least against this type of immune cell. This effect was less evident after 24 h incubation of cells with temoporfin-loaded NPs, probably due to the different extra- and intracellular release profiles of temoporfin from PEGylated and PLGA NPs. These results are consistent with previous studies reporting that PEGylation of PLGA NPs affects the uptake by monocytes during short incubation times, whereas prolonged incubation diminished the effect of PEGylation [23].

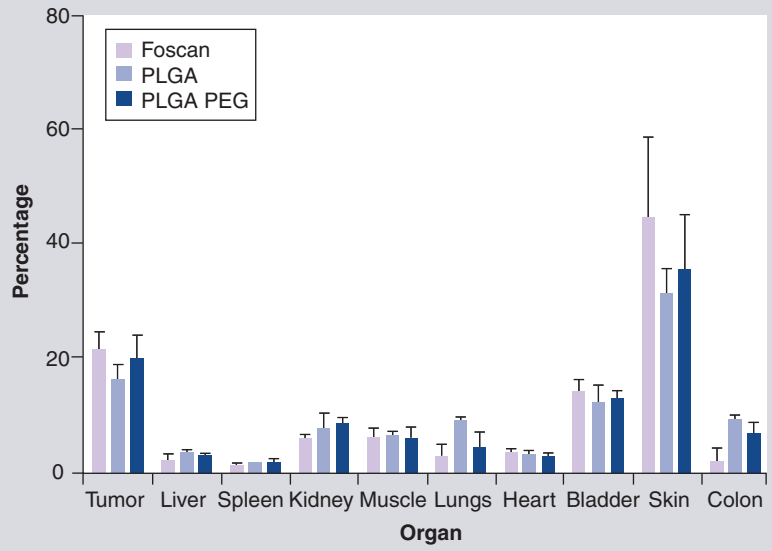

Figure 9. Relative fluorescence of temoporfin in individual organs expressed as the percentage of fluorescence of an organ to the total fluorescence of all organs harvested 24 h postinjection of temoporfin formulations.

The subcellular localization of the PS is one of the key factors governing the outcome of PDT, since it determines the primary sites of photoinduced damage [33]. The preferential sites of accumulation of temoporfin delivered as Foscan were the endoplasmic reticulum and Golgi apparatus, probably as a consequence of its internalization in a complex with serum proteins [24,34]. On the other hand, PLGA NPs are internalized by specific endocytotic processes, mostly through a clathrin-dependent pathway, targeting endosomal–lysosomal compartments [35,36]. Our results of temoporfin intracellular localization suggest two mechanisms of cell internalization when PEGylated PLGA NPs were used as a delivery system. First, temoporfin released from NPs prior to cell internalization binds to serum proteins and follows the same route as the internalization of temoporfin delivered as Foscan, accumulating in the Golgi apparatus and endoplasmic reticulum. By contrast, temoporfin incorporated in NPs is taken up by clathrin dependent endocytosis and is triggered to the endosomal and lysosomal compartments.

The PLGA copolymer is not cytotoxic [37,38] and the same holds for PLGA NPs in concentrations up to 5 mg/ml in A549 cells [36]. Similarly,

in the same cell line, we detected no cytotoxicity for empty PEGylated PLGA NPs at concentrations up to 0.1 mg/ml, both in the dark and after illumination with red light (Figures 5 & 6). Temoporfin-loaded PEGylated NPs showed a moderate dark cytotoxicity which was, however, significantly lower than that of temoporfin as Foscan (Figure 5). Thus, the incorporation of temoporfin into a nanocarrier reduces its dark cytotoxicity. Similarly, the dark cytotoxicity of temoporfin was demonstrated to be lower when loaded in PEGylated liposomes (Fospeg®, Biolitec AG) than in Foscan [39].

The photodynamic effectiveness of temoporfin delivered by PEGylated NPs was assessed by irradiation of A549 cells with red light (600–700 nm) and compared to that of temoporfin as Foscan. The *in vitro* phototoxic effect of the two formulations was similar, although the intracellular availability of temoporfin, as determined by flow cytometry, in cells incubated with temoporfin-loaded PEGylated NPs, was approximately 50% that of the cells incubated with Foscan. However, temoporfin delivered by PEGylated NPs can be completely converted to very photoactive monomers, which may compensate for the reduction in the uptake. Our result is consistent with those obtained by other groups, where incorporation of PS in PLGA NPs has been shown to enhance the photodynamic activity of the PS and give improved phototoxicity results compared with the free PS [16,40].

The distribution of temoporfin applied to mice loaded either in NPs or as Foscan was compared by fluorescence-based imaging. As expected, 24 h postinjection the total body fluorescence of temoporfin delivered by NPs was significantly lower than that delivered by Foscan, which can be accounted for by the delayed release of temoporfin from the PLGA matrix. At 96 h postinjection, the total body fluorescence reached steady levels for both NP formulations, indicating that, in this time period, most of the temoporfin was released from the PLGA NPs. The tissue distribution of temoporfin differed little between the delivery systems (Figure 9). The skin and the tumor uptake indicate that temoporfin loaded to PEGylated PLGA NPs results in a higher tumor-to-skin ratio than Foscan or PLGA NPs, thus limiting the side effects of the treatment [6]. Moreover, PEGylated PLGA NPs show decreased delivery of temoporfin into the lungs and colon than PLGA NPs, which could further reduce side effects in healthy tissues.

Conclusion

A stealth, biodegradable nanosystem has been developed for the systemic delivery and prolonged intracellular release of photodynamic agents for PDT. We demonstrated higher *in vitro* phototherapeutic effectiveness of temoporfin delivered by PEGylated NPs than in standard solution (Foscan). PEGylation significantly reduced the cellular uptake of NPs, especially by the differentiated promonocytic U937 cells, revealing the stealth properties of the delivery system. Importantly, the dark cytotoxicity of temoporfin in the PLGA formulation is substantially lower than that of Foscan, with the consequence that fewer side effects of PDT are envisaged by delivering temoporfin in PLGA NPs. Finally, temoporfin delivered *in vivo* by PEGylated PLGA NPs exhibits favorable tissue distribution to be used in PDT. The selectivity of the delivery system, and hence of PDT, could be further improved by binding biological molecules that specifically recognize tumor cells.

Future perspective

Toxicity of anti-tumor drugs should be limited to tumor cells and tissues with low adverse effects on other organs. PEGylated PLGA NPs enable more specific targeting of the PS temoporfin to tumor cells than the standard solution of temoporfin and may improve PDT of cancer patients. However, for effective tumor targeting, the nanoparticulate delivery system has to contain surface-bound ligands that specifically recognize tumor-associated molecules. Second, the process of preparation of temoporfin-loaded PEGylated PLGA NPs needs to be optimized in order to improve the stability and to prevent aggregation and sedimentation of NPs when dispersed in serum-like media. Finally, additional *in vivo* studies, testing the phototoxic effect of temoporfin are needed to confirm the advantage of new temoporfin formulation over existing studies.

Financial & competing interests disclosure

This research was supported by funding from the European Community's Seventh Framework Programme (FP7/20072-013) under grant agreement No.201031 NANOPHOTO, by the Slovenian Research Agency P4-0127 (J Kos), and the Dutch Cancer Society (RUG20073-784). The authors have no other relevant affiliations or financial involvement with any organization or entity with a financial interest in or financial conflict with the subject matter or materials discussed in the manuscript apart from those disclosed.

No writing assistance was utilized in the production of this manuscript.

Ethical conduct of research

The authors state that they have obtained appropriate institutional review board approval or have followed the principles outlined in the Declaration of Helsinki for all human or animal experimental investigations. In addition, for investigations involving human subjects, informed consent has been obtained from the participants involved.

Executive summary

Aim

- The aim of this study was to prepare a polyethylene glycol (PEG)ylated poly-(D,L-lactide-co-glycolide) (PLGA) nanoparticle (NP) delivery system loaded with temoporfin to be used in photodynamic therapy of cancer.

In vitro *characterization*

- The ζ potential was more negative for non-PEGylated PLGA NPs, indicating the presence of a larger number of free carboxyl groups on the PLGA NP surface than on the PEGylated PLGA NPs.
- Compared with non-PEGylated PLGA NPs, the PEGylation significantly reduced the cellular uptake of NPs by all selected cell lines, especially by the differentiated promonocytic U937 cells, revealing the stealth properties of the delivery system.
- Temoporfin delivered by PEGylated PLGA NPs was localized in the perinuclear region and in endosomal/lysosomal compartments.
- The dark cytotoxicity of temoporfin delivered by PEGylated PLGA NPs was less than that of free temoporfin in standard solution (Foscan® Biolitec AG [Jena, Germany]); however, the phototoxicity was not reduced.

In vivo *characterization*

- PEGylation of NPs influenced time-dependent total body fluorescence of temoporfin.
- The skin uptake of the drug, which results in skin photosensitivity, appeared to be lower for the NPs compared with Foscan.
- PEGylated PLGA NPs show decreased delivery of temoporfin into lungs and colon compared with PLGA NPs, which could further reduce side effects in healthy tissues.

Conclusion

- A stealth, biodegradable nanosystem with therapeutically favorable tissue distribution has been developed for the systemic delivery and sustained release of photodynamic agents for photodynamic therapy.
- The selectivity of the delivery system, and hence of photodynamic therapy, could be further improved by binding biological molecules that specifically recognize tumor cells.

References

Papers of special note have been highlighted as:
- ▪ of interest
- ▪▪ of considerable interest

1 Jori G. Tumour photosensitizers: approaches to enhance the selectivity and efficiency of photodynamic therapy. *J. Photochem. Photobiol. B.* 36(2), 87–93 (1996).

2 Levy JG. Photodynamic therapy. *Trends Biotechnol.* 13(1), 14–18 (1995).

3 Oleinick NL, Evans HH. The photobiology of photodynamic therapy: cellular targets and mechanisms. *Radiat. Res.* 150(5 Suppl.), 146–156 (1998).

4 Dougherty TJ, Gomer CJ, Henderson BW *et al.* Photodynamic therapy. *J. Natl Cancer Inst.* 90(12), 889–905 (1998).

5 Ball DJ, Vernon DI, Brown SB. The high photoactivity of m-THPC in photodynamic therapy. Unusually strong retention of m-THPC by RIF-1 cells in culture. *Photochem. Photobiol.* 69(3), 360–363 (1999).

6 Ris HB, Altermatt HJ, Inderbitzi R *et al.* Photodynamic therapy with chlorins for diffuse malignant mesothelioma: initial clinical results. *Br. J. Cancer* 64(6), 1116–1120 (1991).

7 Tan IB, Dolivet G, Ceruse P, Poorten VV, Roest G, Rauschning W. Temoporfin-mediated photodynamic therapy in patients with advanced, incurable head and neck cancer: a multicenter study. *Head Neck* 32(12), 1597–1604 (2010).

8 Hopper C, Kübler A, Lewis H, Tan IB, Putnam G. Temoporfin-mediated photodynamic therapy for early oral squamous cell carcinoma. *Int. J. Cancer* 111(1), 138–146 (2004).

9 Nathan TR, Whitelaw DE, Chang SC *et al.* Photodynamic therapy for prostate cancer recurrence after radiotherapy: a Phase I study. *J. Urol.* 168(4), 1427–1432 (2002).

10 Sibani SA, McCarron PA, Woolfson AD, Donnelly RF. Photosensitiser delivery for photodynamic therapy. Part 2: systemic carrier platforms. *Exp. Opin. Drug Deliv.* 5(11), 1241–1254 (2008).

11 Cegnar M, Kristl J, Kos J. Nanoscale polymer carriers to deliver chemotherapeutic agents to tumours. *Exp. Opin. Biol. Ther.* 5(12), 1557–1569 (2005).

▪ **Reviews polymeric carriers for the delivery of anti-tumor agents.**

12 Vasir JK, Labhasetwar V. Biodegradable nanoparticles for cytosolic delivery of therapeutics. *Adv. Drug Deliv. Rev.* 59(8), 718–728 (2007).

13 Lü JM, Wang X, Marin-Muller C *et al.* Current advances in research and clinical applications of PLGA-based nanotechnology. *Exp. Rev. Mol. Diagn.* 9(4), 325–341 (2009).

14 Chatterjee DK, Fong LS, Zhang Y. Nanoparticles in photodynamic therapy: an emerging paradigm. *Adv. Drug Deliv. Rev.* 60(15), 1627–1637 (2008).

15 Hu Z, Pan Y, Wang J, Chen J, Li J, Ren L. Meso-tetra (carboxyphenyl) porphyrin (TCPP) nanoparticles were internalized by SW480 cells by a clathrin-mediated endocytosis pathway to induce high photocytotoxicity. *Biomed. Pharmacother.* 63(2), 155–164 (2009).

16 Konan-Kouakou YN, Boch R, Gurny R, Allémann E. *In vitro* and *in vivo* activities of verteporfin-loaded nanoparticles. *J. Control Release* 103(1), 83–91 (2005).

17 Vargas A, Pegaz B, Debefve E *et al.* Improved photodynamic activity of porphyrin loaded into nanoparticles: an *in vivo* evaluation using chick embryos. *Int. J. Pharm.* 286(1–2), 131–145 (2004).

18 Owens DE, Peppas. Opsonization, biodistribution, and pharmacokinetics of polymeric nanoparticles. *Int. J. Pharm.* 307(1), 93–102 (2006).

19 Avgoustakis K, Beletsi A, Panagi Z *et al.* Effect of copolymer composition on the physicochemical characteristics, *in vitro* stability, and biodistribution of PLGA-mPEG nanoparticles. *Int. J. Pharm.* 259(1–2), 115–127 (2003).

20 Beletsi A, Panagi Z, Avgoustakis K. Biodistribution properties of nanoparticles based on mixtures of PLGA with PLGA-PEG diblock copolymers. *Int. J. Pharm.* 298(1), 233–241 (2005).

21 Kocbek P, Teskac K, Brozic P, Lanišnik Rižner T, Gobec S, Kristl J. Effect of free and in poly(ε-caprolactone) nanoparticles incorporated new type 1 17β-hydroxysteroid dehydrogenase inhibitors on cancer cells. *Curr. Nanosci.* 6(1), 69–76 (2010).

22 Welgus HG, Connolly NL, Senior RM. 12-o-tetradecanoyl-phorbol-13-acetate-differentiated U937 cells express a macrophage-like profile of neutral proteinases. High levels of secreted collagenase and collagenase inhibitor accompany low levels of intracellular elastase and cathepsin G. *J. Clin. Invest.* 77(5), 1675–1681 (1986).

23 Segat D, Tavano R, Donini M *et al.* Proinflammatory effects of bare and PEGylated ORMOSIL-, PLGA- and SUV-NPs on monocytes and PMNs and their modulation by f-MLP. *Nanomedicine (Lond).* 6(6), 1027–1046 (2011).

▪▪ **The proinflammatory effects of different nanoparticle systems are presented.**

24 Compagnin C, Baù L, Mognato M *et al.* The cellular uptake of meta-tetra(hydroxyphenyl)chlorin entrapped in organically modified silica nanoparticles is mediated by serum proteins. *Nanotechnology* 20(34), 345101 (2009).

▪ **Dark- and phototoxicity of temoporfin, delivered by silica nanoparticles is discussed.**

25 Konan YN, Chevallier J, Gurny R, Allémann E. Encapsulation of p-THPP into nanoparticles: cellular uptake, subcellular localization and effect of serum on photodynamic activity. *Photochem. Photobiol.* 77(6), 638–644 (2003).

26 Maeda H, Wu J, Sawa Y, Matsumura Y, Hori K. Tumor vascular permeability and the EPR effect in macromolecular therapeutics. *J. Control Release* 65(1–2), 271–284 (2000).

27 Bezdetnaya L, Zeghari N, Belitchenko I *et al.* Spectroscopic and biological testing of photobleaching of porphyrins in solutions. *Photochem. Photobiol.* 64(2), 382–386 (1996).

28 Vargas A, Lange N, Arvinte T, Cerny R, Gurny R, Delie F. Toward the understanding of the photodynamic activity of m-THPP encapsulated in PLGA nanoparticles: correlation between nanoparticle properties and *in vivo* activity. *J. Drug Target* 17(8), 599–609 (2009).

▪ **Provides data on the influence of nanoparticle size on the efficiency of photodynamic therapy.**

29 Lassalle HP, Dumas D, Gräfe S, D'Hallewin MA, Guillemin F, Bezdetnaya L. Correlation between *in vivo* pharmacokinetics, intratumoral distribution and photodynamic efficiency of liposomal temoporfin. *J. Control Release* 34(2), 118–124 (2009).

30 Preuss A, Chen K, Hackbarth S, Wacker M, Langer K, Röder B. Photosensitizer loaded HSA nanoparticles II: *in vitro* investigations. *Int. J. Pharm.* 404(1–2), 308–316 (2011).

31 Hopkinson HJ, Vernon DI, Brown SB. Identification and partial characterization of an unusual distribution of the photosensitizer meta-tetrahydroxyphenyl chlorin (temoporfin) in human plasma. *Photochem. Photobiol.* 69(4), 482–488 (1999).

32 Sasnouski S, Zorin V, Khludeyev I, D'Hallewin MA, Guillemin F, Bezdetnaya L. Investigation of Foscan interactions with plasma proteins. *Biochim. Biophys. Acta* 1725(3), 394–402 (2005).

33 Moor AC. Signaling pathways in cell death and survival after photodynamic therapy. *J. Photochem. Photobiol. B.* 57(1), 1–13 (2000).

34 Teiten MH, Bezdetnaya L, Morlière P, Santus R, Guillemin F. Endoplasmic reticulum and Golgi apparatus are the preferential sites of Foscan localisation in cultured tumour cells. *Br. J. Cancer* 88(1), 146–152 (2003).

35 Panyam J, Zhou WZ, Prabha S, Sahoo SK, Labhasetwar V. Rapid endo-lysosomal escape of poly(DL-lactide-co-glycolide) nanoparticles: implications for drug and gene delivery. *FASEB J.* 16(10), 1217–1226 (2002).

36 Tahara K, Sakai T, Yamamoto H, Takeuchi H, Hirashima N, Kawashima Y. Improved cellular uptake of chitosan-modified PLGA nanospheres by A549 cells. *Int. J. Pharm.* 382(1–2), 198–204 (2009).

37 Athanasiou KA, Niederauer GG, Agrawal CM. Sterilization, toxicity, biocompatibility and clinical applications of polylactic acid/polyglycolic acid copolymers. *Biomaterials* 17(2), 93–102 (1996).

38 Cegnar M, Premzl A, Zavasnik-Bergant V, Kristl J, Kos J. Poly(lactide-co-glycolide) nanoparticles as a carrier system for delivering cysteine protease inhibitor cystatin into tumor cells. *Exp. Cell Res.* 301(2), 223–231 (2004).

▪ **A study on the cytotoxicity of bare-loaded poly-(D,L-lactide-co-glycolide) nanoparticles.**

39 Berlanda J, Kiesslich T, Engelhardt V, Krammer B, Plaetzer K. Comparative *in vitro* study on the characteristics of different photosensitizers employed in PDT. *J. Photochem. Photobiol. B.* 100(3), 173–180 (2010).

40 Konan YN, Berton M, Gurny R, Allémann E. Enhanced photodynamic activity of meso-tetra(4-hydroxyphenyl)porphyrin by incorporation into sub-200 nm nanoparticles. *Eur. J. Pharm. Sci.* 18(3–4), 241–249 (2003).

IV

Targeted delivery of photosensitizers: efficacy and selectivity issues revelead by multifunctional ORMOSIL nanovectors in cellular systems

Francesco Selvestrel,[a,‡] Francesca Moret,[b,‡] Daniela Segat,[c,‡] Josephine H. Woodhams,[d‡] Giulio Fracasso, [e,‡] Iria. Rio Echevarria,[a] Luca Baù,[a] Federico Rastrelli,[a] Chiara Compagnin,[b] Elena Reddi,*[,b] Chiara Fedeli,[c] Emanuele Papini,[c] Regina Tavano, *[,c] Alexandra Mackenzie,[d] Melissa Bovis,[d] Elnaz Yaghini,[d] Alexander J. MacRobert,*[,d] Silvia Zanini,[e] Anita Boscaini,[e] Marco Colombatti,*[,e] and Fabrzio Mancin*[,a]

Abstract

PEGylated and non-PEGylated ORMOSIL nanoparticles prepared by microemulsion condensation of vinyltriethoxy-silane (VTES) were investigated in detail for their micro-structure and ability to deliver photoactive agents. With respect to pure silica nanoparticles, organic modification substantially changes the microstructure and the surface properties. This in turn leads to a modulation of both the photophysical properties of embedded photosensitizers and the interaction of the nanoparticles with biological entities as serum proteins. The flexibility of the synthetic procedure allows the rapid preparation and screening of multifunctional nanosystems for photodynamic (PDT) therapy. Selective targeting of model cancer cells was tested by using folate, integrin specific RGD peptide and anti-EGFR antibodies. Data suggest the interference of the stealth-conferring layer (PEG) with small targeting agents, but not with bulky antibodies. Moreover, we showed that selective photokilling of tumour cells may be limited even in the case of efficient targeting because of intrinsic transport limitations of active cellular uptake mechanisms or suboptimum localization.

Introduction

Over the last few years, silica nanoparticles have attracted a great deal of interest as materials for biomedical applications.[1] At first glance, this may appear quite surprising. Unlike other nanomaterials, silica nanoparticles do not have any nanosize-related properties, nor are they easily biodegraded.[2] So, what makes silica nanoparticles so attractive? The answer lies in their highly cross-linked polymeric nature. Being of polymeric structure they can accommodate in their interior (either in the silica matrix or within pores) active molecules, such as drugs, dyes and photosensitizers.[3] The loading capacity of silica nanoparticles is hence much higher than that achievable with other nanomaterials which allow only surface grafting, and this enables their use for drug delivery applications. On the other hand, their highly cross-linked nature renders silica nanoparticles much more rigid than other polymeric nanoparticles. This makes it possible to process them into very complex structures, including mesoporous particles,[1c,4] nanoshells[5] and multi-shell particles.[3,6] Such versatility has opened the way to the realization of several sophisticated systems, such as gated porous particles for controlled release,[1a,f] multimodal imaging and delivery agents,[1] chemical sensors.[7] Notably, silica does not need to be made only by silicon oxide. Using organosilane precursors in the formation of the silica network, organically modified silica (ORMOSIL) materials can be obtained.[8] Here, the possibilities for tuning the nanoparticles properties, either of the surface and

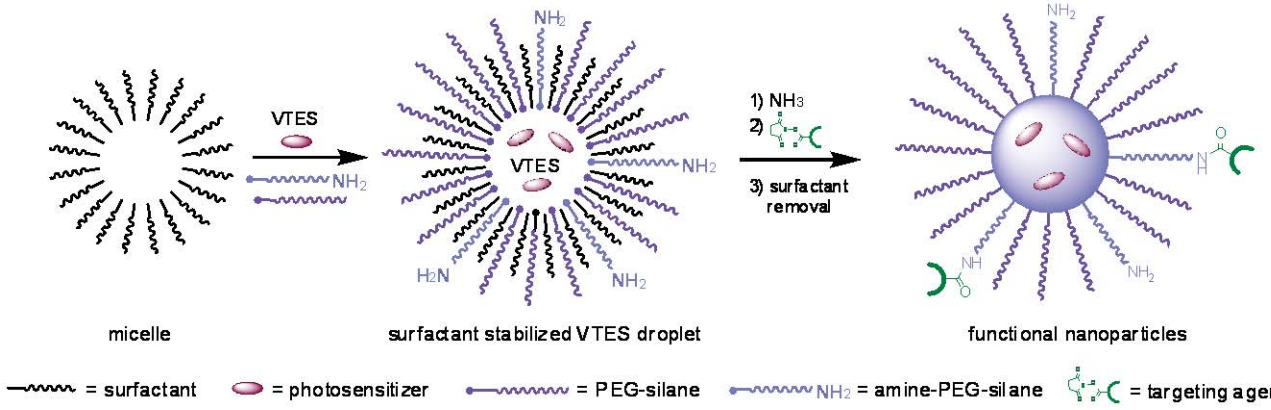

Scheme 1. One-pot synthesis of doped, PEGylated and functional ORMOSIL nanoparticles. Any of the components indicated in the caption, with the exception of the surfactant may be omitted to prepare nanoparticles with different features.

of the bulk phase, or by changing the nature of the organic moiety introduced, are very broad. A class of ORMOSIL nanoparticles that has recently emerged as an attractive candidate for nanomedicine applications comprises those prepared by the base-catalyzed condensation of vinyl-triethoxysilane (VTES, chart 1) in aqueous surfactant solutions.

This synthetic protocol was first proposed by P. N. Prasad and co-workers in 2003 for the development of photosensitizer delivery agents in photodynamic therapy (PDT).[9] This approach enabled a series of very elegant advances stemming from the original photosensitizer loaded particles,[10] including two-photon excitation of the photosensitizer through Förster energy transfer from a co-included antenna[11] and matrix enhancement of the singlet oxygen production quantum yield.[12] Applications for fluorescent probes,[13] encapsulation of other nanoparticles,[14] DNA transfection[15] and targeted delivery[16] were also reported.

Advantages of such ORMOSIL nanoparticles are many. Firstly, the use of the organosilane precursor provides a low polarity interior that favours the inclusion of hydrophobic molecules but does not prevent their release in biological fluids.[17] Secondly, the properties of both the bulk material and probably also of the particles surface may be tailored, as mentioned earlier, by the use of different organosilane precursors. But the most relevant feature is brought about by the microemulsion polymerization protocol used for their preparation. In fact, not only does the surfactant aggregate act as a nanocontainer where the organosilane polymerization is confined, but it can also play the role of a template, where it pre-organizes the nanoparticle components placing them precisely in the site they are needed to perform their function. Hence, as demonstrated by Prasad and also by us, dye-doped surface functionalized nanoparticles can be prepared by a one pot-procedure.[16,18] Indeed, we recently showed, by taking full advantage of such an approach, that densely PEGylated nanoparticles can be prepared[18] and that such a dense coating reduces the toxic[19] and pro-coagulant[20] properties of particles themselves and avoids capture by immune system cells.[18] While these findings further amplify the interest in nanomedicine applications of ORMOSIL nanoparticles, their structure and characteristics have yet to be fully investigated. By a detailed investigation of the chemical, structural and biological properties of PEGylated and non-PEGylated ORMOSIL nanoparticles made with VTES, we have acquired herein a deeper comprehension of their properties and potential for applications.

Results and Discussion

Chemical microstructure and surface properties

The synthesis of the VTES-ORMOSIL nanoparticles (Scheme 1) may be regarded as a variation of the well-known Stöber procedure,[21] involving the ammonia-catalysed polymerization of alkoxysilane precursors in ethanol. The main difference here is that the reactions occur in water and in the presence of a surfactant (AOT, Tween, Brij) that controls the growth of the

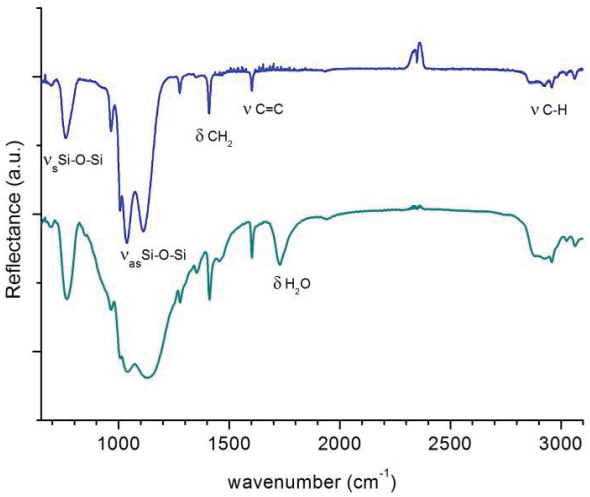

Figure 1. ATR-IR Spectra of lyophilized ORMOSIL nanoparticles (blue) and PEGylated ORMOSIL nanoparticles (green).

nanoparticles. Such modifications of the use of an organosilane precursor may influence the nanoparticles microscopic structure. With this view, we prepared VTES nanoparticles with a diameter of 50 nm using the Brij surfactant for spectroscopic characterization. The ATR-IR spectrum (Figure 1, blue) contains all the main features of VTES-containing materials.[22] The most intensive band, at about 1100 cm^{-1} is due to the asymmetric stretching of the Si–O–Si bridges, and, as usually found for ORMOSIL materials, splits into two separate bands at 1040 (TO mode) and 1110 (LO mode) cm^{-1}. Interestingly, the position of these signals is 20-40 nm red-shifted with respect to the usual values found in VTES containing sol-gel films prepared by acid catalysis,[22] possibly indicating a highly porous structure of the nanoparticles. The symmetric stretching of the same silicon–oxygen bridges is responsible of the band at about 760 cm^{-1}. The sharp signals at 1409 (in plane CH_2 bending) and 1602 (C=C stretching) cm^{-1} arise from the vibrations of the vinyl groups. On the other hand, the sharp signal at 966 cm^{-1}, is likely the result of the overlap of the signals arising from Si-OH stretching and vinyl CH_2 wagging.

More detailed structural information is obtained by MAS solid state NMR. ^{13}C NMR (Figure 2a, blue) confirmed the complete hydrolysis of the alkoxysilane precursor since no signals related to the ethoxy moieties are visible in the spectrum. The two-broad signals at 145 and 135 ppm arise from the two carbon atoms of the vinyl residue. On the other hand, a series of sharp signals is visible between 80 and 20 ppm, which corresponds very well to the Brij surfactant. We were not able to remove the surfactant signals either by extensive ultrafiltration or Soxlet extraction with ethanol, indicating that it is likely physically entrapped in the ORMOSIL matrix. The ^{29}Si spectrum (Figure 2b, blue) shows two signals at -77 and -68 ppm, arising respectively from fully condensed T^3 and partially condensed T^2 silicon atoms.

Integration of the signals indicates that T^2 atoms are only 10% of

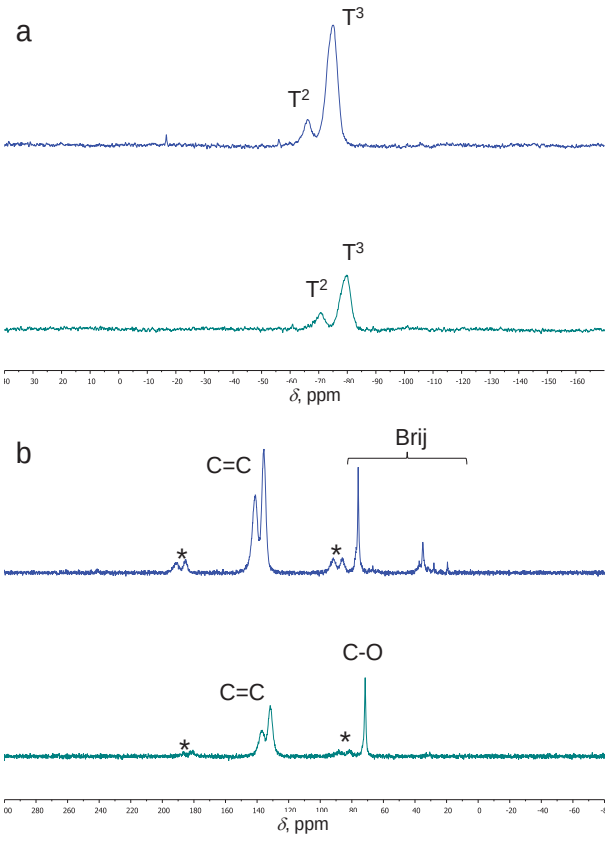

Figure 2. ^{29}Si MAS (a) and ^{13}C MAS solid state NMR of lyophilized ORMOSIL nanoparticles (blue) and PEGylated ORMOSIL nanoparticles (green). C=C indicates the vinylic carbons and C-O the carbons bound oxygen of the PEG polymer. to The symmetric signals (*) at 70 and 170 ppm in the 29Si spectrum are spinning bands.

the total, indicating a highly condensed structure. When compared with pure silica nanoparticles, the VTES ORMOSIL particles reveal interesting differences. Early studies by van Blaaderen indicated that silica nanoparticles prepared either via the Stöber protocol (TEOS condensation in ethanol) or via the micro-emulsion protocol (TEOS condensation in water/cyclohexane microemulsion) are characterized by incomplete hydrolysis of the precursor alkoxysilanes and much less condensed structure (67 and 55% of fully condensed Q^4 silicon atoms, respectively).[23] Only the commercial Ludox particles, that are prepared by condensation of silicates in water, present a similarly highly condensed structure, with 85% of Q^4 silicon atoms.[23]

The degree of hydrolysis and condensation, however, does not influence surface charge, which is one of the most important features of nanoparticles for biomedical applications since it determines their stability in high ionic strength biological fluids and ability to interact with cells. Z-potential measurements performed in PBS buffer at pH 7.4 yielded the values of -5.9, -18.3 and -15.6 mV respectively for ORMOSIL, Stöber and Ludox particles (50 nm diameter). Hence, surface charge is not proportional to the amount of Si-OH groups present on the particles, which is greater in Stöber particles and smaller in ORMOSIL and Ludox. Van Blaaderen calculations reveal that surface silanols account for a very small fraction (2,5% for 50 nm

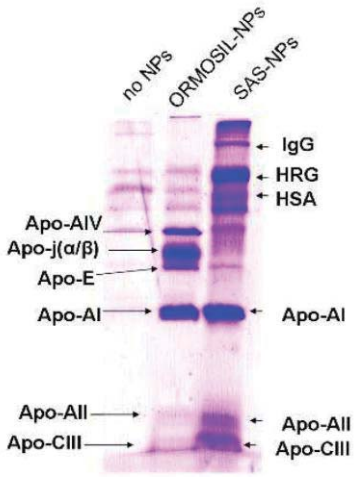

Figure 3. Comassie Blue stained SDS-PAGE analysis of nanoparticle-bound human plasma proteins.

diameter nanoparticles) of the total silicon atoms.[23] Hence, even in the most condensed particles the amount of silanols detected by ^{29}Si MAS NMR groups largely exceed that necessary for a full surface coverage. This explains why Stöber and Ludox particles have similar Z-potential values notwithstanding the large difference in number of silanols. Once all the available sites on the surface are occupied, silanols in excess must locate in the nanoparticles interior not affecting the overall surface charge. Hence, in the case of ORMOSIL particles, the less-negative Z-potential could be explained by postulating that several vinyl moieties are exposed on surface instead of OH groups, and this reduces the overall surface charge. The consequences of such a relevant difference in the surface chemical structure should be observed not only on the Z-potential values but also on the interaction with serum proteins, which is fundamental in determining the biological fate of the nanoparticles.[24] To test this hypothesis the patterns of protein adsorbed on ORMOSIL and Ludox particles, after 3 hours incubation at 37°C in human plasma, were identified by SDS-PAGE and mass spectroscopy (figure 3). Interestingly, both ORMOSIL and Ludox particles recruit few and quite different plasma proteins, with Ludox interacting preferentially with Immunoglobuline-G (IgG), Histidine Rich Glycoprotein (HRG), Human Serum Albumin (HSA) and apolipoproteins ApoA-I, ApoA-II, and ApoC-III, while ORMOSIL exhibit higher affinity for ApoA-IV, ApoE, ApoJ and ApoA-I. Hence, the reduction of the surface charge (which still remains negative) and the exposure of vinyl residues results in a shift of preference from soluble IgG, HSA and HRG proteins to more hydrophobic lipoproteins. We previously observed that hydrophobic photosensitizers entrapped in the ORMOSIL where rapidly released from the nanoparticles when incubated with serum.[17b] The high preference for recruiting lipoproteins, which are known carriers of hydrophobic species, could account for this observation.

As we have shown earlier, addition of an amphiphilic trialkoxysilane PEG derivative to the reaction mixture, as **1** in Chart 1, results in the formation of densely PEGylated nanoparticles.[18] PEGylation produces only minor modifications on the IR spectrum (Figure 1, green) where a broadening of the signals in the 1000-1200 cm^{-1} range, due to the superimposition

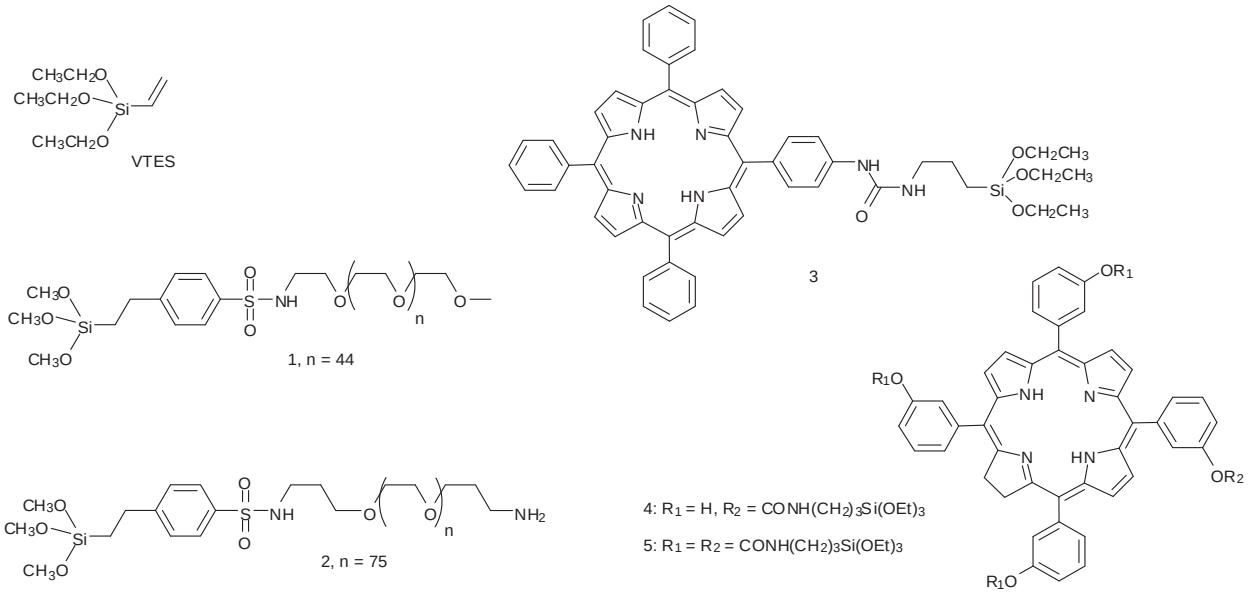

Chart 1. Alkoxysilane derivatives used in this work.

of the PEG signals, is the main difference observed. PEG features are also visible in the ^{13}C MAS solid state NMR signal at 71 ppm, arising from the methylenes of the polyethylene oxide chain (Figure 2b, green). Analysis of this spectrum also reveals the absence of residual surfactant in these samples, in contrast with the non-PEGylated ORMOSIL nanoparticles (Figure 2b, blue). This suggests that the presence of the amphiphilic silane prevents the surfactant from remaining physically entrapped in the ORMOSIL matrix, hence favouring its removal. TGA analysis (ESI) reveals that the dense coat of PEG-2000 accounts respectively for 67, 38 and 25% of NPs weight for nanoparticles with 20, 55 and 70 nm diameters. Such figures lead to estimate a surface density of 1-2 PEG molecules per nm^2.

Finally, ^{29}Si-NMR indicates a smaller degree of condensation of the silicon atoms, with the amount of partially condensed T^2 atoms raised here to 34%. However, both the surface coating with PEG and again the presence of a larger amount of silanol groups in the ORMOSIL matrix appear not to affect the overall surface charge, the Z-potential (in PBS buffer, pH 7.4) being −4.3 mV, only slightly different form that of the "naked" ORMOSIL particles.

Photochemical properties of embedded photosensitizers

Having such a strong influence on the surface properties of the nanoparticles, the presence of the vinyl groups is expected to affect also the interior silica matrix and as a consequence the properties of embedded dyes. This aspect is particularly relevant for one of the most promising application of VTES-ORMOSIL nanoparticles, namely the anticancer modality called photodynamic therapy (PDT). In this approach, a photosensitizing molecule should be selectively delivered inside the tumour and produce, upon activation with light, cytotoxic reactive oxygen species (ROS) that kill the tumour cells. Remarkably, the photosensitizer does not need to be released from the carrier to exert its phototoxic effect and therefore it can be embedded in the nanoparticles without the need of devising effective release mechanisms. However, the essential requirement is that the embedded photosensitizer maintains its photophysical properties and hence its ability to generate ROS, in particular singlet oxygen.

To investigate this point, we initially prepared both Stöber silica nanoparticles and VTES-ORMOSIL nanoparticles (both PEGylated and not) doped with the alkoxysilane porphyrin derivative **3** (we selected this molecule because most of the photosensitizers used in clinic are porphyrins or chlorins) and investigated the photophysical properties of the embedded dye. Inspection of the fluorescence lifetime data reported in Table 1 reveals that all the nanoparticles-embedded dyes (Entries 2-4) show biexponential decays with a long component (~10 ns) that is very similar to the life-time of **3** in ethanol (Entry 1) and a short component (~3 ns) which presumably arise from poorly emissive porphyrin aggregates. However, while the short component is minor in the ORMOSIL particles, it is predominant in the Stöber particles (Entry 2), where this behaviour is accompanied by a broadening of the porphyrin Soret band in the UV-Vis spectrum (ESI). This suggests that the more polar environment provided by silica matrix with respect to that of ORMOSIL favours the formation of weakly fluorescent dye aggregates inside the particles, which are known to be ineffective as photosensitizers.[25] Fluorescence self-quenching through interaction of adjacent photosensitiser moieties results in lower triplet state and singlet oxygen yields, and this interaction should

Table 1. Photophysical properties (fluorescence lifetimes (τ) and their amplitudes (A), and singlet oxygen quantum yields (ϕ_Δ) of photosensitizers embedded in silica (Stöber) and ORMOSIL (OS) nanoparticles.[a,b]

Entry	Dye	Np	Solvent	τ_1/ns (A_1)	τ_2/ns (A_2)	ϕ_Δ[e]
1	**3**	-	EtOH	9.5 (100)		-
2	**3**	Stober[c]	H_2O	9.6 (55)	2.3 (45)	-
3	**3**	OS[c]	H_2O	11.2 (91)	3.0 (9)	-
4	**3**	OS/PEG[c]	H_2O	12.1 (85)	4.7 (15)	-
5	mTHPC	-	MeOH	8.4 (100)	-	0.71
6	**4**	-	MeOH	8.4 (100)	-	0.67
7	**4**	OS/PEG[d]	MeOH	8.5 (91)	0.8 (9)	-
8	**4**	OS/PEG	MeOH	8.6 (94)	1.0 (6)	0.55
9	**4**	OS/PEG	MeOH/H_2O	9.7 (90)	1.7 (10)	-
10	**4**	OS/PEG	H_2O	9.9 (83)	0.8 (17)	0.53
11	**5**	-	MeOH	8.3 (100)	-	0.65
12	**5**	OS/PEG[d]	MeOH	8.7 (78)	3.4 (22)	0.55
13	**5**	OS/PEG	MeOH	8.4 (88)	1.2 (12)	0.58
14	**5**	OS/PEG	MeOH/H_2O	9.9 (52)	0.8 (48)	-
15	**5**	OS/PEG	H_2O	10.0 (18)	0.7 (82)	0.10

[a] Nanoparticles diameter 20 nm and average photosensitizer loading 1.5% w/w unless otherwise stated. [b]Errors within 5%. [c]0.3% w/w photosensitizer loading. [d] 90 nm diameter. [e] ϕ_Δ measured in MeOD except Entries 10 and 15, which were carried out in D_2O.

therefore be minimised as far as possible. The less polar environment provided by the ORMOSIL matrix hence appears to be ideal for accommodating photosensitizer molecules with retention of their optimal photophysical properties.

More insight on this respect was obtained by studying the photochemistry of ORMOSIL nanoparticles containing the alkoxysilane derivatives **4** and **5** of the commercial photosensitizer mTHPC (Chart 1). Likewise in the previous case fluorescence decay profiles are biexponential, with the long component (~8-9 ns) similar to that of the free dye in methanol and a short component (~0.5-1 ns). mTHPC in MeOD ("monomeric mTHPC") exhibited a ϕ_Δ of 0.71, which is in agreement with the literature.[26]

In methanol, either mono- and tetra-functionalization of the parent mTHPC does not significantly alter the photophysical properties of the derivatives (Entries 5, 6 and 11). The singlet oxygen yields measured for mTHPC in MeOD are in good agreement with other studies.[26] Also embedding in the ORMOSIL matrix does not alter the photosensitizer properties (Entries 7-8, 12-13). In fact, in all these cases very similar emission lifetimes are observed with a major long-lived component and a minor short component. However, the situation drastically changes when moving to solvents with higher polarity (1:1 methanol/H_2O, H_2O). In the particles doped with **4** the long component remains predominant with only a slight increase of the short-lived one in more polar solvents (Entries 8-10). However, in the particles doped with **5,** the amplitude of the short component is substantially increased in water so that it becomes the dominant decay component. The fluorescence emission intensity is also substantially quenched compared to methanol (Entries 13-15). The behaviour of the emission quantum yield parallels that of the singlet oxygen quantum yield (measured by singlet oxygen phosphorescence at 1270 nm). Singlet oxygen production of nanoparticles doped by both the dye in methanol and by dye **4** in deuterated water are very similar to that of mTHPC in deuterated methanol, on the other hand, singlet oxygen production by **5**-doped nanoparticles in deuterated water is much lower (Entry 15).

The peculiar behaviour of the embedded dye **5** is not due to aggregation since it is not loading-dependent (not shown). In this case we propose that the penetration of water and resulting H-bonding inside the nanoparticle may lead to distortion of the tetra-coordinated chlorin macrocycle since it is rigidly attached to the silica matrix and cannot compensate by conformational realignment, unlike the mono-coordinated chlorin which is able to rotate. Distortion in the macrocycle planarity is well known to increase the rate of internal conversion resulting in quenching of its emission and singlet oxygen production.[27]

Targeting of the ORMOSIL nanoparticles

As we earlier demonstrated, functional groups for conjugation of the nanoparticles to targeting species can be introduced in the coating layer by simply adding a second PEG-trialcoxysilane derivative bearing a reactive terminal group (Scheme 1).[18] To further explore such possibility we prepared several batches of **4**-doped ORMOSIL nanoparticles targeted with different bioactive molecules, such as folic acid, biotin, the cyclic(RGD) peptide and the antibody Cetuximab (Chart 2). The nanoparticles were prepared in different sizes (20-100 nm) by adding to the reaction mixture different amounts of PEG derivatives **1** and **2** (1-30%). In the case of folic acid and biotin, which can be directly linked to the nanoparticles amino groups via the formation of an amide bond, targeting was performed by directly adding O-hydroxysuccinimmide ester derivatives of the targeting agents to the reaction mixture before the purification (Scheme 1). In this way, dye-doped, PEGylated and targeted nanoparticles could be prepared by a simple one-pot procedure. The grafting of folate and biotin to the nanoparticles was demonstrated by the presence of the characteristic spectral features of this molecule in the UV-Vis spectrum in the case of the first, and by the HABA-Avidin and the EZview Red Streptavidin Affinity Gel tests for the second (see ESI).

On the contrary, the cyclic(RGD) peptide, which targets the $\alpha_v\beta_3$ integrin associated to tumor neovasculature (Chart 2), and the Cetuximab antibody, recognizing the Epithelial Growth Factor receptor (EGFR) overexpressed in many tumours, were conveniently conjugated to the nanoparticles by taking advantage of thiols group inserted in the derivatives (i.e. in the case of Cetuximab thiols group were introduced by reaction with 2-iminothiolane). This required the conversion of the terminal amine groups of the nanoparticles into thiol-reactive maleimide groups via the reaction with the commercial MBS crosslinker (Chart 2). Subsequent reactions with the cyclic(RGD), the inactive analogue cyclic(RAD) and iminothiolane modified Cetuximab antibody provided the targeted nanoparticles. In this case, due to the sensitivity of the maleimide group to nucleophiles, and to prevent unwanted conjugation between the targeting peptide and unreacted MBS, we preferred to perform the conjugation with a three step procedure involving nanoparticles purification after each step (Chart 2). Antibody

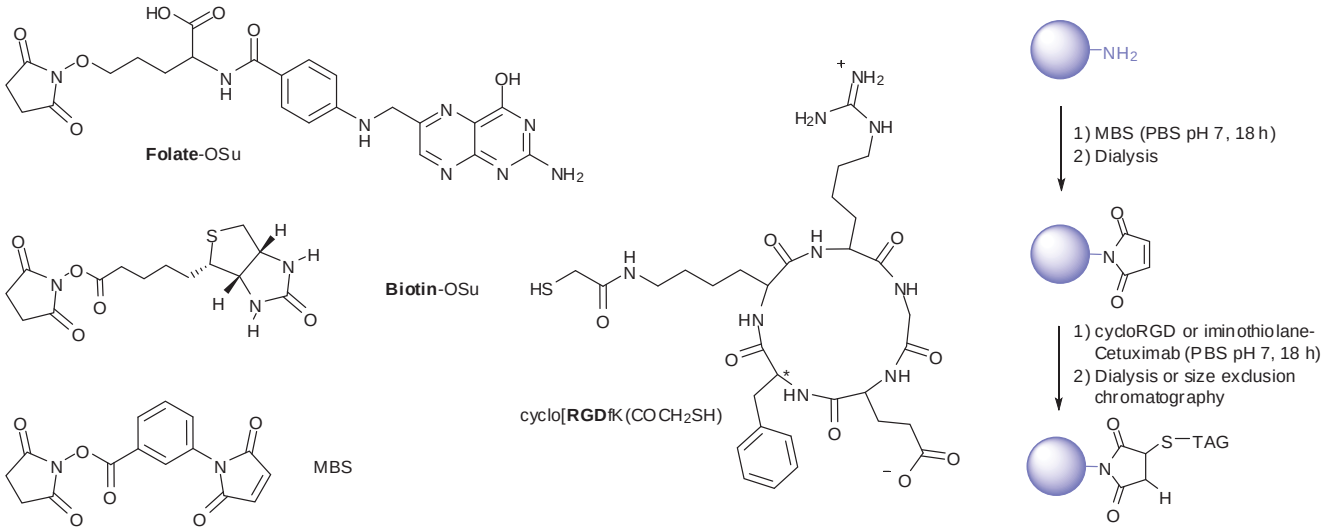

Chart 2. Targeting agents used and scheme for the post-synthetic functionalization of **1**/**2**-coated nanoparticles with the peptides and antibodies (TAG).

conjugation was confirmed by Western Blot analysis (see ESI).

Cellular uptake and targeting

In order to investigate the ability of the PEGylated ORMOSIL nanoparticles to enter cancer and healthy cells, free mTHPC and **4**-doped nanoparticles (90 nm diameter) were incubated, at the same dye concentration, with human lung carcinoma cells A549 and normal lung fibroblasts CCD-34Lu for 24 h at 37 °C in culture medium supplemented with 3% fetal calf serum (FCS). The dye uptake was measured by flow cytometry (FACS) experiments using the fluorescence emission of the chlorins associated to the cells. As expected, the cellular uptake of the drug by both the cancer (Figure 4) and healthy cells (ESI, Figure S10) is greatly reduced by the embedding in the PEGylated nanoparticles, with the uptake of the photosensitizer being only about 5% of that measured when the free dye is incubated with the cells.

These results are important because they clearly indicate that the use of the PEGylated nanoparticles as a carrier for the photosensitizer should minimize unwanted uptake by healthy tissues and by consequence reduce the unwanted systemic toxicity of the therapy. On the other hand, this ability to escape cell capture makes conjugation with targeting agents necessary in order to trigger active uptake mechanisms and ensure that the photosensitizer is delivered to the target cells. We hence investigated the "in vitro" uptake of folate-, RGD- and Cetuximab-conjugated nanoparticles using cell lines over-expressing the targets recognized by each vehicle moieties. The results obtained are quite different with the three guided-nanosystems.

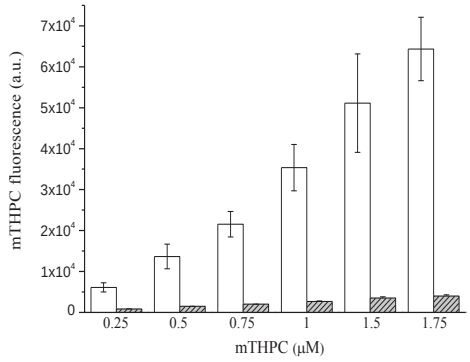

Figure 4. Flow cytometry measurements of mTHPC and derivative **4**uptake in A549 cells incubated for 24 h with increasing concentration of free mTHPC (white) or **4**-doped PEG-ORMOSIL nanoparticles (grey).

In the case of folate, KB cells overexpressing and A549 cells not expressing the folate receptor were used. The presence of the folate in the nanoparticles coating results in (see ESI): i) decreased uptake with respect to nanoparticles coated with only PEG; ii) no difference in the uptake of folate-nanoparticles between KB and A549 cells (not shown) and; iii) no inhibition of the uptake of folate-targeted nanoparticles in KB cells preincubated with 1 mM free folic acid to saturate the receptor and prevent the internalization of the nanoparticles through the receptor-driven specific endocytosis. Such behavior is not affected by the size of the nanoparticles or by the thickness of the PEG coating or the length of the PEG functioning as a linker for folate.

Different results were obtained with the RGD-targeted nanoparticles incubated with HUVEC cells overexpressing the integrin $\alpha_v\beta_3$ receptors for RGD. We evaluated the efficiency of the targeting agent on the same cell line by comparing the uptake of the RGD-targeted nanoparticles with that of identical particles (prepared from the same original batch) targeted with the RAD peptide, where the substitution of the central glycine with an alanine prevents the recognition by the integrins. Inspection of the results reported in Figure 5 provides evidence of higher uptake of the RGD-conjugated nanoparticles with respect to the RAD-conjugated ones. The uptake improves by increasing the amount of RGD peptides present in the nanoparticles coating layer form 15 to 30%, while uptake slightly decreases using smaller nanoparticles (40 nm diameter). The different behaviour

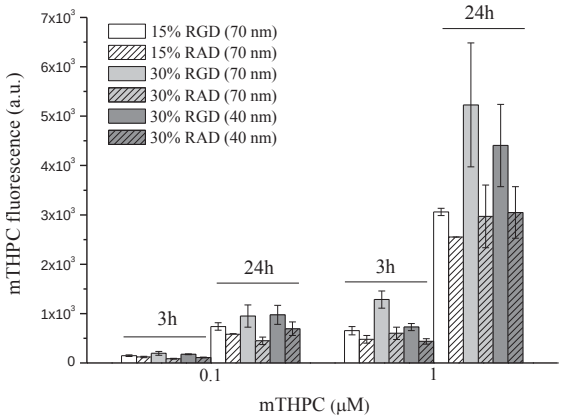

Figure 5. Flow cytometry measurements of mTHPC derivative **4** uptake in HUVEC cells incubated for 3 or 24 h with **4**-doped PEG-ORMOSIL nanoparticles of different size and conjugated with RGD and RAD peptides in different amounts.

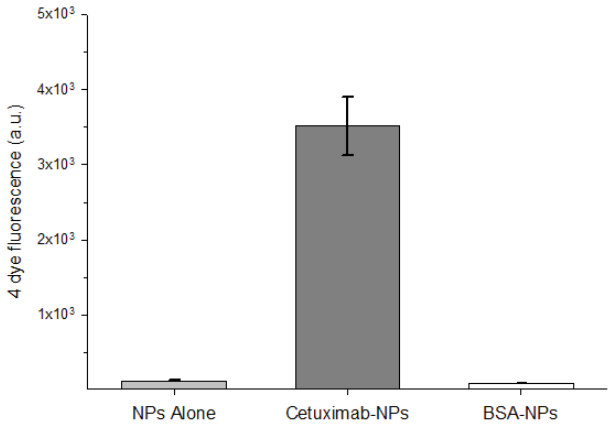

Figure 6. Differential uptake of **4**-doped PEG-ORMOSIL nanoparticles unconjugated (NPs alone), or conjugated with Cetuximab and BSA on A431 cells. Cells were incubated with nanoparticles at1 μM concentration of dye **4** for 90 minutes at 37°C, nanoparticle uptake was analyzed by flow cytometry.

between the two small-molecule targeting agents is not unprecedented in PLGA nanoparticles and was attributed to poor surface exposure of the hydrophobic folate moiety.[28] Moreover, it has been recently reported that a dense PEG layer coating silica nanoparticles can effectively capture and incorporate organic dyes from water solution.[29] It can hence be expected that the long PEG3300 linker, bearing the targeting agent, folds allowing to the folate moiety to hide in the PEG layer. In support of this view, some of us recently found that only liposomes with a degree of PEGylation not higher than 8% folate conjugation slightly improved the selectivity of mTHPC uptake in KB cells.[30] Furthermore, the decreasing uptake of folate ORMOSIL nanoparticles with the increasing of the folate percentage might indicate changes of the surface properties that make cell internalization less efficient. The zwitterionic RGD peptide is much more hydrophilic than folate and hence it likely less attracted by the PEG pseudophase, therefore remaining available for the interaction with the cellular receptor.

Such a picture is confirmed by the results obtained with the **4**-doped nanoparticles conjugated with the antibody Cetuximab (Figure 6). Here the size of the targeting agent (i.e. the average size of an antibody is 15×8×4 nm[31]) is such that the interference of the PEG coating with its binding efficiency appear to be unlikely. In fact, internalization of targeted nanoparticles at 37°C, measured on the A431 cells overexpressing the EGF receptor, is impressive. The uptake of the conjugated nanoparticle is at least 20-fold greater than that of the unconjugated or BSA-conjugates (prepared as negative control systems). The specific uptake of Cetuximab-guided nanoparticles on A431 cells was confirmed by competition experiments performed co-incubating cells, at 37°C, with increased concentrations of free Cetuximab (Figure 7). In fact the co-incubation of targeted nanoparticles with free Cetuximab reduces the nanoparticle uptake of about 93%, whereas no decrease of nanosystem uptake is observed for BSA-conjugated control particles in the same conditions (see ESI).

Further assays were performed to obtain more insight on the internalization mechanism. First the dependence of the uptake by the amounts of Cetuximab or BSA-conjugated nanoparticles added was investigated (see ESI) and demonstrates that the internalization mechanism of the antibody-guided nanovectors is saturable. In fact, the amount of taken-up nanoparticles does not increases linearly with the amount of nanoparticles added and appears to reach a plateau for nanoparticles concentrations of 320 μg/mL (corresponding to a dye concentration of 4 μM). Such behavior suggests that, once all the EGF receptors available on the surface of the cells are bound to antibodies conjugated with the nanoparticles, further increments of the nanoparticles concentrations do not result in increased uptake, as expected for a receptor mediated internalization mechanism. Indeed the BSA-conjugated nanoparticle uptake appears to follow a different trend with a linear concentration-dependent increase of the uptake in the interval studied.

The same picture emerged from time-dependant analysis performed using in this case three different cell lines (see ESI):

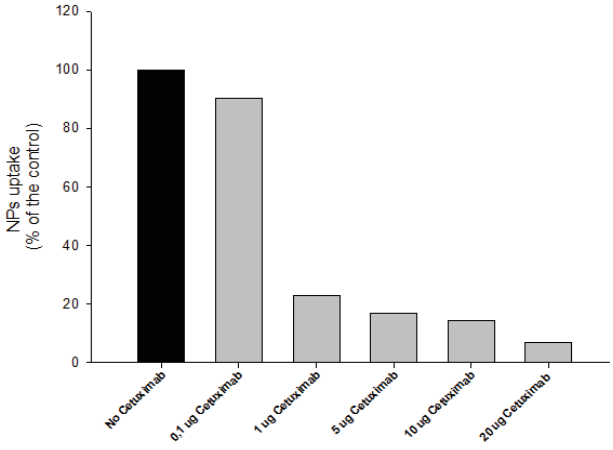

Figure 7. Displacement of the uptake of **4**-doped PEG-ORMOSIL nanoparticle conjugate with Cetuximab on A431 cells by free Cetuximab. Cells were incubated with nanoparticles at 0.25 μM concentration of dye **4** and increasing concentrations of free Cetuximab for 90 minutes at 37°C, nanoparticle uptake was analysed by FACS.

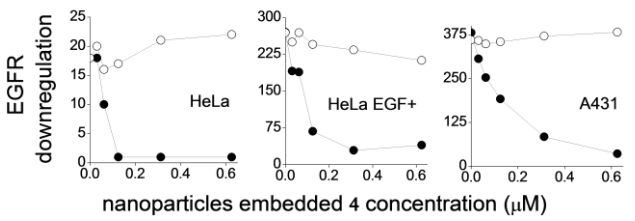

Figure 8. Nanoparticles induced down-regulation (measured as amount of cell bound FITC-labelled anti EGFR antibody) of EGF receptor in different cell lines. Cells were incubated in DMEM 10% FCS with different concentrations of Cetuximab (●) or BSA (○) conjugated nanoparticles for two hours at 37°C; washed and analysed by FACS. Note the different signal intensities in the three cell lines, proportional to plasma membrane EGFR amounts.

normal HeLa cells, expressing basal amounts of plasma membrane located EGFR, a derived HeLa cell lines, permanently transfected to express higher levels of surface EGFR (4-5 folds the parental HeLa cell line) and the above mentioned A431 cells, expressing a high amount of EGFR (10-13 folds in the plasma membrane compared to HeLa cells). As expected, Cetuximab-conjugated nanoparticle uptake is not linear with incubation time and reaches a saturation level after about 2 hours with all the cell lines. Moreover, the amount of nanoparticles taken up at saturation is directly correlated with the extent of EGFR expression levels, with A431 and transfected HeLa internalizing upon prolonged incubation an amount of nanoparticles about 20- and 4-fold larger than normal HeLa. On the other hand, non-specific uptake of BSA-conjugated nanoparticles appears to occur with a slower and cell line-independent kinetic that does not reach saturation values in the time span explored. As a consequence, maximum preferential uptake is observed for short incubation times.

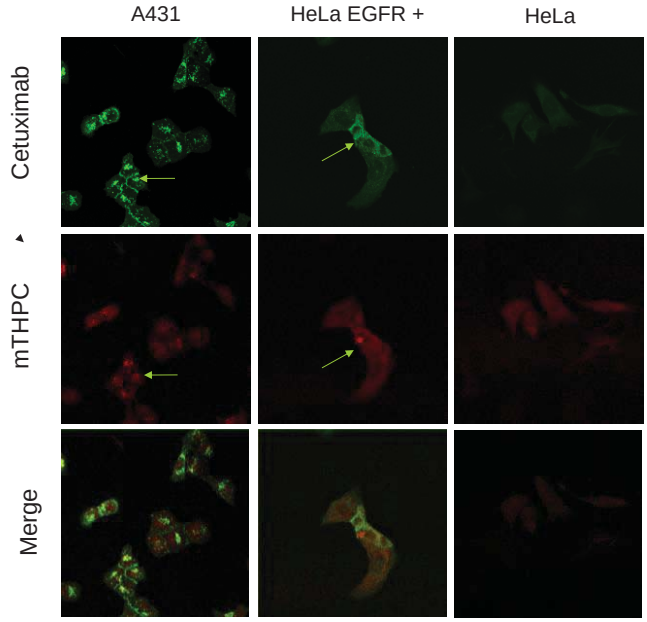

Figure 9. Colocalization of Cetuximab and dye **4** upon incubation of EGFR positive A431 cells, EGFR over-expressing HeLa and parental HeLa (having reduced EGFR levels) with Cetuximab conjugated **4**-doped ORMOSIL nanoparticle at 1 μM mTHPC concentration for two hours at 37°C. Green signal is Cetuximab distribution, red one is mTHPC. Arrows point the colocalisation of Cetuximab and mTHPC.

The specific interaction of the nanoparticles with EGFR, followed by internalisation of the resulting complex, was clearly documented by further experiments in which the amount of surface receptors was quantified by FACS after incubation with nanoparticles using a fluorescein-conjugated Cetuximab as a label (Figure 8). Indeed, Cetuximab-conjugated nanoparticles, but not BSA-conjugated ones, down regulate EGFRs in all cell types, suggesting, in agreement with confocal microscopy (see infra), that Cetuximab-nanoparticles complexes with EGFRs, formed on the plasma membrane, are internalised in endosomes and this leads to a decrease of the amount of receptor on the cell surface. EGFR down regulation is complete at very low nanoparticle concentrations (50 μg/mL for A431 cells, corresponding to a **4** concentration of 0.62μM). Confocal microscopy analysis experiments (Figure 9) enabled localisation of both nanoparticle-linked Cetuximab (by staining with a fluorescein labelled anti-human antibody) and of the nanoparticle-linked dye **4**. The experiment confirmed that the nanoparticles bind more effectively to cells overexpressing the EGFR, with localized emission of dye **4** suggesting endosomial localization, while the high degree of colocalization of Cetuximab and **4** indicates that the nanoparticles maintain their integrity upon internalization.

Taken together, all these experiments confirm an active uptake mechanism, where the targeted nanoparticles bind to the EGF receptors available on the cell surface and are internalized by endocytosis. On the other hand, untargeted nanoparticles are taken up by a slow and non saturable passive mechanism. Hence, optimal selectivity can be achieved for relatively low doses and incubation times.

Finally from the perspective of future "in vivo" evaluations, we investigated the serum stability of our protein conjugated-nanosystems. The nanoparticles functionality, assessed as binding and uptake capabilities on A431 cells, decreases of less than 20% when the incubation of Cetuximab-conjugated nanoparticles was performed in 100% of serum (i.e. 90 minutes at 37°C). The good serum stability was also confirmed when longer incubation times were applied (i.e. 32% of functionality was preserved after 16 hrs of serum pre-treatment, data not shown).

PDT experiments

The phototoxicity of **4** delivered by nanoparticles was determined both in the case of RGD- and Cetuximab-conjugated nanoparticles. In the case of RGD nanoparticles, a significant reduction of the cell viability was found after irradiation of the cells incubated with the **4**-loaded nanoparticles, demonstrating the photokilling activity of the dye embedded in the nanoparticles. Disappointingly, the dose-response curve obtained by treatment of the HUVEC cells with RGD-conjugated nanoparticles was in any case perfectly superimposed (see ESI) to that of RAD-conjugated nanoparticles. A possible explanation of such a behaviour is based on the findings of Allen and co-workers that suggest that RGD, but not RAD, partially protect the cells from PDT induced death by exerting an anti-oxidant and/or anti-apoptotic effect.[32]

Better results were obtained with the Cetuximab-conjugated

nanoparticles (Figure 10), but only when prolonged (6 hours)

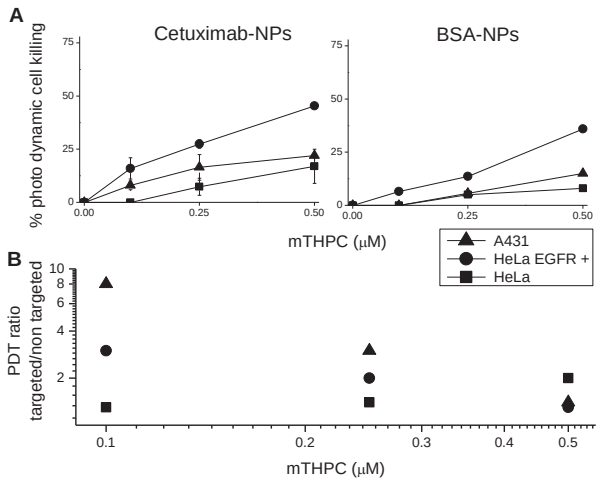

Figure 10. Photokilling efficiency of Cetuximab- and BSA-conjugated **4**-loaded PEG-ORMOSIL nanoparticles upon incubation for 6 hours with different cell lines and light exposure. A) Amount of cells killed with respect to the controls at increasing nanoparticle doses. B) Ratio of photokilling activity between targeted and control nanoparticles on the different cell lines as a function of the dose administered.

incubation times where applied. As revealed from figure 10A, absolute photokilling efficiency does not correlate with uptake in the different cell lines, likely as a result of a different ability of the cell line to resist to cytotoxicity of generated ROS. However, when the attention is focused on the difference between the activity of the targeted and untargeted nanoparticles with each cell line, it appears evident as the Cetuximab-conjugated nanoparticles are substantially more efficient in photokilling A431 cells (up to 8-fold) than the BSA-conjugated counterparts when delivered at doses well below the EGF receptors saturation level. This difference rapidly decreases when the nanoparticles dose is increased, possibly because the non-specific uptake of the untargeted particles becomes more relevant with respect to the receptor-mediated uptake at this prolonged incubation times, or when cells express a lower (HeLa-EGFR, 40% of EGFR with respect to A431) or negligible (HeLa) amount of EGF receptor.

Shorter incubation times at low doses led to negligible photokilling. As a matter of fact, when compared with free mTHPC delivered as standard formulation, Cetuximab-conjugated nanoparticles are still less efficient in producing phototoxicity. The photochemical investigations reported in the previous paragraph exclude the possibility that such a result arises from a lower efficiency of singlet oxygen production by the nanoparticle-embedded photosensitizer. On the other hand, unfavourable localization of the nanoparticles inside the cells could result into a lower cytotoxic activity of the singlet oxygen produced. In fact, it is well-known that mTHPC mainly localises in the Golgi apparatus and the endoplasmic reticulum, while we have showed here that **4**-loaded Cetuximab-conjugated nanoparticles are found essentially in endosomal vesicles.

Conclusions

In summary, the results reported provide interesting insight on how to optimise the properties of VTES-ORMOSIL nanoparticles for biomedical applications, and in particular for targeted therapy. Being designed to operate in a very complex environment such as a living organism, such nanoparticles require a precise design which in turn needs detailed chemical and structural characterization. The first feature that emerges is the flexibility of the synthetic procedure, which enables the one-pot preparation of nanoparticles loaded with the active agent, PEGylated and either targeted or ready for post-targeting. However, realization of such a multifunctional entity requires taking into account all the possible interactions between the components. The organosilica matrix provides a low polarity environment that preserves the photochemical properties of the embedded photosensitizer while maintaining water accessibility, but excessive rigidity of the framework, as here in the case of tetrasilane derivative **5**, may result in an unanticipated perturbation to the photophysical properties in aqueous solution leading to a reduced singlet oxygen yield. Dense PEGylation minimizes toxicity and RES capture, but also uptake by cells. This enables higher selectivity with active targeting strategies, as we demonstrated using the Cetuximab targeting agent. On the other hand, the possibility of adverse interactions between the targeting molecules and the stealth-conferring layer to which they are grafted, as here in the case of folate, must be taken in to account and prevented.

Another important feature is the interaction with proteins, which is fundamental in determining the final fate of a nanoparticle following administration. The results reported herein suggest that not only we can prevent such interactions, as is well known, by coating the particles with PEG or other hydrophilic molecules, but also we can select the interacting proteins by finely tuning the surfaces properties, as here shown in the case of VTES and Stöber particles.

Finally, we explored the crucial point of selective targeting and the importance of the subcellular fate of the nanoparticles. The results we report on RGD and Cetuximab-conjugated nanoparticles clearly show that increased uptake arising from efficient targeting is not sufficient to ensure higher therapeutic efficiency. In particular data obtained with Cetuximab were very informative, since they clearly indicate that differential binding to tumor model cells of nanoparticles and hence of mTHPC loading may be achieved only at doses of ligand-linked nanoparticles that do not saturate the internalization mechanism. Once these specific sites are saturated, non-specific and non-saturable binding sites become more relevant upon increasing the applied nanoparticle concentrations. The resulting paradox is that *selective* photokilling was only achieved under conditions of *partial killing efficacy*. Moreover, subcellular localization may also play an important role in explaining the correlation between uptake and PDT efficacy, since the amount of photosensitizer internalized could not be a good parameter to evaluate the real amount of effective photosensitizer, i.e. the fraction localized at critical sites more susceptible to generated ROS.

These observations may lead to the development of new strategies to improve the intrinsic efficacy of the nanoparticles-carried photosensitizer inside the cell, a parameter that, in the end, appears to be the most critical and limiting to gain effective neoplastic cell disruption. The implementation of active release mechanisms or the addition of other chemical determinants to the nanoparticle coating layer capable of re-directing them to more sensitive intracellular sites/organelles, or helping their

translocation to the cell cytoplasm, could provide solutions to this problem. All this information provides a useful framework in the development of new nanosystems for tumor therapy.

Acknowledgements

Financial support for this research has been provided by European Union (FP7, grant 201031 NANOPHOTO, and FSE post-doc fellowship, DGR n. 1102, to F.S.), by the Italian Ministry of Research (FIRB 2011, RBAP114AMK RINAME) and by the University of Padova (PRAT CPDA110213), by Fondazione Cariverona (Verona Nanomedicine Initiative project), by AIRC 5×1000 and by Fondazione Cariverona/AIRC Progetto Regionale.

The authors thank Matteo Bachicchetto for performing some preliminary experiments and Biolitec research GmbH (Jena, Germany) for supplying Temoporfin (mTHPC).

Notes and references

[a] *Dipartimento di Scienze Chimiche, Università di Padova, via Marzolo 1, Padova, I-35131, Italy. Tel:+39 0498275666; Fax: +39 0498275239. E-mail: fabrizio.mancin@unipd.it*

[b] *Dipartimento di Biologia, Università di Padova, via U. Bassi 58/B, Padova, I-35131, Italy. Tel: +39 0498276335; Fax: +39 8276300. E-mail: elena.reddi@unipd.it*

[c] *Dipartimento di Scienze Biomediche e Centro di Ricerca Inter-dipartimentale per le Biotecnologie Innovative, Università di Padova, via U. Bassi 58/B, Padova, I-35131, Italy. Fax: +39 0498276301 Tel: +39 0498276159. E-mail: emanuele.papini@unipd.it*

[d] *University College London Medical School, National Medical Laser Centre, 67-73 Riding House St, London W1W7EJ, UK. E-mail: E-mail: a.macrobert@ucl.ac.uk*

[e] *Dipartimento di Patologia e Diagnostica, Università di Verona, Piazzale A Scuro 10 , Verona , I-37134, Italy. Fax: +39 045-8124256 Tel: +39 0458126455. E-mail: marco.colombatti@univr.it*

[‡] *These authors equally contributed to the work.*

† Electronic Supplementary Information (ESI) available: Experimental procedures and nanoparticles additional characterization.

1 (a) M. W. Ambrogio, C. R. Thomas, Y.-L. Zhao, J. I. Zink and J. F. Stoddartt, *Acc. Chem. Res.*, 2011, **44**, 903-913; (b) S.-H. Wu, Y. Hung and C.-Y. Mou, *Chem. Commun.*, 2011, **47**, 9972-9985; (c) P. Couleaud, V. Morosini, C. Frochot, S. Richeter, L. Raehm and J.-O. Durand, *Nanoscale*, 2010,**2**, 1083-1095; (d) J. L. Vivero-Escoto, I. I. Slowing, B. G. Trewyn and V. S. Y. Lin, *Small*, 2010, **6**, 1952-196; (e) W. J. M. Mulder, G. J. Strijkers, G. A. F. Van Tilborg, D. P. Cormode, Z. A. Fayad and K. Nicolay, *Acc. Chem. Res.*, 2009, **42**, 904-914; (f) Y. Piao, A. Burns, J. Kim, U. Wiesner and T. Hyeon, *Adv. Funct. Mater.*, 2008, **18**, 3745-3758.

2 *Colloidal Silica: Fundamentals and Applications;*H. E. Bergna and W. O. Roberts, eds.; CRC Press: Boca Raton, 2006.

3 (a) A. Burns, P. Sengupta, T. Zedayko, B. Baird and U. Wiesner, *Small*, 2006, **2**, 723-726; (b) A. Vanblaaderen and A. Vrij, *Langmuir*, 1992, **8**, 2921-2931.

4 B. G. Trewyn, I.I. Slowing, S. Giri, H.-T. Chen and V. S. Y. Lin, *Acc. Chem. Res.*, 2007, **40**, 846-853.

5 (a) J. Hu, M. Chen, X. Fang and L. Wu, *Chem. Soc. Rev.*, 2011, **40**, 5472-5491, (b) X. Du and J. He, *Nanoscale*, 2011, **3**, 3984-4002; (c) L. Bau, B. Bartova, M. Arduini and F. Mancin, *Chem. Commun.*, 2009, 7584-7586.

6 M. Arduini, F. Mancin, P. Tecilla and U. Tonellato, *Langmuir*, 2007, **23**, 8632-8636.

7 L. Bau, P. Tecilla and F. Mancin, *Nanoscale*, 2011, **3**, 121-133.

8 R. Ciriminna, M. Sciortino, G. Alonzo, A. de Schrijver and M. Pagliaro, *Chem. Rev.*, 2011, **111**, 765-789.

9 I. Roy, T. Y. Ohulchanskyy, H. E. Pudavar, E. J. Bergey, A. R. Oseroff, J. Morgan, T. J. Dougherty and P. N. Prasad, *J. Am. Chem. Soc.*, 2003, **125**, 7860-7865.

10 T. Y. Hulchanskyy, I. Roy, L. N. Goswami, Y. Chen, E. J. Bergey, R. K. Pandey, A. R. Oseroff and P. N. Prasad, *Nano Lett.*, 2007, **7**, 2835-2842.

11 S. Kim, T. Y. Ohulchanskyy, H. E. Pudavar, R. K. Pandey and P. N. Prasad, *J. Am. Chem. Soc.*, 2007, **129**, 2669-2675; see also: M. Gary-Bobo, Y. Mir, C. Rouxel, D. Brevet, I. Basile, M. Maynadier, O. Vaillant, O. Mongin, M. Blanchard-Desce, A. Morere, M. Garcia, J. O. Durand, L. Raehm, *Angew. Chem. Int.* Ed. 2011, **50**,11425-11429.

12 S. Kim, T. Y. Ohulchanskyy, D. Bharali, Y. Chen, R. K. Pandey and P. N. Prasad, *J. Phys. Chem. C*, 2009, **113**, 12641-12644.

13 S. Kim, H. E. Pudavar and P. N. Prasad, *Chem. Commun.*, 2006, 2071-2073.

14 W.-C. Law, K.-T. Yong, I. Roy, G. Xu, H. Ding, E. J. Bergey, H. Zeng and P. N. Prasad, *J. Phys. Chem. C*, 2008, **112**, 7972-7977.

15 (a) D. J. Bharali, I. Klejbor, E. K. Stachowiak, P. Dutta, I. Roy, N. Kaur, E. J. Bergey, P. N. Prasad and M. K. Stachowiak, *Proc. Natl. Acad. Sci. U. S. A.*, 2005, **102**, 11539-11544; (b) I. Roy, T. Y. Ohulchanskyy, D. J. Bharali, H. E. Pudavar, R. A. Mistretta, N. Kaur and P. N. Prasad, *Proc. Natl. Acad. Sci. U. S. A.*, 2005, **102**, 279-284.

16 R. Kumar, I. Roy, T. Y. Hulchanskyy, L. N. Goswami, A. C. Bonoiu, E. J. Bergey, K. M. Tramposch, A. Maitra and P. N. Prasad, *ACS Nano*, 2008, **2**, 449-456.

17 (a) A. Gupta, L. N. Goswami, M. Ethirajan, J. Missert, K. V. R. Rao, T. Ohulchanskyy, I. Roy, J. Morgan, P. N. Prasad and R. K. Pandey, *J. Porphyrins Phthalocyanines*, 2011, **15**, 401-411; (b) C. Compagnin, L. Bau, M. Mognato, L. Celotti, G. Miotto, M. Arduini, F. Moret, C. Fede, F. Selvestrel, I. M. Rio Echevarria, F. Mancin and E. Reddi, *Nanotechnology*, 2009, **20**, 345101.

18 I. M. Rio-Echevarria, F. Selvestrel, D. Segat, G. Guarino, R. Tavano, V. Causin, E. Reddi, E. Papini and F. Mancin, *J. Mater. Chem.*, 2010, **20**, 2780-2787.

19 D. Segat, R. Tavano, M. Donini, F. Selvestrel, I. Rio-Echevarria, M. Rojnik, P. Kocbek, J. Kos, S. Iratni, D. Scheglmann, F. Mancin, S. Dusi and E. Papini, *Nanomedicine*, 2011, **6**, 1027-1046.

20 R. Tavano, D. Segat, E. Reddi, J. Kos, M. Rojnik, P. Kocbek, S. Iratni, D. Scheglmann, M. Colucci, I. M. Rio Echevarria, F. Selvestrel, F. Mancin and E. Papini, *Nanomedicine*, 2010, **5**, 881-896.

21 W. Stober, A. Fink and E. Bohn, *J. Colloid. Interface. Sci.*, 1968, **26**, 62-69.

22 (a) Z. Olejniczak, M. Leczka, K. Cholewa-Kowalska, K. Wojtach, M. Rokita and W. Mozgawa, *J. Mol. Struct.*, 2005, **744**, 465-471; (b) Y. J. Eo, D. J. Kim, B. S. Bae, K. C. Song, T. Y. Lee and S. W. Song, *J. Sol-Gel Sci. Technol.*, 1998, **13**, 409-413. (c) D. L. Ou and A. B. Seddon, *J. Non-Cryst. Solids*, 1997, **210**, 187-203.

23 A. Vanblaaderen and A. P. M. Kentgens, *J. Non-Cryst. Solids*, 1992, **149**, 161-178.

24 D. F. Moyano and V. M. Rotello, Langmuir, 2011, **27**, 10376-10385.

25 In contrast, a hydrophilic trianionic phorphyrin covalently embedded into mesoporous silica nanoparticles prepared by the Stöber procedure efficiently produce single oxygen with a quantum yield of 0.57 in ethanol, see: D. Brevet, M. Gary-Bobo, L. Raehm, S. Richeter, O. Hocine, K. Amro, B. Loock, P. Couleaud, C. Frochot, A. Morère, P. Maillard, M. Garcia and J.-O. Durand, *Chem. Commun.*, 2009, 1475-1477

26 a) Y. Ferrand, *Bioorg. Med. Chem. Lett.*, 2003, **13**, 833-835; b) M. Wacker, K. Chen, A. Preuss, K. Possemeyer, B. Roeder and K. Langer, *Int. J. Pharm.*, 2010, **393**, 253-262.

27 a) M. Ravikanth, and T. K. Chandrashekar, *J. Photochem. Photobiol. A: Chem.*, 1993, **74**, 181-187; b) B . Röder, M. Büchner, I. Rückmann and M. O. Senge,*Photochem. Photobiol. Sci.*, 2010, **9**, 1152-1158.

28 P. M. Valencia, M. H. Hanewich-Hollatz, W.Gao, F. Karima, R. Langer, R. Karnik, and O. C. Farokhzad, *Biomaterials,* 2011, **32**, 6226-6233.

29 a) D. Genovese, M. Montalti, L. Prodi, E. Rampazzo, N. Zaccheroni, O. Tosic, K. Altenhoner, F. May and J. Mattay, *Chem. Commun.*, 2011, **47**, 10975-10977; b) E. Rampazzo, S. Bonacchi, R. Juris, M.

Montalti, D. Genovese, N. Zaccheroni, L. Prodi, D. C. Rambaldi, A. Zattoni and P. Reschiglian, *J. Phys. Chem. B*, **2010**, 114, 14605-14613.
30 F. Moret, D. Scheglmann and E. Reddi, *Photochem. Photobiol. Sci*. 2013, *in press*, DOI: 10.1039/c3pp25384h.
31 G. Amit, R. A. Mariuzza, S. E. Phillips, R. J. Poljak, *Science,*1986, **233**, 747-753.
32 C. M. Allen, W.M. Sharman, C. La Madeleine, J. E. van Lier and J. M. Weber, *Photochem. Photobiol. Sci.*, 2002, **1**, 246-254.

Supporting Information

Targeted delivery of photosensitizers: efficacy and selectivity issues revealed by multifunctional ORMOSIL nanovectors in cellular systems

Francesco Selvestrel,[‡] Francesca Moret,[‡] Daniela Segat,[‡] Josephine H. Woodhams,[‡] Giulio Fracasso,[‡] Iria Rio Echevarria, Luca Baù, Federico Rastrelli, Chiara Compagnin, Elena Reddi, Chiara Fedeli, Emanuele Papini, Regina Tavano, Alexandra Mackenzie, Melissa Bovis, Elnaz Yaghini, Alexander MacRobert, Silvia Zanin, Anita Boscaini, Marco Colombatti, and Fabrizio Mancin.

Table of Contents

1. Experimental procedures.

Instrumentation. Ultrafiltration of the nanoparticles was carried out using a 75 ml Amicon® Ultrafiltration Cell, Millipore® using a cellulose membrane with a cut-off of 10,000 Da.
UV-Vis absorption spectra were measured in water on a Perkin-Elmer Lambda 45 UV-Vis spectrophotometer with 1 cm path length quartz cuvettes.
Fluorescence spectra were measured in water on a Perkin-Elmer LS-50B fluorimeter with 1 cm path length quartz cuvettes. Infrared spectra were recorded on a Nicolet 5700 FT-IR instrument.
NMR spectra in the solution state were recorded on a Bruker Avance (250 MHz ^{1}H frequency) or on a Bruker AC-300 (300 MHz ^{1}H frequency). NMR spectra in the solid state were collected on a Varian 400 equipped with a narrow bore, triple resonance T3 MAS probe spinning 4 mm rotors and operating at ^{1}H, ^{29}Si and ^{13}C frequencies of 400.36, 79.51 and 100.68 MHz, respectively. The nominal temperature of the probe was always set to 298 K. ^{13}C CP-MAS spectra were acquired at 5 kHz MAS with 1200 scans and a repetition delay up to 3 s. The contact time for CP was 2 ms, and an acquisition time of 50 ms was used. ^{29}Si spectra were obtained at 5 kHz MAS with a basic pulse-acquire sequence (2048 scans) and a recycle delay of 60 s. The chemical shifts were referenced externally against the $^{13}CH_2$ resonance observed for adamantane at 38.48 ppm (for ^{13}C) or against the signal of Q8M8 (for ^{29}Si).
The hydrodynamic particle size (Dynamic Light Scattering, DLS) and Z-potential were measured with a Malvern Zetasizer Nano-S equipped with a HeNe laser (633nm) and a Peltier thermostatic system. Measurements were performed at 25 °C in water or PBS buffer at pH 7.0.
Transmission electron microscopy (TEM) was recorded on a Jeol 300PX instrument. One drop of sample was placed on the sample grid and the solvent was allowed to evaporate.
Thermogravimetric analysis (TGA) was run on 5 mg lyophilized nanoparticle samples using a SDT-2960 model TA instrument from 30 to 1,200 °C under a continuous air flow.

Solvents and reagents. Solvents were of analytical reagent grade, laboratory reagent grade or HPLC grade. Water was purified using a Milli-Q® water purification system. High surface area hydrophobic Bio-Beads® SM were obtained from Bio-Rad and used according to instructions of the supplier. Haba-Avidin Test and EZview Red Streptavidin Affinity Gel were obtained by Aldrich and used according to the manufacturer instructions. 2-(4-chlorosulfonylphenyl)ethyltrimethoxy silane (50 % solution in dichloromethane) was obtained by ACROS. 5-(4-Aminophenyl)-10,15,20-triphenyl-porphyrin was purchased by Porphyrins Systems. Cyclo[RGDfK(AcSCH$_2$CO)] and cyclo[RGDfK(AcSCH$_2$CO)] where obtained by Peptides International. 5,10,15,20-tetra(3-hydroxyphenyl)-(2,3-dihydro)porphyrin (mTHPC, temoporfin) was gently provided by Biolitec. Derivatives **1**, **2**, Folate-OSu, Biotin-OSu were prepared as previously reported. All the other reagents were used as received from Sigma-Aldrich.

2. Synthesis of derivatives 3-5.

2.1 Synthesis N-[3-(triethoxysilyl)propyl]-N'-[4-(10,15,20-triphenylporphin-5-yl)phenyl]-urea (3).
In a sealed tube, 50 mg (0.08 mmol) of 5-(4-aminophenyl)-10,15,20-triphenylporphyrin and 198 µL (0.8 mmol) of 3-(trimethoxysilyl)propyl isocyanate are dissolved in 6 mL of dry acetonitrile and the reaction mixture is heated at 90°C for 24 hours. The reaction is followed by TLC (eluent: Petroleum Ether/EtOAc = 2:1, Rf = 0.22). The solvent is removed and the solid obtained is redissolved in 2 mL of CH_2Cl_2 and precipitated in 60 mL of n-hexane. The product is recovered by centrifugation at 4,000 g for 20 minutes. The procedure is repeated 3 times providing after drying 52 mg of a violet powder (yield 74%).
^{1}H-NMR (250 MHz, $CDCl_3$): δ -2.78 (s, 2H, N*H*), 0.77 (t, 2H, J = 7.5 Hz, Si*CH_2*), 1.27 (t, 9H, J = 7 Hz, C*H_3*CH_2O), 1.80 (qn, 2H, J = 7.5 Hz, $SiCH_2C$*H_2*), 3.88 (q, 6H, J = 7.5 Hz, CH_3C*H_2*O), 7.73 (m, 11H, Ar*H*), 8.18 (m, 8H, Ar*H*), 8.87 (m, 8H, Ar*H*).
ESI-MS: m/z calcd. for $C_{54}H_{53}N_6O_4Si$ $[M + H]^+$: 877.4; found: 876.9 (100%).

2.2 Synthesis of N-[3-(triethoxysilyl)propyl]-O-[4-(10,15,20-tri(3-hydroxyphenyl)-(2,3-dihydro) porphin-5-yl) phenyl]-carbamate (4).
In a small conical vial, 17 mg (0.025 mmol) of mTHPC, 15.4 □L (0.062 mmol) of 3-(trimethoxysilyl)propyl isocyanate and 8.6 µL (0.062 mmol) of triethylamine are dissolved in 100 µL of dry THF. The reaction is followed by TLC (eluent EtPet: iPrOH = 3:1, $Rf_{mTHPC-Si}$ = 0.3, $Rf_{mTHPC-2Si}$ = 0.4, $Rf_{mTHPC-3Si}$ = 0.5). The solvent is evaporated and the product is used without other purifications.
ESI-MS: m/z calcd. for $C_{54}H_{54}N_5O_8Si$ $[M_{mTHPC-Si} + H]^+$: 928.4; found: 928.7 (100%), $C_{64}H_{75}N_6O_{12}Si_2$ $[M_{mTHPC-2Si} + H]^+$: 1175.5; found: 1175.8 (30%).
UV-vis (toluene): λ_{max} (nm) 420, 518, 545, 601, 654.

2.3 Synthesis of 5,10,15,20-tetra(3-(N-(triethoxysilylpropyl)carbamate)phenyl)-(2,3-dihydro) porphyrin (5).
In a small conical vial, 17 mg (0.025 mmol) of mTHPC, 24.7 µL (0.1 mmol) of 3-(trimethoxysilyl)propyl isocyanate and 13.8 µL (0.1 mmol) of triethylamine are dissolved in 100 µL of dry THF. The reaction is followed by TLC (eluent EtPet: iPrOH = 3:1, $Rf_{mTHPC-3Si}$ = 0.5, $Rf_{mTHPC-4Si}$ = 0.6). The solvent is evaporated and the product is used without other purifications.
ESI-MS: m/z calcd. for $C_{74}H_{96}N_7O_{16}Si_3$ $[M_{mTHPC-3Si} + H]^+$: 1422.6; found: 1422.7 (100%), $C_{84}H_{117}N_8O_{20}Si_4$ $[M_{mTHPC-3Si} + H]^+$: 1669.7; found: 1669.8 (20%).
UV-vis (toluene): λ_{max} (nm) 420, 518, 545, 601, 654.

3. Synthesis and purification of the nanoparticles.

3.1 Stöber nanoparticles.

To a thermostated vessel charged with **3** (4 mg, 0.005 mmol) and ethanol (20 mL), 100 μL (0.45 mmol) of TEOS were added under stirring at 25 °C. Subsequently, 1 mL of a 14.8 M aqueous solution of ammonia was added to initiate the polymerization. After 16 hours, the solution was diluted to 80 mL with ethanol and concentrated to the original volume by ultrafiltration (Amicon stirred cell) through a regenerated cellulose membrane (cut-off 10 kDa) under nitrogen pressure (4 bar). The procedure was repeated five times with ethanol and 7 times with Milli-Q water. The resulting solution was filtered through a 0.22 μm cellulose acetate membrane.

3.2 VTES nanoparticles (OS).

Brij 35 (90 mg, 75 μmol, 15 mM) was dissolved under stirring in 5 ml of water at 25°C into a thermostated reaction vessel. Subsequently, 150 μL (1.64 μmol) of *n*-butanol, 25 μL (10 mM DMSO solution) of **3** and VTES (45 mg, 0.24 mmol) were added. The mixture was vigorously stirred for 30 min (very important) and then 10 μL of a 14.8 M aqueous solution of ammonia were added to initiate the polymerization. After 2 hours, the solution was transferred into an Amicon stirred cell and extensively ultrafiltrated with 1.5 L of Milli-Q water, using a regenerated cellulose membrane (cut-off size 10 kD). The nanoparticles suspension was then collected and filtered through a 0.22 μm cellulose acetate filter.

3.3 PEGylated VTES nanoparticles (OS/PEG).

The appropriate amount of Brij 35 (see the following table), **1** (15.2 μmol, 3 mM), *n*-butanol (150 μL, 1.64 μmol) and, when required, **3**, **4** or **5** (10 mM DMSO solution, 10 to 130 μL) were dissolved under stirring in 5 mL of water into a thermostated reaction vessel. The temperature was adjusted according to the following table and the desired amount of VTES was added:

NP	*Final Size (nm)*	*T (°C)*	*Brij35 (mM)*	*VTES (mM)*
OS/PEG	20	25	15	50
OS/PEG	50	30	5	50
OS/PEG	90	30	5	100

The mixture was vigorously stirred for 30 min (very important) and then 10 μL of a 14.8 M aqueous solution of ammonia were added. The mixture was further stirred for 2 hours at constant temperature. Then 14.3 mg of Bio-Beads® SM per mg of surfactant were added and the suspension was gently stirred for 3 hours. The beads were filtered off with filter paper and the filtrate diluted to 15 mL with Milli-Q water and concentrated to 0.5 mL by ultrafiltration with Amicon Ultra-15 Centrifugal Filter Units (cut-off 10 kDa) at 4,000 g. The procedure (dilution-concentration) was

repeated seven times. The resulting solution was diluted to the original volume and filtered through a 0.22 μm cellulose acetate filter.
When required to prepare **amine/OS/PEG** nanoparticles, part of **1** was replaced with **2 (**0.1 to 30 % in moles) to provide amine groups in the PEG. Some examples are given in the following table.

NP	*Final Size (nm)*	*T (°C)*	*Brij35 (mM)*	***1** (μmol)*	***2** (μmol)*	*VTES (mM)*
OS/PEG **(**1% **2**)	100	30	5	15.0	0.15	100
OS/PEG **(**10% **2**)	100	30	5	13.7	1.5	100
OS/PEG **(**30% **2**)	100	30	5	10.7	4.5	100

Note 1: The amino-PEG derivative **2,** in DMSO solution**,** must be added to the reaction mixture just before the addition of ammonia.
Note 2. 20-nm VTES nanoparticles can be synthesized at 30°C using Tween 80 (33 mg, 25 μmol, 5 mM) in place of Brij 35, in this case *n*-buthanol is not needed.

3.3.1 Folate and Biotin conjugated nanoparticles.
To a preparation of crude (unpurified) **amine/OS/PEG** (as described in the previous paragraph) Folate-OSu or Biotin-OSu dissolved in DMSO (20 equivalents with respect to the amount of **2** used in the synthesis of the nanoparticles) were added and the mixture was further stirred at 25 °C for 16 h. Then 14.3 mg of Bio-Beads® SM per mg of surfactant were added and the mixture was further gently stirred for 3 hours. The beads were filtered off with filter paper and the filtrate diluted to 15 mL with Milli-Q water and concentrated to 0.5 mL by ultrafiltration with Amicon Ultra-15 Centrifugal Filter Units (cut-off 10 kDa) at 4,000 g. The procedure was repeated seven times for biotin-conjugated nanoparticles and 10 times for folate-conjugate nanoparticles. The resulting solution was diluted to the original volume and filtered through a 0.22 μm cellulose acetate filter.

3.3.2 RGD and RAD conjugated nanoparticles.
Into a thermostated reaction vessel, PBS-10x (0.5 mL) was added to a purified preparation of amine/OS/PEG nanoparticles (5 mL). The pH was adjusted to 7.2, then MBS (20 equivalents with respect to the amount of **2** used for the synthesis of the nanoparticles) was added and the mixture was stirred at 30 °C for 16 h. The mixture was then filtered through a 0.45 μm cellulose acetate filter, the filtrate was diluted to 15 mL with Milli-Q water and concentrated to 0.5 mL by ultrafiltration with an Amicon Ultra-15 Centrifugal Filter Unit (cut-off 10 kDa) at 4,000 g. The procedure was repeated seven times. The resulting solution was diluted to the original volume (5.5 mL) and filtered through a 0.22 μm cellulose acetate membrane. HEPES buffer (5 mM, 0.5mL) was added and the pH was adjusted to 7. Then, the solution was split in three fractions of 2 mL each.

RGD or RAD peptides (1 equivalent with respect to the amount of **2** used in the synthesis of the nanoparticles) were deacetylated in 0.1 mL of an HEPES (17 mM)/$NH_2OH{\cdot}HCl$ (17 mM)/ EDTA (10 mM) buffer (pH 7.2) for 1 h at room temperature. Then, the resulting RGD/RAD solution (0.1 mL) was added to one of the nanoparticles aliquots (2 mL). The solutions were stirred overnight at RT. The solution was then diluted to 15 mL with Milli-Q water and concentrated to 0.5 mL by ultrafiltration with an Amicon Ultra-15 Centrifugal Filter Unit (cut-off 10 kDa) at 4,000 g. The procedure was repeated seven times. The resulting solution was diluted to the original volume and filtered through a 0.22 μm cellulose acetate filter.

3.3.3 Cetuximab and Bovine Serum Albumin (BSA) conjugated nanoparticles.

For the conjugation of these proteins to the nanoparticle surface we decided to derivatize the PEG-amino groups with the cross-linker MBS using the same procedures described for the conjugation of RGD and RAD peptides, whereas the proteins (i.e. Cetuximab and BSA) were functionalized by 2-iminothiolane (2-IT) reaction that modified the NH2 of lysine introducing new free sulfhydryl groups. Briefly, the protein functionalization was performed o/n at 4°C, the reaction blocked with glycine 0.2 M for 20 minutes at r.t. and finally the derivatized proteins were purified by gel filtration on PD10 columns (Sephadex G-25M, GE Healthcare) in order to remove the excess of 2-IT. The number of introduced SH groups were calculated using the Ellman's assay; the NP-protein conjugation was performed o/n at 30°C and then a dialysis step was performed for 24 hr at r.t. in PBS EDTA 10 mM.

At last nanoconjugates were purified from the unreacted reagent by a first step of centrifugation at 100,000 g for 45 minutes and a second step of size exclusion chromatography on HiLoad 16/60 column (Superdex 75 prep grade, GE Healthcare) using a FPLC apparatus (Biologic Workstation, Bio-Rad). The purified fractions were concentrated by centrifugation.

4. Characterization of the nanoparticles.

4.1 TEM analysis.

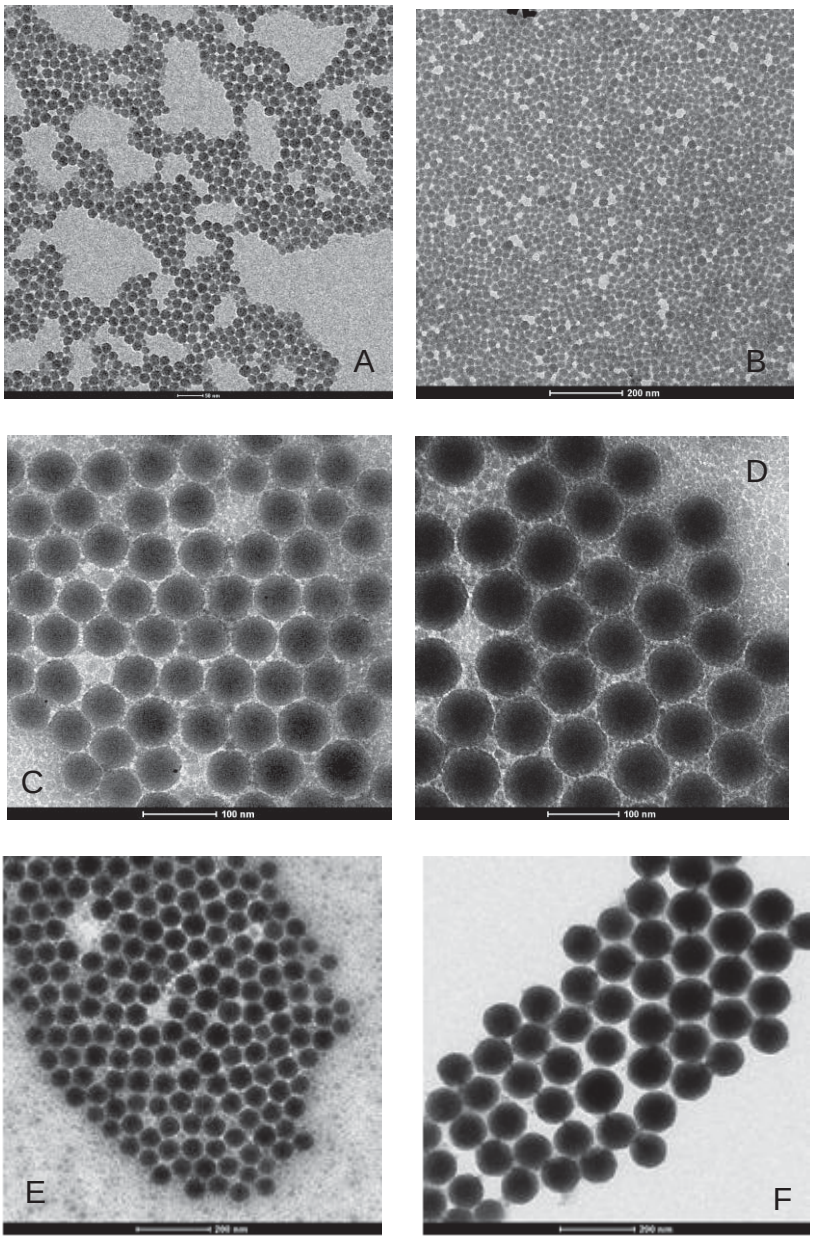

Figure S1. TEM images of **OS/PEG** nanoparticles with different sizes: 20 nm (A, B), 55 nm (C, E), 70 nm (D), 90 nm (F).

4.2 DLS analysis

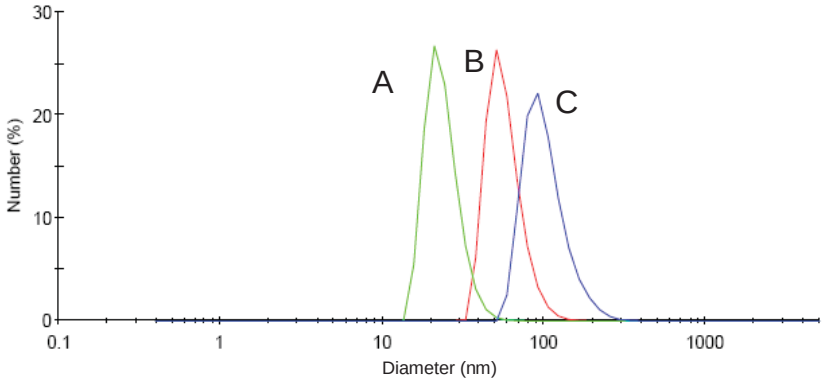

Figure S2. DLS analysis of **OS/PEG** nanoparticles with different sizes: 20 nm (A), 55 nm (B), 90 nm (C).

4.3 UV-Vis and Fluorescence analysis.

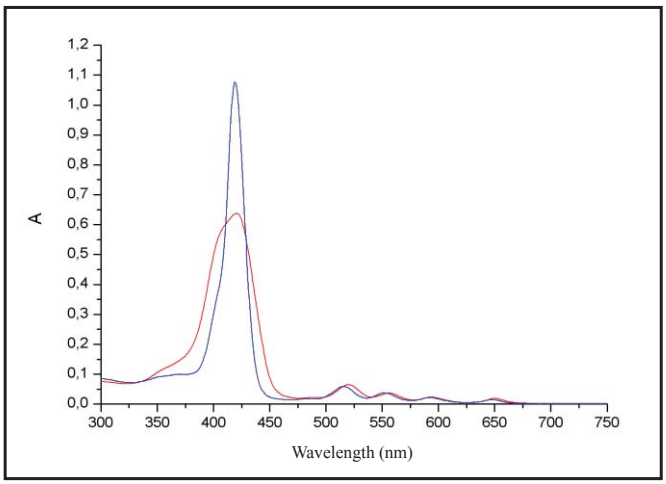

Figure S3. UV-Vis spectrum of 20-nm diameter **Stöber** (red) and **OS** (blue) nanoparticles doped with dye **3** (water, 25 °C). See Table 1, entries 2 and 3.

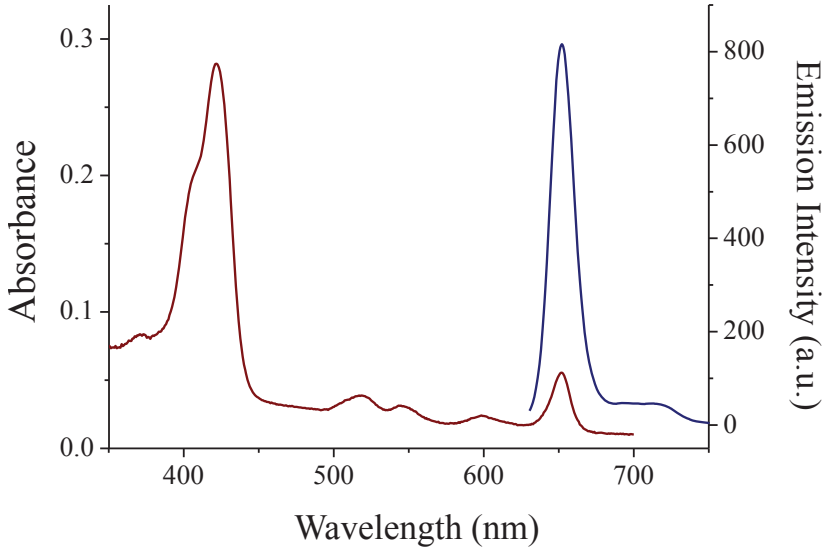

Figure S4. UV-Vis absorption (purple) and emission (blue) spectrum of 90-nm diameter **OS/PEG** nanoparticles doped with dye **4** (water, 25 °C). See Table 1, entry 7.

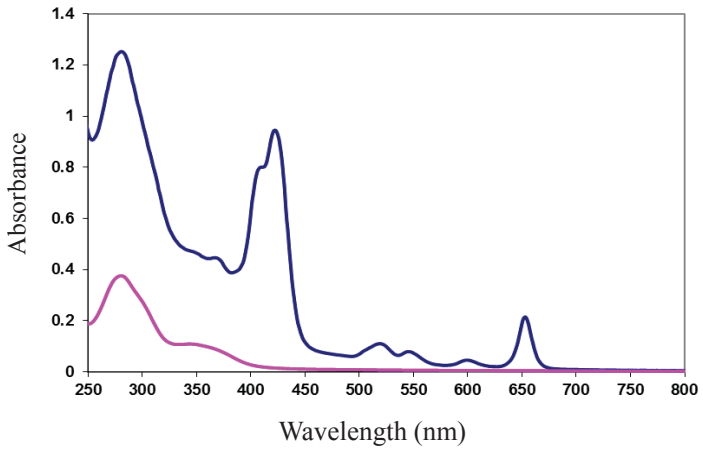

Figure S5. UV-Vis spectrum of 90-nm diameter **amine/OS/PEG** nanoparticles doped with dye **4** and targeted with folic acid (blue, water, 25 °C) and of folic acid (magenta, water, 25 °C).

4.4 TGA analysis.

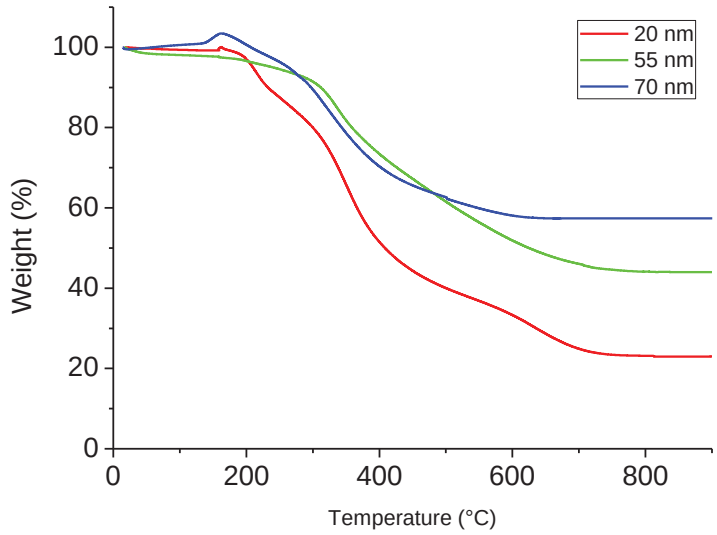

Figure S6. Thermogravimetric (TGA) profiles in air of **OS/PEG** nanoparticles of different sizes: red: 20 nm diameter; green: 55 nm diameter; blue: 70 nm diameter.

Weight fraction of the ORMOSIL cores was calculated by assuming that the residue at 900° is silica (SiO_2) and adding the corresponding weight of the vinyl groups. Weight of a single ORMOSIL core was calculated from the particles diameter using an estimated density of 1.5 g/cm^3, as vinyltriethoxysilane ORMOSIL nanoparticles are considered (see ref. 9) to be less dense than pure silica ones (2.0 g/cm^3). PEG surface density is then easily calculated on the basis of geometrical considerations.

4.5 Avidin tests.

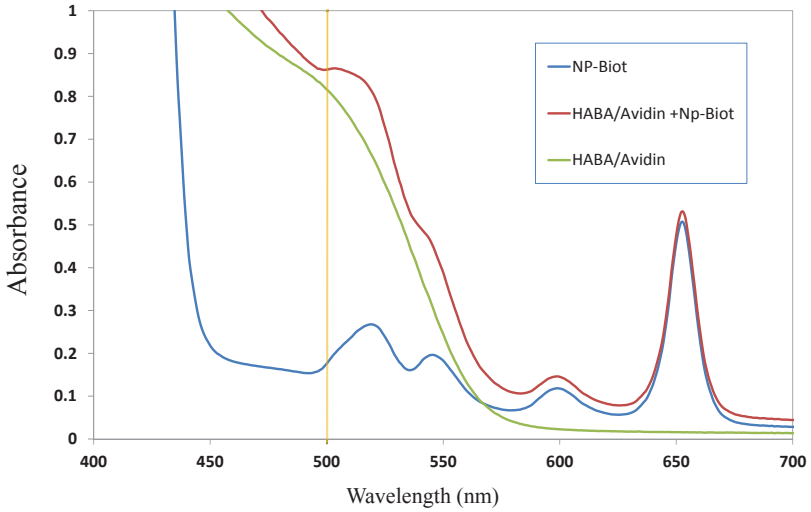

Figure S7. HABA/AVIDIN test on 90-nm diameter **amine/OS/PEG** nanoparticles doped with dye **4** and targeted with biotin. The test is based on the displacement of the HABA dye bound to avidin by biotin. The displacement causes a decrease in the absorption of the HABA dye at 500 nm that allow to measure the amount of biotin present in the sample analyzed.

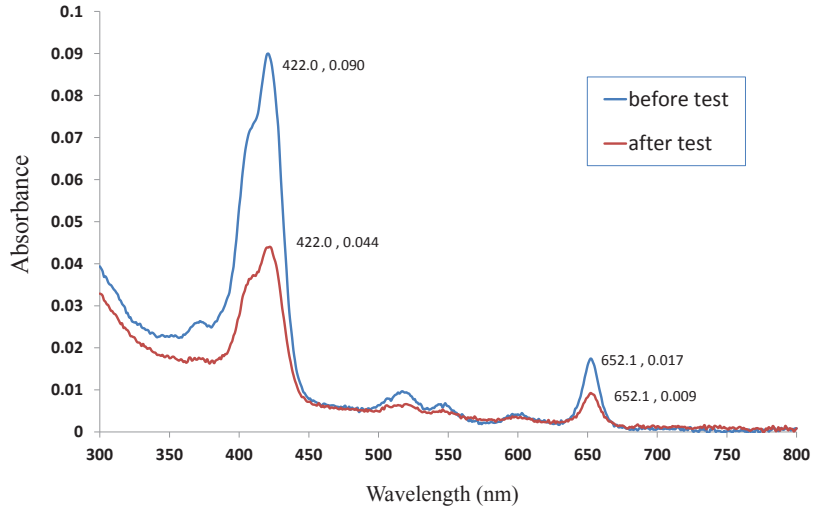

Figure S8. EZview™ Red Streptavidin Affinity Gel test on 90-nm diameter **amine/OS/PEG** nanoparticles doped with dye **4** and targeted with biotin. The test is based on streptavidin coated agarose beads, the nanoparticles are incubated with the beads for 1 hour and the beads are then removed, the difference in the absorbance before and after the beads incubation confirm the conjugation of the particles with the biotin.

4.6 Western blot analysis of Cetuximab-conjugated nanoparticles.

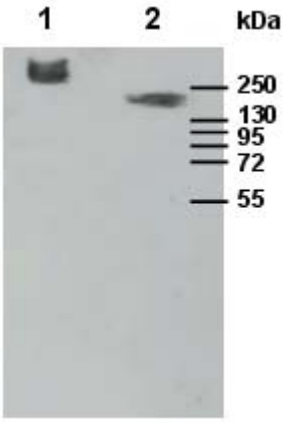

Figure S9. Western blot analysis to confirm the antibody conjugation to the nanoparticles. Cetuximab-conjugated NPs (lane 1) and Cetuximab (lane 2) were separated by SDS-PAGE under non reducing condition and after the transfer onto a membrane of nitrocellulose the antibodies were stained using an anti-human antibody conjugated to HRP. Chemiluminescent signals, developed using ECL substrate, were detected by photographic films.

5. Photophysical studies.

5.1 Absorbance and Fluorescence Measurements.

Absorbance spectra were measured using a Perkin-Elmer (Beaconsfield, UK) Lambda 25 UV/Vis spectrometer with 1 cm path length quartz cuvette. Fluorescence spectra were measured using a Perkin-Elmer LS50-B spectrofluorimeter equipped with a bifurcated fiber-optic probe.

5.2 Fluorescence Lifetime Measurements.

Fluorescence lifetimes were measured using time correlated single photon counting (TCSPC). Dilute solutions were prepared with the dye concentration at 0.5 μM and placed in a 1 cm path length quartz cuvette. A pulsed laser diode module (90 picosecond pulse duration) was used to excite the samples at 405 nm at a 5MHz repetition rate (EPL-405, Edinburgh Instruments Ltd., UK). The fluorescence was detected using a fast multialkali photomultiplier module (model H5773-04, Hamamatusu Photonics K.K., Japan) via a longpass filter (OG510, Schott, UK) and a monochromator (model M300, Bentham Instrument Ltd, UK). A Lyot depolarizer (Thorlabs Ltd, UK) was incorporated to minimize any polarisation anisotropy artefacts. TCSPC was carried out using a PC-mounted TCSPC board (TimeHarp, Picoquant GmbH, Germany) and lifetimes were derived using Fluofit software (PicoQuant GmbH, Germany). The Instrument Response Function (IRF) was obtained from a non-fluorescent scattering Ludox® solution (Sigmal-Aldrich, Gillingham, UK). Optimum fitting with minimization of the residuals was confirmed using a Chi-squared value $\chi^2 < 1.4$.

5.3 Singlet Oxygen Measurements.

The singlet oxygen phosphorescence at 1270 nm was detected using time-resolved photon counting from air-equilibrated, deuterated aqueous or methanolic solutions in quartz cuvettes. For detection in the near-IR, a thermoelectrically cooled photomultiplier (model H10330-45, Hamamatsu Photonics Ltd, UK) was used, and emission was collected via a series of lenses from the cuvette in combination with a long-pass and a band-pass filter centered at 1270 nm (BK Interferenzoptik Electronik, Germany). The solutions were excited using a 532 nm Nd:YAG laser (Lumanova GmbH, Germany) with the beam axis aligned orthogonally to the collection optics. The laser was pulsed at a repetition rate of 3 kHz and a pulse length of 3 ns, giving a mean power of 8 mW, and a fast photodiode (1 ns rise time, Becker-Hickl, Berlin, Germany) was used to synchronize the laser pulse with the photon counting detection system. A series of neutral density filters was used to attenuate the laser power. The photon counting equipment consisted of a PC-mounted multiscaler board (model MSA-300, Becker-Hickl, Germany) and a pre-amplifier (Becker-Hickl, Germany) which gave a resolution of 5 ns per channel. Time-resolved phosphorescence measurements were accumulated by the multiscaler board. The traces were analysed using FluoFit software (PicoQuant GmbH, Germany) to extract the singlet oxygen decay lifetime. To calculate the quantum yield, Rose Bengal was used as the standard which has singlet oxygen yields of 0.76 in D2O and 0.79 in MeOD (R. W. Redmond, and J. N. Gamlin, “A compilation of singlet oxygen yields from biologically relevant molecules” *Photochem. Photobiol.* 1999, **70**, 391-475). The concentrations

were adjusted to give the same absorbance at 532 nm, and to analyze the time-resolved data we used the standard zero-intercept method.

6. Protein binding studies.

6.1 Nanoparticles incubation with human plasma.

Venous blood was taken from healthy volunteers and immediately anticoagulated with 3.8% trisodium citrate (9 vol blood + 1 vol citrate). Plateled poor plasma (PPP) was obtained by centrifuging blood at 2,000 g for 10 min, without use of a brake. Plasma aliquots were frozen in liquid nitrogen and stored at -20°C until time of use. Before use, plasma was thawed and centrifuged at 16000 g at 4°C for 20 min, to eliminate any precipitate. Then, it was diluted in PBS EDTA 1 mM pH 7.4 at a final concentration of 24% (v/v), filtered through a 0.22 µM filter and incubated with PBS (ctrl) and 2 mg of ORMOSIL or Ludox® nanoparticles for 1 hour at 37°C under gentle stirring. Then, nanoparticles were recovered by ultracentrifuging at 100,000 g for 1 h at 4°C, using a XL-70 Ultracentrifuge (Beckman), and washed twice with PBS EDTA 1 mM pH 7.4.

6.2 Identification of plasma proteins adsorbed to nanoparticles surface.

The pellet of nanoparticles was dissolved in 150 µl of non-reducing sample buffer (50 mM Tris HCl pH 6.8, 2% SDS, 0.06% bromophenol blue, 6% glycerol) plus protease inhibitors cocktail (Sigma Aldrich), heated at 95°C for 5 min and loaded on a 12% (v/v) SDS-PAGE. After protein staining with colloidal Comassie G-250, bands of interest were excised and analyzed by mass spectrometry.

7. Biological studies

7.1 Cell culture and incubation experiments.

A549 (human lung carcinoma cells), CCD-34Lu (human normal lung fibroblasts), KB (folate receptor positive cells derived via HeLa contamination), HeLa (human malignant cervical cells expressing low amounts of EGF receptor), A431 (human epidermoid carcinoma cells, expressing high amounts of EGF receptor) and HUVEC (human umbilical vein endothelial cells, overexpressing $\alpha_v\beta_3$ integrin) cell lines were obtained from American Type Culture Collection (ATCC, Rockville, USA). The cells were maintained at 37 °C in a humidified atmosphere containing 5% CO_2 and 90% of humidity. A549 were cultured in F-12K medium containing 2 mM L-glutamine and 2.5 g/L sodium bicarbonate; CCD-34Lu, HeLa and A431 were cultured in Dulbecco Modified Eagle's Medium (DMEM) containing 3.7 g/L sodium bicarbonate, 4.5 g/L glucose and supplemented with 0.1 mM MEM non essential amino acids and 0.02 M HEPES while KB were cultured in Modified Eagle's Medium (MEM). All the media were supplemented with 10% heat-inactivated foetal bovine serum (FBS) (Invitrogen, NY, USA) and antibiotics (38 units/mL streptomycin and 100 units/mL penicillin G (Sigma-Aldrich, St Louis, MO, USA). HUVEC cells were cultured in Medium-200 supplemented with antibiotics and with the Low Serum Supplement Kit (Invitrogen) having a final FBS concentration of 2%. To obtain stabilized EGFR-expressing HeLa cells (HeLa EGFR +), $3x10^6$ cells were transfected with 30 μg of pBABE-EGFR plasmid (Addgene) by means of electroporation treatment (250 V, 950 μF) in 0.45 cm electroporation cuvettes (Gene Pulser, Bio-Rad); after two days, transfected cells were diluted and selected in 2 μg/ml puromycin-containing medium (Sigma).

In all the experiments, the cells (A549, CCD-34Lu, KB, A431, HeLa and HeLa EGFR +) were seeded and maintained for 24 h in culture medium supplemented with 10% FBS (complete medium) before starting the treatment; then, the medium was replaced with fresh medium containing 3% FBS, in which free mTHPC or nanoparticle suspensions were freshly diluted. For HUVEC cells no additional serum was used nor for the seed nor for the treatments.

7.2 Cellular uptake of mTHPC in standard solvent or loaded in ORMOSIL/PEG nanoparticles.

A549 and CCD-34Lu cells (10^5) were seeded in 2 mL of complete medium in 35 mm diameter tissue culture dishes. After 24 h, the cells were incubated with increasing concentrations (0.25-1.75 μM) of mTHPC, delivered by standard solvent (Foscan®, ethanol/poly(ethylene glycol) 400/water; 20:30:50, by vol.) or by **OS/PEG** nanoparticles in the form of dye **4**, (Table 1). After 24 h of incubation, the cells were washed twice with 2 mL of versene, detached with 500 μL of trypsin (Invitrogen) that was neutralized with the addition of 200 μL of FBS. Cells were centrifuged and resuspended in versene before measuring mTHPC fluorescence by flow cytometry with a BD FACSCanto™ II (Becton Dickinson, San Jose, California, USA). The blue laser at 488 nm was used as excitation source and wavelengths longer than 670 nm (PerCP channel) were used for the detection of the mTHPC fluorescence. Ten thousand events/sample were acquired and analyzed with the FACSDiva Software.

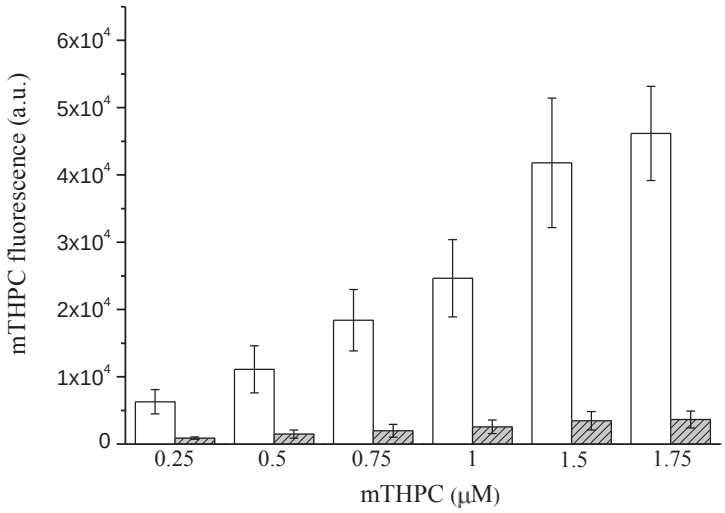

Figure S10. Flow cytometry measurements of mTHPC and derivative **4** uptake in CCD-34Lu normal cells incubated for 24 h with increasing concentration of free mTHPC (white) or **4**-doped **OS/PEG** nanoparticles (grey).

7.3 Specific uptake of mTHPC (dye 4) loaded in targeted ORMOSIL/PEG nanoparticles.
Folate-targeted nanoparticles. 10^5 KB cells were seeded in 2 mL of folate-deficient RPMI medium and 24 h after the seeding were incubated for 5 h with increasing concentration (0.005-1 μM) of mTHPC (dye **4**, Table 1) in folate-targeted (0.1 or 1% folate) or un-targeted (0% folate) **OS/PEG** nanoparticles. After incubation time, the cells were washed, detached from the plates and analyzed by flow cytometry to measure mTHPC fluorescence as described above. Competition experiments with 1 mM of free folic acid (Sigma-Aldrich) were carried out incubating the cells for 1 h prior the addition of NPs in order to saturate folate receptors present on KB cell surface.

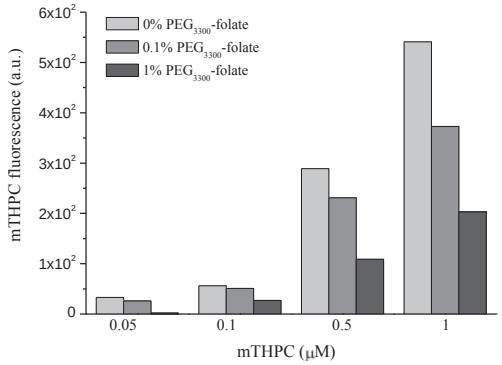

Figure S11. Flow cytometry measurements of mTHPC derivative **4** uptake in folate receptor positive KB cells incubated for 5 h with increasing concentration of **4**-doped **OS/PEG** nanoparticles conjugated with folate in different amounts (light grey: 0%, grey: 0.1%, dark grey 1% PEG_{3300}-folate/PEG_{2000}).

RGD-targeted nanoparticles. 50,000 HUVEC cells were seeded in 500 µl of M-200 medium in 24-well plates. After 24 h, the cells were incubated with 0.1 or 1 µM mTHPC (dye **4**, Table 1) loaded in RGD-NPs or RAD-NPs for 3 or 24 h. After incubation, the cells were washed twice with 500 µl of versene, detached with 200 µL of trypsin and neutralized with 100 µL of FBS before flow cytometry analysis (see text).

Cetuximab-targeted nanoparticles. To analyze the cellular uptake 100,000 A431 cells were seeded in 500 µl of DMEM medium in 24-well plates. After 24 h, the cells were incubated with 1 µM mTHPC (dye **4**, Table 1) loaded in Cetuximab-NPs, NPs-alone or BSA-NPs for 90 minutes at 37°C; finally, the cells were washed twice with 500 µl of versene, detached with 200 µL of trypsin and neutralized with 100 µL of FBS before flow cytometry analysis. For competition experiments Cetuximab and BSA-NPs were mixed with a molar excess of free Cetuximab before the incubation with the cells. In order to investigate if the uptake is dose-dependent, A431 cells were incubated with increasing amounts of mTHPC (dye **4**, Table 1) loaded on Cetuximab-NPs or BSA-NPs for 90 minutes at 37°C and then analyzed by flow cytometry. Finally to evaluate the serum stability, Cetuximab-NPs or BSA-NPs were incubated for 90 minutes at 37°C with increasing concentrations of serum (i.e. ranging from 10% to 100%) before to assess their functionality in uptake experiments on A431 cells.

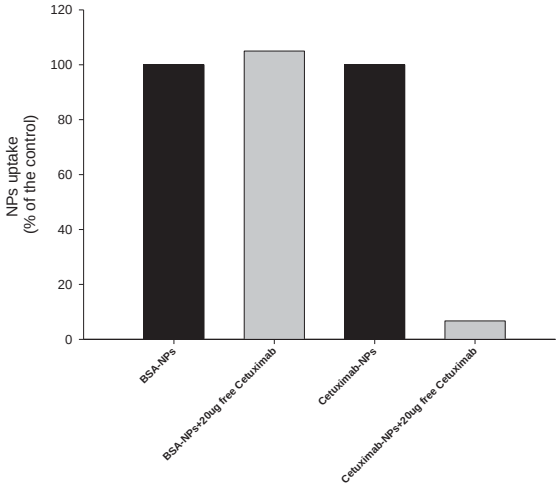

Figure S12. Displacement of the uptake of Cetuximab or BSA-**4** doped **OS/PEG** on A431 cells by free Cetuximab. Live adherent cells were incubated with a fixed NP concentration (concentration of 0.25 µM in dye 4) and with or without an excess of free Cetuximab (20 µg of antibody) for 90 minutes at 37°C. After washings, detachment from the well and a further washing step cells were analyzed by flow cytometry measuring the dye **4** fluorescence (APC channel).

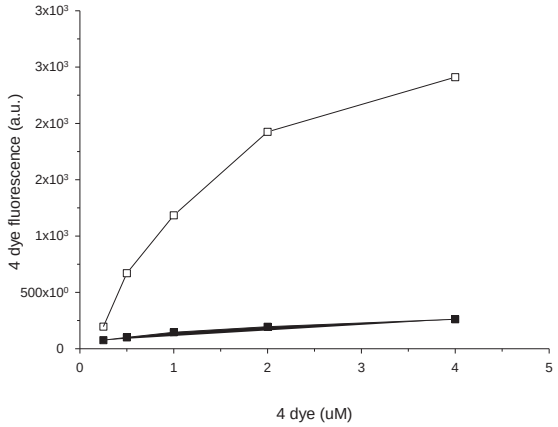

Figure S13. Differential uptake of Cetuximab-NPs (□) and BSA-NPs (■) on A431 cells. Live adherent cells were incubated with increasing concentrations (concentration ranging from 0.25 to 4 μM in dye **4**) of **4**-doped **OS/PEG** for 90 minutes at 37°C. After washings, detachment from the well and a further washing step, cells were analyzed by flow cytometry measuring the dye **4** fluorescence (APC channel).

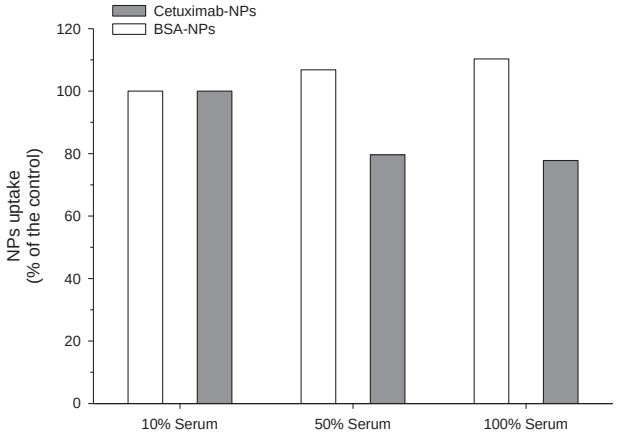

Figure S14. Serum stability of Cetuximab-NPs and BSA-NPs. After a pre-incubation of NP batches in serum at 37°C for 90 minutes, the NP functionality was assessed measuring the uptake on A431 cells. Briefly, serum-treated NPs were incubated on A431 cells for 90 minutes at 37°C; after washings, detachment from the well and a further washing step cells were analyzed by flow cytometry measuring the dye **4** fluorescence (APC channel).

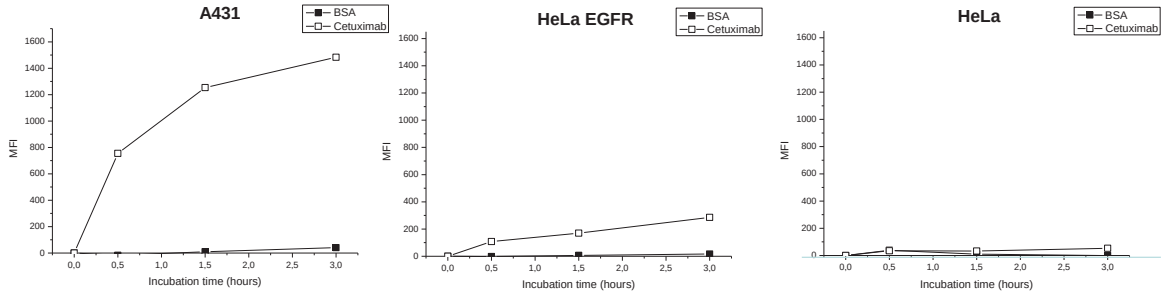

Figure S15. Time-dependant uptake of Cetuximab- and BSA- conjugated nanoparticles with different cell lines. EGFR positive A431 cells, EGFR over-expressing HeLa and parental HeLa, having reduced EGFR levels, were incubated at 37°C for different times (up to 3 hours) with a concentration of Cetuximab-NPs corresponding to 1 μM mTHPC. Cells were then washed and directly analyzed by FACS.

7.4 Measurement of EGFR down regulation induced by Cetuximab-conjugates NPs.

The day before the experiment $1x10^5$ A431, HeLa and HeLa EGFR + cells were seeded on 24 wells plastic plates (Falcon). The day of the experiment, cells were incubated for two hours with different concentrations of Cetuximab or BSA-conjugated NPs (up to 50 μg/ml) at 37°C, then they were washed, trypsinized and stained with a FITC-conjugated anti-EGFR antibody (Abcam) for 30 minutes at 4°C. After washing, cells were analyzed by FACS, acquiring 10,000 events for each sample.

7.5 Confocal analysis of A431, HeLa and HeLa cells incubated with Cetuximab-conjugated NPs.

The day before the experiment, cells ($1x10^5$) were seeded on cover glasses; after 24 hours they were treated for two hours at 37°C with an amount of nanoparticles corresponding to 1 μM mTHPC, washed, fixed with 2% paraformaldehyde (Sigma) in PBS for 20 minutes at room temperature, permeabilized with 0.2% Triton X-100 (Sigma) for 10 minutes at 4°; cells were then washed and saturated with 1% BSA in PBS for 1 hour at room temperature; Cetuximab conjugated to NPs was then stained with a FITC-conjugated anti-IgG antibody (Millipore) for 1 hour at 4°C. After three washings coverslips were mounted in mounting medium (KPL) and were analyzed with a confocal microscope (SP2 Leica), using 488 nm and 630 nm excitation sources. Images have been acquired with the different fluorescence filters, representative pictures were collected as Tiff files and processed with standard imaging programs (Photoshop and Image J).

7.6 Photokilling experiments.

$8x10^3$ A431, HeLa and HeLa EGFR cells were seeded on 96 wells plastic plates (Falcon) and after 24 hours were treated with different amount of Cetuximab- or BSA-conjugated NPs for 6 hours at 37°C. Cells were then washed in PBS and irradiated or not with a red light (Waldmann Meidizintechnik PDT 1200, 60 mW/cm^2) for 10 minutes (36 J/cm^2) at room temperature. Fresh culture medium was added and after 24 hour cell viability was assessed by MTS assay (Promega), following manufacturer instructions.

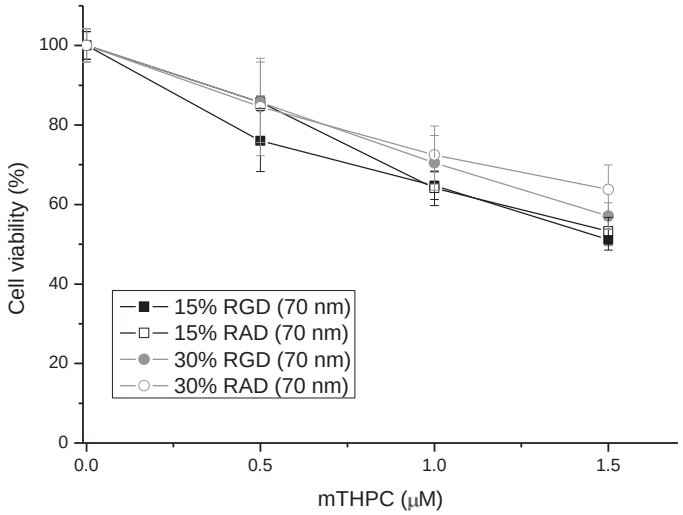

Figure S16. Phototoxicity in HUVEC cells after exposure to different preparations of RGD- or RAD conjugated **4**-doped **OS/PEG** nanoparticles. Cells were irradiated with 2.4 J/cm^2 of red light (Waldmann, 600-700 nm, 12 mW/cm^2) after 24 h incubation with increasing doses of mTHPC in RGD targeted NPs or RAD conjugated NPs as untargeted control. Cell viability was measured 24 h post-irradiation by MTS assay and expressed as mean percentage ± S.D. with respect to not incubated but irradiated, control cells.

V

PEGylation of ORMOSIL nanoparticles abolishes the toxicity toward some lung cells but not alveolar type II epithelial cells *in vitro*

Francesca Moret[1], Francesco Selvestrel[2], Elisa Lubian[2], Chiara Compagnin[1], Maddalena Mognato[1], Lucia Celotti[1,3], Fabrizio Mancin[2] and Elena Reddi[1§]

[1]Department of Biology, University of Padova, Padova, Italy

[2]Department of Chemical Sciences, University of Padova, Padova, Italy

[3]National Laboratory of Legnaro, INFN, Legnaro, Italy

Abstract

Background: The development of novel nanocarriers for drug delivery needs to be accompanied by detailed cytotoxicity studies to guarantee a safe medical use. PEGylated ORganically MOdified SILica (ORMOSIL) nanoparticles (NPs) appear promising for improving drug delivery to cancer cells but a detailed toxicity profile is not yet available. Therefore the responses of human normal and cancer cells of the lung to ORMOSIL NP exposure were studied with the aim to determine the effect of PEGylation on NP cytotoxicity.

Results: The exposure to non-PEG NPs caused a concentration-dependent decreased of viability of all types of cells. On the contrary PEG NPs-caused plasma membrane damage and death only in carcinoma alveolar type II A549 cells while had no effects on CCD-34Lu normal fibroblasts. The similar uptake of NPs in these cells promoted ROS production; superoxide dismutase and catalase reduced ROS levels but did not protect A549 cells from death, suggesting that the oxidative stress was not the main determinant of cytotoxicity. Gene expression analysis showed that only in A549 cells genes involved in inflammation, signal transduction, cell death were differentially expressed, while CCD-34Lu did not modulate significantly transcription, after NP exposure. PEG-NPs localized in the lamellar bodies of A549 cells, reduced the production of surfactant proteins and very likely interfered with the pulmonary surfactant system, peculiar of alveolar epithelial type II cells of which A549 represent a model.

Conclusions: PEGylation did not abolish the cytotoxicity of ORMOSIL NPs toward A549 cells while they were not toxic toward the other lung cells. The death of A549 cells occurred very likely via necrosis and was consequent to impaired functioning of surfactant machinery determined by the interaction of the NPs with the surfactant film. Our *in vitro* results highlight the importance of identifying the characteristics that make the cells sensitive or resistant to stress or damages caused during exposure to nanomaterial.

Keywords: cytotoxicity, ORMOSIL nanoparticles, PEGylation, plasma membrane permeabilization, reactive oxygen species, inflammation, gene expression profiles, pulmonary surfactants, lamellar bodies.

Background

In the recent years there have been tremendous progresses in the synthesis of nanosized materials with controlled structures and functions [1-3]. Such nanomaterials are particularly attractive for biomedical applications especially because they can be exploited as carriers of therapeutic and diagnostic agents [4-6]. It is hence expected that properly engineered nanomaterials will provide powerful tools in the management of many types of important diseases, such as cancer. At the same time, some concern exists about their possible toxic effects [7]. Because of their large surface area, nanoparticles (NPs) exhibit high bioactivity, which is modulated by their physicochemical properties and by the presence of specific functional groups. Moreover, there are increasing evidences that materials, which proved to be biocompatible in bulk, may have very different biological properties in a nanostructured form [8-10]. Therefore, the development of NPs for medical applications has to be associated to detailed cytotoxicity studies in order to assess biocompatibility and safe medical use.

Silica and ORganically MOdified SILica (ORMOSIL) NPs appear particularly appealing as carriers for drug delivery because of some unique properties, which include structural stability in different solvents and at different pH, relative low chemical reactivity, the low cost of synthesis and the possibility of easily obtaining complex structures with different shapes and porosity [11-14]. Silica and ORMOSIL NPs are generally considered biocompatible, however an increasing number of recent reports indicate that they may have several toxic effects [15-25]. Surface charge, aggregation, size and shape have been considered in relation to cytotoxicity of silica NPs but, in some

cases, general conclusions on the precise role of these factors in determining toxic effects are still lacking. Amorphous silica NPs of 15 and 46 nm similarly reduced the viability of human lung carcinoma cells (A549) to 76% of control [15], while silica NPs of 20 nm and 50 nm caused a significant different cytotoxicity toward human embryonic kidney cells (HEK293) [26]. The influence of shape was studied with mesoporous silica NPs and the results indicated that long rod shaped NPs were internalised more efficiently than sphere shaped NPs with consequent greater impact on different cellular functions including proliferation, apoptosis, adhesion and cytoskeleton organisation [27]. The characteristics of the surface of NPs are also particularly important in determining their efficiency of cell internalisation which is strongly influenced by their ability to capture biological molecules from cellular environment or body fluids creating a protein corona [28,29]. Nanoparticles designed for medical use, and in particular for drug delivery, need to be properly functionalised on their surface to guarantee prolonged residence in the bloodstream which is essential prerequisite for sustained release of the drug to the targeted tissue. The coating of NP surface with polyethyleneglycol (PEG) is an effective approach to inhibit adsorption of blood proteins on NPs and capture by the phagocytic cells of the reticulo-endothelial system (RES) [30-33]; PEGylation should also reduce the cytotoxicity of NPs as reported for quantum dots and dendrimers [34-36]. We have previously reported on the preparation of highly PEGylated ORMOSIL NPs (PEG NPs) by one-pot reaction that allows the control of the NP size in the 20-150 nm range [37]. The high density coat of covalently linked PEG confers to NPs excellent stealth properties as demonstrated by the almost negligible capture by human macrophages *in vitro* in comparison to the non PEGylated counterparts (non-PEG NPs). In addition, PEG NPs are not toxic to macrophages and are hemocompatible; importantly, they have a very poor pro-coagulant activity when compared with their non PEGylated version [38].

In this study, we have further investigated the cytotoxicity of non-PEG and PEG ORMOSIL NPs by analysing the responses elicited in different human lung cells *in vitro*. We used the alveolar carcinoma epithelial cell line A549 that has been used in a number of nanotoxicology studies, in particular to assess the cytotoxicity of silica NPs [15,16,23,39] and we compared the responses to ORMOSIL NPs to those elicited in the adenocarcinoma non-small cell lung cells NCI-H2347 and normal fibroblasts CCD-34Lu. We are developing PEG ORMOSIL NPs as carriers of anticancer drugs and for this reason most of the studies were focused on the understanding of the PEG NP-induced morphological and functional alterations in the CCD-34Lu normal fibroblasts and in A549 carcinoma cells as models of healthy and diseased cells. To better understand the cellular effects induced by PEG NPs, we combined some traditional cytotoxicity tests to determine reduction of cell viability, alterations of plasma membrane, ROS production and inflammation with a genome-wide transcriptome analysis to assess NP-induced alterations of gene expression.

Results and Discussion

Characterization of ORMOSIL NPs

The ORMOSIL NPs were prepared by ammonia catalyzed co-polymerization of vinyltriethoxysilane and, for PEGylated NPs, a suitable PEG2000 trimethoxysilane derivative in aqueous solutions of Brij 35, as reported previously [37]. The residual concentration of Brij 35 in the NP preparations was always lower than 1 μM and was not toxic to the cells (data not shown). The NPs had a spherical shape with a mean diameter of 70 ± 10 nm, as determined by Dynamic Light Scattering (DLS) measurements, and confirmed by transmission electron microscopy (TEM) analyses (Figure 1 A,C,D). Zeta potential in phosphate buffered saline (PBS, pH 7.4) was -5.9 and -4.3 mV respectively for non-PEGylated and PEGylated NPs, indicating a scarce electrostatic stabilization of the nanoparticles against aggregation. Thermogravimetric analysis (TGA) of the non-PEGylated NPs revealed an organic content of about 30% of the total weight, as expected on the basis of an average minimal formula of $SiO_{1.5}C_2H_3$ of the VTES-ORMOSIL material (Figure 1 B). In the case of PEGylated NPs TGA revealed that the coat of PEG-2000 accounted for an additional 25% of NPs weight and for an estimated surface footprint of 0.63 nm^2 for each PEG molecule. The presence of such a dense PEG protecting layer provides an effective steric stabilization against aggregation, as confirmed by the observation that the PEGylated NPs were stable for months when kept in an aqueous medium and did not aggregate in solutions of high ionic strength nor in the cell culture medium as indicated by the DLS measurements performed in these media (Additional file 1). On the other hand, we have already reported that non-PEGylated ORMOSIL NPs slowly aggregate in saline aqueous solutions but not in the presence of serum [40].

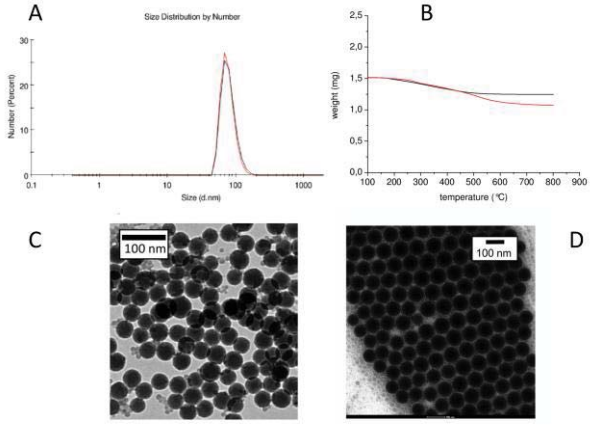

Figure 1 Characterization of ORMOSIL nanoparticles. A) DLS size distribution by number (average size 70 ± 10 nm) of non-PEGylated (black line) and PEGylated NPs (red line). **B**) Thermogravimetric (TGA) profiles in air of non-PEGylated (black line) and PEGylated NPs (red line) (residual weight at 700°C is 57%, coating PEG footprint was calculated by assuming a 1.5 g/cm^3 density for the ORMOSIL core). **C**) TEM micrograph of non-PEGylated NPs. **D**) TEM micrograph of PEGylated NPs.

ORMOSIL NPs exhibit different cytotoxicity toward different types of lung cells

We first analyzed in which manner the coating with a PEG corona of ORMOSIL NPs influenced the cytotoxicity of the particles in CCD-34Lu normal lung fibroblasts and A549 and NCI-H2347 lung cancer cells. Cytotoxicity was assessed with the MTS assay by measuring proliferation/viability of cells incubated with increasing concentrations (up to 1.5 mg/ml) of non-PEG or PEG NPs for 24 h (i.e. 24 h) as well as of cells incubated 24 h with NPs and released for additionally 24 h in NP-free medium (i.e. 24 + 24 h) (Figure 2).

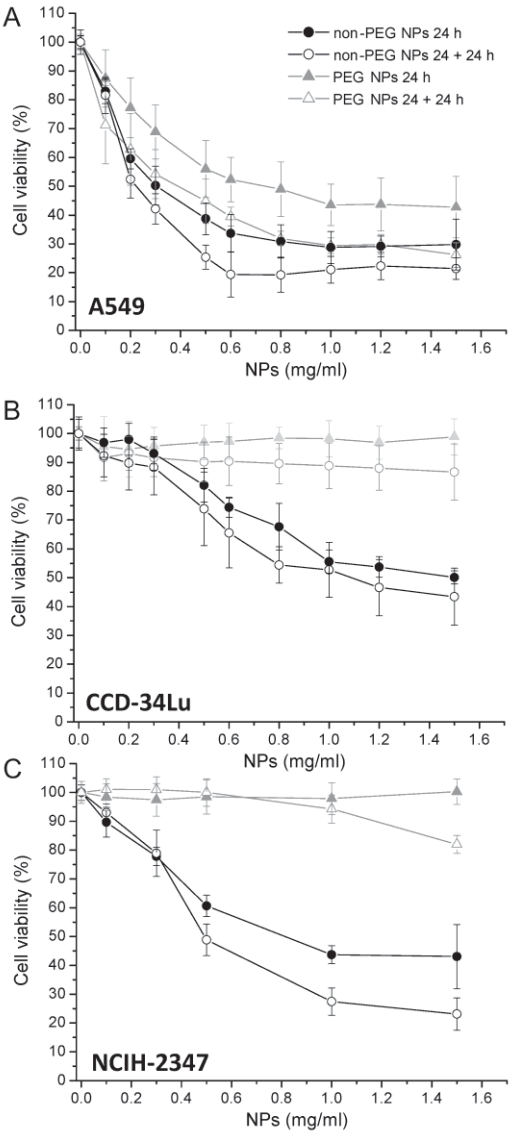

Figure 2 Cytotoxicity of non-PEG and PEG ORMOSIL nanoparticles toward different lung cells. A) alveolar carcinoma A549, **B**) normal fibroblasts CCD-34Lu and **C**) adenocarcinoma NCIH-2347. Cell viability measured by the MTS assay after 24 h of NP exposure (24 h) and after additional 24 h of incubation in NP-free medium (24 + 24 h). The results are means ± SD of at least three independent experiments carried out in triplicate.

Incubation with non-PEG NPs for 24 h caused a severe concentration-dependent loss of the viability in all types of cells with IC_{50} of 0.31, 0.82 and >1.5 mg/ml for respectively A549, NCI-H2347 and CCD-34Lu cells. On the contrary, PEG NPs in the same range of concentrations exerted a significant cytotoxic effect only in A549 cells (IC_{50} 0.74 mg/ml); in CCD-34Lu and NCI-H2347 cells incubated with PEG NPs the viability was significantly reduced only after 24 + 24 h incubation, but by no more than 10-15% at the highest NP concentrations. Thus, it appeared that the coating of NPs with PEG-2000 strongly reduced and almost abolished the cytotoxicity to some types of lung cells, as fibroblasts and adenocarcinoma cells (as NCI-2347 cells), while had only minor effects in decreasing the toxicity toward A549 cells derived from type II cells of the alveolar epithelium. The latter cell type was more sensitive to ORMOSIL NPs than the other two cell lines used in our study, however the loss of viability was similar to that reported by other authors with comparable concentrations of bare silica (SiO_2) NPs of various size [15-17,39]. Interestingly, in a recent work we reported higher cell mortality for CCD-34Lu fibroblasts than for A549 carcinoma cells after exposure to commercial Ludox SiO_2 NPs (SM30, AS30) [41]. Differently to ORMOSIL NPs, Ludox form aggregates in medium added with serum [41,42] and the different cytotoxic profile may be attributed to different interactions of NP aggregates versus mono-dispersed NPs with the cells. Data on the cytotoxicity of PEG ORMOSIL NPs in A549 cells are lacking and only few data are available on PEG NPs of other materials [43] and also in other cell lines [44,45]. Chang and colleagues [17] reported that normal MRC-5 fibroblasts are more susceptible than A549 cells to injury induced by silica and identified in the lower metabolic activity of normal cells, determined by the longer doubling time, the major determinant of the higher susceptibility. In our case, normal CCD-34Lu fibroblasts and A549, or NCI-H2347 carcinoma cells have similar doubling time and very likely a similar metabolic activity; therefore a different metabolic activity does not appear responsible for the higher susceptibility of A549 cells to PEG ORMOSIL. Interestingly, Jing Wang et al. [46] reported that PEG phospholipid micelles induced an endoplasmic reticulum-dependent apoptosis in A549 cells, but not normal MRC-5 and 293T cells, due to ER accumulation of the particles. Our results showed a completely different response to PEG NPs in the two cancer cell lines (i.e. A549 and NCI-H2347), excluding a correlation between NP cytotoxicity and tumoral phenotype. To gain insight into the factors determining the different cytotoxicity we selected CCD-34Lu normal fibroblasts and A549 cancer cells for detailed studies on the uptake and intracellular fate of ORMOSIL NPs.

Cell interaction and uptake of ORMOSIL NPs

In general, it is expected that the efficiency of cell internalization correlates with the extent of NP cytotoxicity. Thus, because of the different toxicity of non-PEG and PEG ORMOSIL toward A549 and CCD-34Lu cells, we found important to determine the modalities of NP interactions with

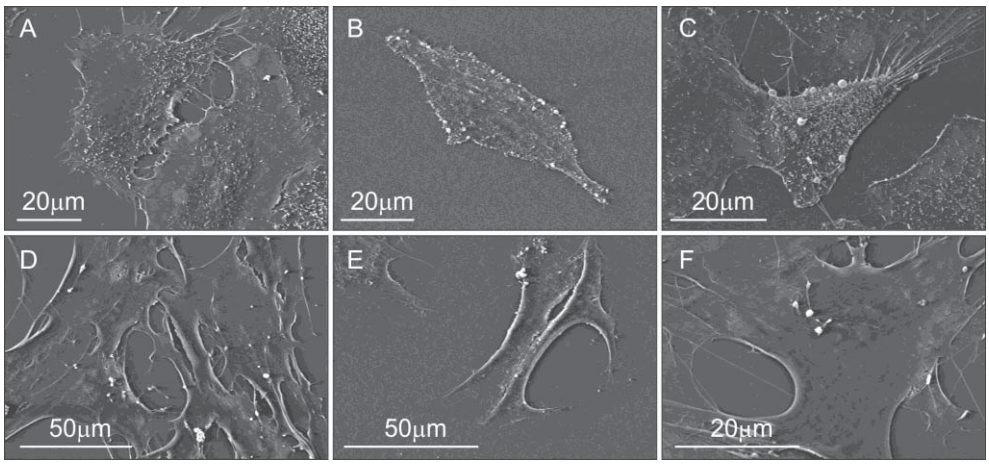

Figure 3 SEM images of A549 and CCD-34Lu cells incubated with non-PEGylated and PEGylated ORMOSIL for 24 h. A549 cells not incubated with NPs **(A)**, incubated with 0.3 mg/ml non-PEGylated **(B)**, or PEGylated NPs **(C)**. CCD-34Lu cells not incubated with NPs **(D)**, incubated with 0.5 mg/ml non-PEGylated (**E**), or PEGylated NPs **(F)**.

the two types of cells and the efficiency of internalisation. We used scanning electron microscopy (SEM) to analyze particle interactions with cell surface as well as cell morphological alterations induced by a 24 h exposure to NPs. In agreement with the cell viability results (Figure 2A), A549 cells exposed to 0.1 mg/ml (Additional file 2) or 0.3 mg/ml of non-PEG or PEG NPs (Figure 3 B and C) showed profound alterations of the morphology with respect to controls, with numbers of blebs on cell surface. On the contrary, advanced cell death features were visible in CCD-34Lu only when exposed to 0.5 mg/ml of non-PEG NPs (Figure 3 E). As expected, the hydrophilic character of the coat of PEG diminished the interactions of NPs with cells. As shown in the images of Figure 3 and in the additional file 3, non-PEG NPs tightly interacted with and covered almost completely several areas of the surfaces of both types of cells while PEG NPs were much less abundant. To assess if the reduced cell adhesion of PEG NPs decreased cell internalization, we measured the uptake of ORMOSIL labeled with rhodamine covalently linked to the matrix of NPs. Fluorescence microscopy investigations confirmed the "stealthy" properties of our PEG NPs and showed clear reduced uptake in both cell types with respect to their bare counterpart (Figure 4). Furthermore, flow cytometry measurements of cells incubated with the sub-lethal NP concentration of 0.1 mg/ml, indicated an uptake of PEG NPs equivalent to about 24 and 19% that of non-PEG NPs respectively in A549 and CCD 34Lu cells. Interestingly, PEG NPs were internalized to a very similar extent in the two cell lines (mean rhodamine fluorescence intensities (a.u.) of 153.6 ± 37.72 and 163.2 ± 29.1 respectively in A549 and CCD-34Lu), indicating that the NP-induced cytotoxicity in A549 cells cannot be ascribed to a higher ability to capture PEG NPs. Subsequently, TEM was used to better investigate on the NP-induced ultrastructural damages as well as the intracellular localization of NPs. TEM images of control A549 cells (Figure 5 A-D) showed the typical ultrastructural features of alveolar type II (AE2) epithelial cells [47], such as microvilli, tonofilaments and lamellar bodies (LBs). In fact, AE2 cells synthesize and store pulmonary surfactants in these lamellate structures [48], which are secreted together with their content in the lumen of alveoli to form a lipid monolayer film in order to maintain low surface tension at the air-liquid interface to prevent alveolar collapse during expiration. TEM images of A549 cells incubated for 24 h with non-PEG NPs (Figure 5 E-H) showed evident vacuolation of cytoplasm and of LBs containing numbers of particles internalized mainly in

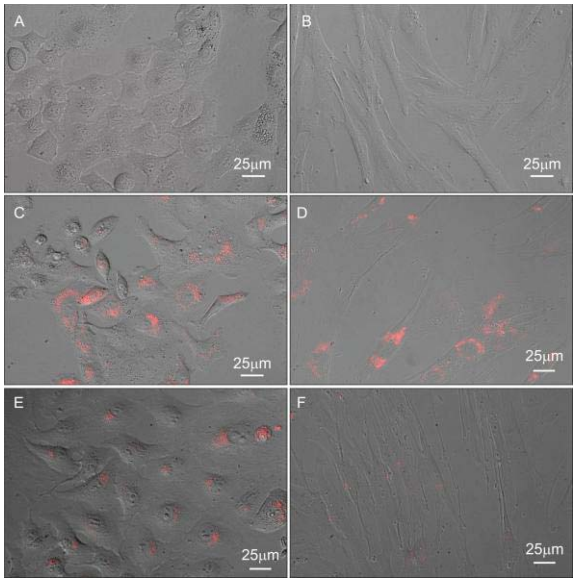

Figure 4 Intracellular uptake of rhodamine-labelled ORMOSIL NPs in A549 and CCD-34Lu cells. Fluorescence microscopy images of cells exposed for 24 h to NPs. A549 control cells **(A)**, A549 cells incubated with 0.1 mg/ml of non-PEGylated NPs (**C**) or PEGylated NPs **(E)**. CCD-34Lu control cells **(B)**, CCD-34Lu cells incubated with 0.1 mg/ml of non-PEGylated NPs **D**) or PEG NPs **F**).

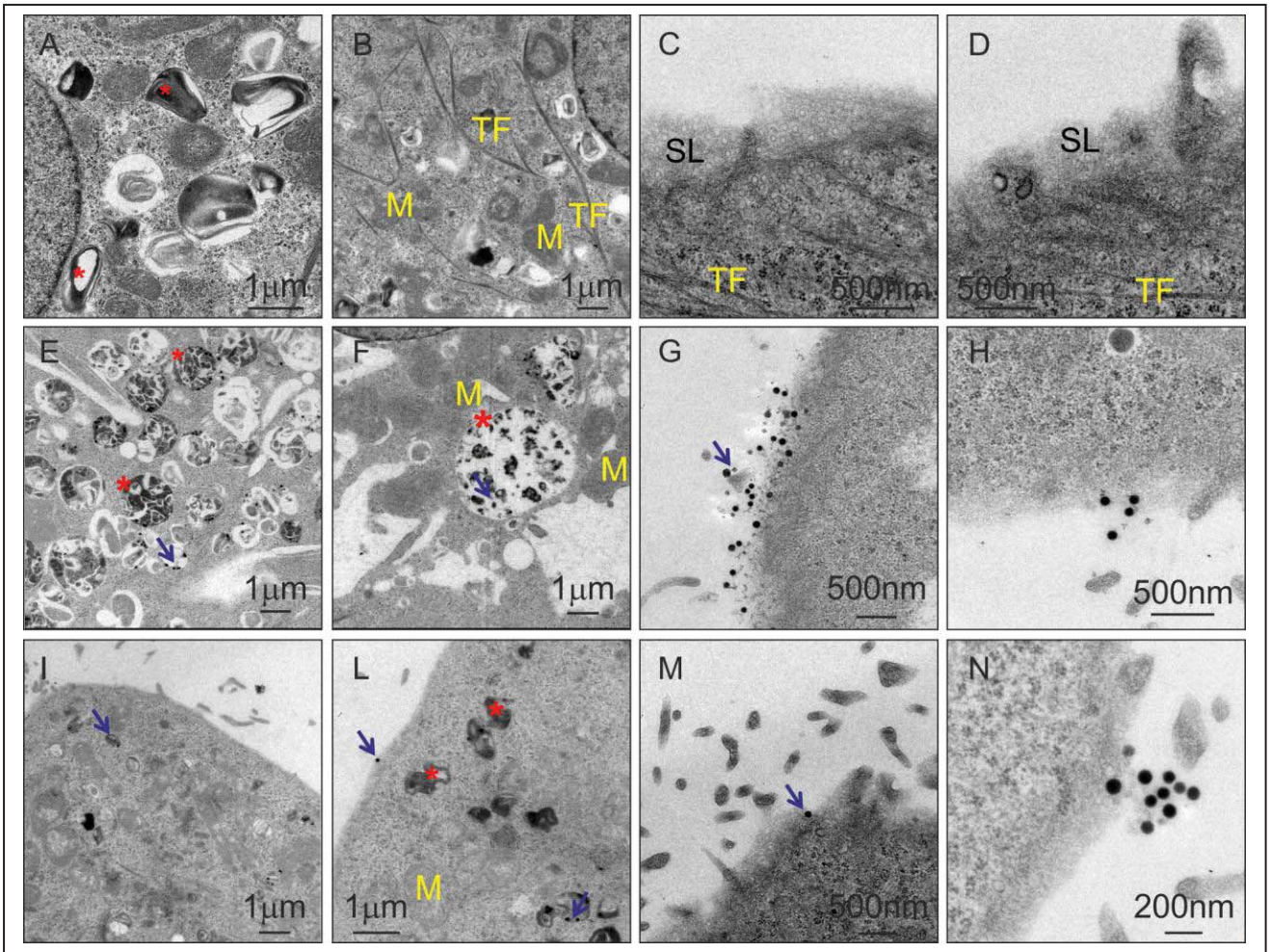

Figure 5 Intracellular uptake of ORMOSIL NPs in A549 cells. TEM micrographs of cells exposed for 24 h to nanoparticles. **A-D**) cells not incubated with NPs; **E-H**) cells incubated with 0.3 mg/ml of non-PEGylated NPs; **I-M**) incubated with 0.3 mg/ml of PEGylated NPs. Blue arrows denote NPs, asterisks indicate lamellar bodies while M, TF and SF indicate mitochondria, tonofilaments and the surfactant film, respectively.

these lipid vesicles, many of which appeared to have lost their characteristic multivesicular/multilamellar structure. As already observed with SEM, many NPs lied on plasma membrane and were entrapped within the surfactant layer that appeared less dense and with fewer vesicles when compared to controls. Vacuoles were not visible in A549 cells incubated with the same dose of PEG NPs (Figure 5 I-N). However, some NPs were internalized and localized in the LBs, which appeared much reduced in numbers and size as compared to controls; in addition some NPs interacted with the components of the surfactant film. Both type of particles, with PEG NPs to a minor extent, induced mitochondrial swelling and disappearance of tonofilaments in A549 cells. On the other hand, CCD-34Lu fibroblasts treated with non-PEG NPs (Figure 6 E-H) showed an increased number of vacuoles and of NP-containing vesicles while those treated with the PEGylated NPs showed no evident ultrastructural alterations (Figure 6 I-N) with respect to controls (Figure 6 A-D). In these cells NPs free in the cytosol as well as entrapped in endosomes/lysosomes or associated to microtubules were observed. Non-PEG NPs were probably taken up by cells by clathrin-mediated endocytosis since a number of coated pits were clearly visible throughout the cell membrane (Figure 6 H). It appeared that for non-PEG NPs and in both types of cells, the cytotoxic effect was mainly induced by the high numbers of particles internalized which promote cytoplasmatic vacuolization as well as by the particles interacting with plasma membrane.

PEGylated ORMOSIL NPs increased the permeability of plasma membrane

Being interested mainly at evaluating the safety in using PEGylated ORMOSIL NPs as nanocarriers for the delivery of anticancer drugs, further investigations aimed at elucidating the mechanism of cytotoxicity were restricted to the PEGylated version of ORMOSIL NPs. To better understand the effects of NPs on plasma membrane, we measured the release of the cytosolic enzyme lactate dehydrogenase (LDH). Upon a 24 h of exposure to NPs, considerable amounts of LDH were released

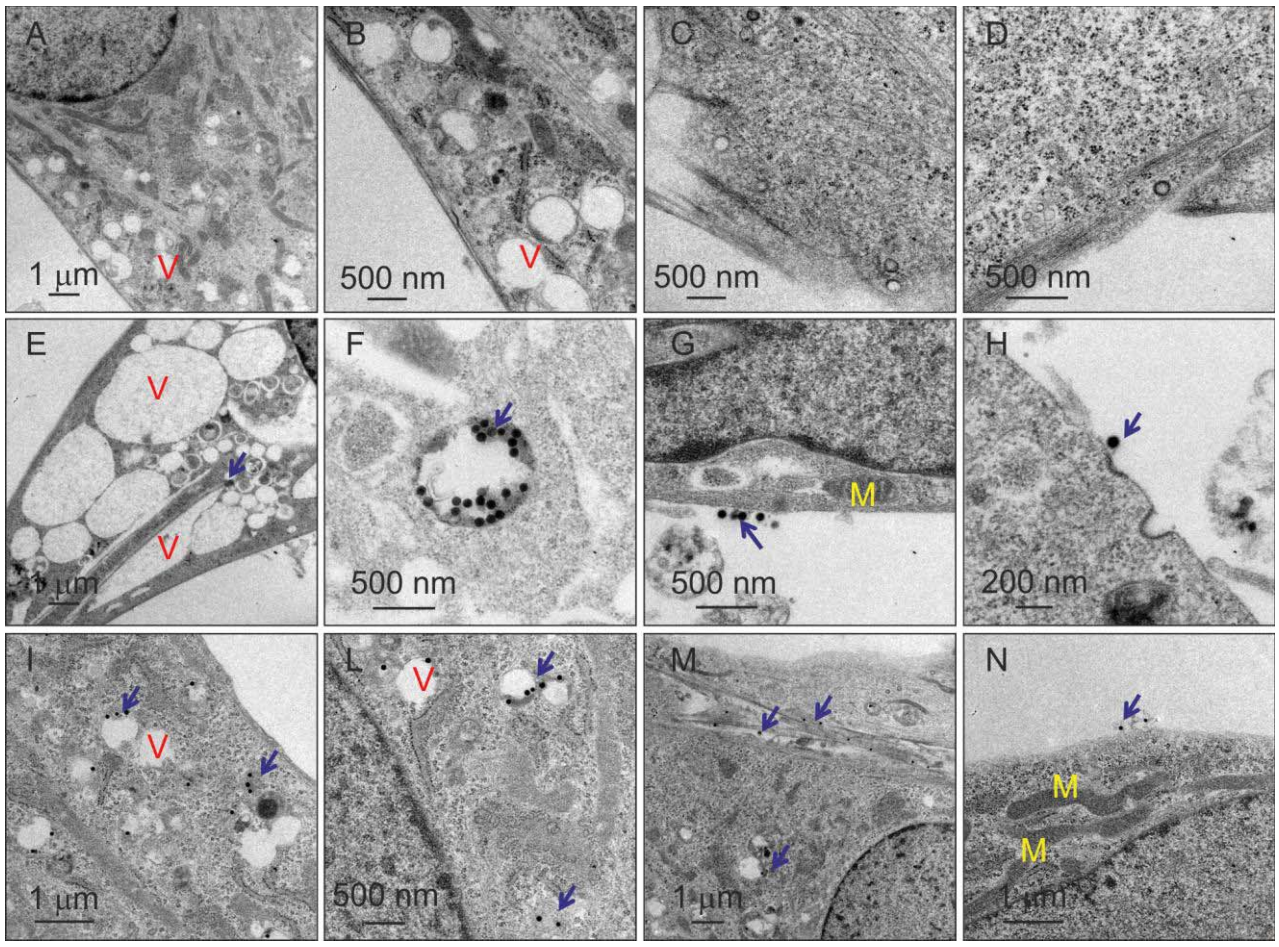

Figure 6 Intracellular uptake of ORMOSIL NPs in CCD-34Lu cells. TEM micrographs of cells exposed for 24 h to nanoparticles. A-D) cells not incubated with NPs; E-H) cells incubated with 0.5 mg/ml of non-PEGylated NPs; I-M) incubated with 0.5 mg/ml of PEGylated NPs. Blue arrows denote NPs while M and V indicate mitochondria and vacuoles, respectively.

in the culture medium only by A549 cells (Figure 7 A). This assay indicated that an increased permeability of the plasma membrane induced by PEG-NPs could be responsible for the death of A549 cells. Accordingly, by increasing the NP dose, an increasing number of A549 cells became positive to PI staining (Figure 7 B), with almost 100% of positive cells at the highest tested concentration of 1.5 mg/ml (Additional file 4), indicating occurrence of cell death very likely by necrosis; indeed, morphological changes typical of apoptosis could not be detected during the TEM analysis. On the other hand, consistently with the results of cell viability and LDH release, in CCD-34Lu the PI staining showed increased permeability of the plasma membrane only in ~ 20% of the cells after incubation with 1.5 mg/ml of NPs (Additional file 4).

Production of intracellular ROS triggered by PEGylated ORMOSIL was not the major determinant of death in A549 cells

It is well accepted that oxidative stress is implicated in NP induced-cytotoxicity and most of the cellular responses are explained with the activation of different pathways leading to cell death, inflammation, induction of antioxidant agents subsequent to the formation of reactive oxygen species (ROS) [8,19]. Thus, we measured the production of ROS in cells exposed and not exposed to NPs (endogenous ROS level) by flow cytometry, after staining the cells with a specific probe that is converted to a fluorescent product only in the presence of intracellular ROS. In both cell lines exposed to 0.1 mg/ml NPs, we could not measure a production of ROS above the basal level at all time points considered of 5, 24 and 24 + 24 h (data not shown). On the contrary, with NP concentrations of 0.3 and 0.5 mg/ml, in A549 cells the level of ROS was significantly increased at all time points (Figure 8 A), while in CCD-34Lu cells ROS exceeded the basal level only at the end of the 24 h of NP exposure (Figure 8 B). Twenty four h after the removal of NPs from the medium, in A549 cells the level of ROS was still higher than the basal level, while CCD-34Lu cells had already restored the basal oxidative stress conditions. Thus it appeared that PEG NPs, notwithstanding their reduced uptake when compared to the non-PEGylated version, can cause an oxidative stress to the cells, as do many types of nanomaterials [39,49,50] and in particular bare commercial

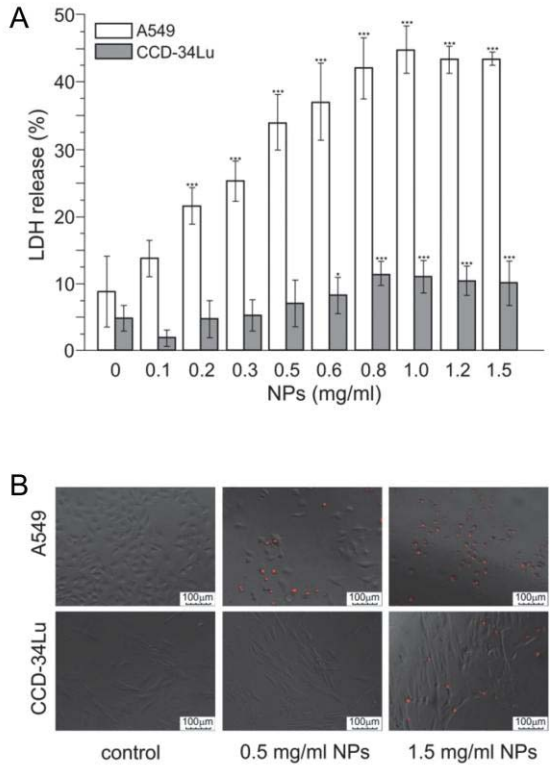

Figure 7 Effects of PEGylated ORMOSIL NPs on permeability of plasma membrane in A549 and CCD-34Lu cells. A) LDH release in the culture medium of cells incubated for 24 h with increasing doses of NPs; the data show the percentage of the total LDH content of the cells and are means ± SD of at least three independent experiments carried out in triplicate. * $p < 0.05$; ** $p < 0.01$; *** $p < 0.001$ vs controls (t test). **B**) Images of A549 and CCD-34Lu cells incubated for 24 h with NPs and stained with propidium iodide.

silica NPs [16,16,19-22,51]. It is also expected that antioxidant agents such as superoxide dismutase (SOD), catalase (CAT) and N-acetylcysteine (NAC), are able to protect the cells from the oxidative stress induced by NPs [16,50, 52]. To gain more insight into the types of ROS produced in the cells following the exposure to NPs, we performed experiments in which the cells were incubated with PEG NPs in the presence of the antioxidant agents SOD and CAT given alone or in combination (Figure 8 A, B). In general, CAT alone was much more effective than SOD alone in reducing the level of ROS suggesting that hydrogen peroxide was the most abundant among the ROS produced. SOD alone caused a slight decrease of ROS level only in A549 cells indicating that some superoxide anion is also produced. In all cases when SOD and CAT were combined, the highest reduction of ROS level was observed. Nevertheless, while SOD and CAT were effective in reducing the level of intracellular ROS they were unable to protect A549 cells from death induced by NPs. In fact A549 cells incubated for 24 h with 0.3 mg/ml of NPs in the presence of SOD and CAT, alone or in combination, showed a reduction of viability similar to that of the cells incubated with NPs in the absence of antioxidants (Figure 8 C). Therefore, these data suggest that the oxidative stress is not the major determinant of the cytotoxic effect induced by PEG ORMOSIL NPs in A549 cells.

PEG ORMOSIL NPs modulate the gene expression profiles of A549 cells

To understand if PEG NPs exposure forced the cells to modulate their gene expression profiles, we performed microarray analyses hybridizing mRNA, extracted from samples treated with 0.1 mg/ml of NPs, on the Agilent Human Whole microarray platform. SAM analysis revealed that mRNA expression was significantly altered only in A549 cells, with 133 and 45 genes differentially expressed at 24 h and at 24 + 24 h, respectively (Figure 9). The complete lists of differentially expressed genes (d.e.g.) in A549 cells at the two time points are provided in the Additional files 5 and 6. The heat map profiles of d.e.g shown in Figure 9 (A and B) emphasized that in A549 cells incubated for 24 h with NPs most genes were over-expressed (110/133). Generally, the expression values of up-regulated genes returned to values close to zero during the following 24 h of cell incubation in NP-free medium, indicating that up-regulation was mainly promoted by the presence of NPs in the medium and suggesting that cell damages elicited by 0.1 mg/ml of NPs were not severe enough to compromise the regulation of the gene expression. On the contrary, down-regulated genes maintained negative expression values. Indeed, no d.e.g. were found in NP-treated fibroblasts with respect to controls, confirming the unresponsiveness of CCD-34Lu cells to PEG NPs also from a transcriptional point of view.

For few selected A549 d.e.g. (IL8, PTGS2, KRT4) microarray data were confirmed by quantitative RT-PCR (qRT-PCR, Additional file 7). In general, the results of qRT-PCR showed a gene induction greater than that measured by microarray analysis, probably due to the higher sensitivity of qRT-PCR technique. Microarray results were confirmed with the exception of PTGS2 gene which was found down-regulated only in qRT-PCR analysis, in both cell lines at 24 + 24 h.

To assess the effect of PEG NP exposure on cellular functions, we uploaded A549 d.e.g. in DAVID annotation tool to classify them based on the Gene Ontology (GO) categories. The most significant GO terms were regrouped and represented in Figure 9 D and E, while the complete lists of GO functional categories identified by DAVID are reported in the Additional files 8 and 9. The d.e.g. at the end of the 24 h of NP incubation belonged to 42 different GO terms (Additional file 8) which can be grouped in 5 major biological processes, namely, signal transduction, cell death, cell proliferation, response to stimulus and inflammation (Figure 9 D).

Several authors reported that the exposure to nanomaterials activates the transcription of inflammatory mediators/activators both *in vivo* and *in vitro* [9,53,54], with oxidative stress identified as the major underlying mechanism driving NP-induced inflammation, especially in lung tissues [55]. In particular, commercial silica NPs stimulate mRNA over-expression of inflammation-related genes, such as IL-8, IL-6,

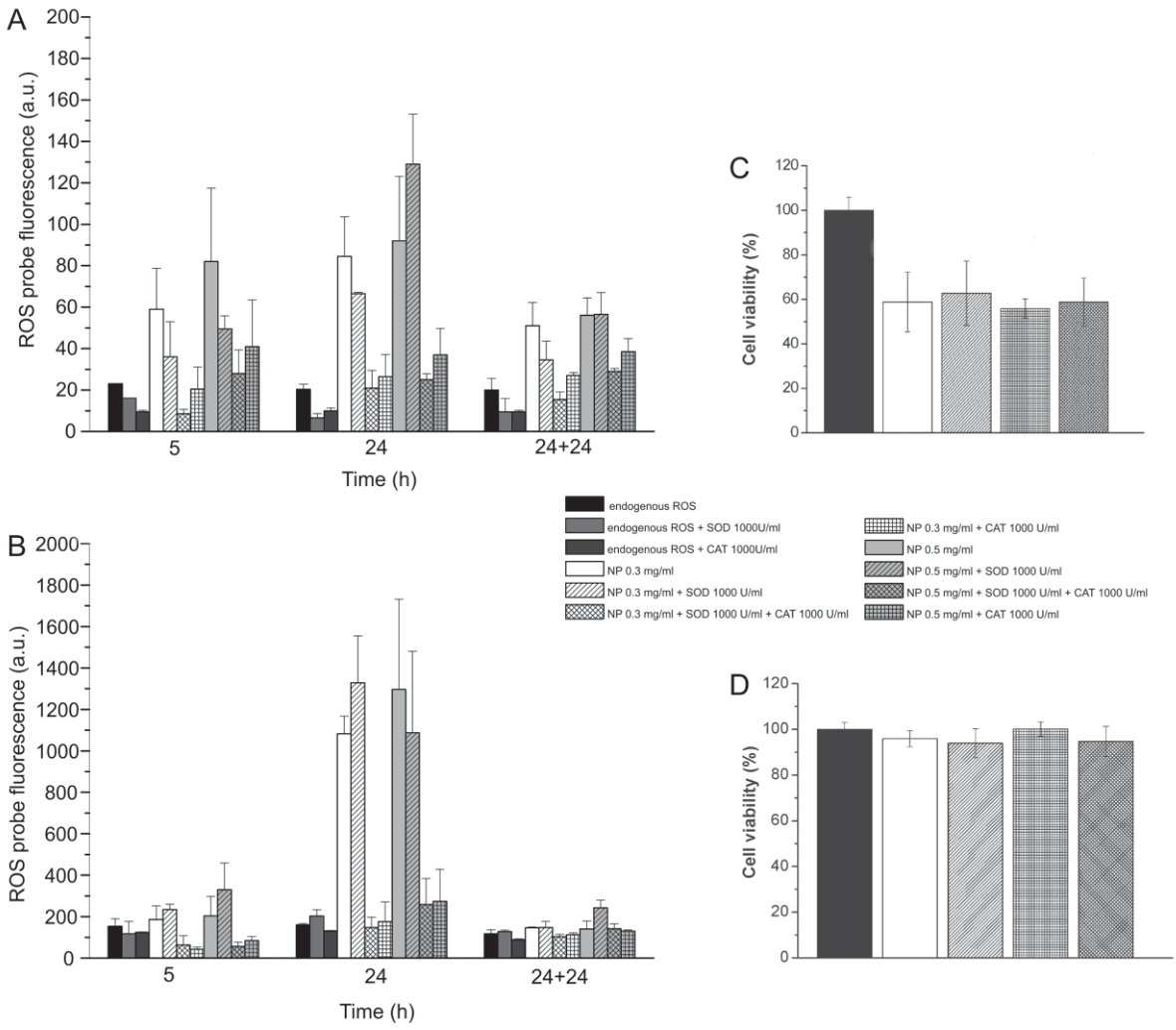

Figure 8 ROS production induced by PEGylated ORMOSIL NPs in A549 and CCD-34Lu cells. ROS produced in A549 **A**) and CCD-34Lu **B**) cells after exposure to PEG ORMOSIL NPs. Cells were incubated with 0.3 or 0.5 mg/ml of NPs for 5 h, 24 h or 24 + 24 h. Incubation with NPs was carried out in the absence and presence of ROS inhibitors SOD, CAT or SOD + CAT. At the end of incubation time cells were analyzed by flow cytometry after staining with ROS Detection probe. Cell viability determined by the trypan blue exclusion test, of A549 cells **C**) or CCD-34Lu cells **D**) incubated for 24 h with 0.3 mg/ml of PEGylated NPs in the absence or in the presence of ROS inhibitors. The results are means ± SD of at least three independent experiments.

IL-1ß, TNF-α, iNOS in various cell lines [18,39,56]. Segat et al. [57] studied the pro-inflammatory effects of bare and PEG ORMOSIL NPs and showed NP stimulation of IL-1ß, IL-6, TNF-α and IL-8 in monocytes and IL-8 in polymorphonuclear leukocytes (PMNs) *in vitro*. Similarly, our microarray data showed that PEG NPs triggered an inflammatory response in A549 cells by stimulating the transcription of several inflammation-related genes (ADRB2, CSF1R, CXCL5, CXCR7, IL8, IL11, LTB, NT5E, OSMR, PTGS2, SERPINF1, TGM2; Additional file 5). Since expression and release of cytokines have an important role in the induction and in the regulation of the inflammatory response, we measured the mRNA expression level of IL-8, IL-6 and IL-1ß by qRT-PCR. IL-8 mRNA was the most over-expressed transcript in A549 cells exposed to PEG NPs, but also IL-6 and IL-1ß mRNA transcription was found to be increased during the 24 h of NP exposure (Figure 10 A). Indeed, after NP removal, mRNA transcription of IL-8 and IL-1ß decreased dramatically, while IL-6 transcription did not change significantly with the incubation times and after NP removal. In addition, an ELISA-based immunoassay was used to confirm that the NP-promoted transcriptional activation of the interleukin genes (IL8 in particular) correlated with the increased synthesis of the corresponding proteins (Figure 10 B). Our results on IL-8 protein release are similar to those obtained by Choi et al. [39] after exposure of A549 cells to non-PEGylated Aerosil®-200 silica nanoparticles, suggesting that the PEG-coating does not abolish the inflammatory response in this cell line.

The PTGS2 gene, also known as cyclooxygenase 2 (COX-2), is a pro-inflammatory related gene that encodes for an enzyme

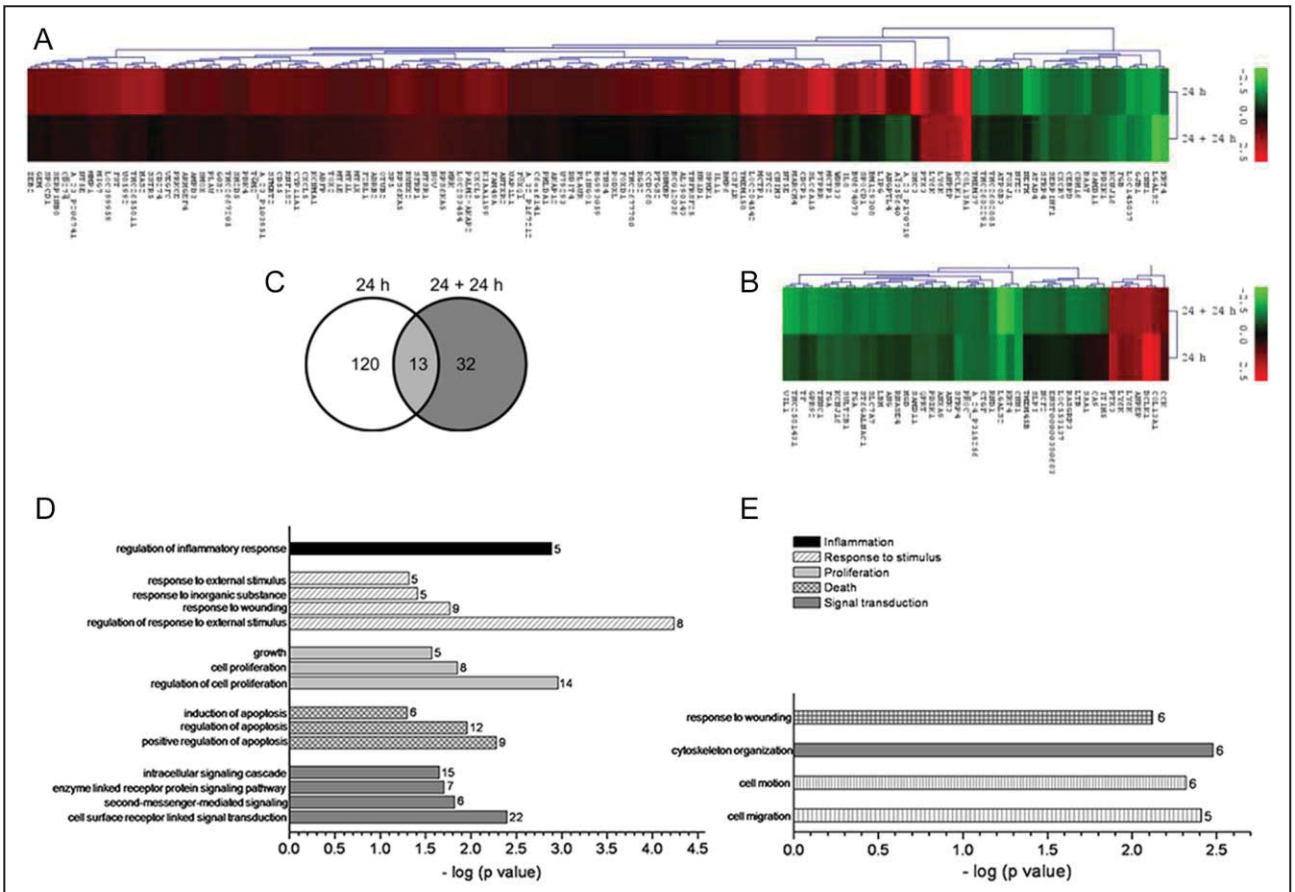

Figure 9 Gene expression profile alterations induced by PEGylated ORMOSIL NPs in A549 cells and GO analysis of differentially expressed genes. Heat map profiles of differentially expressed genes in A549 cells, identified using TMEV 4_5_1 **A, B**): pseudo-color scale indicates the expression value [log_2 (NP-treated cells/controls)]; range of expression value is from -0.7 (green, down-regulation) to 0.7 (red, up-regulation). In the upper heat map **A**), expression values of the 133 differentially expressed genes at 24 h are correlated with their expression values after NP removal (24 + 24 h), while in the bottom heat map **B**) expression values of the 45 differentially expressed genes at 24 + 24 h are correlated with their expression values during NP incubation (24 h). The Venn diagram **C**) shows the total number of differentially expressed genes at the end of 24 h of NP incubation and after additional 24 h of cells incubation in NP-free medium. Comparison of the gene ontology (GO) categories among the annotatable genes differentially expressed during the 24 h of NP incubation **D**) and 24 h after NP removal **E**). GO terms of biological processes (BP) were represented at FAT level using the Database for Annotation, Visualization and Integrated Discovery functional annotation tool (DAVID, http://david.abcc.ncifcrf.gov/). BP are plotted as a function of significance (-log p value), using $p < 0.05$ as cut-off threshold; the number of genes involved in each GO BP is indicated on the right of each bar.

that catalyzes the conversion of arachidonic acid to prostaglandins [58]. Our microarray and qRT-PCR analysis showed an up-regulation of this gene in A549 cells at 24 h and the GO research indicated that it is involved in different biological processes such as response to extracellular stimulus, second-messenger mediated signalling, regulation of inflammatory response, cell proliferation and apoptosis (Additional file 8). Over-expression of PTGS2 has been already reported as a consequence of the oxidative stress induced in cells exposed to different nanomaterials [50,59]. In some cases PTGS2 expression was preceded by the activation of MAPKs signalling pathway, which is one of the most widespread mechanism pertaining to eukaryotic cell regulation [60], but we found no direct evidence of the activation of the MAPKs signalling pathway in A549 cells exposed to PEG ORMOSIL NPs. Also the transcription of genes as JNK, p53 and NF-kB, implicated in silica NP-induced apoptosis and inflammation [39], was not affected, very likely because necrosis is the predominant mechanism of cell death induced by our PEG NPs. Furthermore, the GO analysis of A549 d.e.g. revealed that the most enriched biological processes were those of the signal transduction; in particular, the relevant GO terms were related to cell surface receptor linked signal transduction (Additional file 8). These data suggest that NP interaction from the outside of the cell involved some membrane receptors, which in turn activated a signalling cascade of activation/perturbation of cellular processes, such as induction of inflammatory response together with regulation of proliferation and activation of death programs. Also for PEG NPs the interaction with cell membrane can be mediated by proteins adsorbed on their surface [61-64]. Previously, we have shown that serum proteins adsorb very efficiently on the surface of bare ORMOSIL NPs and PEGylation reduced but did not abolish protein adsorption [40]. Therefore, the possibility still exists of interaction

between NP-associated proteins and cell surface receptors. Moreover, adsorption of different proteins may trigger the activation of different membrane receptors in different types of cells. Recently, it was shown that the clathrin dependent endocytosis of amorphous silica engineered NPs and the secretion of proinflammatory cytokines are strongly correlated with the expression of scavenger receptor A [65]. Thus, future investigations may be addressed to the identification of proteins and plasma membrane receptors involved in PEG ORMOSIL NPs uptake and/or responsible for the NP-promoted activation of intracellular signalling cascade leading to cell death.

After NP removal (24 + 24 h), only GO terms related to response to wounding, cell motility and cell migration remained perturbed in A549 cells (Figure 9 E, Additional file 9). Interestingly, enrichment in genes involved in the cytoskeleton organization (ANG, ANK3, CNN1, KRT4, RND1, VIL1) was found, suggesting that this type of rebound on cell organization and morphology is a persisting and irreversible effect. In fact, after NP removal, the down-regulation of these genes, some of which are correlated with actin-filament interaction and consequently with cell structure organization, proliferation, cell cycle progression (CNN1 excluded) increased [66,67]. Cytoskeleton disturbance induced by NPs, as well as reduced cell adhesion were confirmed by TEM and SEM analyses (Figure 5 and 3) respectively. TEM clearly showed decreased presence of tonofilaments very likely due to the reduced expression of keratin proteins, while SEM images, showing wizen cells with spherical shape, indicated loss of cell adhesion in agreement with the microarray data indicating that some genes involved in cell adhesion (CDCP1, CDH16, CNN1, COL13A1, FGB, GJB1, NOV, PHLDA1, PODXL, ZEB2) and extracellular matrix degradation (ANPEP, ANTXR2, MMP1, PLAU) were differentially expressed.

We attempted to find reasons for the completely different responses elicited by PEGylated ORMOSIL NPs in A549 and CCD-34Lu cells by comparing the gene expression profiles of the two types of untreated cells. SAM analysis reported 2842 d.e.g between the two cell lines (data not shown) and the GO analysis classified the annotated genes in 401 significant GO terms (cut-off of $p < 0.05$ and filtering out of processes represented by less than 10 genes). However, this comparison was very time consuming and poorly informative with few exceptions. By uploading in DAVID only genes over-expressed in CCD-34Lu cells with respect to A549 cells, an enrichment of about 30 genes involved in response to inorganic substances and response to oxidative stress was found (Additional file 10). The SOD3 gene encoding a member of the superoxide dismutase protein family, was expressed 9.57-fold more in fibroblasts with respect to A549 cells, together with other genes such as SEPP1 and SCARA3 (Additional file 10) encoding for antioxidants active in extracellular space and able to deplete ROS. Consistently with the microarray data, qRT-PCR showed a relative fold change of SOD3 mRNA in CCD-34Lu with respect to A549 of 6.96. This highlighted that fibroblasts possess more efficient mechanisms of defence against oxidative stress in agreement with the faster return, when compared to A549 cells, to basal ROS levels found when NPs were removed from the medium (Figure 8).

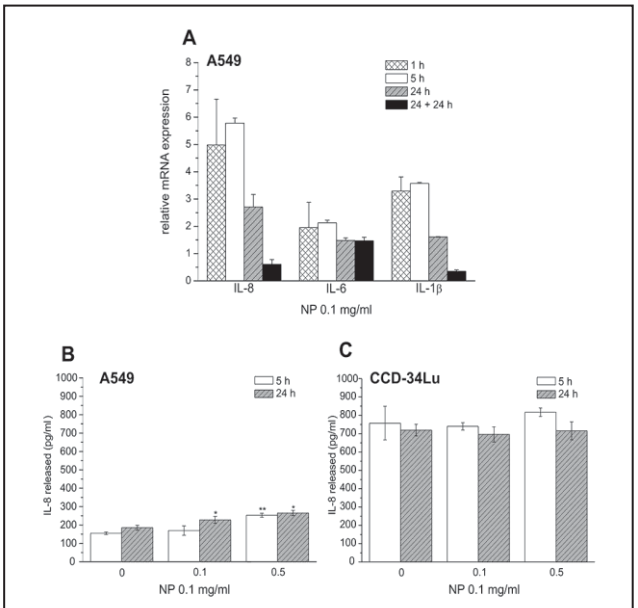

Figure 10 Cytokine mRNA over-expression and release of IL-8 protein induced by PEGylated ORMOSIL NPs. A) Quantitative RT-PCR measurements of mRNA expression of IL-8, IL-6 and IL-1β genes in A549 cells incubated for 1, 5, 24 and 24 + 24 h with 0.1 mg/ml PEGylated ORMOSIL NPs. ELISA measurements of protein IL-8 released in the supernatants of A549 cells (**B**) and CCD-34Lu (**C**) cells incubated for 5 or 24 h with 0, 0.1, 0.5 mg/ml of PEGylated ORMOSIL NPs. The results are mean ± SD of at least three independent experiments each carried out in duplicate. * $p < 0.01$; ** $p < 0.001$ vs controls (t test).

PEG ORMOSIL NPs interacted with pulmonary surfactant components of A549 cells

The evidence that in A549 cells ORMOSIL NPs localized in LBs, suggested that this unique intracellular localization could be the reason leading to cytotoxicity, differently to CCD-34Lu cells. Similarly to our PEG ORMOSIL, fine and ultrafine TiO_2 particles [68,69], single walled carbon nanotubes [70] and lipid-coated gold NPs [71] were reported to localize in the LBs of A549. It was suggested that gold NPs are endocytosed and then excreted by the cells using the same pathways of pulmonary surfactants [71]. Thus, we can speculate that similarly to gold NPs, also ORMOSIL NPs may negatively interfere with surfactant machinery, leading to cytotoxicity. The association of lipids and surfactant proteins with nanomaterials has been well investigated with surfactant monolayer models *in vitro* [72-76] while less in known about these interactions in cellular systems. Mühlfeld and colleagues [77] hypothesized that the particles internalized by the cells interfered with surfactant metabolism and decreased the levels of surfactant proteins because of adsorption to NPs with consequent increased pulmonary inflammatory status. This is well in agreement with our results showing a reduced number LBs (Figure 5 I and L) and an inflammatory response in A549 cells exposed to PEG ORMOSIL. Thus, to assess whether PEGylated ORMOSIL

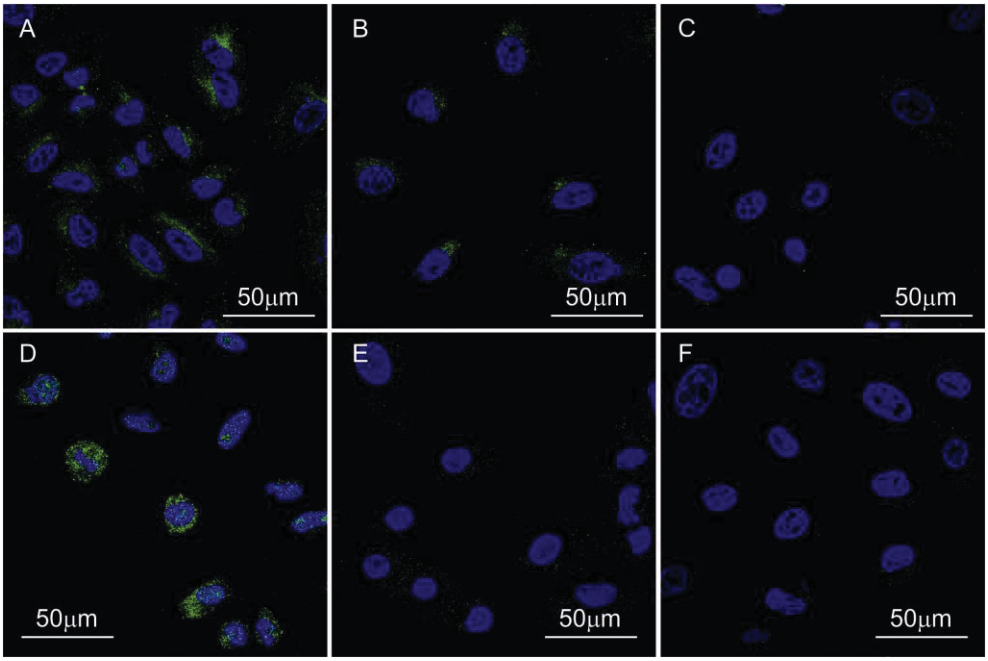

Figure 11 PEGylated ORMOSIL NPs affected the expression of surfactant protein (SP) A and C in A549 cells. Representative immunofluorescence images showing the decrease expression of SP-A **A-C**) and SP-C protein **D-F**) in A549 cells incubated for 24 h with PEGylated ORMOSIL NPs. **A and D** cells not exposed to NPs; **B** and **E** cells incubated with 0.1 mg/ml NPs; **C** and **F** cells incubated with 0.3 mg/ml of NPs.

could interfere with secretion/recycling of the surfactant components, we used immunofluorescence to detect possible alterations of the level and distribution of surfactant protein A (SP-A) and surfactant protein C (SP-C) in A549 cells. SP-A is a hydrophilic protein and, together with surfactant protein D (SP-D), plays a role in the innate immune defense of the lung [78] and surfactant lipid metabolism and homeostasis [79] while the small hydrophobic polypeptides SP-C, with surfactant protein B (SP-B), is mainly involved in the surface activity of the surfactant film. As shown in Figure 11, while the expression of SP-A was only slightly reduced after exposure to PEG NPs, SP-C gradually disappeared by increasing the NP concentration. SP-C localizes within LBs and is co-secreted with LB content while SP-A secretion is LB-independent [80]; thus the immunofluorescence data confirmed an interference of PEG ORMOSIL NPs with LB functioning as suggested by the TEM analyses (Figure 5 I and L). We can speculate that the stronger reduction of SP-C with respect to SP-A may be related to the hydrophobic nature of this protein that favors the association with the PEG coat of our NPs. In any case, further investigations are needed to quantitatively/qualitatively measure the association of lipids and proteins of the surfactant with PEG-ORMOSIL NPs. SPs and lipids are normally recycled by alveolar epithelial type II cells via clathrin-mediated endocytosis [81] and re-included in LBs, with SPs playing an important role in the stimulation of this recycling mechanism. Thus, it may be that NP association with SPs on plasma membrane triggered recycling, with NPs internalized together with surfactants and included in LBs. Sachan and colleagues [75] studied the interaction of AmOrSil20 NPs with a model surfactant monolayer and reported strong association at high concentration of NPs (3 mg/ml) with surfactant components with consequent slowing down of vesicle insertion rate and inhibition of surfactant recycling. NP interference with surfactant regeneration very likely occurred also in our experiments, as shown by the reduction of the film thickness (Figure 5 G, H, M, N) and disappearance of the lipid vesicles clearly visible in the TEM images of the control cells (Figure 5 C and D). Reduction of vesicle size was measured also in the model film Infasurf exposed to hydroxyapaptite (HA) NPs [73] and the adsorption of proteins on NPs was identified as determinant of smaller vesicles formation with consequent inhibited surface activity of the surfactant film. In addition, it has been reported that NPs covered themselves with lipids [74,82] becoming integral part of surfactant film and disturbing lipid surface structure and function [72]. Translating these observations to our alveolar epithelial cell model, it may be that the destabilization of surfactant layer lead to the enhanced plasma membrane permeability measured after PEG ORMOSIL NP exposure.

Taking together, all these information indicated that the higher sensitivity of A549 cells to ORMOSIL NP treatment with respect to other lung cell lines may be attributed to interactions of the NPs with the surfactant film as well as to an impaired re-spreading/recycling of surfactants.

Conclusions

We have reported on the responses elicited in different lung cell

lines by PEGylated ORMOSIL NPs designed for medical application. Our data showed that the addition of the PEG corona abolished the toxicity of ORMOSIL NPs toward normal fibroblasts CCD-34Lu and adenocarcinoma cells NCI-H2347 while had only a minor effect in reducing the toxicity toward A549 carcinoma cells. The uptake of PEG NPs in the cells was about 20% that of their bare counterpart, due to reduced interactions of NPs with plasma membrane as expected because of the hydrophilic PEG coating. In spite of the reduced uptake, PEG ORMOSIL were still toxic to A549 cells. Investigations on the effects of PEG NPs on cellular functions in A549 alveolar cells and in CCD-34Lu fibroblasts revealed ROS production in both types of cells even if the oxidative stress was not the major cause of A549 NP-induced cytotoxicity. Only in A549 cells, PEG NP exposure caused alteration of plasma membrane permeability and up-regulation of genes involved mainly in inflammation, cell death and cell signalling mediated by membrane receptors, with consequent death via necrosis. All the above mentioned cellular events were probably triggered by NP interactions and interference with the surfactant production and recycling peculiar of alveolar type II epithelial cells. The TEM images clearly showed that NPs were internalized in the lamellar bodies, very likely interacted with surfactant film components (i.e. lipids/proteins) sequestering part of them as well as interfering with film functions and surfactant recycling. However, additional investigations are needed to identify the surfactant components which interact with PEGylated ORMOSIL NPs.

Methods

Preparation and characterization of ORMOSIL nanoparticles

The detailed procedure of preparation of PEGylated and non-PEGylated ORMOSIL NPs was described previously [37,38]. Briefly, Brij 35 (5 mM) was dissolved under stirring in 5 ml of water into a thermostated reaction vessel. A DMSO solution (10 μl) of a rhodamine-triethoxysilane derivative (11 mM) [83] and, when required, O-(2-(4-(2-trimethoxysilyl-ethyl)-benzensulfonammido))ethyl)-O'-methylpolyethylene glycol ($MPEG_{2000}$triethoxysilane, (3 mM)), 150 μL of *n*-butanol and finally 80 μl of VTES were added. The mixture was stirred for 30 min and then 5 μl of aqueous ammonia were added to start the polymerization. The stirring was continued overnight at 30 °C, the reaction mixture was then extensively ultrafiltered with Milli-Q water, using a cellulose membrane with a cut-off size of 10 kDa and eventually filtered with a 0.20 μm cellulose acetate membranes. In the case of PEGylated nanoparticles, to reduce ultrafiltration times, the crude reaction mixture was stirred with Bio-Beads® SM (14.3 mg per mg of Brij 35) for 3 hours before ultrafiltration.

The particle sizes were measured by Dynamic Light Scattering (DLS) with a Malvern Zetasizer Nano-S with a HeNe laser (633 nm): temperature of 25 °C, aqueous suspension, viscosity of 0.8872 cP. Zeta potenzial (ζ) was measured with the same instrument using disposable cells. Transmission electron microscopy (TEM) analysis was carried outwith a Jeol 300PX instrument. One drop of NP suspension was placed on the sample grid and the solvent as allowed to evaporate. For fluorescence-labelled NPs, dye content was determined on the basis of rhodamine absorption at 566 nm, using the ε value of 95000 cm^{-1} M^{-1}, measured with a Lambda 45 Perkin-Elmer spectrophotometer. Dye emission was measured using a LS50B Perkin-Elmer fluorimeter. Thermogravimetric analysis (TGA) were run on 1 mg lyophilized nanoparticle samples using a Q5000-IR model TA instrument from 30 to 1000 °C under a continuous air flow.

Cell culture and incubation with ORMOSIL NPs

A549 human lung carcinoma cells, CCD-34Lu human normal lung fibroblasts and NCI-H2347 human adenocarcinoma non-small lung cells were obtained from American Type Culture Collection (ATCC, Rockville, MD, USA). The cells were maintained at 37 °C in a humidified atmosphere containing 5% CO_2. A549 cells were cultured in F-12K medium supplemented with 10% heat-inactivated foetal bovine serum (FBS, Life Technologies, Milan, Italy), 2 mM L-glutamine, 2.5 g/l sodium bicarbonate, 38 units/ml streptomycin and 100 units/ml penicillin G (Sigma-Aldrich, St Louis, MO, USA). CCD-34Lu fibroblasts were grown in DMEM medium with 3.7 g/l sodium bicarbonate, 4.5 g/l glucose, and supplemented with 38 units/ml streptomycin and 100 units/ml penicillin G, 0.1 mM MEM non essential amino acids, 0.02 M HEPES and 10% FBS. NCI-H2347 cells were grown in RPMI-1640 medium with 1.5 g/l sodium bicarbonate, and supplemented with 38 units/ml streptomycin and 100 units/ml penicillin G, 4.5 g/l D-glucose, 2 mM glutamine, 10 mM HEPES, 1 mM sodium piruvate and 10% FBS. In all cases, the cells were seeded and maintained for 24 h in culture medium supplemented with 10% FBS before starting the NP treatment; then, the medium was replaced with DMEM, F-12K or RPMI-1640 containing 3% FBS, in which the NP stock suspensions were freshly diluted. Cells were incubated for 24 h with increasing concentrations of NPs (0.1-1.5 mg/ml). Afterwards, cell responses were analyzed immediately (24 h time point), or after additional 24 h of incubation of cells in NP-free complete medium (24 + 24 h time point).

Assessment of NP cytotoxicity

MTS assay. Reduction of cell proliferation/viability after NP incubation was measured by MTS [(3-(4,5-dimethylthiazol-2-yl)-5-(3-carboxymethoxyphenyl)-2-(4-sulfophenyl)-2H-tetrazolium)] assay. The CellTiter 96® Aqueous One Solution Cell Proliferation Assay (Promega Co, Madison, WI, USA) was used. Briefly, A549, CCD-34Lu and NCI-H2347 cells were seeded in triplicate in 96-well plates (3000 cells/well) and 24 h later incubated with increasing concentrations of non-PEG or PEG NPs. Cell viability was measured at 24 h time point as well as at 24 + 24 h. For the assay, the cell medium was replaced with 100 μl of serum free medium plus 20 μl of CellTiter 96® Reagent and the plates were incubated for 1.5 h at 37°C. Afterward, the absorbance at 492 nm of the formazan produced was measured with a Biotrak II (GE Healthcare,

Piscataway, NJ, USA) visible plate reader. The viability of treated cells was expressed as percentage of the absorbance of controls that was taken as 100% viability.

LDH release assay. The activity of lactate dehydrogenase (LDH) released in the cell culture medium during incubation with PEG NPs was measured using the CytoTox 96® Non-Radioactive Cytotoxicity Assay (Promega Co, Madison, WI, USA). The cells were seeded in 96-well plates and treated as for the MTS assay. Following the 24 h of treatment, the LDH activity was measured according to the manufacturer's instructions. The activities of the total cellular LDH content and of that released in the cell culture medium were measured in order to calculate the percentage of enzyme released during the exposure of the cells to PEG NPs.

Propidium iodide (PI) staining. Morphological changes and plasma membrane permeabilization in cells treated for 24 h with PEG NPs were analyzed using the DM 5000B fluorescence microscope (Leica Microsystems Srl; Milan, Italy). At the end of NP incubation, cells were incubated with 10 µg/ml of PI (Sigma-Aldrich, St Louis, MO, USA) in phosphate buffered saline (PBS) for 5 minutes at room temperature and then visualized under the microscope. The percentage of PI positive cells (% of necrotic cells) in each sample was obtained counting at least 400 cells/sample.

Scanning electron microscopy (SEM) and transmission electron microscopy (TEM)

A549 and CCD-34Lu cells were seeded in 35 mm culture dishes (100000 cells/well) and, after 24 h of growth, were treated with non-PEG or PEG NPs for 24 h. For SEM, the cells seeded on a coverslip, were primary fixed in 2.5% glutaraldehyde in 0.1 M phosphate buffer at pH 7.4 for 1 h at room temperature and then washed 3 times with phosphate buffer (10 min each wash). The samples were post-fixed in 1% osmium tetroxide in 0.1 M phosphate buffer pH 7.4 for 1 h at room temperature and dehydrated in ethanol from 10% to100% (3 times) for 10 min each step. The samples were then critical point dried, gold sputtered and observed with a Stereoscan 260 scanning electron microscope (Cambridge Scientific Instruments Ltd., Ely, UK) operating at 15 kV. For TEM, cells were fixed and dehydrated in ethanol as for SEM and finally included in epoxy resin. The samples were sectioned with a Ultrotome V ultramicrotome (LKB instruments, Victoria, TX, USA). Thin sections (80-100 nm) were counterstained with uranyl acetate and lead citrate and then observed with a Tecnai G^2 transmission electron microscope (FEI Company, Hillsboro, OR, USA) operating at 100 kV.

Uptake of rhodamine labeled non-PEG and PEG ORMOSIL NPs

Flow cytometry was used for a comparative evaluation of the uptake of NPs in A549 and CCD-34Lu cells. The cells were incubated for 24 h with a sub-lethal dose (0.1 mg/ml) of NPs covalently labelled with rhodamine. After cell harvesting, 10000 events/sample were acquired and analysed by flow cytometry. The internalization and localisation of rhodamine-labeled NPs in the cells was also inspected with a DM 5000B fluorescence microscope (Leica Microsystems Srl, Milan, Italy).

ROS measurements

ROS generation within cells was measured using the Total ROS Detection Kit (Enzo Life Sciences International Inc., Plymouth Meeting, PA, USA). The kit includes a non-fluorescent cell permeable probe (Oxidative Stress Detection Reagent) which reacts directly with various types of ROS, yielding a green fluorescent product indicative of cellular ROS production. Cells were seeded in 24-well plates (15000 cells/well) and, after 24 h of growth, were treated with PEG NPs for 5, 24 or 24 + 24 h. Afterwards, the cells were washed twice with 1X Wash Buffer, harvested and centrifuged for 5 min at 400xg. Cell pellets were incubated with 500 µl of ROS Detection Solution (25 µM Oxidative Stress Detection Reagent in Wash Buffer 1X) and incubated at 37° C in the dark for 30 min. Ten thousand events/sample were analyzed by flow cytometry (BD FACSCanto™ II instrument, Becton Dickinson, San Jose, CA, USA) using 488-nm laser and FITC detection channel (515-545 nm). The capability of antioxidant agents such as catalase (CAT) and superoxide dismutase (SOD) to deactivate ROS was analyzed in cells exposed to PEG NPs. The cells were pre-incubated for 1 h with CAT (1000 U/ml), SOD (1000 U/ml) or SOD + CAT (1000 U/ml of each) (Sigma-Aldrich, St Louis, MO, USA) and then NPs were added for 24 h. The viability of the cells exposed to NPs in the presence of CAT and SOD was measured with the trypan blue exclusion test. This test was used because of the interference of antioxidants with the MTS test [84]. The cells treated as those for ROS detection experiments were harvested, centrifuged and 30 µl of cell suspension were stained with 30 µl of trypan blue (Sigma-Aldrich, St Louis, MO, USA). Cells negative to trypan blue staining were counted using a Burker Chamber and the viability of treated cells was expressed as percentage of the cell number of controls that was taken as 100% viability.

Gene expression analysis

Microarray experiments. 0.5 x 10^6 A549 or CCD-34Lu cells were seeded in 100 mm culture dishes for 24 h and then exposed to a sub-lethal dose (0.1 mg/ml) of PEG NPs for 24 h or 24 + 24 h. Total RNA was extracted from control and NP-treated cells with TRIZOL (Life Technologies, Milan, Italy) according to the manufacturer's instructions. Extracted RNA was quantified by spectrophotometric analysis (NanoDrop® ND-1000, CELBIO, Milan, Italy) and checked for quality and integrity with an Agilent Bioanalyzer 2100 (Agilent Small RNA kit and Nano kit, Agilent Technologies, Palo Alto, CA, USA). The One-Color Microarray-Based Gene Expression Analysis was performed using the Whole Human Genome (4x44K) Oligo Microarray Kit with SurePrint (Agilent), according to the manufacture's guidelines. One µg of RNA from three different experimental replicates/sample was amplified and labeled using the Quick Amp Labeling Kit (Agilent) to generate Cyanine-3-CTP labeled complementary

RNA (cRNA) using T7 RNA polymerase. Spike-in control transcripts were added to each sample and monitored to verify hybridization integrity. cRNA samples were purified with RNeasy Mini spin columns (Qiagen Sciences, Germantown, MD, USA) and quantified using NanoDrop®. Before the hybridization on the microarray platform, 1.65 µg of RNA/samples was fragmented using the Gene Expression Hybridization Kit (Agilent) by incubation with 25x Fragmentation Buffer and 10x Blocking Agent for 30 min at 60°C. Fragmented RNA was hybridized to 4x44 K Whole Genome Human Chip that contains about 41000 60-mer oligoprobe for human genes and transcripts that have been empirically and experimentally validated. Samples were hybridized in Hybridization Buffer of Gene Expression Hybridization kit using gasket slides within the Agilent SureHib chamber for 17 h at 65° C and with a rotation of 10 rpm. Slides were scanned at 5 µm resolution on a DNA Microarray Scanner (Agilent). Images were analyzed with the Agilent Feature Extraction Software 10.5.1.1 and 4 Quality Control (QC) for array were extracted. Microarray data were first normalized both intra-array (multiplicatively detrended analysis) and inter-array (quantile analysis) and then filtered according to the parameters of spots recognition and background exclusion. Using TMEV 4_5_1 [85], the Significance Analysis of Microarray (SAM) two class unpaired statistic analysis was performed: normalized values of gene expression were converted to a logarithmic scale and genes resulting with Log_2 (expression values NPs/controls) > +0.7 and < −0.7 and with a False Discovery Rate (FDR) < 4% were considered as up-regulated and down-regulated, respectively. SAM was used also to obtain d.e.g. between A549 and CCD-34Lu un-treated cells, applying for the analysis a FDR of 0%. Raw data of microarray experiments are available on the National Center for Biotechnology Information Gene Expression Omnibus (GEO) website (http://www.ncbi.nlm.nih.gov/geo/) [GSE25991].

Cluster and Gene ontology analysis. Heat map images and cluster analysis of d.e.g. in A549 cells were performed using TMEV 4_5_1. Lists of d.e.g were uploaded in the Database for Annotation, Visualization and Integrated Discovery functional annotation tool (DAVID 6.7b version; http://david.abcc.ncifcrf.gov/) which is able to extract biologically relevant gene ontology terms (GO terms) [86,87]. The analysis was focused on the enrichment in GO-terms in biological processes on FAT level (GOTERM_BP FAT chart) which filters out very broad GO terms based on a measured specificity of each term (not level-specificity). For a biological process term to be considered significantly enriched, we used a cut-off of $p < 0.05$ after multiple testing corrections. Moreover, the processes represented by less than 5 genes were filtered out to identify only those pathways most perturbed by NPs. Biological processes terms that represented complete subsets of other biological processes were rolled up to the highest level of GO hierarchy, eliminating redundancy.

Quantitative Real time PCR (qRT-PCR)

One µg of total RNA/sample extracted from cells untreated or treated with PEG NPs was converted to complementary DNA (cDNA) via reverse transcriptase with oligo-dT priming (Improm-II™ Reverse Transcription System, Promega Co., Madison, WI, USA) according to the manufacturer's instructions. Primer pairs designed to amplify cDNA encoding target genes were prepared using the Universal ProbeLibrary Assay Design Center (Roche Applied Science, Indianapolis, IN, USA). qRT-PCR analysis was performed using the 7500 Real-Time PCR system (Applied Biosystems, Life Technologies Corporation, Carlsbad, CA, USA) and data were analyzed using the Sequence Detection software version 1.4 (Applied Biosystems). Differences in gene expression were normalized to GAPDH transcript levels with invariant abundance in our experimental conditions. Normalized ratios in NP-treated samples were reported as mean fold-change (sometimes transformed in Log_2 scale) compared with untreated controls (Relative Expression, RE).

Detection of IL-8 protein in culture supernatants

The concentrations of IL-8 protein in the supernatant of cells treated for 5 h or 24 h with different doses of PEG NPs were measured with the Human IL-8/NAP-1 Instant ELISA assay (Bender MedSystems, Wien, Austria) according to the manufacturer's instructions.

Immunofluorescence of pulmonary surfactant proteins

The surfactant protein A (SP-A) and the surfactant protein C (SP-C) were selected among the four specific proteins of pulmonary surfactant, secreted by alveolar type II cells, and the modulation of their expression was analyzed by immunofluorescence in A549 after incubation with PEG NPs. The cells (10^5) were grown in 35 mm tissue culture dishes containing a glass cover slip for 24 h and then exposed to 0.1 or 0.3 mg/ml of NPs for 24 h. Cells were then washed twice with PBS and fixed in 4% paraformaldehyde in PBS for 15 min at room temperature. The fixed cells were washed again three times with PBS, permeabilized in 0.2% Triton X-100 PBS (permeabilization solution) for 10 min at 37 °C and then incubated in 10% goat serum (GS) in PBS for 1 h at room temperature to suppress non specific antibody binding. The cells were then incubated for 90 min at room temperature with the primary antibodies: rabbit polyclonal anti-Prosurfactant Protein C antibody and mouse monoclonal anti-surfactant Protein A antibody (Abcam, Cambridge, UK) diluted 1:200 and 1:100, respectively, in permeabilization solution added with 10% GS. The slides were washed three times in PBS and incubated in the dark for 1 h with the secondary antibodies Alexa Fluor 488 donkey anti-rabbit and Alexa Fluor 488 goat-anti-mouse for SP-C and SP-A, respectively, diluted 1:350 in permeabilization solution added with 10% GS. After three additional washes in PBS, cells were counterstained with 2 µg ml^{-1} DAPI (4,6-diamidino-2-fenilindole) in antifade solution (Vectashield, Vector Laboratories, Burlingame, CA, USA) and glass cover slip were mounted and analyzed with a Leica SP5

confocal laser microscope (Leica Microsystems Srl, Milan, Italy).

Statistical analysis

The Primer software for biostatistics (McGraw-Hill, Columbus, OH, USA) was used for statistical analysis of the data. The data are expressed as means ± standard deviations (S.D.) of at least 3 experiments. The differences between groups were evaluated with the Student's *t*-test and considered significant for $p < 0.05$.

Additional files

Additional file 1: Size distribution of PEGylated ORMOSIL nanoparticles in different media.

Additional file 2: SEM micrographs of A549 cells incubated for 24 h with 0.1 mg/ml of non-PEG A) or PEG B) ORMOSIL NPs.

Additional file 3: Further SEM images of A549 and CCD-34Lu cells exposed for 24 h to ORMOSIL NPs. This series of images are at higher magnification with respect to those of Figure 3 and show NP adhesion on cell membrane.

Additional file 4: Percentage of propidium iodide positive A549 and CCD-34Lu cells after 24 h exposure to PEG NPs.

Additional file 5: List of A549 differentially expressed genes after 24 h of incubation with PEG NPs.

Additional file 6: List of A549 differentially expressed genes after 24 + 24 h of incubation with PEG NPs.

Additional file 7: qRT-PCR measurements of mRNA expression of IL-8, PTGS2 and KRT4 gene in A549 cells incubated with 0.1 mg/ml of PEG NPs for 24 h or 24 + 24 h. The table shows validation of microarray expression results.

Additional file 8: List of GO terms relative to A549 differentially expressed genes after 24 h PEG NP incubation. The list was used to extrapolate data for Figure 9 D.

Additional file 9: List of GO terms relative to A549 differentially expressed genes after 24 + 24 h PEG NP incubation. The list was used to extrapolate data for Figure 9 E

Additional file 10: List of genes, obtained uploading in DAVID genes over-expressed in untreated CCD-34Lu with respect to untreated A549, showing only those genes belonging to 4 different GO terms related to the response to oxidative stress and/or inorganic substances.

Competing interests

The authors declare that they have no competing interests.

Authors' contributions

FMoret participated in the design of the study, performed the microarray and qRT-PCR experiments, the ROS measurements, the MTS and LDH assays, the fluorescence microscopy, SEM and TEM analyses and drafted the manuscript. FS and EL were involved in the preparation and characterization of the nanoparticles. CC was involved in the cell viability tests. MM contributed to the analyses of the microarray data. LC participated in the design of the study and helped with the manuscript revision. FMancin supervised the nanoparticle preparation and characterization, contributed to manuscript drafting and revision. ER was the project leader, participated in the study design and planning experiments, contributed to the interpretation of the results and critically revised the manuscript. All authors read and approved this final version of the manuscript.

Acknowledgements

The research leading to these results has received funding from the European Community's Seventh Framework Programme (FP7/2007-2013) under grant agreement no. 201031 NANOPHOTO. We thank Dr. Cristiano De Pittà (CRIBI, Padova) for the submission to GEO of the microarray data. Microarray analysis was performed by CRIBI Gene Expression Service (MicroCribi, http://microcribi.cribi.unipd.it) of the University of Padova, Via Ugo Bassi, No. 58/B, 35131 Padova, Italy. The acquisition of the SEM and TEM images was performed by the electron microscopy service of the University of Padova, Via Ugo Bassi, No. 58/B, 35131 Padova, Italy.

References

1. Ruiz-Hitzky E, Darden M, Azauda P, Ariga K: **Advances in biomimetic and nanostructured biohybrid materials**. *Adv Mat* 2010, **22:**323-336.
2. Kim KT, Meeuwisser SA, Nolte RJ, van Hest JC: **Smart nanocontainers and nanoreactors.** *Nanoscale* 2010, **2:**844-858.
3. Ray S, Chandra H, Srivastava S: **Nanotechniques in proteomics: current status, promises and challenges.** *Biosens Bioelectron* 2010, **25:**2389-2401.
4. Dong X, Mumper RJ: **Nanomedicinal strategies to treat multidrug-resistant tumors: current progress.** *Nanomedicine (Lond)* 2010, **5:**597-615.
5. Shi J, Votruba AR, Farokhzad OC, Langer R: **Nanotechnology in drug delivery and tissue engineering: from discovery to applications.** *Nano Lett* 2010, **10:**3223-3230.
6. Davis ME, Chen Z, Shin DM: **Nanoparticles therapeutics: an emerging treatment modality for cancer.** *Nat Rev Drug Discov* 2008, **7:**771-782.
7. Fadeel B, Garcia-Bennett AE: **Better safe than sorry: understanding the toxicological properties of inorganic nanoparticles manufactured for biomedical application.** *Adv Drug Del Rev* 2010, **62:**362-374.
8. Nel A, Xia T, Mädler L, Li N: **Toxic potential of nanomaterials at the nanolevel.** *Science* 2006, **311:**622-627.
9. Card JW, Zeldin DC, Bonner JC, Nestmann ER: **Pulmonary applications and toxicity of engineered nanoparticles.** *Am J Physiol Lung Cell Mol Physiol* 2008, **295:**400-411.
10. Singh N, Manshian B, Jenkins GJS, Griffith SM, Williams PM, Maffeis TG, Wright CJ, Doak SH: **NanoGenotoxicology: the DNA damaging potential of engineered nanomaterials.** *Biomaterials* 2009,

30:3891-3914.

11. Couleaud P, Morosini V, Frochot C, Richeter S, Raehm L, Durand JO: **Silica-based nanoparticles for photodynamic therapy applications.** *Nanoscale* 2010, **2:**1083-1095.
12. Slowing II, Vivero-Escoto JL, Wu CW, Lin VSY: **Mesoporous silica nanoparticles as controlled release drug delivery and gene transfection carriers.** *Ad Drug Del Rev* 2008, **60:**1278-1288.
13. Trewyn BG, Slowing II, Giri S, Chen HT, Lin VSY: **Synthesis and functionalization of a mesoporous silica nanoparticle based on the sol-gel process and applications in controlled release.** *Acc Chem Res* 2007, **40:**846-853.
14. Slowing II, Trewyn BG, Giri S, Lin VSY: **Mesoporous silica nanoparticles for drug delivery and biosensing applications.** *Adv Funct Mater* 2007, **17:**1225-1236.
15. Lin W, Huang YW, Zhou XD, Ma Y: **In vitro toxicity of silica nanoparticles in human lung cancer cells.** *Tox Applied Pharmacol* 2006, **217:**252-259.
16. Akhtar MJ, Ahamed M, Kumar S, Siddiqui H, Patil G, Ashquin M, Ahmad I: **Nanotoxicity of pure silica mediated through oxidant generation rather than glutathione depletion in human lung epithelial cells.** *Toxicology* 2010, **276:**95-102.
17. Chang JS, Chang KLB, Hwang DF, Kong ZL: **In vitro cytotoxicity of silica nanoparticles at high concentrations strongly depends on the metabolic activity type of the cell line.** *Environ Sci Technol* 2007, **41:**2064-2068.
18. Park EJ, Park K: **Oxidative stress and pro-inflammatory responses induced by silica nanoparticles in vivo and in vitro.** *Toxicol Lett* 2009, **184:**18-25.
19. Eom HJ, Choi J: **Oxidative stress of silica nanoparticles in human bronchial epithelial cell, Beas-2B.** *Toxicol in Vitro* 2009, **23:**1326-1332.
20. Liu X, Sun J: **Endothelial cells dysfunction induced by silica nanoparticles through oxidative stress via JNK/P53 and NF-κB pathways.** *Biomaterials* 2010, **31:**8198-8209.
21. Choi J, Zheng Q, Katz HE, Guilarte TR: **Silica-based nanoparticle uptake and cellular response by primary microglia.** *Environ Health Perspect* 2010, **118:**589-596.
22. Lu X, Qian J, Zhou H, Gan Q, Tang W, Lu J, Yuan Y, Liu C: **In vitro cytotoxicity and induction of apoptosis by silica nanoparticles in human HepG2 hepatoma cells.** *Int J Nanomedicine* 2011, **6:**1889-1901.
23. Mohamed BM, Verma NK, Prina-Mello A, Williams Y, Davies AM, Bakos G, Tormey L, Edwards C, Hanrahan J, Salvati A, Lynch I, Dawson K, Kelleher D, Volkov Y: **Activation of stress-related signalling pathway in human cells upon SiO_2 nanoparticles exposure as an early indicator of cytotoxicity.** *J of Nanobiotechnology* 2011, **9:**29.
24. Mu Q, Hondow NS, Krzemiński, Brown AP, Jeuken LJC, Routledge MN: **Mechanism of cellular uptake of genotoxic silica nanoparticles.** *Part Fibre Toxicol* 2012, **9:**29-40.
25. Yang X, Liu J, He H, Zhou L, Gong C, Wang X, Yang L, Yuan J, Huang H, He L, Zhang B, Zhuang Z: **SiO_2 nanoparticles induce cytotoxicity and protein expression alteration in HaCaT cells.** *Part Fibre Toxicol* 2010*,* **7:**1-12.
26. Wang F, Gao F, Lan M, Yuan H, Liu J. **Oxidative stress contributes to silica nanoparticle-induced cytotoxicity in human embryonic kidney cells.** *Toxicol In Vitro* 2009, **23:**808-815.
27. Huang X, Teng X, Chen D, Tang F, He J: **The effect of the shape of mesoporous silica nanoparticles on cellular uptake and cell function.** *Biomaterials* 2010, **31:**438-448.
28. Lundqvist M, Stigler J, Elia G, Lynch I, Cedervall T, Dawson KA: **Nanoparticle size and surface properties determine the protein corona with possible implications for biological impacts.** *Proc Natl Acad Sci USA* 2008, **105:**14265-14270.
29. Nel AE, Madler L, Velegol D, Xia T, Hoek EM: **Understanding biophysicochemical interaction at the nano-bio interface.** *Nat Mater* 2009, **8:**543-557.
30. Wattendorf U, Merkle HP: **PEGylation as a tool for the biomedical engineering of surface modified microparticles.** *J Pharm Sci* 2008, **97:**4655-4669.
31. Jain A, Jain SK: **PEGylation: an approach for drug delivery. A review.** *Crit Rev Ther Drug Carrier Syst* 2008, **25:**403-447.
32. Jain K, Kesharwani P, Gupta U, Jain NK: **Dendrimer toxicity: let's meet the challenge.** *Int J Pharm* 2010, **394:**122-42.
33. Jiang YY, Tang GT, Zhang LH, Kong SY, Zhu SJ, Pei YY: **PEGylated PAMAM dendrimers as a potential drug delivery carrier: in vitro and in vivo comparative evaluation of covalently conjugated drug and noncovalent drug inclusion complex.** *J Drug Target* 2010, **18:**389–403.
34. Zhang T, Stilwell JL, Gerion D, Ding L, Elboudwarej O, Cooke PA, Gray JW, Alivisatos AP, Chen FF: **Cellular effect of high doses of silica-coated quantum dot profiled with high throughput gene expression analysis and high content cellomics measurements.** *Nano Lett* 2006, **6:**800-808.
35. Clift MJD, Varet J, Hankin SM, Bownlee B, Davidson AM, Branderberger C, Rothen-Rutishauser B, Bown DM, Stone V: **Quantum dot cytotoxicity in vitro: an investigation into the cytotoxic effects of a series of different surface chemistries and their core/shell materials.** *Nanotoxicol* 2011, **5:**664-674.
36. Wang W, Xiong W, Zhu Y, Xu H, Yiang X: **Protective effect of PEGylation against poly(amidoamine) dendrimer-induced hemolysis of human red blood**

cells. *J Biomed Mater Res B Appl Biomater* 2010, **93:**59-64.
37. Rio-Echevarria IM, Selvestrel F, Segat D, Guarino G, Tavano R, Causin V, Reddi E, Papini E, Mancin F: **Highly PEGylated silica nanoparticles: "ready to use" stealth functional nanocarriers.** *J Mater Chem* 2010, **20:**2780-2787.
38. Tavano R, Segat D, Reddi E, Kos J, Rojnik M, Kocbek P, Iratni S, Scheglmann D, Colucci M, Rio Echevarria IM, Selvestrel F, Mancin F, Papini E: **Procoagulant properties of bare and highly-PEGylated vinyl-modified silica nanoparticles.** *Nanomedicine (Lond)* 2010, **5:**881-896.
39. Choi SJ, Oh JM, Choy JH: **Toxicological effects of inorganic nanoparticles on human lung cancer A549 cells.** *J Inorg Biochem* 2009, **103:**463-471.
40. Compagnin C, Baù L, Mognato M, Celotti L, Miotto G, Arduini M, Moret F, Fede C, Selvestrel F, Rio Echevarria IM, Mancin F, Reddi E: **The cellular uptake of meta-tetra(hydroxyphenyl)chlorin entrapped in organically modified silica nanoparticles is mediated by serum proteins.** *Nanotechnology* 2009, **20:**345101.
41. Fede C, Selvestrel F, Compagnin C, Mognato M, Mancin F, Reddi E, Celotti L: **The toxicity outcome of silica nanoparticles (Ludox®) is influenced by testing techniques and treatment modalities.** *Anal Bional Chem* 2012, **404:**1789-1802.
42. Drescher D, Orts-Gil G, Laube G, Natte K, Veh RW, Österle W, Kneipp J: **Toxicity of amorphous silica nanoparticles on eukaryotic cell model is determined by particle agglomeration and serum protein adsorption effects.** *Anal Bional Chem* 2011, **440:**1367-1373.
43. Rojnik M, Kocbek P, Moret F, Compagnin C, Celotti L, Bovis MJ, Woodhams JH, MacRobert AJ, Scheglmann D, Helfrich W, Verkaik MJ, Papini E, Reddi E, Kos J: **In vitro and in vivo characterization of temoporfin-loaded PEGylated PLGA nanoparticles for use in photodynamic therapy.** *Nanomedicine (Lond)* 2012, **7:**663-677.
44. Mano SS, Kanehira K, Sonezaki S, Taniguchi A: **Effect of polyethylene glycol modification of TiO_2 nanoparticles on cytotoxicity and gene expressions in human cell lines.** *Int J Mol Sci* 2012, **13:**3703-3717.
45. Gyenge EB, Darphin X, Wirth A, Pieles U, Walt H, Bredell M, Maake C: **Uptake and fate of surface modified silica nanoparticles in head and neck squamous cell carcinoma.** *Journal of Nanobiotechnology* 2012, **9:**32-46.
46. Wang J, fang X, Liang W: **Pegylated phospholipid micelles induce endoplasmic reticulum-dependent apoptosis of cancer cells but not normal cells.** *ACS Nano* 2012, **6:**5018-5030.
47. Foster KA, Oster CG, Mayer MM, Avery ML, Audus KL: **Characterization of the A549 cell lines as a type II pulmonary epithelial cell model for drug metabolism.** *Exp Cell Res* 1998, **243:**359-366.
48. Haagsman HP, van Holde LMG: **Synthesis and assembly of surfactant.** *Annu Rev Physiol* 1991, **53:**441-464.
49. Ye SF, Wu YH, Hou ZQ, Zhang QQ: **ROS and NF-kappaB are involved in upregulation of IL-8 in A549 cells exposed to multi-walled carbon nanotubes.** *Biochem Biophys Res Commun* 2009, **379:**643-648.
50. Huang CC, Aronstam RS, Chen DR, Huang YW: **Oxidative stress, calcium homeostasis, and altered gene expression in human lung epithelial cells exposed to ZnO nanoparticles.** *Toxicol in Vitro* 2010, **24:**45-55.
51. Nabeshi H, Yoshikaea T, Matsuyama K, Nakazato Y, Tochigi S, Kondoh S, Hirai T, Akase T, Nagano K, Abe Y, Yoshioka Y, Kamada H, Itoh N, Tsunoda S, Tsutsumi Y: **Amorphous nanosilica induce endocytosis-dependent ROS generation and DNA damage in human keratinocytes.** *Part Fibre Toxicol* 2011, **8:**1-10.
52. Yu M, Mo Y, Wan R, Chien S, Zhang X, Zhang Q: **Regulation of plasminogen activator inhibitor-1 expression in endothelial cells with exposure to metal nanoparticles.** *Toxicol Lett* 2010,**195:**82-89.
53. Gras R, Almonacid L, Ortega P, Serramia MJ, Gomez R, de la Mata FJ, Lopez-Fernandez LA, Muñoz-Fernandez MA: **Changes in gene expression pattern of human primary macrophages induced by carbosilane dendrimer 2G-NN16.** *Pharm Res* 2009, **26:**577-586.
54. Cho WS, Kim S, Han BS, Son WC, Jeong J: **Comparison of gene expression profiles in mice liver following intravenous injection of 4 and 100 nm-sized PEG-coated gold nanoparticles.** *Toxicol Lett* 2009, **191:**96-102.
55. Li JJ, Muralikrishnan S, Ng CT, Yung LYL, Bay BH: **Nanoparticle-induced pulmonary toxicity.** *Exp Biol Med* 2010, **235:**1025-1033.
56. Waters KM, Masiello LM, Zangar RC, Tarasevich BJ, Karin NJ, Quesenberry RD, Bandyopadhyay S, Teeguarden JG, Pounds JG, Thrall BD: **Macrophages responses to silica nanoparticles are highly conserved across particle sizes.** *Toxicol Sci* 2009, **107:**553-569.
57. Segat D, Tavano R, Domini M, Selvestrel F, Rio Echevarria IM, Rojnik M, Kocbek P, Kos J, Iratni S, Scheglmann D, Mancin F, Dusi S, Papini E: **Proinflammatory effects of bare and PEGylated ORMOSIL-, PLGA-, and SUV-NPs on monocytes and PMNs and their modulation by f-MLP.** *Nanomedicine (Lond)* 2011, **6:**1027-1046.
58. Park GY, Christman JW: **Involvement of cyclooxygenase-2 and prostaglandins in the molecular pathogenesis of inflammatory lung diseases.** *Am J Physiol Lung Cell Mol Physiol* 2006,

290:797-805.
59. Kagan VE, Bayir H, Shvedova AA: **Nanomedicine and nanotoxicology: two sides of the same coin.** *Nanomedicine* 2005, **1:**313-316.
60. Jiang J, Wang J, Zhang X, Huo K, Wong HM, Yeung KW, Zhang W, Hu T, Chu PK: **Activation of mitogen-activated protein kinases cellular signal transduction pathway in mammalian cells induced by silicon carbide nanowires.** *Biomaterials* 2010, **31:**7856-7862.
61. Dutta D, Sundaram SK, Teeguarden JG, Riley BJ, Fifield LS, Jacobs JM, Addleman SR, Kaysen GA, Moudgil BM, Weber TJ: **Adsorbed proteins influence the biological activity and molecular targeting of nanomaterials.** *Toxicol Sci* 2007, **100:**303-315.
62. El-Ansary A, Al-Daihan S: **On the toxicity of therapeutically used nanoparticles: an overview.** *J Toxicol* 2009, 754810.
63. Marano F, Hussain S, Rodrigues-Lima F, Baeza-Squiban A, Boland S: **Nanoparticles: molecular targets and cell signalling.** *Arch Toxicol* 2011, 85:733-741.
64. Lesniak A, Fenaroli F, Monopoli MP, Åberg C, Dawson KA, Salvati A: **Effects of the presence or absence of a protein corona on silica nanoparticle uptake and impact on cells.** *ACS Nano* 2012, **7:**5845-5857.
65. Orr GA, Chrisler WB, Cassens KJ, Tan R, Tarasevich BJ, Markillie LM, Zangar RC, Thrall BD: **Cellular recognition and trafficking of amorphous silica nanoparticles by macrophage scavenger receptor A.** *Nanotoxicology* 2011, **5:**296-311.
66. Khurana S, George SP: **Regulation of cell structure and function by actin-binding proteins: villin's perspective.** *FEBS Lett* 2008, **582:**2128-2139.
67. Riou P, Villalonga P, Ridley AJ: **Rnd proteins: multifunctional regulators of the cytoskeleton and cell cycle progression.** *Bioessays* 2010, **32:**986-992.
68. Singh S, Shi T, Duffin R, Albrecht C, van Verlo D, Höhr D, Fubini B, Martra G, Fenoglio I, Borm PJA, Schins RPF: **Endocytosis, oxidative stress and IL-8 expression in human lung epithelial cells upon treatment with fine and ultrafine TiO2: role of the specific surface area and of surface methylation of the particles.** *Toxicol Appl Pharmacol* 2007, **222:**141-151.
69. Stearns RC, Paulauskis JD, Godleski JJ: Endocytosis **of ultrafine particles by A549 cells.** *Am J Respir Cell Mol Biol* 2001, **24:**108-115.
70. Davoren M, Herzog E, Casey A, Cottineau B, Chambers G, Byrne HJ, Lyng FM: **In vitro toxicity evaluation of single walled carbon nanotubes on humanA549 lung cells.** *Toxicol in Vitro* 2007, **21:**438-448.
71. Wang M, Petersen NO: **Lipid-coated gold nanoparticles promote lamellar body formation in A549 cells.** *Biochim Biophys Acta* 2013, http://dx.doi.org/10.1016/j.bbalip.2013.01.018.
72. Harishchandra RK, Saleem M, Galla HJ: **Nanoparticle interaction with model lung surfactant monolayers.** *J R Soc Interface* 2010, **7:**S15-S26.
73. Fan Q, Wang YE, Zhao X, Loo JSC, Zuo YY: **Adverse biophysical effects of hydroxyapatite nanoparticles on natural pulmonary surfactant.** *ACS Nano* 2011, **8:**6410-6416.
74. Bakshi MS, Zhao L, smith R, Possmayer F, Petersen NO: **Metal nanoparticle pollutants interfere with pulmonary surfactant function in vitro.** *Biophys J* 2008, **94:**855-868.
75. Sachan AK, Harishchandra RK, Bantz C, Maskos M, Reichelt R, Galla HJ: **High-resolution investigation of nanoparticle interaction with a model of pulmonary surfactant monolayer.** *ACS Nano* 2012, **2:**1677-1687.
76. Schle C, Mühlfeld C, Pulskamp K, Schmiedl A, Nassimi M, Lauenstein HD, Braun A, Krug N, Erpenbeck VJ, Hohlfed JM: **The effect of titanium dioxide nanoparticles on pulmonary surfactant function and ultrastructure.** *Resp Res* 2009, **10:**90.
77. Mühlfeld C, Rothen-Rutishauser B, Blank F, Vanhecke D, Ochs M, Gehr P: **Interactions of nanoparticles with pulmonary structure and cellular responses.** *Am J Physiol Lung Cell Mol Physiol* 2008, **294:**817-819.
78. Crouch E, Wright JR: **Surfactant proteins A and D and pulmonary host defence.** *Annu Rev Physiol* 2001, **63:**521-554.
79. Hawgood S, Poulain F: **The pulmonary collectins and surfactant metabolism.** *Annu Rev Physiol* 2001, **63:**495-519.
80. Andreeva AV, Kutuzov MA, Voyno-Yasenetskaya TA: **Regulation of surfactant secretion in alveolar type II cells.** *Am J Physiol Lung Cell Mol Physiol* 2007, **293:**L259-L271.
81. Rooney SA, Young SL, Mendelson CR: **Molecular and cellular processing of lung surfactant.** *FASEB J* 1994, **8:**957-967.
82. Bothum G: **Hydrophobic silver nanoparticles trapped in lipid bilayers. Size distribution, bilayer phase behavior, and optical properties.** *J Nanobiotechnology* 2008, **6:**13.
83. Rampazzo E, Bonacchi S, Juris R, Montalti M, Genovese D, Zaccheroni N, Prodi L, Rambaldi DC, Zattoni A, Reschiglian P: **Energy transfer from silica core-surfactant shell nanoparticles to hosted molecular fluorophores.** *J Phys Chem B* 2010, **114:**14605-14613.
84. Berridge MV, Tan AS, McCoy KD, Wang R: **The biochemical and cellular basis of cell proliferation assays that use tetrazolium salts.** *Biochemica* 1996, **4:**14-19.
85. Saeed AI, Sharov V, White J, Li J, Liang W, Bhagabati N, Braisted J, Klapa M, Currier T, Thiagarajan M, Sturn A, Snuffin M, Rezantsev A, Popov D, Ryltsov A,

Kostukovic E, Borisovsky I, Liu Z, Vinsavich A, Trush V, Quackenbush A: **TM4: a free, open-source system for microarray data management and analysis.** *BioTechniques* 2003, **34:**374-378.

86. Dennis G Jr, Sherman BT, Hosack DA, Jang J, Gao W, Lane HC, Lempicki RA: **DAVID: Database for Annotation, Visualization, and Integrated Discovery.** *Genome Biol* 2003, **4:**P3.
87. Huang da W, Sherman BT, Lempicki RA: **Systematic and integrative analysis of large gene lists using DAVID bioinformatics resources.** *Nat Protoc* 2009, **4:**44-57.

Additional files

PEGylation of ORMOSIL nanoparticles abolishes the toxicity toward some lung cells but not alveolar type II epithelial cells *in vitro*

Francesca Moret, Francesco Selvestrel, Elisa Lubian, Chiara Compagnin, Maddalena Mognato, Lucia Celotti, Fabrizio Mancin and Elena Reddi.

Additional file 1. DLS size distribution of PEGylated ORMOSIL nanoparticles in different media. DLS size distribution of PEG NPs incubated in water (blue curve, average size 67 ± 15 nm), cell culture medium (red curve, average size 73 ± 15 nm), cell culture medium supplemented with 10% serum (green curve, average size 78 ± 15 nm).

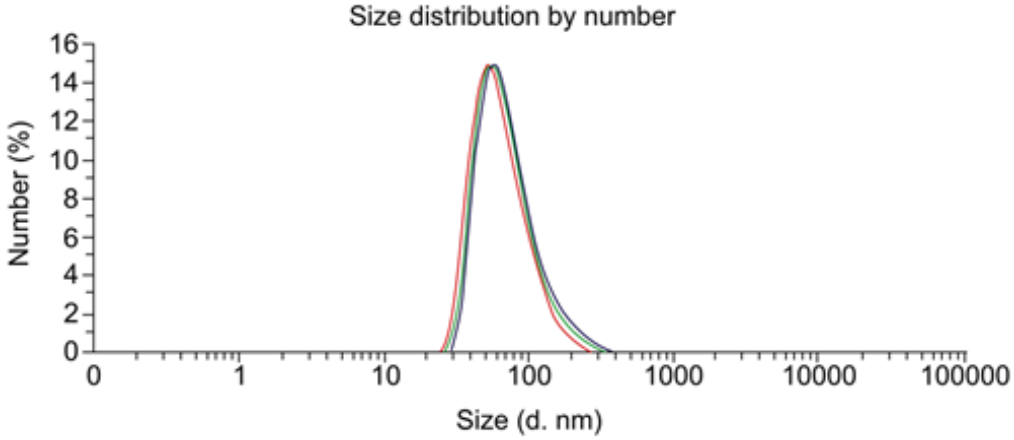

Additional file 2. SEM micrographs of A549 cells incubated 24 h with 0.1 mg/ml of non-PEGylated (A) or PEGylated ORMOSIL NPs (B).

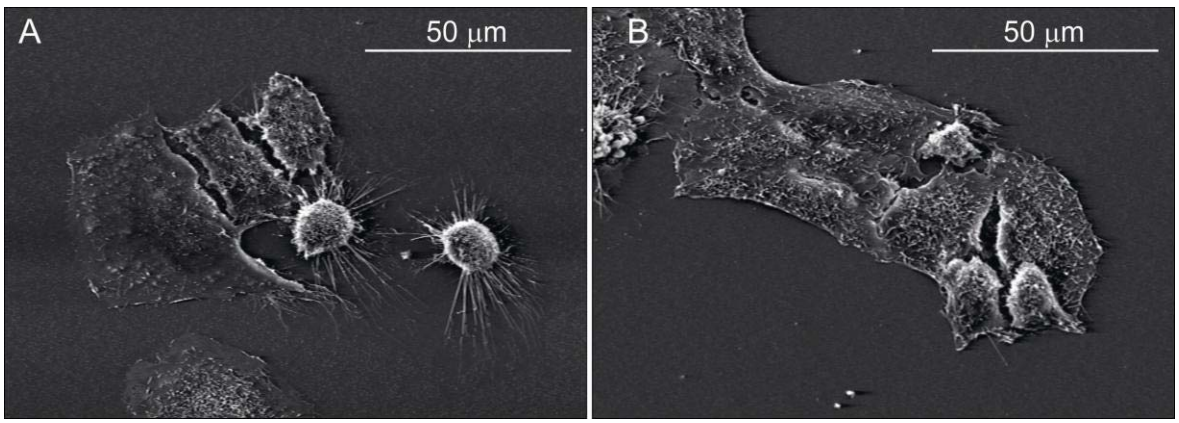

Additional file 3. SEM images of A549 and CCD-34Lu cells exposed 24 h to ORMOSIL NPs. A549 cells **A**) not incubated with NPs, **B**) incubated with 0.3 mg/ml non-PEGylated NPs, **C**) incubated with 0.3 mg/ml PEGylated NPs. CCD-34Lu cells **D**) not incubated with NPs, **E**) incubated with 0.5 mg/ml non-PEGylated NPs, **F**) incubated with 0.5 mg/ml PEG NPs.

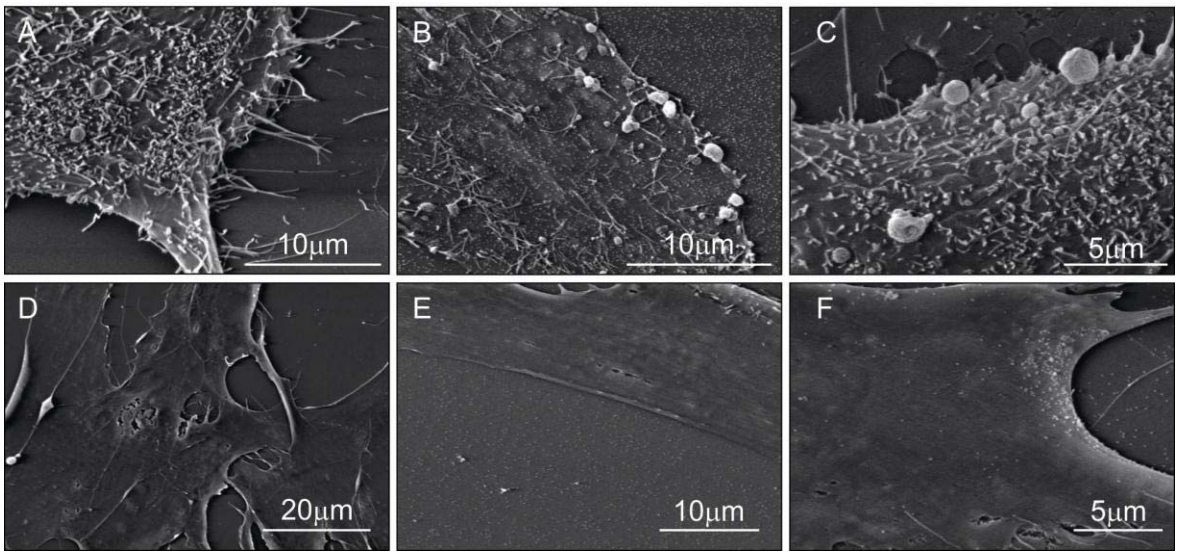

Additional file 4. Percentage of propidium iodide positive A549 and CCD-34Lu cells. The cells were stained with PI after exposure for 24 h to increasing concentrations of PEG ORMOSIL NPs.

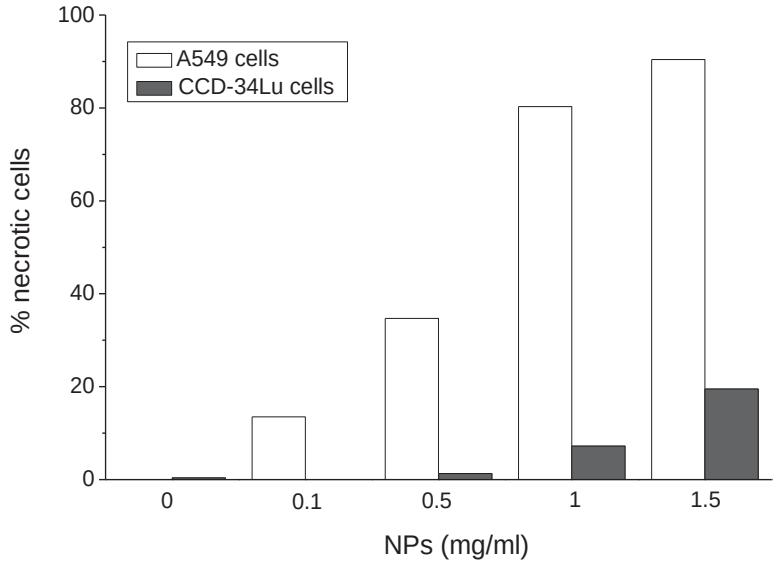

Additional file 5. List of genes differentially expressed in A549 cells after 24 h incubation with 0.1 mg/ml PEGylated NPs. Data from this table were used to obtain heat map diagrams (Figure 9 A) and the GO terms related to biological function perturbed by NP treatments (Figure 9 D).

Gene name	Systematic name	Description	Log_2 NPs/C **24h**	FDR (%)
A_23_P103951	A_23_P103951	unknown	0.98	4%
A_23_P170719	A_23_P170719	unknown	0.95	0%
A_23_P206741	A_23_P206741	unknown	1.05	4%
A_32_P167212	A_32_P167212	unknown	0.73	4%
ADFP	NM_001122	adipose differentiation-related protein	0.87	0%
ADRB2	NM_000024	adrenergic ß-2-receptor	0.81	0%
AI359640	AI359640		0.88	4%
AKAP12	NM_144497	kinase A anchor protein 12 (PRKA)	0.73	4%
AL390143	AL390143		0.93	4%
AMPD3	NM_000480	adenosine monophosphate deaminase	0.80	4%
ANGPTL4	NM_139314	angiopoietin-like 4	0.90	4%
ANPEP	NM_001150	alanyl aminopeptidase (membrane)	1.37	4%
ANTXR2	NM_058172	anthrax toxin receptor 2	1.01	4%
ARHGEF4	NM_032995	Rho guanine nucleotide exchange factor 4	0.84	4%
ATAD4	NM_024320	ATPase family, AAA domain containing 4	-1.41	0%
ATP8B3	NM_138813	ATPase, Class I, type 8B, member 3	-0.84	4%
BAAT	NM_001701	bile acid Coenzyme A	-1.10	4%
BC012036	BC012036		1.05	4%
BG993059	BG993059		0.77	4%
BM129308	BM129308	Melton normalized human islet 4	1.5	4%
BMP6	NM_001718	bone morphogenetic protein 6	0.95	4%
BU674073	BU674073		1.24	4%
C6orf141	BC036917	chromosome 6 open reading frame 141	0.72	4%
CCDC68	NM_025214	coiled-coil domain containing 68	0.87	4%
CD274	NM_014143	CD274 molecule	1.31	4%
CD274	ENST00000381577	programmed death ligand 1	1.06	4%
CD55	NM_000574	CD55 molecule	0.92	0%
CDCP1	NM_022842	CUB domain containing protein 1	1.37	0%
CDH16	NM_004062	cadherin 16	-0.98	4%
CEBPD	NM_005195	CCAAT/enhancer binding protein	-0.85	4%
CNIH3	NM_152495	cornichon homolog 3	1.27	4%
CNN1	NM_001299	calponin 1	-1.47	4%
COL13A1	NM_005203	collagen, type XIII	2.09	0%
CSF1R	NM_005211	colony stimulating factor 1 receptor	0.77	4%
CXCL5	NM_002994	chemokine ligand 5	0.92	0%
CXCL5	NM_002994	chemokine ligand 5	1.10	4%
CXCR7	NM_020311	chemokine receptor 7	-0.85	4%
CYP11A1	NM_000781	cytochrome P450, family 11, subfamily A	0.9	4%
DCLK1	NM_004734	doublecortin and CaM kinase-like 1	2.41	4%
DDIT4	NM_019058	DNA-damage-inducible transcript 4	0.70	0%
DNMBP	BC041628	dynamin binding protein	1.02	0%
F2RL1	NM_005242	coagulation factor II thrombin receptor	0.80	4%
FAM49A	NM_030797	family with sequence similarity 49	1.09	4%
FGB	NM_005141	fibrinogen beta chain	-1.02	4%
FOXD1	NM_004472	forkhead box D1	0.86	4%
FOXJ1	NM_001454	forkhead box J1	-0.78	4%
FOXQ1	NM_033260	forkhead box Q1	0.74	4%
FST	NM_013409	follistatin	1.29	0%
G0S2	NM_015714	G0/G1 switch 2	0.82	0%
GEM	NM_005261	GTP binding protein	1.01	0%
GJB1	NM_000166	gap junction protein, ß 1	-1.33	4%
HAS2	NM_005328	hyaluronan synthase 2	1.45	4%
HRK	NM_003806	BCL2 interacting protein	0.95	0%
IL11	NM_000641	interleukin 11	0.97	0%
IL8	NM_000584	interleukin 8	1.16	4%
KCNJ16	NM_170741	potassium inwardly-rectifying channel	-0.81	4%
KCNMA1	NM_001014797	potassium calcium-activated channel	0.89	4%
KIAA1199	NM_018689		1.19	0%
KRT4	NM_002272	keratin 4	-1.02	4%
LGALS2	NM_006498	lectin, galactoside-binding	-1.50	0%
LINGO1	NM_032808	leucine rich repeat and Ig domain	0.72	4%
LIPG	NM_006033	endothelial lipase	1.71	4%

LOC145837	BC064586	hypothetical protein	-1.45	4%
LOC283454	AK094730		0.90	0%
LOC284542	AK090467	FLJ00388 protein	1.57	4%
LOC399959	AK021552	FLJ11490 fis clone	1.23	4%
LY6K	NM_017527	lymphocyte antigen 6 complex	1.16	0%
LY6K	NM_017527	lymphocyte antigen 6 complex	1.09	0%
MARCH4	NM_020814	membrane-associated ring finger 4	1.33	0%
MCTP1	AK025997		1.80	0%
MCTP1	NM_024717	transmembrane multiple C2 domains	1.57	0%
MIG7	DQ080207	MIG7 mRNA	1.23	4%
MMP1	NM_002421	matrix metallopeptidase 1	1.17	0%
MT1E	NM_175617	metallothionein 1E	0.73	4%
MT1L	X97261	metallothionein isoform 1R	0.76	4%
MT1X	NM_005952	metallothionein 1X	0.74	4%
NEFH	NM_021076	neurofilament, heavy polypeptide 200kDa	-1.58	4%
NFE2	NM_006163	nuclear factor (erythroid-derived 2), 45kDa	-0.86	4%
NOV	NM_002514	nephroblastoma overexpressed gene	0.82	4%
NR1D1	NM_021724	nuclear receptor subfamily 1, member 1	0.91	4%
NT5E	NM_002526	5'-nucleotidase (CD73)	1.27	0%
NT5E	NM_002526	5'-nucleotidase (CD73)	1.13	4%
NTSR1	NM_002531	neurotensin receptor 1	0.81	4%
OTUB2	NM_023112	OTU domain, ubiquitin aldehyde binding 2	0.75	4%
PALM2-AKAP2	NM_007203	PALM2-AKAP2 protein	1.11	4%
PDK4	NM_002612	pyruvate dehydrogenase kinase, isozyme 4	0.75	4%
PDZK1	NM_002614	PDZ domain containing 1	-0.76	4%
PHLDA1	NM_007350	pleckstrin homology-like domain	0.71	4%
PLAU	NM_002658	plasminogen activator, urokinase	0.83	0%
PLAUR	NM_001005377	plasminogen activator, urokinase receptor	0.73	4%
PODXL	NM_005397	podocalyxin-like , transcript variant 2	0.82	0%
PRKCE	NM_005400	protein kinase C	0.80	4%
PTGS2	NM_000963	prostaglandin synthase and cyclooxygenase	1.01	0%
PTPRR	NM_002849	protein tyrosine phosphatase receptor	1.98	4%
PTX3	NM_002852	pentraxin-related gene, induced by IL-1 ß	1.62	4%
RGS2	NM_002923	regulator of G-protein signalling 2	0.88	0%
RNF182	NM_152737	ring finger protein 182	0.96	0%
RPS6KA5	NM_004755	ribosomal protein S6 kinase, 90kDa	0.93	0%
RPS6KA5	NM_004755	ribosomal protein S6 kinase, 90kDa	1.08	4%
RUNX2	NM_004348	runt-related transcription factor 2	1.05	4%
SAMD11	NM_152486	sterile α motif domain containing 11	-0.70	4%
SERPINB8	NM_198833	serpin peptidase inhibitor, clade B, member 8	1.03	4%
SERPINF1	NM_002615	α-2 antiplasmin epithelium derived factor	-0.91	0%
SFMBT2	ENST00000361972	Scm-like with four MBT domains protein 2	0.98	4%
SFRP1	NM_003012	secreted frizzled-related protein 1	0.90	4%
SFRP4	NM_003014	secreted frizzled-related protein 4	-1.10	4%
SH2D5	AK124869		0.71	4%
SHC3	NM_016848	Src2 domain containing transforming protein 3	2.75	4%
SLC6A15	NM_018057	solute carrier family 6	1.80	4%
SMOX	NM_175839	spermine oxidase	0.85	4%
SP5	NM_001003845	Sp5 transcription factor	1.00	4%
SPHK1	NM_021972	sphingosine kinase 1	0.88	0%
SPOCD1	AK097227		1.56	4%
SPOCD1	NM_144569	SPOC domain containing 1	1.05	4%
SSTR5	NM_001053	somatostatin receptor 5	1.48	4%
STC2	NM_003714	stanniocalcin 2	1.30	0%
TGM2	NM_004613	transglutaminase 2	0.98	4%
THC2655811	THC2655811	unknown	1.44	0%
THC2667205	THC2667205	unknown	0.71	4%
THC2677780	THC2677780	unknown	0.89	4%
THC2682291	THC2682291	unknown	-1.10	4%
THC2682885	THC2682885		-0.88	4%
TMEM158	NM_015444	transmembrane protein 158	1.50	0%
TMEM37	NM_183240	transmembrane protein 37	-1.02	4%
TNFRSF25	NM_148965	tumor necrosis factor receptor superfamily	0.88	4%
TNS4	NM_032865	tensin 4	0.80	4%
TOX2	NM_032883	TOX high mobility group box family member 2	0.73	4%
U79293	U79293		0.70	4%
U85992	U85992		1.46	0%
UAP1L1	NM_207309	UDP-N-acteylglucosamine pyrophosphorylase	0.74	4%
VEGFC	NM_005429	vascular endothelial growth factor C	0.82	4%
WDR33	NM_018383	WD repeat domain 33	1.15	4%
ZEB2	NM_014795	zinc finger E-box binding homeobox 2	1.00	4%

Additional file 6. List of genes differentially expressed in A549 cells after 24 + 24 h of PEG NP incubation. Data from this table were used to obtain heat map diagrams (Figure 9 B) and the GO terms related to biological function perturbed by NP treatments (Figure 9 E).

Gene name	Systematic name	Description	Log_2 NPs/C **24 + 24 h**	FDR (%)
A_24_P315256	A_24_P315256	unknown	-0.91	4%
ANG	NM_001145	angiogenin, ribonuclease, RNase A family, 5	-1.02	4%
ANK3	NM_020987	ankyrin 3, node of Ranvier	-0.73	4%
ANPEP	NM_001150	alanyl aminopeptidase	1.43	0%
ANXA9	NM_003568	annexin A9	-0.80	4%
CA9	NM_001216	carbonic anhydrase IX	-0.94	4%
CCK	NM_000729	cholecystokinin	1.00	4%
CNN1	NM_001299	calponin 1	-1.38	0%
COL13A1	NM_005203	collagen, type XIII	1.20	0%
CTGF	NM_001901	connective tissue growth factor	-0.82	4%
DCLK1	NM_004734	doublecortin and CaM kinase-like 1	1.55	0%
ENST00000380683	ENST00000380683	unknown	-0.86	4%
FGA	NM_021871	fibrinogen alpha chain	-1.05	0%
FGA	NM_000508	fibrinogen alpha chain	-1.22	4%
GPR92	NM_020400	G protein-coupled receptor 92	-1.42	4%
HGD	NM_000187	homogentisate 1,2-dioxygenase	-0.96	0%
ITIH5	NM_030569	inter-α (globulin) inhibitor H5	-0.73	4%
KCNJ16	NM_170741	potassium channel, subfamily J, member 16	-1.13	0%
KRT4	NM_002272	keratin 4	-1.84	0%
LBH	NM_030915	limb bud and heart development homolog	-1.10	4%
LGALS2	NM_006498	lectin, galactoside-binding 2	-2.10	0%
LOC553137	AK124400		-0.74	4%
LTB	NM_002341	lymphotoxin ß (TNF superfamily, member 3)	-1.05	4%
LY6K	NM_017527	lymphocyte antigen 6 complex	1.39	4%
LY6K	NM_017527	lymphocyte antigen 6 complex	1.33	4%
NCF2	NM_000433	neutrophil cytosolic factor 2	-0.87	4%
PDZK1	NM_002614	PDZ domain containing 1	-0.84	4%
PROC	NM_000312	protein C	-0.95	4%
PTX3	NM_002852	pentraxin-related gene, induced by IL-1 ß	1.35	0%
QPRT	NM_014298	quinolinate phosphoribosyltransferase	-0.83	4%
RASGRP3	NM_170672	RAS guanyl releasing protein 3	-1.07	4%
RNASE4	NM_194430	ribonuclease, RNase A family 4	-0.92	4%
RND1	NM_014470	Rho family GTPase 1	-1.22	4%
SAA1	NM_000331	serum amyloid A1	-0.99	4%
SAMD11	NM_152486	sterile alpha motif domain containing 11	-0.77	4%
SFRP4	NM_003014	secreted frizzled-related protein 4	-0.90	4%
SLC7A7	NM_003982	solute carrier family 7	-1.01	0%
SLPI	NM_003064	secretory leukocyte peptidase inhibitor	-0.93	4%
ST6GALNAC1	NM_018414	ST6	-1.08	4%
SULT2B1	NM_004605	sulfotransferase family, member 1	-0.94	0%
TF	NM_001063	transferrin	-1.23	4%
THC2581431	THC2581431	VIL1 protein	-1.49	0%
TMEM45B	NM_138788	transmembrane protein 45B	-0.82	4%
TNNC1	NM_003280	troponin C type 1 (slow)	-1.27	0%
VIL1	NM_007127	villin 1	-1.58	0%

Additional file 7. qRT-PCR measurements of mRNA expression of IL-8, PTGS2 and KRT4 gene in A549 cells incubated with 0.1 mg/ml of PEG NPs for 24 h or 24 + 24 h. Data are represented as Log_2 (Relative Expression) ± range derived from quadruplicate RT-PCR reactions.

	Gene name	time (h)	Microarray (Log2 NPs/C)	RT-PCR (log2 RE)
A549	IL8	24	1.16	1.44 ± 0.46
	PTGS2	24	1.01	1.49 ± 0.04
	KRT4	24	-1.02	-1.86 ± 0.02
	IL8	24 + 24	-0.13	-0.71 ± 0.18
	PTGS2	24 + 24	0.0008	-1.11 ± 0.01
	KRT4	24 + 24	-1.84	-2.4 ± 0.01
CCD-34Lu	IL8	24	not significant	-0.41 ± 0.17
	PTGS2	24	not significant	0.39 ± 0.01
	KRT4	24	not significant	0.09 ± 0.07
	IL8	24 + 24	not significant	-0.1 ± 0.01
	PTGS2	24 + 24	not significant	-1.75 ± 0.01
	KRT4	24 + 24	not significant	-0.23 ± 0.06

Additional file 8. List of GO terms relative to differentially expressed genes in A549 cells after 24 h PEG NP incubation. Full list of significant GO terms (p value < 0.05) obtained uploading in DAVID genes differentially expressed in A549 cells at the end of the 24 h of NP incubation. F.E.: Fold Enrichment.

GO Term	Description	p value	F.E.	Gene
GO:0007166	cell surface receptor linked signal transduction	4,00E-03	1,9	AKAP12, CD274, GEM, SHC3, ADRB2, BMP6, CXCL5, CXCR7, F2RL1, CSFR1, FST, IL8, NTSR1, RPS6KA5, SFRP1, SFRP4, SSTR5, SPHK1, STC2, TGM2, TNFRSF25, VEGFC
GO:0023034	intracellular signaling cascade	2,20E-02	1,9	GEM, ARHGEF4, SHC3, ADRB2, CNIH3, DCLK1, IL8, LINGO1, MCTP1, PRKCE, RPS6KA5, SSTR5, SPHK1, TGM2
GO:0042127	regulation of cell proliferation	1,10E-03	2,8	CD274, ADRB2, CXCL5, FOXJ1, IL11, IL8, KRT4, PLAU, PTGS2, RUNX2, SSTR5, SPHK1, TGM2, VEGFC
GO:0042981	regulation of apoptosis	1,10E-02	2,4	ARGHGEF4, ADRB2, ANGPLT4, HRK, PHLDA1, KCNMA1, PTGS2, PRKCE, SFRP1, SPHK1, TGM2, TNFRSF25
GO:0043067	regulation of programmed cell death	1,10E-02	2,4	ARGHGEF4, ADRB2, ANGPLT4, HRK, PHLDA1, KCNMA1, PTGS2, PRKCE, SFRP1, SPHK1, TGM2, TNFRSF25
GO:0010941	regulation of cell death	1,20E-02	2,3	ARGHGEF4, ADRB2, ANGPLT4, HRK, PHLDA1, KCNMA1, PTGS2, PRKCE, SFRP1, SPHK1, TGM2, TNFRSF25
GO:0043065	positive regulation of apoptosis	5,20E-03	3,3	ARHGEF4, ADRB2, HRK, PHLDA1, KCNMA1, PTGS2, PRKCE, TGM2, TNFRSF25
GO:0043068	positive regulation of programmed cell death	5,40E-03	3,3	ARHGEF4, ADRB2, HRK, PHLDA1, KCNMA1, PTGS2, PRKCE, TGM2, TNFRSF25
GO:0010942	positive regulation of cell death	5,50E-03	3,3	ARHGEF4, ADRB2, HRK, PHLDA1, KCNMA1, PTGS2, PRKCE, TGM2, TNFRSF25
GO:0007610	behavior	8,60E-03	3,1	CXCL5, CYP11A1, IL8, KCNMA1, NTSR1, PLAU, PLAUR, PTGS2, SHC3
GO:0006928	cell motion	9,20E-03	3	DCLK1, FOXJ1, IL8, PLAU, PLAUR, PODXL, PTGS2, VEGFC, ZEB2
GO:0009611	response to wounding	1,70E-02	2,7	BMP6, CD55, F2RL1, FGB, IL11, IL8, PLAU, PLAUR, PTX3
GO:0032101	regulation of response to external stimulus	5,80E-05	8	ADRB2, F2RL1, IL8, NT5E, PLAU, PTGS2, SERFPINF1, TGM2
GO:0051094	positive regulation of developmental process	1,70E-03	4,6	ADRB2, ANGPTL4, BMP6, FST, RUNX2, SERPINF1, SPHK1, VEGFC
GO:0008284	positive regulation of cell proliferation	1,40E-02	3,1	ADRB2, CXCL5, IL11, PTGS2, RUNX2, SPHK1, TGM2, VEGFC
GO:0008283	cell proliferation	1,90E-02	2,9	ADRB2, CXCL5, IL11, PTGS2, RUNX2, SPHK1, TGM2, VEGFC
GO:0050878	regulation of body fluid levels	2,40E-04	7,9	F2RL1, FGB, IL11, NFE2, PLAU, PLAUR, KCNMA1
GO:0016477	cell migration	7,40E-03	4	DCLK1, FOXJ1, IL8, PLAU, PODXL, VEGFC, ZEB2
GO:0048870	cell motility	1,20E-02	3,6	DCLK1, FOXJ1, IL8, PLAU, PODXL, VEGFC, ZEB2
GO:0051674	localization of cell	1,20E-02	3,6	DCLK1, FOXJ1, IL8, PLAU, PODXL, VEGFC, ZEB2
GO:0007167	enzyme linked receptor protein signaling pathway	2,00E-02	3,3	ADRB2, BMP6, CSFR1, FST, RPS6KA5, SHC3, VEGFC
GO:0007599	hemostasis	5,50E-04	8,8	F2RL1, FGB, IL11, NFE2, PLAU, PLAUR
GO:0048514	blood vessel morphogenesis	1,00E-02	4,5	ANPEP, ANGPTL4, IL8, PLAU, TGM2, VEGFC
GO:0019932	second-messenger-mediated signaling	1,50E-02	4,1	ADRB2, IL8, MCTP1, SSTR5, SPHK1, TGM2
GO:0051240	positive regulation of multicellular organismal process	1,80E-02	3,9	ADRB2, BMP6, FST, LIPG, PTGS2, SPHK1
GO:0001568	blood vessel development	1,80E-02	3,9	ANPEP, ANGPTL4, IL8, PLAU, TGM2, VEGFC
GO:0001944	vasculature development	2,00E-02	3,8	ANPEP, ANGPTL4, IL8, PLAU, TGM2, VEGFC
GO:0007626	locomotory behavior	2,80E-02	3,5	CXCL5, IL8, NTSR1, PLAU, PLAUR, KCNMA1
GO:0044057	regulation of system process	4,30E-02	3,1	ADRB2, CNN1, FST, KCNMA1, PTGS2, SPHK1
GO:0006917	induction of apoptosis	4,90E-02	3	ARGHGEF4, HRK, PHLDA1, PRKCE, TGM2, TNFRSF25
GO:0012502	induction of programmed cell death	4,90E-02	3	ARGHGEF4, HRK, PHLDA1, PRKCE, TGM2, TNFRSF25
GO:0006937	regulation of muscle contraction	1,00E-03	11,1	ADRB2, CNN1, KCNMA1, PTGS2, SPHK1
GO:0050727	regulation of inflammatory response	1,30E-03	10,5	ADRB2, NT5E, PTGS2, SERPINF1, TGM2
GO:0050817	coagulation	3,70E-03	7,8	F2RL1, FGB, IL11, PLAU, PLAUR
GO:0007596	blood coagulation	3,70E-03	7,8	F2RL1, FGB, IL11, PLAU, PLAUR
GO:0010038	response to metal ion	8,50E-03	6,2	CYP11A1, FGB, MT1X, KCNMA1, PTGS2
GO:0001525	angiogenesis	1,40E-02	5,4	ANPEP, ANGPTL4, IL8, PLAU, VEGFC
GO:0040007	growth	2,70E-02	4,3	BMP6, DCLK1, PLAU, PLAUR, PTGS2
GO:0042060	wound healing	3,10E-02	4,2	F2RL1, FGB, IL11, PLAU, PLAUR
GO:0031667	response to nutrient levels	3,40E-02	4	CYP11A1, FGB, LIPG, PTGS2, STC2
GO:0010035	response to inorganic substance	3,90E-02	3,9	CYP11A1, FGB, MT1X, KCNMA1, PTGS2
GO:0009991	response to extracellular stimulus	4,80E-02	3,6	CYP11A1, HRK, LIPG, PTGS2, STC2

Additional file 9. List of GO terms relative to differentially expressed genes in A549 cells after 24 + 24 h PEG NP incubation. Full list of significant GO terms (p value < 0.05) obtained uploading in DAVID genes differentially expressed in A549 cells incubated for 24 h with NPs and released in NP-free medium for additional 24 h (24 + 24 h). F.E.: Fold Enrichment.

GO Term	Description	p value	F.E.	Gene
GO:0009611	response to wounding	7,60E-03	4,6	CTGF, FGA, PTX3, PROC, SAA1, TF
GO:0006928	cell motion	4,80E-03	5,2	ANG, ANK3, CCK, CTGF, DCLK1, SAA1
GO:0007010	cytoskeleton organization	3,30E-03	5,6	ANG, ANK3, CNN1, KRT4, RND1, VIL1
GO:0044057	regulation of system process	5,80E-03	6,6	CNN1, CCK, LTB, TF, TNNC1
GO:0051674	localization of cell	5,70E-03	6,7	ANG, CCK, CTGF, DCLK1, SAA1
GO:0048870	cell motility	5,70E-03	6,7	ANG, CCK, CTGF, DCLK1, SAA1
GO:0016477	cell migration	3,90E-03	7,4	ANG, CCK, CTGF, DCLK1, SAA1
GO:0051050	positive regulation of transport	1,80E-03	9,2	PDZK1, ANG, LTB, PTX3, SAA1
GO:0006461	protein complex assembly	3,00E-02	4,1	ANG, FGA, QPRT, SCL7A7, VIL1
GO:0070271	protein complex biogenesis	3,00E-02	4,1	ANG, FGA, QPRT, SCL7A7, VIL1

Additional file 10. List of genes, obtained uploading in DAVID genes over-expressed in CCD-34Lu controls with respect to A549 controls, showing only those genes belonging to 4 different GO terms related to the response to oxidative stress and/or inorganic substance.

Gene name	Systematic name	Description	Log2 (CCD-34Lu)	Log2 (A549)	Log2 (CCD-34Lu/A549)
ABAT	NM_020686	4-aminobutyrate aminotransferase	7,82	5,58	2,24
BCL2	NM_000633	B-cell CLL/lymphoma 2	6,96	4,87	2,09
SEC31A	NM_014933	SEC31 homolog A	12,21	10,28	1,93
AHRR	NM_020731	aryl-hydrocarbon receptor repressor	9,42	4,75	4,67
COL1A1	Z74615	mRNA for prepro-α1 collagen	15,92	6,48	9,44
CRYAB	NM_001885	crystallin α B	13,12	6,79	6,32
CYBRD1	NM_024843	cytochrome b reductase 1	13,07	10,69	2,38
ERCC2	NM_000400	excision repair cross-complementing 2	10,43	7,55	2,88
GJA3	NM_021954	gap junction protein, α 3	8,90	3,71	5,19
GSN	NM_198252	gelsolin, transcript variant 2	14,14	11,86	2,27
HVCN1	NM_032369	hydrogen voltage-gated channel 1	8,27	4,03	4,24
LCAT	NM_000229	lecithin-cholesterol acyltransferase	8,73	6,60	2,13
MMP14	NM_004995	matrix metallopeptidase 14	10,59	4,92	5,68
MT1H	NM_005951	metallothionein 1H	16,25	12,96	3,29
MT1X	NM_005952	metallothionein 1X	9,37	6,19	3,18
PXDN	NM_012293	peroxidasin homolog	8,88	3,41	5,47
PDGFRA	AA599881	bone marrow stromal cells cDNA clone	11,12	4,51	6,61
KCNMA1	NM_001014797	potassium large conductance calcium-activated channel	8,72	5,45	3,27
PML	NM_033244	promyelocytic leukemia, transcript variant 5	12,20	10,16	2,04
PTGS1	NM_000962	prostaglandin-endoperoxide synthase 1	13,10	5,81	7,29
SCARA3	NM_016240	scavenger receptor class A, member 3	15,70	12,92	2,78
SEPP1	NM_005410	selenoprotein P	8,09	4,54	3,55
SLC8A1	NM_021097	solute carrier family 8 (sodium/calcium exchanger), member 1	11,43	5,68	5,74
SOD3	NM_003102	superoxide dismutase 3	13,00	3,43	9,57
SNCA	NM_007308	synuclein α	8,92	6,59	2,33
TXNIP	NM_006472	thioredoxin interacting protein	9,98	5,56	4,42
THBS1	NM_003246	thrombospondin 1	13,80	10,81	2,99
TRPA1	NM_007332	transient receptor potential cation channel, subfamily A, member 1	9,92	5,86	4,06
TNFRSF11B	NM_002546	tumor necrosis factor receptor superfamily, member 11b	14,20	3,92	10,28

Conclusions and future perspectives

Despite the improvements of photodynamic therapy clinical outcomes obtained using second generation PSs, the use of PS engineered nanoparticle-based formulations appears to offer unique opportunities for limiting the side effects observed with the conventional PS formulations. Recently, unlike the first general enthusiasm demonstrated towards nanosized drug delivery systems and despite the approval of several nano-drugs for clinical trials, criticism arises also toward nanomedicine approaches. In this context, in this PhD thesis a critical evaluation on the benefits but also the limits connected to the delivery of the PS *m*-THPC by liposomes, PLGA NPs or ORMOSIL NPs, properly PEGylated or functionalized for targeted PDT is presented.

In general, the *in vitro* studies on *m*-THPC uptake in different cellular systems revealed that all the nanovehicles were internalized by cells and were able to deliver the PS, even if reduced amounts of drug were measured with respect to the drug delivered by the standard formulation (Foscan®). The reduced uptake was very like related to the different interaction of the particles and of the free drug with serum proteins and in turn with the cells, with a strong influence of the presence of the PEG corona on NP surface. In fact, the PEGylation of the delivery system minimized NP/cell surface interactions leading to a reduced uptake of the nanovehicles and of its cargo, as measured for PLGA and for ORMOSIL NPs. In particular, the presence of a high density PEG layer coating the surface of ORMOSIL NPs, negatively affects PS internalization, as measured with an about 95% reduced delivery of *m*-THPC using these NPs with respect to the delivery using the *m*-THPC standard formulation. Nevertheless, since PEGylation represents one of the most successful strategies for imparting stealth properties to NPs improving their circulation in the bloodstream *in vivo*, the density and the length of the PEG chains which compose the corona have to be properly modulated in order to balance the reduced clearance by the RES with an efficient drug delivery in target tissues. The effect of PEGylation on *m*-THPC delivery was well characterized using liposomes (Fospeg®). Only modest differences in the uptake and in the phototoxicity of four different liposomal formulations were found *in vitro*, but the results indicated Fospeg® with 8% of PEGylation was the most suitable to improve liposome uptake but also to reduce *m*-THPC dark cytotoxicity. In fact, from the data of paper I and III, it is clear that the presence of the delivery system, despite decreasing *m*-THPC cellular uptake, significantly reduced the drug cytotoxicity in the absence of light, toxicity that represents one of the major side effects of PS administration for photodynamic treatments.

Regarding drug release, it is widely reported in literature that PSs physically entrapped in NPs, tend to escape from NPs when incubated in the presence of serum proteins. The phenomenon, that can be explains with a higher affinity of the hydrophobic PS for serum proteins leading to the formation of PS-protein complexes, can occurs before cell internalization as well as after the drug has entered the cells still entrapped in the delivery system. The results on *m*-THPC PLGA NPs, while indicating that ~ the 20% and the 50% of the PS is released in the first 24 h of

incubation from non-PEG and PEG NPs, respectively,, showed the characteristic intracellular localization of Foscan® in Golgi apparatus and endoplasmic reticulum but also accumulation in endosomes/lysosomes as expected for PLGA NPs. Very likely the release of *m*-THPC was much more sustained from Fospeg® and it occurred after as well as before cell internalization of liposomes. This is based on the fact that differently from liposomes labelled with covalently linked rhodamine which localized in the acidic compartments of cells, *m*-THPC delivered with Fospeg® accumulated exclusively in the Golgi apparatus and endoplasmic reticulum also in the absence of serum in the incubation medium. The problem of drug escape from NPs was elegantly abolished by the derivatisation of *m*-THPC with silane moieties that allowed covalent attachment of the PS to the matrix of ORMOSIL NPs, without perturbing to a great extent the PS photophysical properties. Nevertheless, because of poor internalization of PEGylated ORMOSIL NPs measured in cells *in vitro*, higher *m*-THPC and light doses were required to obtained uptake and phototoxic effects comparable to those obtained with the free drug. In A549 cells irradiated with 0.24 J/cm^2 the IC_{50} for *m*-THPC NPs and for Foscan® was corresponding to *m*-THPC doses of 0.47 μM and 0.07 μM, respectively (unpublished results, see Appendix Figure 1). On the other hand, the higher PDT efficiency measured for Fospeg® and PEG PLGA NPs is very likely related to *m*-THPC release from particles before entering cells. Therefore, it can be hypothesized that, despite the significant reduced PS uptake, the intracellular localization of *m*-THPC in Golgi apparatus and endoplasmic reticulum regardless the type of delivery, only slightly affects PDT-induced cellular damages. On contrary, different intracellular targets of PDT damages have to be considered using PEG ORMOSIL NPs which after cellular internalization, localized together with the transported *m*-THPC in endosomes and lysosomes.

Thus, the functionalisation of the drug delivery systems with targeting agents in order to improve both uptake and selectivity of *m*-THPC delivery in tumour cells was extensively explored with PEGylated liposomes and ORMOSIL NPs while only few attempts were directed to the conjugation of PEG PLGA NPs with epidermal growth factor (EGF), which in turn demonstrated to be ineffective as targeting molecule (data not shown).

Regarding the targeting of nanocarriers with folate, despite the higher PDT efficiency obtained using FA-Fospeg with respect to un-targeted liposomes, in Paper II it was clearly demonstrated that only a little fraction of targeted liposomes entered the cells by specific endocytosis mediated by folate-receptor, being non-specific internalization the prevailing mechanism of liposome uptake. Instead, targeting efficiency was completely abolished when folate was conjugated to PEG ORMOSIL NPs (Paper IV) The inefficient targeting is very likely explained with the poor exposure of the hydrophobic folate molecules on the surface of the ORMOSIL NPs due to interference with the PEG corona has hypothesized by others (Valencia *et al.* 2011) for different types of NPs. Thus, it can be that not only folate but also the long PEG spacers carrying the targeting agent (PEG 5000 for liposomes and PEG 3300 for ORMOSIL NPs) folds and buries in the PEG corona. The extent of PEGylation, being the 8% for Fospeg and approx. 25% for ORMOSIL NPs, seem to affect targeting efficiency with the lower PEG density favourably

affecting cell internalisation of NPs with more encouraging results. NP selective uptake was improved using RGD peptide or Cetuximab antibody as targeting agents, with increased NP accumulation in target cells of ~2 and 20-fold, respectively. The modest selectivity showed by RGD conjugated NPs may be explained again with PEG interference hypothesis while the size of Cetuximab limited the interaction with the corona. In any case, the *m*-THPC phototoxicity measured with our targeted ORMOSIL NPs was only slightly improved and this highlighted the difficulties of obtaining significant improvement of PDT effects. With ORMOSIL targeted with Cetuximab good selectivity of uptake was obtained but the amount of internalised *m*-THPC was too low to produce efficient cell photokilling. Thus, new strategies have to be developed in order to increase drug-cell loading using particles and in order to promote drug accumulation in intracellular target sites more suitable for the improvement of PDT effectiveness. Instead of using PEG for NP coating alternative polymers can be evaluated both for liposomes and silica NPs, but also the addition of different targeting molecules can be considered in the future design of targeted nanovehicles. A very interesting example of multicomponent NP for the targeting of hepatocellular carcinoma was reported recently by Ashley and co-workers which combined features of mesoporous silica NPs and liposomes in the so called 'protocell'. They synthesized a particle-supported lipid bilayer with a nanoporous silica core with very high capacity to carry therapeutics and imaging agents and conjugated with a targeting peptide (SP94) displaying high affinity for hepatocellular receptors as well as with a histidine-rich fusogenic peptide (H5WYG) able to prevent the degradation of sensitive cargos in the acidic compartments of cells and to promote endosomal escape and cytosolic dispersion of the cargos. Therefore, using this multivalent protocell loaded with DOX or with a drug cocktail (DOX, 5-fluorouracil and cisplatin) they measured a 10^6-fold improvement of the killing efficiency of drug-resistant hepatocellular carcinoma cells with respect of using liposomes *in vitro*. Nevertheless, it must be considered that promising *in vitro* results not always translated into comparable *in vivo* outcomes, and therefore studies on animal models are of fundamental importance during the design of drug delivery systems. Regarding the *in vivo* behaviour of our *m*-THPC delivery systems, a study recently published by our collaborators (Bovis *et al.* 2012) compared the biodistribution and the PDT efficacy of Foscan® and Fospeg® (2%, 8%) in normal and tumour bearing rats. They found increased tumour selectivity for Fospeg® with respect to Foscan® very likely related to the combination of increased blood plasma circulation and increased accumulation in the tumour vasculature due to PEGylation-induced EPR effect. In addition they reported a maximal tumour to skin ratio $\leq$ 24 h for both Fospeg® formulations, suggesting that a shorter drug light interval could be used with respect to the longer intervals currently adopted in clinic for Foscan®. Moreover, improved PDT-induced tumour necrosis was measured for Fospeg® with respect to Foscan® in rats i.v injected with 0.05 mg kg^{-1} of *m*-THPC and irradiated (2 J) 24 h post-injection.

Therefore, these *in vivo* results together with the *in vitro* results reported in this thesis, propose PEGylated liposomes as the most promising *m*-THPC carrier, even if further efforts have to be

directed to the optimisation of targeting and to the prevention of drug release. Similarly, the promises offered by PLGA NPs *in vitro* have to be investigated *in vivo* as well as targeting strategies have to be developed to further improve the selective delivery of *m*-THPC.

Finally, the potential adverse effects to human health related to nanoparticle use represents one of the major concern on the introduction of non biodegradable NPs in the medical field. Thus, the potential toxicity of ORMOSIL NPs was faced in Paper V by evaluating their cytotoxic profiles in different lung cell models. It was shown that the PEGylation of NPs completely abolish the high NP-induced cytotoxicity in some type of cells (CCD-34Lu, NCIH-2347) but not in the alveolar epithelial II lung (A549) cells. As it has been reported often in the literature, these results highlight the strong dependence of NP cytotoxicity profiles on the cell model used *in vitro.* Therefore it is expected that a more realistic portrait on the safe use of ORMOSIL NPs as drug delivery systems has be to carried out *in vivo*.

Appendix

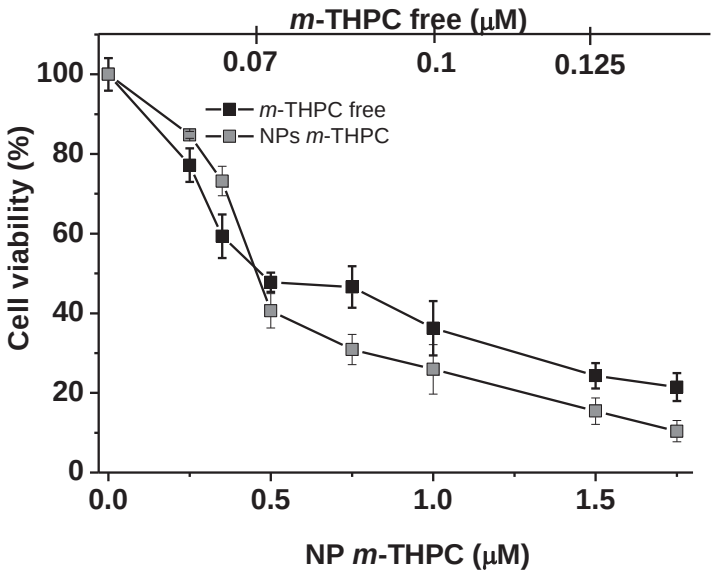

Figure 1: PDT efficacy in A549 cells incubated for 24 h with increasing concentrations of *m*-THPC free or covalently linked in PEGylated ORMOSIL NPs and irradiated with 2.4 J/cm^2 of red light (600-700 nm). Cell viability was measured with MTS test 24 h after irradiation. Free *m*-THPC or *m*-THPC-loaded NP doses had comparable uptake in correspondence of the irradiation time as measured by flow cytometry experiments (data not shown).

References

Albanese A, Tang PS, Chan WCW, "The effect of nanoparticle size, shape and surface chemistry on biological systems", 2012, *Annu Rev Biomed Eng*, **14**, 1-16.

Allison BA, Pritchard PH, Levy JG, "Evidence for low-density lipoprotein receptor-mediated uptake of benzoporphyrin derivative", 1994, *Br J Cancer*, **69**, 883-839.

Allison RR, Downie GH, Cuenca R, Hu XH, Childs CJH, Sibata CH, "Photosensitizers in clinical PDT", 2004, *Photodyn Ther*, **1**, 27-42.

Allison RR, Bagnato VS, Cuenca R, Downie GH, Sibata CH, "The future of photodynamic therapy in oncology", 2006, *Future Oncol*, **2**, 53-71.

Agostinis P, Berg K, Cengel KA, Foster TH, Girotti AW, Gollnick SO, Hahn SM, Hamblin MR, Juzeniene A, Kessel, Korbelik M, Moan J, Mroz P, Nowis D, Piette J, Wilson BC, Golab J, "Photodynamic therapy of cancer: an update", 2011, *CA Cancer J Clin*, **61**, 250-281.

Aguilar ZP, "Nanomaterials for medical applications", 10/2012; Edition: 1st, Publisher: Elsevier, ISBN: 978-0-12-385089-8.

Ahmed N, Fessi H, Elaissari A, "Theragnostic application of nanoparticles in cancer", *Drug Discov Today*, 2012, **17**, 928-934.

Allen TM, Cullis PR, "Drug delivery systems: entering the mainstream", 2004, *Science*, **303**, 1818-1822.

Amoozgar Z, Yeo Y, "Recent advances in stealth coating of nanoparticle drug delivery systems", 2012, *Wires Nanomed Nanotech*, **4**, 219-233.

Arora S., Rajwade JM, Paknikar KM, "Nanotoxicology and in vitro studies: the need of the hour", 2012, *Toxicol Appl Pharm*, **258**, 151-165.

Ashley CE, Carnes EC, Phillips GK, Padilla D, Durfee PN, Brown PA, Hanna TN, Liu J, Phillips B, Carter MB, Carroll NJ, Jiang X, Dunphy DR, Willman CL, Petsev DN, Evans DG, Parikh AN, Chackerian B, Wharton W, Peabody DS, Brinker CJ, "The targeted delivery of multicomponent cargos to cancer cells by nanoporous particle-supported lipid bilayers", 2011, *Nat Mater*, **10**, 389-397.

Ball DJ, Vernon DI, Brown SB, "The high photoactivity of m-THPC in photodynamic therapy. Unusually strong retention of m-THPC by RIF-1 cells in culture", 1999, *Photochem Photobiol*, **69**, 360-363.

Bangham JA, Lea EJ, "The interaction of detergents with bilayer lipid membranes", 1978, *Biochim Biophys Acta*, **511**, 388-396.

Berlanda J, Kiesslich T, Engelhardt V, Krammer B, Plaetzer K, "Comparative in vitro study on the characteristics of different photosensitizers employed in PDT", 2010, *J Photochem Photobiol B*, **100**, 173–180.

Bhuvaneswari R, Gan YY, Soo KC, Olivo M, "The effect of photodynamic therapy on tumor angiogenesis", 2009, *Cell Mol Life Sci*, **66**, 2275–2283.

Bonnet R, Djelai BD, A Nguyen, "Physical and chemical studies related to the development of m-THPC (FOSCAN®) for the photodynamic therapy (PDT) of tumours", 2001, *J Phorphyrins Phtalocyanines*, **5**, 652-661.

Borm PJA, Kreylin W, "Toxicological hazards of inhaled nanoparticles-potential implications for drug delivery", 2004, *J Nanosci Nanotechno*, **4**, 521-531.

Bourdon O, Laville I, Carrez D, Croisy A, Fedel P, Kasselouri A, Prognon P, Legrand P, Blais J, "Biodistribution of meta-tetra(hydroxyphenyl)chlorin incorporated into surface-modified nanocapsules in tumor-bearing mice", 2002, *Photochem Photobiol Sci*, **1**, 709–714.

Bovis MJ, Woodhams JH, Loizidou M, Scheglmann D, Bown SG, MacRobert AJ, "Improved *in vivo* delivery of m-THPC via pegylated liposomes for use in photodynamic therapy", 2012, *J Control Release*, **157**, 196-205.

Buchholz J, Kaser-Hotz B, Khan T, Rohrer BC, Melzer K, Schwendener RA, Roos M, Walt H, "Optimizing photodynamic therapy: in vivo pharmacokinetics of liposomal meta-(tetra-hydroxyphenyl)chlorin in feline squamous cell carcinoma", 2005, *Clin Cancer Res*, **11**, 7538–7544.

Burgaj AM, "Targeted photodynamic therapy – a promising strategy of tumour treatment", 2011, *Photochem Photobiol Sci*, **10**, 1097-1109.

Calzavara-Pinton PG, Venturini M, Sala R, "Photodynamic therapy: update 2006. Part 1", 2006, *Photochem Photobiol*, **21**, 293-302.

Canelas DA, Herlihy KP, De Simone JM, "Top-down particle fabrication: control of size and shape for diagnostic imaging and drug delivery", 2009, *Wires Nanomed Nanotech*, **1**, 391–404.

Carstensen H, Muller RH, Muller BW, "Particle-size, surface hydrophobicity and interaction with serum of parental fat emulsions and model-drug carriers as parameters related to RES uptake", 1992, *Clin Nutr*, **11**, 289-297.

Castano AP, Demidova TN, Hamblin MR, "Mechanisms in photodynamic therapy: Part two-Cellular signalling, cell metabolism and modes of cell death", 2005, *Photodiagn Photodyn Ther*, **2**, 1-23.

Cattaneo AG, Gornati R, Sabbioni E, Chiriva-Internati M, Cobos E, Jenkins MR, Bernardini G, "Nanotechnology and human health: risks and benefits", 2010, *J Appl Toxicol*, **30**, 730-744.

Cedervall T, Lynch I, Lindman S, Berggård T, Thulin E, Nilsson H, Dawson KA, Linse S, "Understanding the nanoparticle-protein corona using methods to quantify exchange rates and affinities of proteins for nanoparticles", 2007, *Proc Natl Acad Sci USA*, **104**, 2050-2055.

Chatterjee DK, Yong Z, "Upconverting nanoparticles as nanotransducers for photodynamic therapy in cancer cells", 2008, *Nanomedicine (London)*, **3**, 73-82.

Chen J, Zhao JX, "Upconversion nanomaterials: synthesis, mechanism, and applications in sensing", 2012, *Sensors Basel*, **12**, 2414-2435.

Chen XJ, Sanchez-Gaytan BL, Qian Z, Park SJ, "Noble metal nanoparticles in DNA detection and delivery", 2012, *Wires Nanomed Nanobiotechnol*, **4**, 273-290.

Chen W, Zhang J, "Using nanoparticles to enable simultaneous radiation of photodynamic therapy for cancer treatment", 2006, *J Nanosci Nanotechnol*, **6**, 1159-1166.

Cheng Z, Al Zaki A, Hui JZ, Muzykantov VR, Tsourkas A, "Multifunctional nanoparticles: cost versus benefit of adding targeting and imaging capabilities", 2012, *Science*, **338**, 903-910.

Clift MJD, Stone V, "Quantum Dots: an insight and perspective of their biological interaction and how this relates to their relevance for clinical use", 2012, *Theranostics*, **2**, 668-680.

Dysart JS, Patterson MS, "Characterization of Photofrin photobleaching for singlet oxygen dose estimation during photodynamic therapy of MLL cells in vitro", 2005, *Phys Med Biol*, **50**, 2597–2616.

Collaud S, Juzeniene A, Moan J, Lange N, "On the selectivity of 5-aminolevulinic acid-induced protoporphyrin IX formation", 2004, *Curr Med Chem Anti-Canc Agents*, **4**, 301-316.

Compagnin C, Baù L, Mognato M, Celotti L, Miotto G, Arduini M, Moret F, Fede C, Selvestrel F, Rio Echevarria IM, Mancin F, Reddi E, "The cellular uptake of meta-tetra(hydroxyphenyl)chlorin entrapped in organically modified silica nanoparticles is mediated by serum proteins", 2009, *Nanotechnology*, **20**, 345101.

Couleaud P, Morosini V, Frochot C, Richeter S, Raehma L, Durand JO, "Silica-based nanoparticles for photodynamic therapy applications", 2010, *Nanoscale*, **2**, 1083-1095.

Cui S, Chen H, Zhu H, Tian J, Chi X, Qian Z, Achilefu S, Gu Y, "Amphiphilic chitosan modified upconversion nanoparticles for *in vivo* photodynamic therapy induced by near-infrared light", 2012, *J Mater Chem*, **22**, 4861-4873.

Curtis J, Greenberg M, Kester J, Phillips S, Krieger G, "Nanotechnology and nanotoxicology: a primer for clinicians", 2006, *Toxicol Sci*, **25**, 245-260.

Da Silva AR, Inada NM, Rettori D, Baratti MO, Vercesi AE, Jorge RA, "In vitro photodynamic activity of chloro(5,10,15,20-tetraphenylporphyrinato)indium(III) loaded-poly(lactide-co-glycolide) nanoparticles in LNCaP prostate tumour cells", 2009, *J Photochem Photobiol B*, **94**, 101-112.

Danhier F, Ansorena E, Silva JM, Coco R, Le Breton A, Préat V, "PLGA-based nanoparticles: An overview of biomedical applications", 2012, *J Control Release*, **161**, 505-522.

D'Cruz AK, Robinson MH, Biel MA, "mTHPC-mediated photodynamic therapy in patients with advanced, incurable head and neck cancer. A multicenter study of 128 patients", 2004, *Head Neck*, **26**, 232-240.

D'Hallewin MA, Kochetkov D, Viry-Babel Y, Leroux A, Werkmeister E, Dumas D, Gräfe S, Zorin V, Guillemin F, Bezdetnaya L, "Photodynamic therapy with intratumoral administration of lipid-based mTHPC in a model of breast cancer recurrence", 2008, *Lasers Surg Med*, **40**, 543–549.

Donaldson K, Stone V, Tran CL, Kreyling W, Borm PJA, "Nanotoxicology", 2004, *Occup Environ Med*, **61**, 727-728.

Dos SN, Allen C, Doppen AM, Anantha M, Cox KA, Gallagher RC, Karlsson G, Edwards K, Kenner G, Samuels L, Webb MS, Bally MB, "Influence of poly-(ethyleneglycol) grafting density and polymer length on liposomes: relating plasma circulation lifetimes to protein binding", 2007, *Biochim Biophys Acta,* **1768**, 1367-1377.

Dougherty TJ, Gomer CJ, Henderson BW, Jori G, Kessel D, Korbelik M, Moan J, Peng Q, "Photodynamic therapy", 1998, *J Natl Cancer Inst*, **90**, 889–905.

Duncan R, Gaspar R, "Nanomedicine(s) under the microscope", 2011, *Mol Pharmaceutics*, **8**, 2101-2141.

Ebbesen M, Jensen TG, "Nanomedicine: techniques, potentials, and ethical implication", 2006, *J Biomed Biotechnol*, **5**, 1-11.

Fadeel B, Garcia-Bennet AE, "Better safe than sorry: understanding the toxicological properties of inorganic manufactured for biomedical applications", 2010, *Adv Drug Del Rev*, **62**, 362-374.

Fadel M, Kassab K, Fadeel DA, "Zinc phthalocyanine-loaded PLGA biodegradable nanoparticles for photodynamic therapy in tumor-bearing mice", 2010, *Lasers Med Sci*, **25**, 283-292.

Ferrari M., "Cancer nanotechnology: opportunities and challenges", *Nat Rev Cancer*, 2005, **5**, 161-171.

Friberg EJ, Čunderlìková B, Pettersen EO, Moan J, "pH effects on the cellular uptake of four photosensitizing drugs evaluated for use in photodynamic therapy of cancer", 2003, *Cancer Lett*, **95**, 73-80.

Gabizon A, Horowitz AT, Goren D, Tzemach D, Shmeeda H, Zalipsky S, "In vivo fate of folate-targeted polyethylene-glycol liposomes in tumor-bearing mice", 2003, *Clin Cancer Res*, **9**, 6551–6559.

Gabizon A, Horowitz AT, Goren D, Tzemach D, Mandelbaum-Shavit F, Qazen MM, Zalipsky S, "Targeting folate receptor with folate linked to extremities of Poly(ethylene glycol)-grafted liposomes: in vitro studies", 1999, *Bioconjugate Chem*, **10**, 289-298.

Garnett MC, Kallinteri P, "Nanomedicine and nanotoxicology: some physiological principles", 2006, *Occup Med-Oxford*, **56**, 307-311.

Gref R, Domb A, Quellec P, Blunk T, Muller RH, Verbavatz JM, Langer R, "The controlled intravenous delivery of drugs using PEG-coated sterically stabilized nanospheres", 1995, *Adv Drug Deliver Rev*, **16**, 215-233.

Gref R, Luck M, Quellec P, Marchand M, Dellacherie E, Harnisch S, Blunk T, Muller RH, "'Stealth' corona-core nanoparticles surface modified by polyethylene glycol (PEG): influences of the corona (PEG chain length and surface density) and of the core composition on phagocytic uptake and plasma protein absorbtion", 2000, *Colloid Surf B-Biointerfaces*, **18**, 301-313.

Gref R, Couvreur P, Barratt G, Mysiakine E, "Surface-engineered nanoparticles for multiple ligand coupling", 2003, *Biomaterials*, **24**, 4925-4937.

Gu F, Zhang L, Teply BA, Mann N, Wang A, Rodovic-Moreno AF, Langer R, Forokhzad OC, "Precise engineering of targeted nanoparticles by using self-assembled biointegrated block copolymers", 2008, *Proc Natl Acad Sci USA*, **105**, 2586–2591.

Hagens WI, Oomen AG, De Jong WH, Casee FR, Sips AJAM, "What do we (need to) know about the kinetic properties of nanoparticles in the body", 2007, *Regul Toxicol Pharm*, **49**, 217-229.

Hamblin MR, Hasan T, "Photodynamic therapy: a new antimicrobial approach to infectious disease?", 2004, *Photochem Photobiol Sci*, **3**, 436-450.

Hatakeyama H, Akita H, Harashima H, "A multifunctional envelope type nano device (MEND) for gene delivery to tumours based on the EPR effect: a strategy for overcoming the PEG dilemma", 2011, *Adv Drug Deliver Rev*, **63**, 152–160.

Hirsjarvi S, Passirani C, Benoit JP, "Passive and active tumour targeting with nanocarriers", 2011, *Curr Drug Discov Technol*, **8**, 188-196.

Hofman JW, Carstens MG, Van Zeeland F, Helwig C, Flesch FM, Hennink WE, Van Nostrum CF, "Photocytotoxicity of mTHPC (temoporfin) loaded polymeric micelles mediated by lipase catalyzed degradation", 2008, *Pharmaceut Res*, **25**, 2065–2073.

Hopper C, Krubler A, Lewis H, Tan IB, Putnam G, "mTHPC-mediated photodynamic therapy for early oral squamous cell carcinoma", 2004, *Int J Cancer*, **111**, 138-146.

Huang YW, Wu CH, Aronstam RS, "Toxicity of transition metal oxide nanoparticles: recent insights from in vitro studies", 2010, *Materials*, **3**, 4842-4859.

Idris NM, Gnanasammandhan MK, Zhang J, Ho PC, Mahendran R, Zhang Y, "*In vivo* photodynamic therapy using upconversion nanoparticles as remote-controlled nanotransducers", 2012, *Nat Med*, **18**, 1580–1585.

Ishida O, Maruyama K, Tanahashi H, Iwatsuru M, Sasaki K, Eriguchi M, Yanagie H, "Liposomes bearing polyethyleneglycol-coupled transferrin with intracellular targeting property to the solid tumors in vivo", 2001, *Pharm Res*, **18**, 1042–1048.

Kawano K, Maitani Y, "Effects of polyethylen glycol spacer lenght and ligand density on folate receptor targeting of liposomal Doxorubicin in vitro", 2011, *J Drug Del*, 160967.

Khdair A, Handa H, Mao G, Panyam J, "Nanoparticle-mediated combination chemotherapy and photodynamic therapy overcomes tumor drug resistance in vitro", 2009, *Eur J Pharm Biopharm*, **71**, 214-222.

Kiesslich, T, Berlanda J, Plaetzer K, Krammer B, Berr F, "Comparative characterization of the efficiency and cellular pharmacokinetics of Foscan®- and Foslip®- based photodynamic treatment in human biliary tract cancer cell lines", 2007, *Photochem Photobiol Sci*, **6**, 619–627.

Klesing, J, Wiehe A, Gitter B, Gräfe S, Epple M, "Positively charged calcium phosphate/polymer nanoparticles for photodynamic therapy", 2010, *J Mater Sci Mater Med*, **21**, 887–892.

Kocbek P, Teskac K, Brozic P, Lanišnik Rižner T, Gobec S, Kristl J, "Effect of free and in poly(e-caprolactone) nanoparticles incorporated new type 1 17ß-hydroxysteroid dehydrogenase inhibitors on cancer cells", 2010, *Curr Nanosci*, **6**, 69–76.

Konan Y, Gurny R, Allèmann E, "State of the art in the delivery of photosensitizers for photodynamic therapy", 2002, *J Photochem Photobiol B*, **66**, 89-106.

Kopelman R, Koo YL, Philbert M, Moffat BA, Reddy GR, McConville P, Hall DE, Chenevert TL, Bhojani MS, Buck SM, Rehemtulla A, Ross BD, "Multifunctional nanoparticle platforms for in vivo MRI enhancement and photodynamic therapy of a rat brain cancer", 2005, *J Magn Magn Mater*, **293**, 404-410.

Korbelik M, "PDT-associated host response and its role in the therapy outcome", 2006, *Lasers Surg Med*, **38**, 500–508.

Konan YN, Chevallier J, Gurny R, Allèman E, "Encapsulation of p-THPP into nanoparticles: cellular uptake, subcellular localization and effect of serum on photodynamic activity", 2003, *Photochem Photobiol*, 77, 638-644.

Krammer B, Plaetzer K, "ALA and its clinical impact, from bench to bedside", 2008, *Photochem Photobiol Sci*, **7**, 283-289.

Kuai R, Yuan W, Qin Y, Chen H, Tang J, Yuan M, Zhang Z, He Q, "Efficient delivery of payload into tumor cells in a controlled manner by TAT and thiolytic cleavable PEG co-modified liposomes, 2010, *Mol Pharmaceutics*, **7**, 1816-1826.

Kumari A, Yadav SK, Yadav SC, "Biodegradable polymeric nanoparticles based drug delivery systems", 2010, *Colloids Surf B Biointerfaces*, **75**, 1–18.

Lam S, Kostashuk EC, Coy EP, Laukkanen E, LeRiche CJ, Mueller HA, Szasz IJ, "A randomized comparative study of the safety and efficacy of photodynamic therapy using Photofrin II combined with palliative radiotherapy versus palliative radiotherapy alone in patients with inoperable obstructive non-small cell bronchogenic carcinoma", 1987, *Photochem Photobiol*, **46**, 893-897.

Lammers T, Kiessling F, Hennink WE, storm G, "Drug targeting to tumours: principles, pitfalls, and (pre) clinical progress", 2012, *J Control Release*, **161**, 175-181.

Lasalle HP, Dumas D, Gräfe S, D'Hallewin MA, Guillemin F, Bezdetnaya L, "Correlation between in vivo pharmakinetics, intratumoral distribution and photodynamic efficiency of liposomal mTHPC", 2009, *J Control Release*, **134**, 118–124.

Levy JG, Obochi M, “New application in photodynamic therapy introduction, 1996, *Photochem Photobiol*, **64**, 737-739.

Lewinski N, Colvin V, Drezek R, “Cytotoxicity of nanoparticles”, 2008, *Small*, **4**, 26-49.

Lin MM, Kim do K, El Haj AJ, Dobson J, “Development of superparamagnetic iron oxide nanoparticles (SPIONS) for translation to clinical applications”, 2008, *IEEE Trans Nanobioscience*, **7**, 298-305.

Liu Z, Chen K, Davis C, Sherlock S, Cao Q, Chen X, Dai H, “Drug delivery with carbon nanotubes for *in vivo* cancer treatment”, 2008, *Cancer Res*, **68**, 6652-6660.

Longmire MR, Ogawa M, Choyke PL, Kobayashi H, “Biologically optimized nanosized molecules and particles: more than just size”, 2011, *Bioconjugate Chem*, **22**, 993–1000.

Lynch I, Dawson KA, “Protein-nanoparticle interactions”, 2008, *Nano Today*, **3**, 40-47.

Maeda H, Wu J, Sawa T, Matsumara Y, Hori K, “Tumour vascular permeability and the EPR effect in macromolecular therapeutics: a review”, 2000, *J Control Release*, **65**, 271-284.

Marchasin S, Wallerstein RO, “The treatment of iron-deficiency anemia with intravenous iron dextran”, 1964, *Blood*, **23**, 354-58.

Master A, Livingston M, Gupta AS, “Photodynamic nanomedicine in the treatment of solid tumours: perspectives and challenge”, 2013, *J Control. Release*, http://dx.doi.org./10.1016/j.jconrel.2013.02.020.

Mazzola L, “Commercializing nanotechnology”, 2003, *Nat Biotechnol*, **21**, 1137-1143.

Mitra S, Foster TH, “Photophysical parameters, photosensitizer retention and tissue optical properties completely account for the higher photodynamic efficacy of meso-Tetra-Hydroxyphenyl-Chlorin *vs* Photofrin”, 2005, *Photochem Photobiol*, **81**, 849-859.

Mlkvy P, Messmann H, Regula J, Conio M, Pauer M, Millson CE, MacRobert AJ, Bown SG, “Photodynamic therapy for gastrointestinal tumors using three photosensitizers-ALA induced PPIX, Photofrin and MTHPC. A pilot study”, 1998, *Neoplasma*, **45**, 157-161.

Moghimi SM, “Opsono-recognition of liposomes by tissue macrophages”, 1998, *Int J Pharmaceut,* **162**, 11–18.

Moghimi SM, Patel HM, “Serum-mediated recognition of liposomes by phagocytic cells of the reticuloendothelial system - The concept of tissue specificity”, 1998, *Adv Drug Deliver Rev*, **32**, 45–60.

Moghimi SM, Hunter AC, Murray JC, “Long-circulating and target-specific nanoparticles: theory to practice”, 2001, *Pharmacol Rev*, **53**, 283-318.

Moghimi SM, Szebeni J, “Stealth liposomes and long circulating nanoparticles: critical issues in pharmacokinetics, opsonization and protein-binding properties”, 2003, *Prog Lipid Res*, **42**, 463-478.

Namiki Y, Fuchigami T, Tada N, Kawamura R, Matsunuma S, Kitamoto Y, Nakagawa M, “Nanomedicine for cancer: lipid-based nanostructures for drug delivery and monitoring”, 2011, *Accounts Chem Res*, **44**, 1080-1093.

Nel A, Xia T, Madler L, Li N, “Toxic potential of materials at the nanolevel”, 2006, *Science*, **311**, 622-627.

Nyman ES, Hynninen PH, “Research advances in the use of tetrapyrrolic photosensitizers for photodynamic therapy”, 2004, *J Photochem Photobiol B*, **73**, 1-28.

Norman ME, Williams P, Illum L, “Human serum-albumin as a probe for surface conditioning (opsonization) of block copolymer-coated microspheres”, 1992, *Biomaterials*, **13**, 841-849.

O’Brien ME, Wigler N, Inbar M, Rosso R, Grischke E, Santoro A, Catane R, Kieback DG, Tomczak P, Ackland SP, Orlandi F, Mellars L, Alland L, Tendler C, “Reduced cardiotoxicity and comparable efficacy in a phase III trial of pegylated liposomal doxorubicin HCl (CAELYX/Doxil) versus conventional doxorubicin for first-line treatment of metastatic breast cancer”, 2004, *Ann Oncol*, **15**, 440-449.

Oberdörster G, Oberdörster E, Oberdörster J, “Nanotoxicology: an emerging discipline evolving from studies of ultrafine particles”, 2005, *Environ Health Persp*, **113**, 823-839.

Oenbrink G, Jürgenlimke P, Gabel D, “Accumulation of porphyrins in cells: influence of hydrophobicity aggregation and protein binding”, 1988, *Photochem Photobiol*, **48**, 451–456.

Ohulchanskyy TY, Roy I, Goswami LN, Chen Y, Bergey EJ, Pandey RK, Oseroff AR, Prasad PN, "Organically modified silica nanoparticles with covalently incorporated photosensitizer for photodynamic therapy of cancer", 2007, *Nano Lett*, **7**, 2835-2842.

Oleinick N, Morris R, Belichenko I, "The role of apoptosis in response to photodynamic therapy: What, where, why and how", 2002, *Photochem Photobiol Sci*, **1**, 1-21.

Osseo-Asare K, Arriagada FJ, "Growth kinetics of nanosize silica in a nonionic water-in-oil microemulsion: a reverse micellar pseudophase reaction model", 1999, *J Colloid Interface Sci*, **218**, 68-76.

Owens III DE, Peppas NA, "Opsonization, biodistribution, and pharmacokinetics of polymeric nanoparticles", 2006, *Int J Pharmaceut*, **307**, 93-103.

Pan X, Lee RJ, "Tumour-selective drug delivery via folate receptor-targeted liposomes", 2004, *Expert Opin Drug Deliv*, **1**, 7–17.

Pantarotto D, Singh R, McCarthy D, Erhardt M, Briand JP, Prato M, Kostarelos K, Bianco A, "Functionalized carbon nanotubes for plasmid DNA delivery", 2004, *Angew Chem Int Ed Engl*, **43**, 5242-5246.

Park W, Hong K, Kirpotin DB, Colbern G, Shalaby R, Baselga J, Shao Y, Nielsen UB, Marks JD, Moore D, Papahadjopoulos D, Benz CC, "Anti-HER2 immunoliposomes: enhanced efficacy attributable to targeted delivery", 2002, *Clin Cancer Res*, **8**, 1172–1181.

Peer D, Karp JM, Hong S, Farokhzad OC, Margalit R, Langer R, "Nanocarriers as an emerging platform for cancer therapy", 2007, *Nat Nanotechnol*, **2**, 751-760.

Pegaz B, Debefve E, Ballini JP, Wagnieres G, Spaniol S, Albrecht V, Scheglmann DV, Nifantiev NE, Van der Bergh H, Konan-Kouakou YN, "Photothrombic activity of m-THPC-loaded liposomal formulations: pre-clinical assessment on chick chorioallantonic membrane model", 2006, *Eur J Pharm Sci*, **28**, 134–140.

Peng CL, Yang LY, Luo TY, Lai PS, Yang SJ, Lin WJ, Shieh MJ, "Development of pH sensitive 2-(diisopropylamino)ethyl methacrylate based nanoparticles for photodynamic therapy", 2010, *Nanotechnology*, **21**, 155103.

Prahabaran M, Grailer JJ, Pilla S, Steeber DA, Gong S, "Gold nanoparticles with a monolayer of doxorubicin-conjugated amphiphilic block copolymer for tumour targeted drug delivery", 2009, *Biomaterials*, **30**, 6065-6075.

Polo L, Valduga G, Jori G, Reddi E, "Low-density lipoprotein receptors in the uptake of tumour photosensitizers by human and rat transformed fibroblasts", 2002, *Int J Biochem Cell B*, **34**, 10-22.

Popovic Z, Liu W, Chauan VP, Lee J, Wong C, Greytak AB, Insin N, Nocera DG, Fukumura D, Jain RK, Bawendi MG, "A nanoparticle size series for in vivo fluorescence imaging", 2010, *Angew Chem Int Ed Engl*, **49**, 8649-8652.

Reddy GR, Bhojani MS, McConville P, Moody J, Moffat BA, Hall DE, Kim G, Koo YE, Woolliscroft MJ, Sugai JV, Johnson TD, Philbert MA, Kopelman R, Rehemtulla A, Ross BD, "Vascular targeted nanoparticles for imaging and treatment of brain tumors", 2006, *Clin Cancer Res*, **12**, 6677-6686.

Remaut K, Lucas B, Braeckmans K, Demeester J, de Smed SC, "Pegylation of liposomes favours the endosomal degradation of the delivered phosphodiester oligonucleotides", 2007, *J Control Release*, **117**, 256–266.

Reshetov V, Kachatkou D, Shmigol T, Zorin V, D'Hallewin M, Guillemin F, Bezdetnaya L, "Redistribution of meta-tetra(hydroxyphenyl)chlorin (m-THPC) from conventional and PEGylated liposomes to biological substrates", 2011, *Photochem Photobiol Sci*, **10**, 911–919.

Ricci-Júnior E, Marchetti JM "Preparation, characterization, photocytotoxicity assay of PLGA nanoparticles containing zinc (II) phthalocyanine for photodynamic therapy use", 2006, *J Microencapsul*, **5**, 523-538.

Rio-Echevarria IM, Selvestrel F, Segat D, Guarino G, Tavano R, Causin V, Reddi E, Papini M, Mancin F, "Highly PEGylated silica nanoparticles: "ready to use" stealth functional nanocarriers", 2010, *J Mater Chem*, **20**, 2780-2787.

Roco MC, "Broader societal issues of nanotechnology", *J Nanopart Res*, 2003, **5**, 181-189.

Romberg B, Hennink WE, Storm G, "Sheddable coatings for long-circulating nanoparticles", 2008, *Pharm Res*, **25**, 55-71.

Roser M, Fischer D, Kissel T, "Surface-modified biodegradable albumin nano- and microspheres. II. Effect of surface charges on in vitro phagocytosis and biodistribution in rats", 1998, *Eur J Pharm Biopharm*, **46**, 255-263.

Roy I, Ohulchanskyy TY, Pudavar HE, Bergey EH, Oseroff AR, Morgan J, Dougherty TJ, Prasad PN, "Ceramic-based nanoparticles entrapping water-insoluble photosensitizing anticancer drug. A novel drug-carrier system for photodynamic therapy", 2003, *J A Chem Soc*, **125**, 7860-7865.

Roy I, Ohulchanskyy TY, Bharali DJ, Pudavar HE, Mistretta RA, Kaur N, Prasad PN, "Optical tracking of organically modified silica nanoparticles as DNA carriers: A nonviral, nanomedicine approach for gene delivery", 2005, *Proc Natl Acad Sci USA*, **102**, 279-284.

Sasnouski S, Zorin V, Khludeyev I, D'Hallewin MA, Guillemin F, Bezdetnaya L, "Investigation of Foscan® interactions with plasma proteins", 2005, *Biochim Biophys Acta*, **1725**, 394-402.

Senge MO, Brandt JC, "Temoporfin (Foscan®, 5,10,15,20-Tetra(m-hydroxyphenyl)chlorin)- A second-generation Photosensitizer", 2011, *Photochem Photobiol*, **87**, 1240–1296.

Schiffelers RM, Koning GA, ten Hagen TLM, Fensa MHAM, Schraac AJ, Janssena APCA, Kokd RJ, Molemac G, Storm G, "Anti-tumor efficacy of tumor vasculature-targeted liposomal doxorubicin", 2003, *J Control Release*, **91**, 115–122.

Shenoy D, Fu W, Li J, Crasto C, Jones G, Di Marzio C, Sridhar S, Amiji M, "Surface functionalisation of gold nanoparticles using hetero-bifunctional poly(ethylene glycol) spacer for intracellular tracking and delivery", 2006, *Int J Nanomedicine*, **1**, 51-57.

Shieh MJ, Peng CL, Chiang WL, Wang CH, Hsu CY, Wang SJ, Lai PS, "Reduced skin photosensitivity with meta-tetra(hydroxyphenyl)chlorin loaded micelles based on a poly(2-ethyl-2-oxazoline)-bpoly(D,L-lactide) diblock copolymer *in vivo*", 2010, *Mol Pharm*, 7, 1244–1253.

Shen H, Sun T, Ferrari M, "Nanovector delivery of siRNA for cancer therapy", 2012, *Cancer Gene Therapy*, **19**, 367-373.

Shmeeda H, Tzemach D, Mak L, Gabizon A, "Her2-targeted pegylated liposomal doxorubicin: retention of target-specific binding and cytotoxicity after in vivo passage", 2009, *J Control Rel*, **136**, 155–160.

Shvedova AA, Kisin ER, Mercer R, Murray AR, Johnson VJ, Potapovich AI, Tyurina YY, Gorelik O, Arepalli S, Schwegler-Berry D, Hubbs AF, Antonini J, Evans DE, Ku BK, Ramsey D, Maynard A, Kagan VE, Castranova V, Baron P, "Unusual inflammatory and fibrogenic pulmonary responses to single-walled carbon nanotubes in mice", 2005, *Am J Physiol*, **289**, L698-708.

Silverstein SB, Rodgers GM, "Parental iron therapy options", 2004, *Am J Hematol*, **76**, 74-78.

Stöber W, Fink A, Bohn E, "Controlled growth of monodisperse silica spheres in the micron size range", 1968, *J Colloid Interface Sci*, **26**, 68-76.

Sumer B, Gao J, "Theranostic nanomedicine for cancer", 2008, *Nanomedicine*, **3**, 137-140.

Sun D, "Nanotheranostics: integration of imaging and targeted drug delivery", 2010, *Mol Pharm*, **7**, 1879.

Svensson, J, Johannson A, Bendsoe N, Gräfe S, Trebst T, Andersson-Engels S, Svanberg K, "Pharmacokinetic study of a systemically administered novel liposomal Temoporfin formulation in an animal tumor model", 2007, *Proc SPIE Int Soc Opt Eng*, **6427**, 64270T.

Svensson J, Johansson A, Gräfe, Gitter B, Trebst T, Bendsoe N, Andersson-Engels S, Svanberg K, "Tumor selectivity at short times following systemic administration of a liposomal temoporfin formulation in a murine tumor model", 2007, *Photochem Photobiol,* **83**, 1211–1219.

Svenson S, "Dendrimers as versatile platform in drug delivery applications", 2009, *Eur J Pharm Biopharm*, **71**, 445-462.

Syu WJ, Yu HP, Hsu CY, Rajan YC, Hsu YH, Chang YC, Hsieh WY, Wang CH, Lai PS, "Improved photodynamic cancer treatment by folate conjugated polymeric micelles in a KB xenografted animal model", 2012, *Small*, **13**, 2060–2069.

Takhar P, Mahant S, "*In vitro* methods for nanotoxicity assessment: advantages and applications", 2011, *Arch Appl Sci Res*, **3**, 389-403.

Torchilin VP, "Drug targeting", 2000, *Eur J Pharm Sci*, **11** (Suppl. 2), S81-91.

Torchilin VP, "Multifunctional nanocarriers", 2006, *Adv Drug Deliver Rev*, **58**, 1532-1555.

Uehlinger P, Zellweger M, Wagnieres G, Juillerat-Jeanneret L, van der Bergh H, Lange N, “Aminolevulinic acid and its derivatives: physical chemical properties and protoporphyrin IX formation in cultured cells”, 2000, *J Photochem Photobiol B*, **54**, 72-80.

Unfried K, Albrecht C, Klotz LO, Von Mikecz A, Grether-Beck S, Schins RPF, “Cellular responses to nanoparticles: Target structures and mechanisms”, 2007, *Nanotoxicology,* **1**, 52-71.

Valencia PM, Hanewich-Hollatz MH, Gao W, Karima F, Langer R, Karnik R, Farokhzad OC, “Effects of ligands with different water solubilities on self-assembly and properties of targeted nanoparticles”, 2011, *Biomaterials*, **32**, 6226-6233.

Van Geel IP, Oppelaar H, Oussoren YG, van der Valk MA, Stewart FA, “Photosensitizing efficacy of MTHPC-PDT compared to Photofrin-PDT in the RIFl mouse tumour and normal skin”, 1995, *Int J Cancer,* **60**, 388-394.

Van Vlerken LE, Amiji MM, “Multi-functional polymeric nanoparticles for tumour-targeted drug delivery”, 2006, *Expert Opinion on Drug Delivery,* **3**, 205-216.

Vargas A, Lange N, Arvinte T, Cerny R, Gurny R, Delie F, “Toward the understanding of the photodynamic activity of m-THPP encapsulated in PLGA nanoparticles: correlation between nanoparticle properties and in vivo activity”, 2009, *J Drug Target*, **17**, 599-609.

Vega-Villa KR, Takemoto JK, Yáñez JA, Remsberg CM, Forrest ML, Davies NM, “Clinical toxicities of nanocarrier systems”, 2008, *Adv Drug Deliver Rev*, **60**, 929-938.

Vert M, Mauduit J, Li S, “Biodegradation of PLA/GA polymers: increasing complexity”, 1994, *Biomaterials*, **15**, 1209-1213.

Wacker M, Chen K, Preuss A, Possemeyer K, Röder B, Langer K, “Photosensitizer loaded HSA nanoparticles. I: Preparation and photophysical properties”, 2010, *Int J Pharmaceut*, **393**, 253–262.

Wang X, Wang Y, Chen ZG, Shin DM, “Advances of cancer therapy by nanotechnology”, 2009, *Cancer Res Treat*, **41**, 1-11.

Wang M, Thanou M, “Targeting nanoparticles to cancer”, 2010, *Pharmacol Res*, **62**, 90-99.

Warner S, “Diagnostics plus therapy = theranostics”, 2004, *Scientist*, **18**, 38-39.

Weeldon I, Farhadi A, Bick AG, Jabbari E, Khademhosseini A, “Nanoscale tissue engineering: spatial control over cell-materials interactions”, 2011, *Nanotechnology*, **22**, 212001.

Weetall HH, “Storage stability of water-insoluble enzymes covalently coupled to organic and inorganic carriers”, 1970, *Biochim Biophys Acta*, **212**, 1-7.

Yang L, Peng XH, YA Wang, Wang X, Cao Z, Ni C, Karna P, Zhang X, Wood WC, Gao X, Nie S, Mao H, “Receptor-targeted nanoparticles for in vivo imaging of breast cancer”, 2009, *Clin Cancer Res*, **15**, 4722–4732.

Yamaoka T, Tabata T, Ikada Y, “Distribution and tissue uptake of poly(ethylene glycol) with different molecular weights after intravenous administration to mice”, 1994, *J Pharm Sci*, **83**, 601-606.

Yan F, Kopelman R, “The embedding of metatetra(hydroxyphenyl)-chlorin into silica nanoparticle platforms for photodynamic therapy and their singlet oxygen production and pH-dependent optical properties”, 2003, *Photochem Photobiol*, **78**, 587–591.

Yan X, Kuipers F, Havekes LM, Havinga R, Dontje B, Poelstra K, Scherpof GL, Kamps JA, “The role of Apolipoprotein E in the elimination of liposomes from blood by hepatocytes in the mouse”, 2005, *Biochem Biophys Res Commun*, **328**, 57-62.

Yu YJ, Zhang Y, Kenrick M, Hoyte K, Luk W, Lu Y, Atwal J, Elliott JM, Prabhu S, Watts RJ, Dennis MS, “Boosting brain uptake of a therapeutic antibody by reducing its affinity for a transcytosis target”, 2011, *Sci Transl Med*, **3**, 84ra44.

Yu MK, Park J, Jon S,. “Targeting strategies for multifunctional nanoparticles in cancer imaging and therapy”, 2012, *Theranostics*, **2**, 3-44.

Zalipsky S, “Chemistry of polyethylene glycol conjugates with biologically active molecules”, 1995, *Adv Drug Deliv Rev*, **16**, 157-182.

Zhang M, Murakami T, Ajima K, tsuchida K, Sandanayaka ASD, Ito O, Iijima S, Yudasaka M, "Fabrication of ZnPc/protein nanohorns for double photodynamic and hyperthermic cancer phototherapy", 2008, *Proc Natl Acad Sci USA*, **105**, 14773-14778.

Zeisser-Labouèbe M, Vargas A, Delie F, "Nanoparticles for photodynamic therapy of cancer", 2006, C.S. Kumar (Ed.), Nanomaterials for Cancer Therapy, Vol. 6 Wiley-VCH, Weinheim, pp. 40–86.

Acknowledgements

Firstly I would like to acknowledge my tutors Prof.ssa Lucia Celotti and Dott.ssa Elena Reddi for gave me the opportunity to work with them and to actively participate to the project Nanophoto.
Thanks to my old and new family.